GAS LIFT OPTIMIZATION AND FLOW INSTABILTIY

KHALID M. O. ELMABROK

School of Computing, Sciences and Engineering
University of Salford

Manchester, UK

Submitted in Partial Fulfilment of Requirements of the Degree of
Doctor of Philosophy, September

Ph.D. Thesis   **2017**

ABSTRACT

Gas lift is an artificial lift method used in the oil industry to lift reservoir fluid to the surface, by supplementing the reservoir pressure when it is depleted or insufficient. During oil production, this method can be affected by two-phase (gas-liquid) flow instability within the production tubing, which results in a reduction in the total oil recovered. There are three main flow instabilities caused by, the density wave oscillation, the casing heading pressure and the flow perturbation within the two-phase flow regime.

Within this investigation of the flow structure, behaviours and instability of two-phase flow have been investigated experimentally using a high-speed motion imaging with a dedicated processing package "Dynamic studio 2015a" in a vertical transparent pipe (ID: 66 mm, Length: 2 m) thus simulating the prototype sizing of the common artificial gas lift. Numerically a Computational Fluid Dynamics (CFD) models were used with air and water as the working fluids for various cases.

The experimental results demonstrated that initial bubble size plays a major role in the development and instability of the upward two-phase flow in the vertical pipe. A new Multiple Nozzle Injection Technique (MNIT) with the aim of reducing initial bubble size and distribution across the simulated vertical column was also utilised, thereby stabilising the gas lift system. Thus the present findings are compared with the current Single Nozzle Injection Technique (SNIT) (or so- called sharp-edge) that are utilised in normal gas lift operation. It has thus been manifested that the new method has the potential to increase the total oil production rate from gas lifted wells. It was found that this new injection technique reduced the overall average bubble size from 7.01 to 5.47 mm and the average overall minimum bubble size from 1.23 to 1.03 mm. The average large bubble size of the Taylor bubble was also reduced from 44.07 to 39.95 mm in the simulated pipe. This perceived to increase in production rate from 40 to 43.05 l/min, which give overall increment of 7.5% at different operating conditions. This is in comparison with the single orifice injection technique at the same operating conditions. Throughout this investigation, water was used as working fluid since the column of corresponding water in the petroleum production tubing has the highest hydrostatic pressure 0.20 bar compared with crude oil. Hence, during the gas lift process crude oil will be less cumbersome to produce than water.

Moreover, it was found that when using the Multiple Nozzle Injection Technique the distribution of gas bubbles could changed from the middle of the vertical pipe (core peaking) to across the entire pipe area (wall peaking). This minimised the two-phase flow development and flow instability, even when the mixture velocity was increased. This was due to a reduction in the coalescence process of the gas bubbles as a result of improved bubble distribution when compared with the Single Nozzle Injection Technique with the same dimensions.

The numerical three-dimensional CFD model using the multi-fluid volume of fluid (VOF) gas-lift with the same dimensions and operating conditions compared qualitatively with bubble distribution similar to those found by experimental trials. In addition, the pressure drop long the simulated test section was calculated numerically. It was also found that the pressure drop was reduced from 0.18 bar to 0.11 bar when the new MNIT was used as compared with the SNIT that are normally used in gas lift operation practise.

DECLARATION

Unless otherwise stated, the work in this thesis is that of the author, and has not previously been submitted in part or in whole, in this or in any other work.

Author:

Khalid M .O. Elmabrok ………………………….

Supervisors:

Dr Martin Burby ………………..………….

Professor Ghasem Nasr ……………………….

LIST OF PUBLICATIONS (see Appendix C)

1- Elmabrok, K. ; Burby, M. ; Nasr, G. (2016), 'The Effect of Development of Two-Phase Flow Regimes on the Stability of Gas Lift Systems', World Academy of Science, Engineering and Technology, International Science Index 114, International Journal of Electrical, Computer, Energetic, Electronic and Communication Engineering, 10(6), 719 - 725.

2- Elmabrok, K. ; Burby, M. ; Nasr, G. ; (2017) Stabilising Gas Lift Systems by Reducing Initial Gas Bubble Size, Society of Petroleum Engineers.(under review)

ACKNOWLEDGMENTS

I would first of all like to thank Allah the most gracious and merciful for His many blessings and guidance, without which I do not believe, I could have accomplished this PhD thesis.

To, Dr Martin Burby, you have been the most patient, supportive, and cooperative supervisor I have ever worked with, and I would like to show my sincere gratefulness to you and to the joint-supervisor Prof. G.G.Nasr and also to all the academic team in the petroleum and gas engineering department.

I would also like to deeply thank my parents, my brothers and my sisters for their prayers, encouragement and support. This is, and always will be, highly appreciated in my life.

Last but not least, to my friends who felt most of the time like family during my stay in the city of Manchester and to the members of staff in the Petroleum and Gas Engineering Division at the University of Salford, especially Alan Wells and Paul Done for their technical supports.

LIST OF CONTENTS

LIST OF TABLES

LIST OF FIGURES

CONVERSION TABLE

Parameter	SI	Other Conversion Factors
Pressure	101.325 kpa	1 atm
		1.01325 bar
		101325 Pa
		14.7 psi
		35.32 ft^3/s
		219.96 gal(UK)/s
Flow	1m^3/s	1000 litre/s
		1000 mm
		0.001 km
		3.28 ft
Length	1m	39.37 in
Temperature	0°C	32 F
		273.15 K
		492 R

GLOSSARY

MNIT	Multiple Nozzles Injection Technique
SNIT	Single Nozzle Injection Technique
ESP	Electrical submersible pump
GLV	Gas lift valve
PI	Productivity Index (psi/bbl)
CAD	Computer aided design-modelling tool
CFD	Computational fluid dynamic (fluent)
BHP	Bottom hole static pressure (psi)
GOR	Gas/oil ratios of oil reservoirs
ID	Internal diameter of pipe, mm
ECT	Electrical capacitance tomography
OD	Outside diameter of pipe, mm
Cp	Centipoise viscosity unit
GLR	Gas liquid ratio
Pt	Production tubing pressure (psi)
Pc	Casing pressure (psi)
LPR	Gas lift performance curve
Cv	Flow coefficient
Xt	Differential pressure ratio across the orifice inside the valve
r_p	Seat of port size bottom radius
r_T	Seat of port size top radius
GOAL	Gas lift optimisation allocation model
GLMS	Gas lift monitoring system
GRAMP	Steady state flow with one-dimensional code
HYTAF	Transient flow code for upward co-current annular

CHAPTER 1

Introduction

1.1 Background

Generally, in oil production, crude oil flows through well tubing naturally by primary oil recovery, which involves natural drive mechanisms that lift crude oil from the oil reservoir to the surface without any artificial method or aid. Nevertheless, in most cases, this primary oil recovery will not last for a long period and becomes inefficient production process. This is due to the reservoir pressure being depleted and lacking sufficient energy to lift the crude oil to the surface. Also, there is still a substantial amount of residual oil in the reservoir, making this the most common production problem in oil fields. Therefore, to extract the remaining crude oil from the reservoir, future reservoir developments, studies and methods must be considered including the secondary oil recovery methods such as gas injection and water injection. These methods are designed depending on reservoir data and driving mechanisms. Other artificial lift methods can also be used to lift crude oil to production facilities, such as electric submersible pumps (ESPs), sucker rod pumps, hydraulic pumps and gas lift methods (Schlumberger, 1999, Forero *et al.*, 1993).

The gas lift method is known as an effective artificial lift technique. The principle of the gas lift method is underlined by its ability to increase drawdown pressure in the reservoir by injecting gas at the bottom of the oil production tubing, where the gas mixes with the reservoir fluid. Since the gas has a lower density than the reservoir fluid, it will lower the overall density of fluid in the tubing and the hydrostatic pressure of the fluid. When bottom-hole pressure decreases, this allows the production from the reservoir to increase (Guet, 2004). Moreover, it is known that, when the crude oil flows from the oil reservoir, it encounters a drop in pressure through the production scheme. Starting from the reservoir to the well bore, through well perforations and then the backpressure that is caused by the hydrostatic pressure in the production tubing string, as well as the fall in gas/oil ratio and increase of water cut.

These pressure drop stages can have a negative impact, either decreasing or stopping the total production flow rate from gas lifted wells. The optimisation of the gas lift method mainly relies on a good understanding of the reduction effects that each parameter is capable of

causing on the total oil production. These parameters include gas flow rate, gas injection pressure, port size, depth, gas lift valve spacing and the two-phase flow behaviours along production tubing which has a crucial phenomenon known as gas lift flow instability (Ebrahimi, 2010).

1.2   Research Problem

During the gas lifting method process, gas is injected into the casing annulus, down to the well into the production tubing through gas lift valves, in order to lift the crude oil column to the surface. However, a very critical and chaotic unstable production phenomenon occurs, known as flow instability. Flow instability can cause serious flow oscillations and turbulence, which can lead to a reduction in total oil production from gas lifted wells. In some cases when the flow instability becomes very severe, it may stop oil production completely in some wells. Flow instability is believed to be a result of three main problems:

(i) Casing heading

(ii) Density wave oscillations

(iii) Flow perturbations

These are briefly explained as a matter of completeness and further clarity of the physical arrangement of the gas lifting operation.

1.2.1   Casing Heading Concept

Casing heading is a dynamic cyclic process that occurs when there is no equilibrium between tubing flow pressure and casing annulus pressure. This cyclic process can be summarised in the following steps; initially casing heading begins in the gas lift valves at the orifice injection point, especially when there is a sudden decrease in the tubing pressure, resulting in an increase in gas flow rate to the tubing column through the orifice. Secondly, when the gas rate is continuously flowing for a certain period to the tubing string, this causes a reduction in the tubing flow pressure. Since the gas supply at the surface choke (compressor facility unit) cannot maintain the high gas flow rate and pressure to the casing for a period, the upstream pressure in the casing annulus will be reduced, causing a decrease in gas flow rate to the tubing column, thereby gradually increasing the tubing pressure because of the reduction of

gas flow rate from the casing. Finally, since tubing pressure increases due to low discharging pressure from upstream while at the same time gas is supplied at the surface, by injection of gas upstream into the casing annulus, and then pressure begins to build up again in the casing annulus and the cycle is repeated. These were comprehensively described by also (Hu, 2005, Torre *et al*., 1987).

1.2.2   Density Wave Oscillation

Density wave oscillation is defined as a density wave instability, and it is related to the kinematic wave propagation phenomena of fluid. Density wave oscillation is caused when fluids with different densities flow together and create very abnormal fluid behaviours that cause turbulence in the system. This is commonly defined as a void wave or continuity wave.

1.2.3   Flow Perturbations

When the gas injection occurs through the gas lift valve into the tubing column, a reaction occurs between the gas phase and liquid phase, resulting in small bubbles. These bubbles are flowing upward in the vertical column as superficial velocity increases, and the flow develops, resulting in different flow patterns such as bubbly flow, slug flow, churn flow and annular flow. However, as the flow develops, a powerful dominant fluid behaviour occurs in the transitional regions including the bubbly to slug, slug to churn and churn to annular flow regions. The cause of this behaviour is related to bubble collapse and backflow, which will lead to a random dispersion and distribution of bubbles in this region. Therefore, abnormal fluid behaviour occurs and causes flow perturbations that can sometimes become very severe, particularly when the velocity increases and the flow reaches the annular region. As results of this, undesired situations such as production of more injected gas than crude oil from the oil reservoir, reducing oil production considerably and causing operational problems such as shutdown of the gas compressor.

1.3 Research Contribution

The contribution to research is the development of a novel technique to reduce flow instability within two-phase flow (gas and liquid). This technique is to reduce the initial gas bubble sizes and pressure drop flowing upward within the production tubing and also improve the bubble distribution across the pipe (production tubing). This has the potential to increase overall oil production for gas-lifted wells, within the operating conditions that have been adopted throughout this investigation.

1.4 Aims

The aims of the thesis are to:

1- Design an apparatus in investigating a two-phase flow experiment for the flow instability in a vertical column when injecting gas in a cross flow.

2- Study the reduction in bubble size and distributions in minimising the flow instability in the simulated production tubing in gas lifted wells.

1.5 Objectives

The prime objectives of the thesis are to:

1. To carry out various trials in order to characterise the flow instability in two-phase flow in a vertical column using advanced image-processing techniques.

2. To construct a numerical simulation model using Computational Fluid Dynamics (CFD) to investigate the effect of all identified variables that are capable of causing this phenomenon during the gas lift operation and benchmark them with experimental data as appropriate.

3. Propose a novel approach that could be used within gas-lifted wells to improve oil production.

4. To contribute to a better understanding of fluid unsteady state and flow instability behaviours.

1.6 Thesis Structure

The thesis is comprises of seven chapters, as follows:

Chapter 1: Introduction

Chapter 1 gives a general insight into the gas lift method, and the associated issues surrounding this method. The chapter then highlights the main aims and objectives of the research.

Chapter 2: Literature Review

Chapter 2 provides a detailed description of the concept of the gas lift method and the types thereof. It also describes the experimental investigations of two- and multi-phase flow which have been carried out over the years to show the developments of the research, including previous attempts and techniques that have been used to overcome the research problem.

Chapter 3: Experimental apparatus, set-up and method of data processing

This chapter presents the experimental design, apparatus and set-up of the research experiment. In addition, the experimental procedure and measurement techniques that have been used to investigate the instability and behaviours of the two-phase flow are also described.

Chapter 4: Experimental Results and Discussion

This chapter presents the experimental results and discussions of the variables that will influence bubble sizes within upward two-phase flow and lead to flow instability. In addition, a novel technique is described that reduces initial bubble size, flow instability and increases

total oil production during the lifting process without increasing the backpressure to the lifting system and restrictions of the flow path inside the vertical pipe.

Chapter 5: Two-Phase Flow Modelling using CFD-Fluent

This chapter introduces ANSYS Fluent computational fluid dynamics modelling, a literature survey of using CFD simulating fluid behaviours in a vertical column and a detailed description of the concept of a comprehensive three-dimensional CFD VOF gas-lift model, which was developed to simulate the gas-liquid flow in a vertical column for both valves.

Chapter 6: Numerical Results, Analysis and Discussion

This chapter presents the numerical simulation results, analysis and discussions of variables that influence the upward two-phase flow behaviours in a vertical pipe related to the gas lift method in the oil industry. In addition, a comparison between the performances of the new multiple nozzles technique and the single orifice (sharp edge) technique is presented.

Chapter 7: Conclusion and Future works

This chapter provides the conclusions from this study and suggestions for future work.

CHAPTER 2

LITERATURE REVIEW

2.1 Introduction

Transportation of fluids from the oil reservoir to the surface can occur naturally, however, occasionally it requires special artificial lift methods, especially when the reservoir energy is insufficient to obtain the desired and profitable oil flow rate. There are several artificial lift methods used in the oil industry to maintain or supplement oil reservoir energy, such as the gas injection method, water injection method, electrical submersible pump (ESP), hydraulic pump and gas lift method. The design of any artificial lift method is largely dependent on the existing reservoir driving mechanisms. The oil reservoir driving mechanism is the ability of the reservoir to deliver fluid to the surface naturally, including gas cap solution, water drive mechanism, dissolved gas drive and a combination of all of these. Gas lift method is one of artificial lift methods, which widely used in the oil industry. In addition, there are a number of requirements to make the gas lift project successful and petroleum engineers must be aware of the golden rules of the gas lift. Firstly, there is the availability of a gas source in the oil field. Secondly, well completion should be considered in the design for a single point lift and with all modes of operation in mind. Finally, detailed attention must be paid to the stability of the gas lift, which can be achieved by understanding the unloading process and multi-phase flow behaviours in the vertical production string (Forero *et al*., 1993).

2.2 Gas Lift Concept

Gas lift is one of the most common artificial lift methods used in the oil production industry. The principle of gas lift is explained by the injection of external energy such as natural gas through a casing annulus down into the tubing through subsurface gas lift valves. This thus enables and assists the formation mechanism to lift the fluid to the surface, depending on the productivity index (PI) of the reservoir. Moreover, this high-pressure gas is injected into the bottom of the production tubing to reduce the mixture density of the fluid by creating gas bubbles, which decrease the liquid hydrostatic pressure and then lift the fluid through the column to the surface. As a result, oil flows from the reservoir to the wellbore, due to the decrease in pressure that occurs in the production tubing; thus as the bottom-hole pressure

decreases, the oil production increases. This method has surface and subsurface equipment. The surface equipment consist of a gas source which is separated from crude oil by production facilities (production separators), and then this gas is dehydrated by a special dehydration unit or filters and then compressed to a certain pressure depending on the injection pressure of the oil reservoir in the compressor station. Thereafter, the gas can be distributed through a gas injection manifold by gas pipelines to the wellheads as shown Figure 2-1, (Schlumberger, 1999).
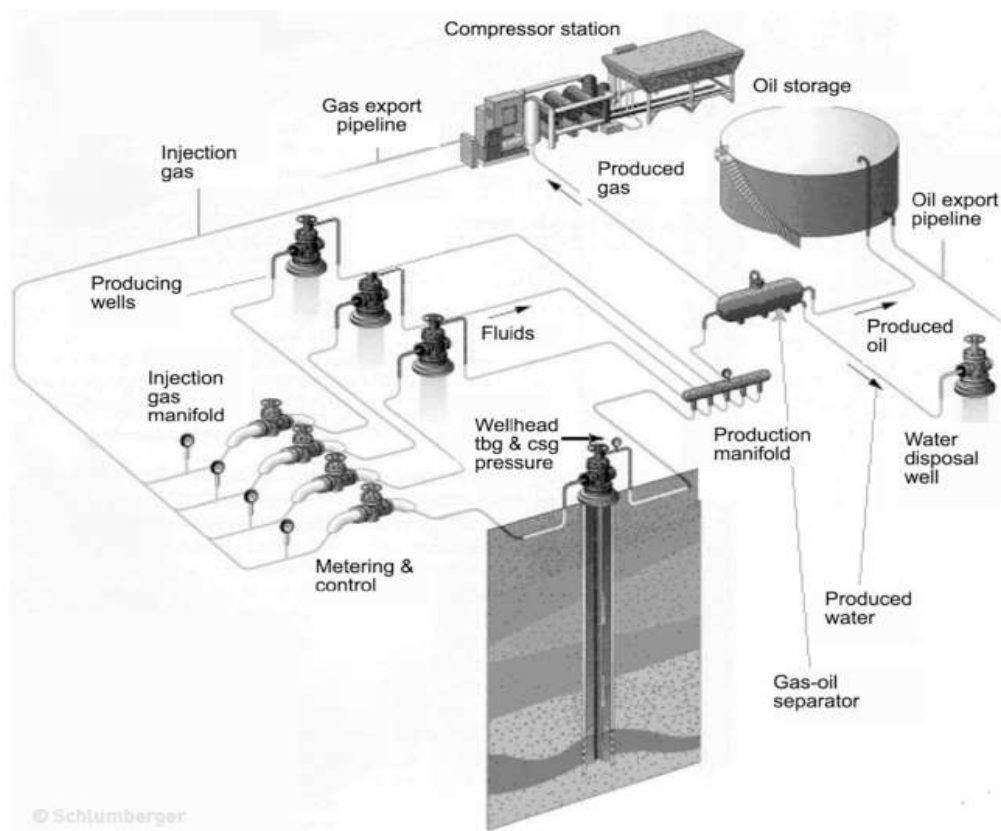
Figure 2-1: Gas lift method components (Schlumberger, 1999).

Figure 2-2 illustrates a schematic view of subsurface gas-lift system equipment. The gas is injected from the surface to the casing annulus down to the well and then it enters the production tubing through unloading valves to lift the long accumulated fluid column above these valves. This process is known as the kick operation. Thereafter, these valves will be closed automatically after some time, depending on their pressure settings. Subsequently, the operating gas lift valve at the bottom of the column will be open during the lifting process to reduce bottom-hole pressure (BHP) to the reservoir. In addition, there are two types of gas lift

method; intermittent gas lift and continuous flow gas lift. These systems are designed depending on the productivity index of the reservoir (PI), which is the ability of fluids to flow through surrounding reservoir rocks to the wellbore under certain operating conditions (Sanderford and W, 1981).
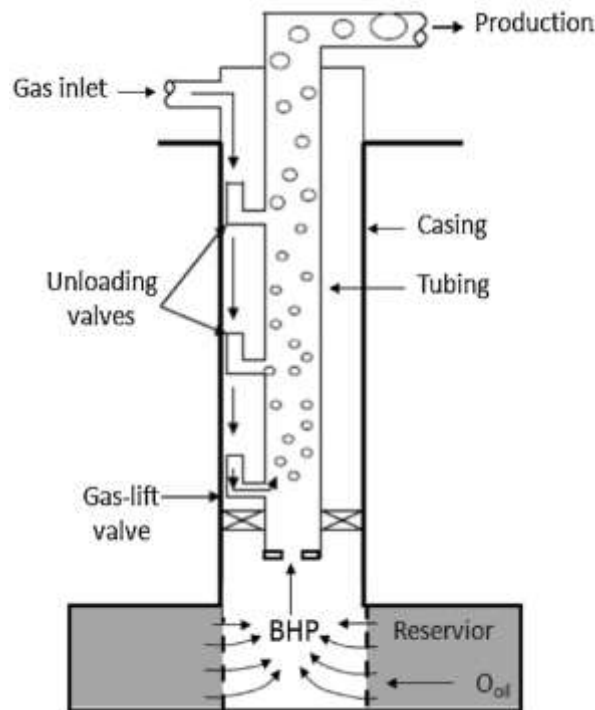
Figure 2-2: Schematic view of a gas-lift system. The gas enters the tubing and lift reservoir (Shaded in grey) to the surface (Sanderford and W, 1981).

2.2.1   Continuous Flow Gas lift System

In terms of fluid dynamics, continuous gas lift is very similar to natural flow. The gas is injected continuously via a casing annulus down to the well into the bottom of the tubing, through the gas lift valves as an additional source of energy to supplement the formation driving mechanism and to reduce the hydrostatic pressure gradient over the injection point. This thereby allows the natural reservoir pressure to cause the reservoir fluid to flow to the well bore and then up to the surface facilities. This is dependent on certain factors such as high productivity index (PI), highly deviated wells, high-static bottom-hole pressure (BHP) and high gas/oil ratios (GORs) reservoirs are considered good candidates for the continuous flow gas lift method. Moreover, continuous gas lift can also be applied to offshore fields, due to its influential water drive mechanism compared to other artificial lift methods; but this

depends on the availability of gas in that particular field. Figure 2-3 shows the principle of continuous gas lift (Kaji et al., 2009, Eikrem, 2006a).
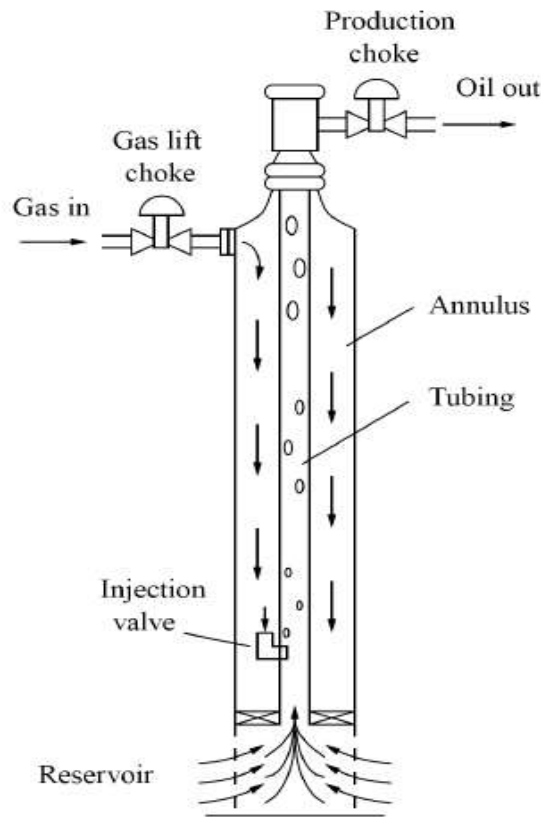
Figure 2-3: The principle of continuous gas lift (Eikrem, 2006b).

2.2.2 Intermittent Flow Gas Lift System

As the name implies, intermittent flow gas lift method is the discontinuous flow of high-pressure gas injected into tubing through subsurface valves for a certain length of time, according to the design settings and fluid accumulation in the tubing column, which is then stopped at intervals Figure 2-4. This cyclic process is repeated after a certain amount of time. The intermittent gas flow lift method is considered as an excellent approach in cases of low productivity index (PI) (< 0.5 psi/bbl), low flowing bottom-hole pressure and low volume production fluid wells (Schlumberger, 1999). The main disadvantage of this method is the interruption (on/off) caused by the discontinuous flow, which makes the gas handling on the surface utilities more difficult, leading to surging in the pipeline and the flowing bottom-hole pressure (Kaji *et al.*, 2009).
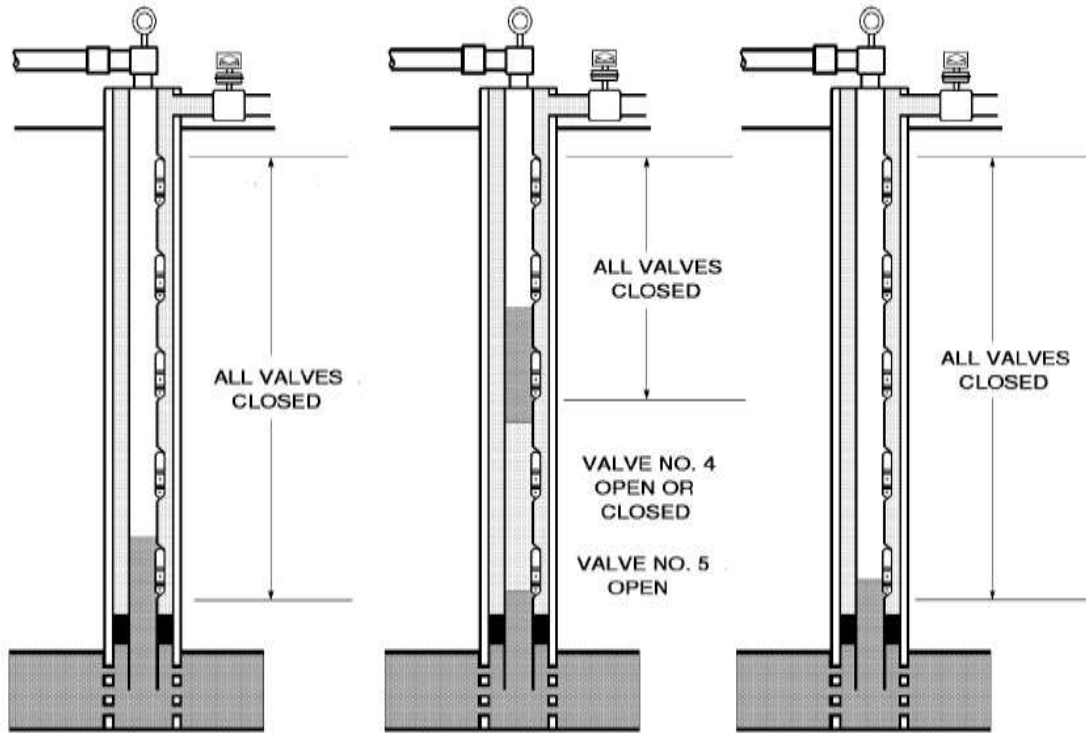
Figure 2-4: Intermittent Gas Lift (Schlumberger, 1999).

Moreover, the gas injection rate through the orifice plate in the intermittent flow gas lift method is calculated by using the following equation (2.1):

$$Q = \frac{155.5\ C_d\ (A)\ P_1\ \sqrt{2g\left(\frac{k}{k-1}\right)\left[r^{\frac{a2}{k}} - r^{\frac{ak+1}{k}}\right]}}{G * T} \qquad (2.1)$$

Where:

Q   =   Flow rate of the gas at standard conditions (14.7 psia and 60°F), Mscf/D,

C_d =   discharge coefficient, determined experimentally and dimensionless,

A   =   area of orifice or choke opening to gas flow, in^2,

P1   =   gas pressure upstream of an orifice or choke, psia,

P2   =   gas pressure downstream of an orifice or choke, psia,

g   =   acceleration of gravity, = 32.2 ft/sec^2,

k   =   ratio of specific heats (Cp/Cv), dimensionless, G = Specific gravity (Air =1),

11

T = Inlet gas temperature, °R, k = Ratio $\frac{C_p}{C_V} = \frac{Specific\ heat\ at\ constant\ pressure}{Specific\ heat\ at\ constant\ volume}$

r = pressure ratio, $P_2/P_1 \geq r_o$, $r_o = \left[\frac{2}{k+1}\right]^{\frac{k}{k+1}}$ = critical flow pressure ratio
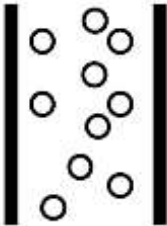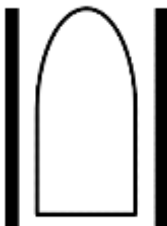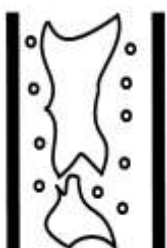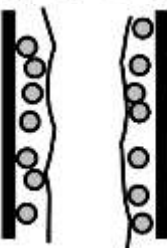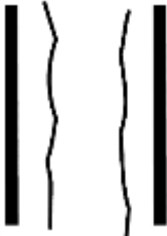
2.3 Two-Phase Flow in Vertical Column

Two-phase flow behaviours and transportation (gas-liquid) are very challenging in many industrial applications, such as air lift pumps, boilers, nuclear power plant steam generators, chemical reactors and the oil and gas industries. Particularly in the oil industry, the gas lifting method is affected by two-phase flow behaviours. The transportation mechanisms of this type of flow is largely affected by the pipe wall, the gradual decrease in the pressure drop, the length of the pipe, as well as the interfacial transfer between the two phases. These effects have a negative impact on the oil production in terms of quantity, and it depends on the stability of the flow . Recently, several attempts have been carried out in order to identify the flow regimes, and these methods are the signals that represent the phase distribution, such as pressure and capacitance (Pan *et al*., 2016).

Furthermore, Sun *et al.* (1999) have experimentally analysed the void fraction waves in different two-phase flow regimes, using an impedance void fraction meter. The authors have reported that the propagating velocities alternate with a change in the type of flow regime and increase as the void fraction rises and become higher at a disturbance point in the vertical pipe. Furthermore, the disturbance wave affects the void fraction wave as its wavelength increases. Also, the frequency of the disturbance wave is largely reliant on the growth rate of void fraction waves. Therefore, when the void fraction growth rate increases, the void fraction fluctuations increase. This accelerates the transition from bubbly flow to other flow regimes and leads to the development of flow.

According to Brill (1987) and Guet (2004), the development of two-phase flow in the vertical pipes created four major flow regimes, which are known as bubbly flow, slug flow, churn flow and annular flow, which occur in accordance with the increase in the superficial velocity as shown in Table 2-1. Each of these flow regimes will be defined in the following section. These flow patterns in a vertical pipe are categorised according to the superficial velocities of liquid and gas. However, the flow patterns depend on specific operating conditions.

Table 2-1: Flow regimes in gas-liquid vertical flow

Flow Transition	Flow Regime	Formation Description	Geometry
Dispersed Flows	Bubbly	Gas bubbles in liquid	
Mixed Flows	Cap or Slug turbulent flow	Gas pocket in liquid	
	Churn Flow	Gas bubbles coalescing in liquid	
	Bubbly annular	Gas bubbles in liquid film with gas core	
Separated Flows	Annular	Gas core and liquid film	

Sources; (Levich and Krylov, 1969).

2.3.1 Bubbly flow

Bubbly flow is divided into two different turbulent sub-regimes; first the bubble is dispersed in the liquid phase and second the sub-regimes are determined by their bubble size. The transition from low to moderate liquid bubbly flow is identified by small bubbles compared to the diameter of the pipe which are spread randomly in the fluid flow within the pipe (Cheng *et al.*, 1998). In addition, the gas bubbles are usually spherical. The characteristics of

this pattern can be noticed by the low void fraction conditions, no bubble break-up occurs, and it is affected by the inlet. On the other hand, the other sub-regime is the finely dispersed bubble-flow regime with large liquid input, which takes place away from the inlets. Then the bubbles start to collapse, which is due to the turbulent eddies and the bubble flow is connected to the turbulence conditions and surface tension properties as the fluid flow moves along the vertical pipe.

2.3.2 Slug flow

Another pattern of gas-liquid flow is known as slug flow. In comparison to the bubbly flow regime, the slug flow regime has a larger value of void fraction, creating less distance between the bubbles and leading to the bubbles colliding and coalescing to form bigger bubbles. The flow consists of large pockets of liquid and gas and also contains dispersed bubbles in the pipe. The regime exhibits strong fluctuations in the liquid flow rate and pressure. Slug flow pattern has a bullet-shaped bubble (Taylor bubble), flowing upward of the pipe separated by a thin film of liquid near the pipe wall. Figure 2-5 illustrates gas bubbles deforming from a spherical bubble to a cap and lastly to a Taylor bubble in the slug flow pattern (Levich and Krylov, 1969, Alamu, 2010).
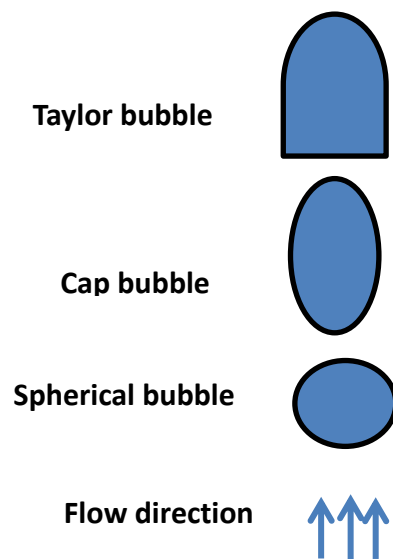
Figure 2-5: The formation and shapes of gas bubbles in the slug flow pattern (Levich and Krylov, 1969).

2.3.3 Churn flow

Moreover, a different pattern that occurs during the gas-liquid flow is the churn flow pattern. The main characteristics of the churn flow regime are defined by the large gas input and moderate void fraction. The pressure and void fraction during the churn flow pattern are constantly fluctuating as the bubble travels up the pipe. This flow instability is mainly caused by the shear stress and gravity. The structure of the fluid becomes unsteady due to fluid fluctuation when the velocity of the flow is increased (Levich and Krylov, 1969, Alamu, 2010).

2.3.4 Annular flow

The last two-phase flow pattern (gas-liquid) that takes place in a vertical direction is known as annular flow, where the annular flow possesses an annular film of liquid near the wall of the pipe with a large flow of gas and small droplets of liquid at the centre of the pipe. The flow is continuous at the centre of the pipe with a higher velocity of gas and liquid droplets being pushed away in both sides of the gas phase (Alamu, 2010).

In addition, previous studies by Da Hlaing *et al*. (2007) carried out an isothermal two-phase flow experiment in a vertical pipe to investigate the effect of liquid viscosity on flow patterns and the corresponding pressure gradient for each flow regime using air with water and air with glycerol solutions respectively as a working fluid. The authors reported that the increasing liquid viscosity has a remarkable impact on the boundaries of the flow patterns in the pipe, especially for transitional region bubble-slug flow regime, where the Reynold numbers of air of each regime were found to be laminar. Figure 6-2 illustrates the relationship between air and water Reynold numbers during the flow. The results showed that the pressure gradient fluctuations occurred between the bubbly and slug flow regimes. Furthermore, these oscillations became severe at the slug to churn transition regime. However, they reduced between the annular and mist flow regimes.
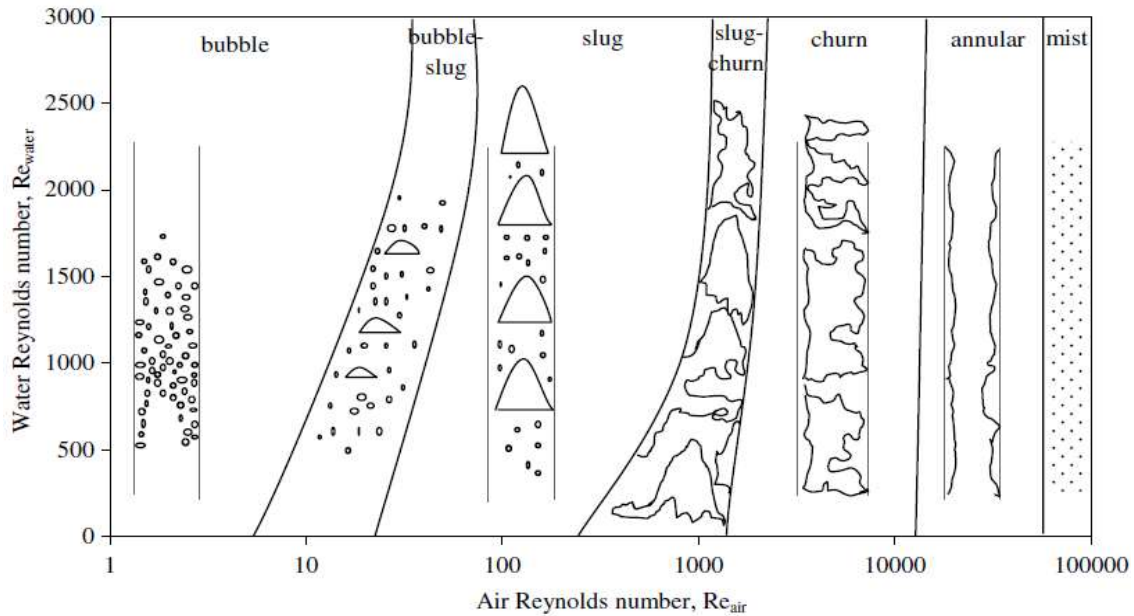
Figure 2-6: Flow pattern regimes for air and pure water mixture (Da Hlaing *et al.*, 2007).

In addition, Sardeshpande *et al.* (2015) have performed two-phase flow experiments in a small vertical tube, 1m long and with 19 mm ID to mimic boiling flows in the reboilers at various mass and heat flux operating conditions. The results have shown that it was possible to identify flow regimes by analysing the accurate pressure drop and pressure fluctuation measurements. Furthermore, it was observed that as heat flux increases, the fluid vapour increases, while the pressure drop decreases. Although the effect of increasing temperature on pressure drop was clearly noticed and significant from pressure analysis, the increase in temperature is not the only parameter that can cause pressure oscillations. Two-phase pressure drop can be affected by several parameters such as geometric configuration, pressure, mass and volume fractions of each phase, fluid properties, mass flux, and also the development of flow patterns (Orkiszewski, 1967) .

On the other hand, a different approach was studied by Ansari and Azadi (2016). The authors experimentally investigated the effect of tube diameter on two-phase flow behaviours in vertical pipes using tubes standing in vertical position made of transparent acrylic with inner diameters of 40 mm and 70 mm. The authors used two different sets of air and water superficial velocities of 0.054-9.654 m/s and 0.015-0.877 m/s for the 40 mm diameter tube, and 0.038-20.44 m/s and 0.036-1.530 m/s for the 70 mm diameter tube. The authors reported that an increase in the tube diameter from 40 mm to 70 mm did not have any significant

16

effect on the transition from bubbly to slug flow and its transition boundary. However, it shrinks the transition region from slug to churn pattern considerably. Furthermore, as a result of using image-processing techniques, the study has reported that the bubbly flow in the 40 mm tube can be divided into three sub-patterns: dispersed, agitated and agglomerated bubbly. Also, two types of slug pattern are also noticed in the same tube diameter, which are named as small and large slugs, whereas a semi-annular flow is clearly noticed as an independent pattern in the 70 mm tube that does not behave like known churn or annular patterns. Although the study has positively contributed to understanding two-phase flow pattern behaviours, they did not report the main cause of Taylor bubble instability, especially when Taylor bubbles reach the critical diameter and then burst. Isao and Mamoru (1987) reported that this collapse leads to fluctuations and undesired operating conditions, which reduce production rate.

On a similar note, Omebere-Iyari and Azzopardi (2007) conducted an experimental study to investigate the flow pattern transitions in a 5mm vertical pipe using conductance probes and a high-speed camera for observations. The result of this study did not massively differ from the previously developed flow model studies. However, it did give better delineat-ing predictions for the churn to annular flow transition compared with the study of Taitel *et al.* (1980), as shown in Figure 2-7. However, the bubbles coalescence and disturbances will be addressed throughout the present investigation.
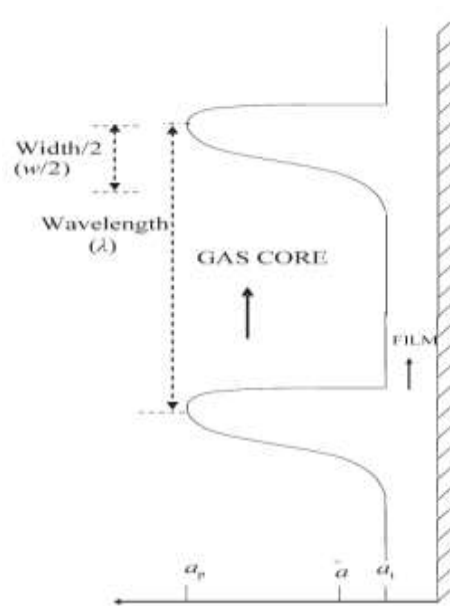
Figure 2-7: Description of film thickness parameters in vertical annular flow (Taitel *et al.*, 1980).

17

Pringle *et al*. (2015) performed an experiment to investigate the effect of pipe diameter on the behaviours of Taylor bubbles and their stability in two vertical tubes with different internal dimeters (0.121 m and 0.290 m) and a height of 9.3 m, using high-speed digital cameras. The authors observed stable Taylor bubbles in a bigger pipe, which had not previously been reported in the literature. Although their Taylor bubble observations were novel, the bubble rise rate measurements only matched when the gas injection was cut. This means that there was no flow and the condition of the column was stagnant, and also there was no bubble break and coalescence mentioned, which is the main cause of the flow instability. The present study aims to critically investigate the main cause of the flow instability.

2.4 Flow Pattern Modelling

Gas-liquid two-phase flow is commonly faced in the petroleum, chemical, and geothermal industries. For example, in the petroleum industry, there are certain complex problems related to two-phase flow behaviours in pipes, vessels and artificial methods. This includes the calculation of flow rate, liquid holdup and pressure loss. These factors are crucial in the design of production vessels, starting from the section of production tubing in the oil well to other surface facilities. Gas-liquid two-phase flow in vertical pipes can be classified into five main patterns: bubbly, slug, churn, annular and dispersed flow (E.Brown and Beggs, 1977). However, there is no single model to capture all these flow pattern behaviours due to their complexity. For that reason, several attempts have been undertaken over the years since the 1950s to model gas-liquid two-phase flow. Previously, (Hasan and Kabir, 1988) have developed a physical model to predict the multi-phase flow patterns in vertical pipes and analysed the transitional flow patterns under hydrodynamic conditions. They have reported that the difference between flow patterns depends on the depth of the vertical well, which near the bottom-hole may only have a single phase. Moreover, as the fluid flows upward in the vertical pipe, its pressure decreases gradually until it reaches a point less than bubble point pressure, where the gas starts to vaporise from the fluid mixture, and then the flow patterns – bubbly flow, slug flow, churn flow and annular flow – will be created respectively, as shown in Figure 2-8.
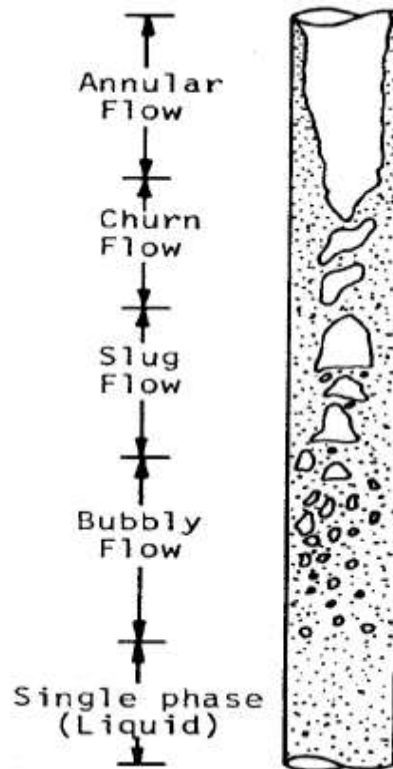
Figure 2-8: Flow pattern transitions in vertical pipe (Hasan and Kabir, 1988).

Bordalo and Gaspari (1997) conducted an extensive analysis to determine the most suitable conditions to stabilise the upward flow in a vertical pipe and also analyse the flow instability, especially for the annular flow regime. The authors used two approaches: a transient flow model that treats phases individually and a linear analysis known as Akin, which was developed by Kelvin-Helmholtz. Both models took into account the effect of the gas compressibility factor in the calculations and how it could influence the prediction within interphase and patterns of two-phase flow as shown in Figure 2.9. The results showed that the gas compressibility had a considerable effect on flow instability and it was the main governing parameter.
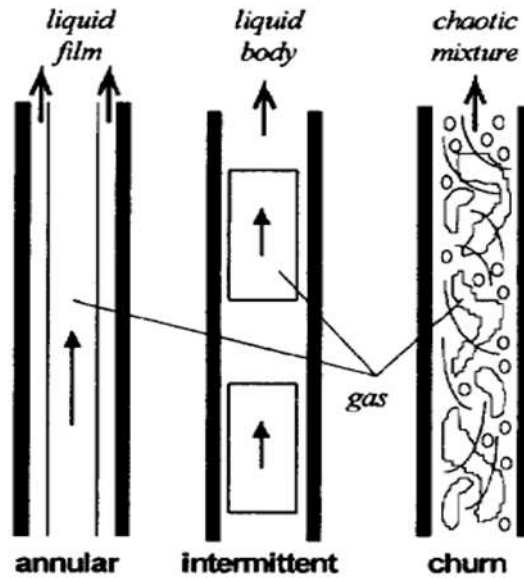
Figure 2-9: Pictorial presentation of vertical annular, intermittent and churn flow (Bordalo and Gaspari, 1997)

Furthermore, they reported that as the gas compressibility decreased, the system became unstable. Moreover, the gas critical flow rate does not rely on the liquid flow rate, but is dependent on the gas compressibility due to the unstable behaviour of the gas, reaching equilibrium quickly (quasi-steady flow). Therefore, the flow stability might depend on the gas composition (molecular composition and flow pressure and temperature). The authors concluded that the surface tension has a positive effect but at low rates only; however, the compressibility is the stabilising parameter, particularly in vertical annular flow at high velocities, because it dominates the interphase fluid system.

(Asheim, 1999) developed an analytical solution to predict the dynamic behaviour of multi-phase flow in the gas lifted wells in comparison to the commercially available simulator OLGA. His analytical solution includes flow friction, interface slippage and certain assumptions in the physical system that is known as the gas lift pumps. This system consists of a vertical pipe submerged in liquid, with gas injected at the bottom inlet. These assumptions have reservoir pressure and outlet pressure as constants, and the fluid flow is assumed incompressible.

20

In addition, the author has stated that OLGA gave good predictions for steady state fluid behaviour compared to his analytical solution; however, there were different predictions in the dynamic conditions, especially when his analytical solution showed certain oscillations that the OLGA simulator did not predict. It seems that his analytical solution was developed only for gas lift pumping research purposes rather than for application to practical gas-lift design and operation. Therefore, no field trial or experiment or any application cases were reported. On the other hand, Grimstad and Foss (2014) developed a non-linear two-phase flow model of an oil producing well with gas lift. This model was based on several assumptions and topside measurements to estimate the well flow rates and downhole pressure. Despite the fact that the model gave good agreements with downhole pressure, no details were mentioned about the prediction of flow instability within the gas lift system.

Moreover, another study was carried out by Waltrich and Barbosa (2011) who investigated the liquid loading in a synthetic vertical well by using the market-leading software package and two research codes; the first code is known as GRAMP, which is used for steady state flow with one-dimensional and two-phase flow in a vertical pipe. The second code is known as HyTAF and it is used for transient flow with one-dimensional, upward co-current annular flow. They focused on the capabilities and limitations of these simulators and how to capture the onset liquid loading and to diagnose the following characteristics in a vertical pipe, as shown in Figure 2-10: pressure drop and liquid up profiles, the transient between churn and annular flow and liquid droplets and flow reversal characteristics.
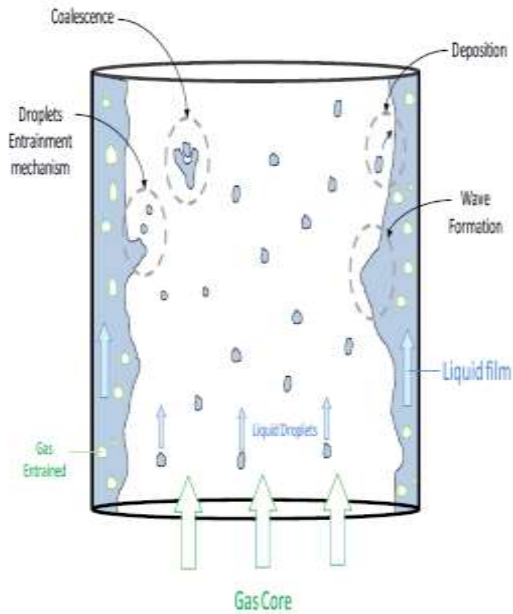
Figure 2-10: Mass transfer mechanisms between phases in annular flow (Waltrich and Barbosa, 2011).

In addition, Waltrich and Barbosa (2011) have stated that the GRAMP code is reliable in measuring the experimental pressure gradient during the steady state conditions for annular flow; however, the authors have shown less confidence in liquid hold up and liquid film velocities. On the other hand, they have suggested that the HyTAF code was not able to capture pressure waves and transient flow in a vertical pipe, which is very important to solve in research on gas lifted wells.

Moreover, a previous attempt was carried out by Waltrich *et al*. (2013), where they compared several transitional models for slug, churn and annular flow regimes with their visual experimental observations in 0.048 m ID, 42 m length vertical pipe under operating conditions where slug, churn, and annular were observed. Results showed a reasonable agreement with the models. Also, they confirmed the existence of churn flow regime as a separate flow regime. However, the flow structure frequency did not show significant variation for gas velocities between 0.2 and 1.6 m/s. One model was proposed by Jayanti and Hewitt (1992) for slug to churn transition triggered by flooding in the Taylor bubble as gas superficial velocity; they studied the critical value at which Taylor bubbles developed as shown in Figure 2.11. The present study aims to investigate the relationship between behaviours of Taylor bubbles and the flow instability within two-phase flow and propose new technique to remedy its development.
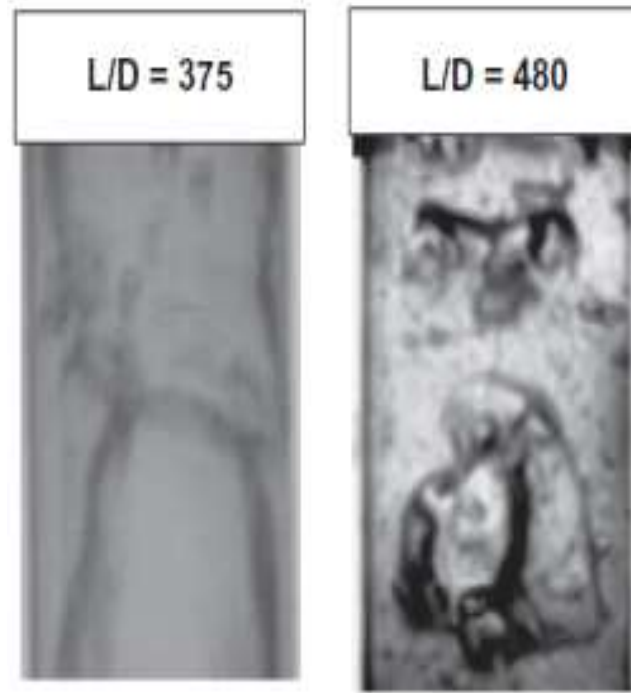
Figure 2-11: The development of Taylor bubble (Waltrich *et al*., 2013).

2.4.1 The Effect of Bubble Velocity on Bubble Size

The bubble rise velocity is an important parameter that characterises the bubble behaviours and most of the previous research studies have investigated the bubble rise velocity on single isolated bubbles. However, the hydrodynamic behaviours of an individual bubble in a gas-liquid system generally differ from those of a single isolated bubble due to interactions with its neighbouring bubbles. Because the mechanism of bubble-bubble interactions is extremely complex, the bubble rise velocity could affect the bubble shape, bubble coalescence process, breakup, bubble size distribution, and gas-liquid interfacial area. Therefore understanding the velocity of the bubbles rising could provide significant innovation of the bubble-bubble interaction mechanism (Zhang and Fan, 2003, Tan *et al*., 2013). Furthermore, another study by Liu *et al*. (2016) investigated the terminal rising velocity of a single bubble in stagnant water and glycerol aqueous solution using high-speed photography and digital image analysis. The results showed that the bubble terminal velocity increases while the aspect ratio decreases in water, and does so almost linearly in the region where d < 0.83 mm. However the terminal velocity and aspect ratio tended to scatter, especially when the diameter of

bubbles was in the range of 0.8-6 mm. The authors concluded that the terminal velocity increases gradually with increasing bubble diameter.

In addition, Acuña and Finch (2010) carried out a study to identify and track individual bubbles flowing in a bubble swarm with diameters ranging between 0.2-5 mm using a 2D column, slot-type spargers, a digital high-speed camera and image analysis software developed for tracking multiple moving objects. The results showed that 60,000 bubbles were matched and tracked per test. Further, the faster moving large bubbles speed up slower small moving bubbles less than 2.5 mm. On the other hand, Krishna *et al.* (1999) performed experimental work to investigate the rise velocity of a swarm of bubbles in a bubble column operating in churn flow regime and proposed two correction factors.

These correction factors are represented by the scale correction factor (SF), which takes into account the influence of the column diameter as a function of the ratio of bubble diameter (d_b) to the column diameter (D_T), and the second factor is known as the correction factor (AF) which considers the increase in rise velocity of the bubble due to its interaction with the wake of a bubble preceding it. The authors found that increasing liquid viscosity reduces the wake acceleration effect and the large bubbles' swarm velocity increases six times more than a single isolated bubble. Although their investigation results showed good agreement with the volume-of-fluid (VOF) simulation, they did not notice any pressure fluctuations due to bubble breakup when the velocity increased.

Azzopardi *et al.* (2015) reported that the use of the capacitance techniques, which consist of electrodes mounted on the side or the outside of an acrylic resin pipe of 67 mm diameter, improves the drift equation for bubble rise velocity, which is quite different from the present. This has also helped to make a useful observation of the flow. The authors have suggested that the void fraction, the mean void fraction in the slug region, the dimensionless length of the liquid slug, all increase with the reduction of the gas superficial velocity. On the other hand, when the gas superficial velocity increases, the Taylor bubble velocity increases as shown in Figure 2.12. Consequently, a new version of the drift flux equation for bubble velocity was proposed and was found to perform well against the present data derived from the literature. This new approach to calculate the Taylor bubble superficial velocity proves to be more accurate, as it takes into account the shape of the nose of the Taylor bubbles, which is affected by the small bubbles in the liquid slug (Abdulkadir *et al.,* 2014a).
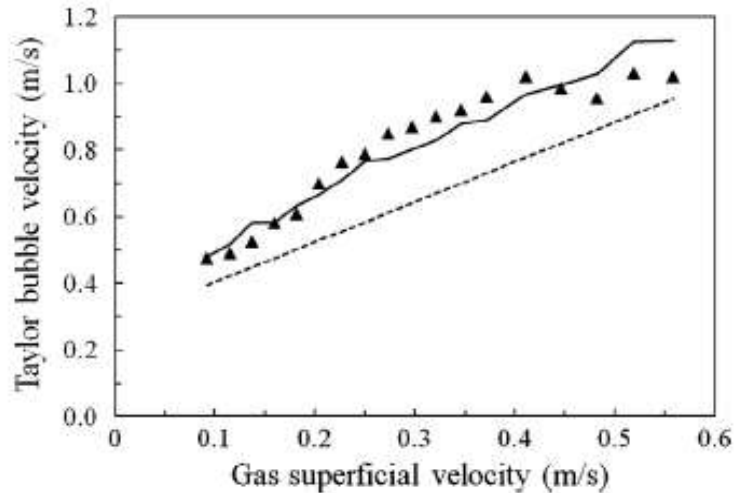
Figure 2-12: Predicted and measured Taylor bubble velocities (Azzopardi *et al*., 2015).

2.5 Multi-phase Flow in a Vertical Pipe

Multi-phase flow is when various fluid phases (oil, water and gas) are flowing together simultaneously. This type of flow is characterised by its abnormal behaviours (concurrent movement of three phases or more such as solid). According to the visual appearance of the flow, flow regimes play a role in categorising the flow development depending on the geometry and direction of the multi-phase flow domain, and whether that is vertical, horizontal or inclined). In addition, when this type of flow reaches a fully developed flow, it causes huge oscillations and interactions in the pipe, which can lead to unstable operational conditions. This has a negative impact on the oil production, as it significantly decreases the amount of crude oil produced by the wells. For example, during a gas-lift system process in the oil industry, fluid flow instabilities occur when the gas is injected into the production tubing and mixed with the reservoir fluid (Guet and Ooms, 2006).

Another approach by Duns Jr and Ros (1963) demonstrated that pressure losses in gas-liquid vertical flow do not always increase the oil production due to the gas in the tubing tending to slip through the liquid phase without lifting the whole liquid in the pipe. The focus of these studies was centred on how to predict the characteristics of multi-phase flow behaviours during the process, which is very critical and complex. Therefore, this research work is aimed at developing a new approach or technique in order to optimise and stabilise the multi-phase flow in gas-lift systems.

25

Previously, different studies had been carried out to study the multi-phase characteristics, including that of Descamps *et al.* (2007), where they performed a multi-phase flow (oil-water and air) experiment in a vertical pipe using optical fibre probes. The main aim of this study was to investigate the phase inversion phenomenon region. This phenomenon occurs when the continuous phase changes to a dispersed phase and vice versa. The authors mentioned that the pressure gradient and pressure increase when they reach the phase inversion region and observed that the dispersed phase (oil and water) had a major effect on bubble size. In addition, the authors reported that the gas flow rate has a significant effect on the distribution of oil and water phases in the cross-section of the vertical pipe. Despite the fact that this research demonstrated extensive understanding of the multi-phase flow behaviours, the study did not provide enough specific information about bubble shapes using these two-point probes and failed to discover the main cause of inversion phenomena. Their approach was not practically applicable to real oil fields, because putting any tool such as a ring inside the production tubing would create a restriction to the flow from the reservoir to the surface and for wireline unit operations. Therefore, another method should be developed for injecting the gas into the column without causing any restriction to the vertical column.

In addition, another attempt was reported by (Zabaras, 1994) to develop a new method to predict pressure profiles of a multi-phase flow in a vertical pipe. This method includes flow pattern transition criteria, and models to calculate pressure loss and liquid hold up for each flow pattern in the vertical pipe. Furthermore, the author applied a method based on physically modelling multi-phase flow in the calculations, which divided the pipe into several segments from bottom to top or vice versa, and involved calculation of pressure and temperature. Also fluid physical properties of gas, oil and water were calculated for each segment. The authors used a convenient pressure gradient model to determine average pressure drop for every segment. This obtained pressure drop and considered the pressure and temperature. Although the study provided sufficient data of the pressure drop, however did not mention how to reduce the pressure drop along the pipe, which can cause the development of flow and flow instability.

On the other hand, Kaji *et al.* (2009) investigated the slug flow pattern using gas and liquid at different flow rates and at different vertical riser axial lengths, with similar pipe diameters: 3a .5 m riser with 51.2mm ID and a 9 m riser with 52.3 mm ID. The authors' approach was to

use a wire mesh sensor and ultrasonic flow in order to determine the void fraction of Taylor bubbles as shown in Figure 2-13, liquid slug lengths, and slug frequency for a slug flow regime. Their study made a remarkable contribution to two-phase flow in vertical risers, however, it did not mention any details or observations regarding the Taylor bubble breakdown and backflow, which causes the flow instability phenomena in two-phase flow.
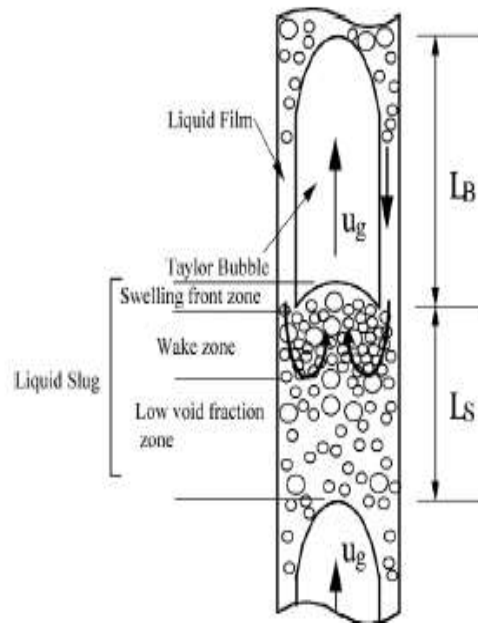
Figure 2-13: The schematic model of slug flow pattern (Kaji *et al*., 2009).

On a similar note, Kaji and Azzopardi (2010) investigated the periodic structure of two-phase flow in a 7m riser for a range of different pipe diameters (0.5 mm to 70 mm). They applied ring-type conductance probes to obtain film thicknesses, pressure gradients and frequencies. The authors reported that as the pipe diameter increased, the flow transitional regions (slug to churn transition and churn to annular) clearly occurred. Their results relied only on the visual observations of flow regime transitions and periodic structures, but they did not focus in their investigations on any variables that were dominant in causing abnormal two-phase behaviours or periodic structure and flow instability.

Another attempt to study two-phase behaviour was carried out by Szalinski *et al.* (2010). The authors employed a wire-mesh sensor as shown in Figure 2-14 in a vertical transparent 6 m pipe with ID of 67mm using air/water and air/silicone. They reported that the void fraction time series of cross-sectional figures was used to characterise amplitude and frequency space. Furthermore, volume fraction profiles and bubble size distribution were determined and then

both scenarios were compared. These data were then processed to identify the flow patterns for each flow rate. Interestingly the bubbles in the air/water tended to be larger than those in air/silicone under similar operational conditions and superficial velocities. Even though the results of the study were promising in understanding the behaviour of two-phase flow in a vertical column, and determined important relationships between variables, and the system recorded acceptable data for both liquids with different densities, the transitional regions from slug to churn and churn to annular could not be 'predicted', and these flow regions are where oscillations are dominant and cause unstable flow.
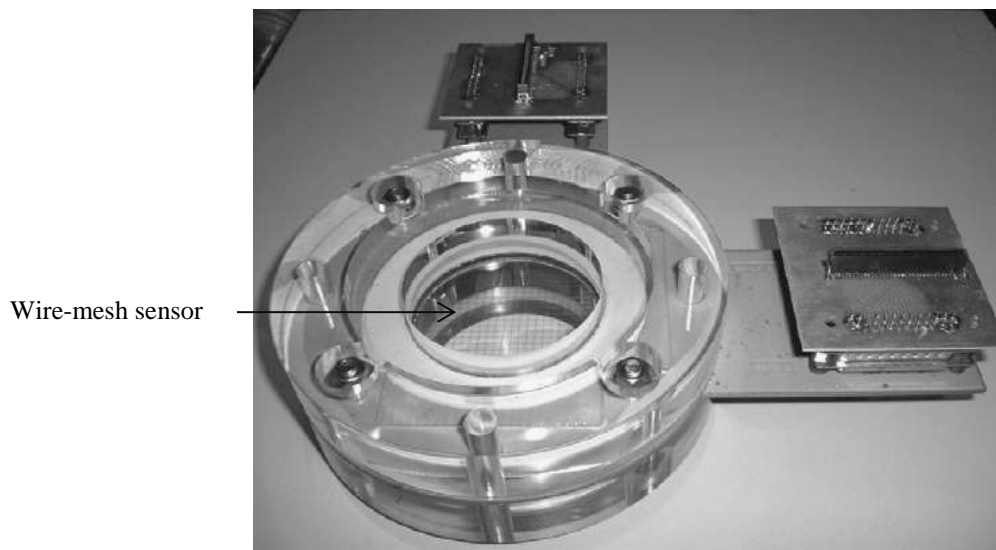
Wire-mesh sensor

Figure 2-14: A wire-mesh sensor (Szalinski *et al.*, 2010)

Furthermore, Alamu and Azzopardi (2011) demonstrated drop concentration frequency by using a laser diffraction technique and a light scattering technique on ID 19 mm, 7m length vertical pipe. This study used air and water as the working fluids and their experiment operated at 13-43 m/s for gas superficial velocity and 0.05 to 0.15 m/s for liquid velocity. Their main research focus was on annular flow regime and they analysed the fluctuation of drop concentration and film hold up with time and reported that flow structure frequencies showed that wave frequency was higher than drop frequency. Moreover, they observed that there was a link between coalescence rate and turbulent diffusion Figure 2-15.
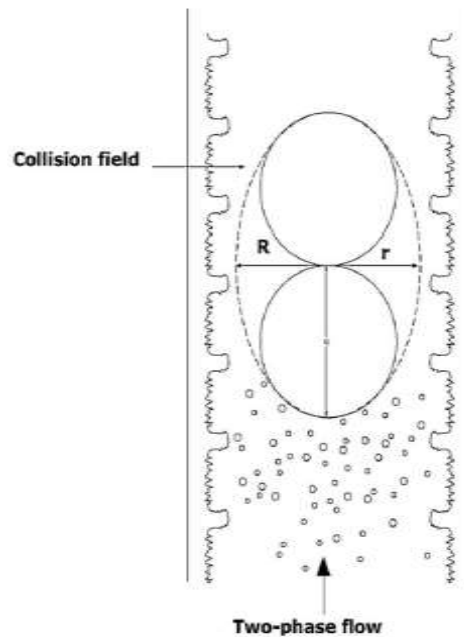
Figure 2-15: Collision field and coalescence of drops in annular two-phase flow (Alamu and Azzopardi, 2011).

Although their study was comprehensive and used advanced techniques to determine drop concentration and frequency and flow structure frequencies on an annular flow regime, it did not provide clear evidence about the main cause of bubble collapse: bubble distributions and flow instability, especially at the transitional regions. In addition, Xu *et al*. (2012) carried out multi-phase flow (oil, water and air) experiment in a vertical pipe to investigate the effect of gas injection pressure on multi-phase flow and the average in situ phase fraction. The results indicated that gas injection pressure had a small effect on the phase invasion phenomena and the average in situ gas fraction decreased when the phase invasion point was reached. Moreover, injecting gas into a liquid phase (oil and water) reduced the gravity gradient. This caused the total pressure gradient to drop in the vertical column. However, the gas phase can increase the mixture velocity, which raises the fractional pressure. Although there was little agreement between the experimental data, the available prediction methods for multi-phase flow pressure gradient still gave poor predictions, due to assumptions in the methods considering the flow as homogenous or oil and water as a single phase. The total pressure gradient, which includes gravity pressure and fractional pressure, can be calculated for fully developed three-phase dispersed flow in a vertical pipe.

Abdulkadir *et al*. (2014b) examined two-phase flow behaviour in a vertical riser of 6 m with 67 mm ID using electrical capacitance tomography (ECT) and a differential pressure transducer. Their main research focus was particularly on the slug flow regime and they determined the velocity of Taylor bubbles, liquid slugs, the slug frequencies, and the length of Taylor bubbles, liquid slug, void fraction with Taylor bubbles, liquid slug, and liquid film thickness. In this experiment, the film thickness could not be measured using ECT directly.

Although their investigations were precise, the bubble dispersion, backflow after Taylor bubbles collapsed, and distribution of Taylor bubbles, which are the main causes of flow instability and chaotic behaviour in the transitional regions, were not mentioned in this study. A different approach was followed by Azzopardi *et al.* (2014) to investigate the Taylor bubbles that coalesced, and small bubbles formed in a 6.5 m riser with 240 mm ID using an advanced tomographic instrument on highly viscous liquid. The authors focused on slug flow regime and reported that as the void fraction increased rapidly, gas superficial velocity increased at low gas flow rate, however it rose slowly at higher gas velocities. Despite the fact that they used advanced instruments for their measurements in this experiment, dispersion and backflow of Taylor bubbles, and bubbles collapsing (especially at the transitional region) were not investigated.

2.6   Gas Lift Flow Instability

Continuous and intermittent gas lifted wells have very abnormal fluid behaviours and unstable operating conditions. Because of the development of two-phase flow in these gas lift systems small fluid perturbations can develop into big fluctuations and flow oscillations along the production tubing. In addition to this, most gas lift wells in the oil fields use gas lift single (sharp edge) orifice valves and (Nova) venturi valves, and these types of valve operate in subcritical flow conditions at the injection point and causing subcritical operating conditions especially at low differential pressure between tubing and casing pressure. This leads to uncontrolled cyclic operating conditions of the flow. As a result of this, there is a reduction in the total oil production from this method along with other disadvantages. First, the pressure surges in the surface production facilities can cause serious operational problems such as the gas compressor shutting down. Second, gas allocation and distribution to other wells becomes difficult. This may affect the overall measurement of production rates when these wells are tested (Alhanati *et al*., 1993). According to Guet and Ooms (2006), there are

several fluid-flow phenomena influencing vertical gas-liquid flows. Figure 2.16 demonstrates the flow instability in a gas-lift system. The flow instability effects contain the radial distribution of void fraction, flow regime changes and system stability problems. The main instabilities in the gas-lift system are due to changes in tubing pressure when the gas pressure is not high enough. If the injected gas pressure becomes higher, then the flow can be critical. The gas lift valve port size cannot be too large, as this can cause considerable instability (Bellarby, 2009).

Lift gas enters annulus and displaces liquid to valve depth- well not flowing.

Gas enters tubing and starts to lower tubing pressure, but effect is slight as pressures are high and gas is compressed.

More gas enters tubing; tubing pressure drops, allowing the annulus gas to expand into the tubing. Runaway flow of a gas results.

Eventually, the high volume of gas in the tubing reaches the surface as large slugs. Flow from annulus stops due to depleted annulus and tubing back pressure.

Figure 2-16: Gas-lift instability (Guet and Ooms, 2006)

The flow instability of the gas lift method can be classified into two types depending on the degree of its severity and impact in the entire gas lift system: microscopic and macroscopic flow instabilities.

31

2.6.1 Microscopic instability

Every two-phase flow in a pipe has small-scale flow instability and perturbations due to bubbles forming and collapsing during the flow of the liquid phase and gas phase together in the same path. The hydrodynamic slugs always occur in two-phase flow but are considered as disturbances and would not cause any trouble within the system. These are known as microscopic instabilities, and happen locally within the liquid-gas interface (Hu, 2005). In gas-lift optimisation, the critical parameter for greater efficiency is 'the bubble coalescence and breakup effects'. Wu *et al.* (1998a) considered five mechanisms responsible for bubble coalescence and breakup. The mechanisms are coalescence due to: random collisions driven by turbulence, breakup due to impact of turbulent eddies, coalescence due to wake entrainment, breakup of large cap bubbles due to interfacial instabilities and shearing-off of small bubbles from cap bubbles. There is a relative velocity between single gas bubbles and the liquid in the pipe resulting in gravity and drag force. Gravity is the main force for large bubbles and therefore, as bubble size increases, so too does bubble terminal velocity. Also the terminal velocity is changing constantly because of the changes in bubble shape in the pipe, affecting the drag force coefficient (Guet *et al*., 2004).

The void fraction is defined as the ratio of the volume of gas to the volume of liquid occupying the pipe. According to Guet and Ooms (2006), the void faction radial profiles depends on the flow conditions. This was demonstrated at the peak near the pipe wall or at the centre line. The authors suggested that the void fraction radial profile evolves from a wall-peak to a core-peak trend as the gas input increases. However, Koide et al. (1968) showed that the bubble size can be increased with gas input and the type of gas injection point. A further study by Liu (1997) considered the effect of bubble size and gas injection rate separately under certain operating conditions. The author concluded that as gas input increased, the bubble size increased. In the study of Taitel *et al.* (1978), different models for each flow were used in predicting the void fractions and the pressure drop. Further work undertaken by Taitel *et al.* (1980) demonstrated that small bubbles coalesce to create Taylor bubbles and the void fraction in this flow regime is at least 0.25.

2.6.2   Macroscopic instability

This type of flow instability is called systematic instability and it involves the entire two-phase flow system and depends on the boundary conditions. The systematic flow instability can cause serious flow oscillations within the system. In most cases, these oscillations are a major cause of production losses and are harmful to operational smoothness, safety and efficiency (Hu, 2005). Therefore, several experimental investigations and attempts have been conducted throughout the literature to understand the main cause of two- and multi-phase flow macroscopic instability. Another previous attempt by Gilbert (1954) performed a study using vertical performance curves, inflow performance curves and bean (choke) performance curves to analyse the behaviours of natural flowing fluid, especially for gas lift wells. The research focus was in understanding and distinguishing between flow patterns along a vertical pipe for petroleum engineers. The author demonstrated the fundamental effect of the depth pressure gradient in two-phase vertical flow by using gradient curves, which showed different ranges of gas-liquid ratios, rate of liquid flow and tubing sizes. The analyses were very useful and important for predicting the overall pressure gradient along the pipe. However, the author did not use any technique to reduce the flow oscillations in production tubing in the gas lifted wells and natural flow wells.

A previous study by Poettman and Carpenter (1952) was conducted to develop correlations and calculations for predicting the overall pressure gradient for multi-phase flow of gas and liquid through a vertical pipe, considering flowing bottom-hole pressure, down-hole pressure (DHP), the depth at which gas is injected into the well, injection rate, the ideal horsepower needed to lift the oil to the well surface, production rate and tubing size. However, the authors neglected the gas flow rate in the casing annulus, which affects the tubing pressure in this study. Another approach by Bertuzzi *et al.* (1953) tested the gas lift well performance under specific conditions by reducing the tubing diameter to ¾ of an inch and observing the gas injection at a certain injection point. The results showed that the surface gas injection pressure was regulated by the flow rate controller valve, however, there was no packer in the well to seal the casing annulus between the casing and tubing. Thus, the system pressure was minimised and the valve's injection depth could be changed. The operating conditions could also be changed by lowering and raising the tubing, depending on the productivity index of the reservoir (PI) and hydrostatic fluid level in the tubing string. The gas lift valves can be adjusted before installation. However, these types of valve could not be controlled in the opening and closing positions from the surface, since the valves were operated under

pressurised conditions. Thus, this approach led to unstable flow rate (unsteady state conditions), which affects the vertical performance.

Hagedorn and Brown (1964) conducted an experiment to investigate the effect of viscosity on pressure gradient in two-phase flow along a vertical pipe. The experiment consisted of 1¼ inches tubing diameter and 1500 ft length. The authors considered different variables in their investigations such as air injection pressure, temperature and surface pressures. The results showed that when the liquid viscosity was less than 12 cp, the influence on the flow rate was low. However, when it was above 12 cp, it caused huge reductions in the liquid flow rates, especially when the flow reached the laminar flow regime. As result of this, there was remarkable energy loss due to friction. Therefore, liquid viscosity must be taken into account in any two-phase flow investigation, because it increases the friction within fluid interfaces.

The authors reported that liquid viscosity plays the main role in increasing fractions within the liquid phase and raises slippage between the gas phase and liquid phase. Furthermore, when flow rate was low, slippage in the fluid interfaces was observed, which causes velocity distribution inside the liquid phase, because of the effect of the pipe wall. The authors concluded that as liquid viscosity decreased, the slippage and friction of the interface decreased. In addition, as the gas-liquid ratio increased, the slippage decreased, especially at high rates, and this led to an increase in energy losses due to friction.

On the other hand, Asheim (1988) developed two gas lift stability criteria: inflow response and pressure depletion response. Firstly, the inflow response criterion dictates that when the reservoir fluid reaction (PI) is fast and sufficiently sensitive to the tubing pressure, then the reservoir fluid will flow into the tubing column quickly and then increase the fluid mixture density as the tubing pressure decreases. This leads to an increase in tubing column pressure, thereby stabilising the well. This inflow instability criterion can be expressed as shown in equation (2-2).

$$F_1 = \frac{\rho_{gsc}\, B_Q\, q_{gsc}^2}{q_{Lsc}} \frac{J}{(EA_i)^2} > 1 \qquad (2.2)$$

Where:

34

p_{gsc} = Gas lift density at standard surface conditions, Kg/m^3, q_{gsc} = Flow rate of lift gas at STD conditions, m^3/s. q_{Lsc} = Flow of liquids at STD conditions, m^3/s J = Productivity of reservoir $STDm^3/s$. Pa. E = Orifice efficiency factor, here assumed to equal 0.9, A = Injection port size, m^2, F_1 = inflow response criterion.

Secondly, the pressure depletion response criteria occurs when tubing pressure decreases; then gas injection flow rate will increase as well as liquid flow rate. This leads to a reduction in the tubing pressure and also a drop in the casing annulus pressure. Therefore, if the annulus pressure is depleted faster than the tubing pressure, this will minimise the differential pressure between the tubing and casing annulus and gas lifting rate, thus stabilising the well. This pressure depletion response criterion can be expressed as shown in equation (2-3):

$$F_2 = \frac{V_t}{V_c}\frac{1}{gD}\frac{P_t}{(\rho_{fi}-\rho_{gi})}\frac{q_{fi}+q_{gi}}{q_{fi}(1-F1)} > 1 \qquad (2.3)$$

Where:

F_2 = pressure depletion response criteria, V_t = tubing volume downstream of gas injection point, m^3, V_c = gas conduit volume, m^3, g = acceleration of gravity, m/s^2, D = vertical depth to injection point, m, P_t = tubing pressure, Pa, ρ_{fi} = reservoir fluid density at injection point, kg/m^3, ρ_{gi} = lift-gas density at injection point, kg/m^3, q_{fi} = flow rate of reservoir fluids at injection point, m^3/sec, q_{gi} = flow rate of lift gas at injection point, m^3/sec.

Furthermore, Alhanati *et al.* (1993) investigated the stability criteria proposed by Asheim (1988) and then stated that certain assumptions were not correct, because some gas lift components were neglected in Asheim's criteria, such as gas injection choke, tubing-casing annulus and subsurface gas lift valves, especially at low flow rate and gas-liquid ratio (GLR). Furthermore, the gas-liquid ratio of reservoir fluid is less than the gas-liquid ratio during the gas lifting process, because the gas liquid ratio of the gas lift method is equal to the reservoir GLR plus the injected gas ratio. Therefore, the formation's response to well-bore should not be neglected. Moreover, Alhanati suggested a simple and reliable full transient simulator, with low accuracy and not for design purposes. The authors recommended unified criteria for continuous gas lift instabilities, including the reservoir dynamic response to bottom-hole pressure variation which Asheim (1988) had neglected.

Ter Avest and Oudeman (1995) developed a dynamic gas lift simulator to aid in the diagnosis of gas lift problems associated with the casing heading stability problem. The simulator includes valve model to capture gas passage through gas lift valve. The main goal of the developed simulator was to improve the gas lift performance curve and optimise the unloading procedure. The results showed that when gas injection rates were low, wells became unstable. However, at high gas rates, the pressure drop along the production tubing was dominated by the friction of phases. In addition, the optimisation of gas injection port size was an important parameter. However, reducing the port size of the gas lift valve is not the solution for two-phase flow instability, because it will decrease the gas flow rate and pressure passage upstream to downstream (tubing), which will thus reduce total oil production from this method, regardless of the simulator predictions of improved gas lift performance. However, a technique should be developed to optimise two-phase flow unstable behaviours at the same time as not increasing the backpressure to the casing annulus or to the tubing from the wellhead at the surface.

Another approach by Bordalo and Gaspari (1997) improved an extensive analysis to determine the most suitable operating conditions to stabilise upward two-phase flow in a vertical pipe. The authors analysed the flow instability, especially for annular flow regime as shown in Figure 2-17. The authors used two approaches in their investigations: a transient flow model, which treats phases individually, and a linear analysis called Akin, which was developed by Kelvin-Helmholtz and is one-dimensional. These two methods considered the effect of gas compressibility in the calculations and predictions within interphase. The authors stated that gas compressibility has a considerable effect on the stability of two-phase flow, and is the main governing parameter.
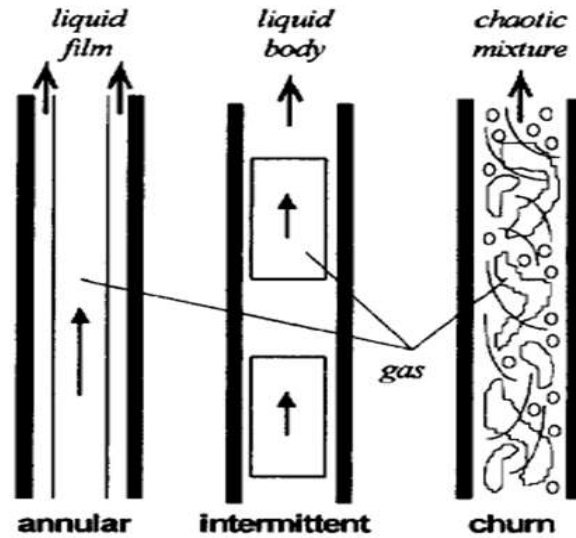
Figure 2-17: Pictorial presentation of vertical annular, intermittent and churn flow (Bordalo and Gaspari, 1997).

The unloading process and type of gas lift valve have a major impact on fluid behaviours. Another practical attempt by Faustinelli *et al.* (1999) investigated the performance of the Nova gas lift valve and conventional (square edge) orifice gas lift valve to eliminate two-phase flow instability and minimise fluctuations of tubing pressures in continuous gas-lift wells. The authors indicated that the casing heading and the flow fluctuations within gas lift systems occur due to subcritical flow conditions at the injection point. This process occurs when there is low differential pressure between the casing pressure and tubing pressure. As a result of this, there is insufficient pressure differential to maintain critical flow conditions. These fluctuations can be monitored from a pressure and differential pressure recorder in the wellhead. Figure 2-18 shows pressure and differential pressure recorder charts. The red circular outer line is the tubing pressure when there is no gas injection to tubing (static pressure) and the blue fluctuating line is the differential pressure during gas injection to tubing (flowing injection pressure). This creates a critical flow conditions such as sonic velocity, critical pressure and critical temperature due to interaction between injected gas and reservoir fluids and development of two-phase flow when large gas bubbles collapse. This causes a huge pressure drop within two-phase flow. The authors stated that the Nova valve and square edge orifice valve have limitations under operating conditions. The authors mentioned that if the ratio obtained from dividing the tubing pressure (Pt) and casing pressure (Pc) is more than 0.9, then the Nova valve cannot handle and perform these critical conditions. However, it may be used if the ratio is between 0.6 and 0.9.
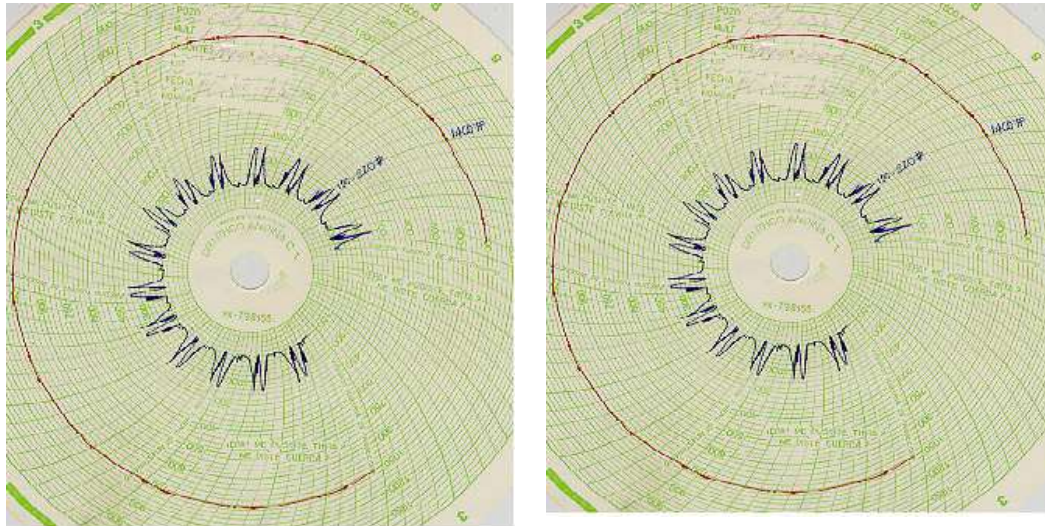
Figure 2-18: Tubing pressure fluctuations at wellhead pressure recorder (Faustinelli *et al.*, 1999).

Furthermore, if the ratio is less than 0.6 then conventional (square edge) orifice valves can be used. However, these valves still require optimisation for every particular well and also have limitations, especially when the ratio is more than 0.9, when very severe fluid behaviours will occur as well as flow instability phenomena. Therefore, there must be another technique to reduce these fluctuations within fluid flow and increase oil production.

Furthermore, Posenato and Rosa (2012) have proposed a procedure for the well unloading process through gas lift valves to eliminate erosion at the gas injection point due to liquid flow rate and pressure drop variations. This erosion causes an increase in port size diameter and gas injection rate to the tubing. Therefore, this leads to an undesired situation and vibrations due to cavitation, which happens after the valve throat due to pressure recovery and a huge pressure drop between upstream and downstream. These initial fluid behaviours are crucial in causing the severe oscillations and the flow instability in the entire gas lift system, even though the unloading process is important in the gas lift process. This protocol has worked with wells equipped with single gas lift valves. However, this procedure is not applicable for wells equipped with more than one gas lift valve due to the complexity of dynamic fluid behaviours that occurs in front of the injection point. Another similar study by Guerrero-Sarabia and Fairuzov (2013) considered the gas lift instability by using linear and nonlinear methods. The authors investigated the effect of the heading severity on the amount of production loss in gas lift systems. The results showed that as flow fluctuations due to heading severity increased, the production rate decreased. Thus, a new technique should be developed to solve this problem in gas lifted wells.

2.7 Gas Lift Optimisation

The improvement in design of gas lift valves to achieve the optimum total oil production rate from an existing gas lift system is the main concern of many oil companies with low investment costs to increase oil recovery and maximise profit. The optimisation can be obtained from collecting data from gas lifted wells, including the design, well test data, well schematics and pressure surveys. There is very important well data that reflects the efficiency and optimisation of gas lifed wells, such as gas injection rate, formation GLR, total production, water cut, tubing pressure and casing pressure (Mantecon, 1993).

The optimisation of a gas lift system aims to achieve the maximum oil production rate, profit and output under specified operating conditions. For example, the gas lift performance curve (LPR) of a gas lift well, as shown in Figure 2.19, indicates that the production rate increases considerably and reaches a peak at the beginning. Thereafter, it starts to decrease gradually at the same gas injection rate. This is because of the pressure drop increasing due to friction losses within the flow phases and pipe wall. This leads to the development of two- phase and turbulent gas slugs along the pipe, thus creating unstable operating conditions (Hu, 2005).
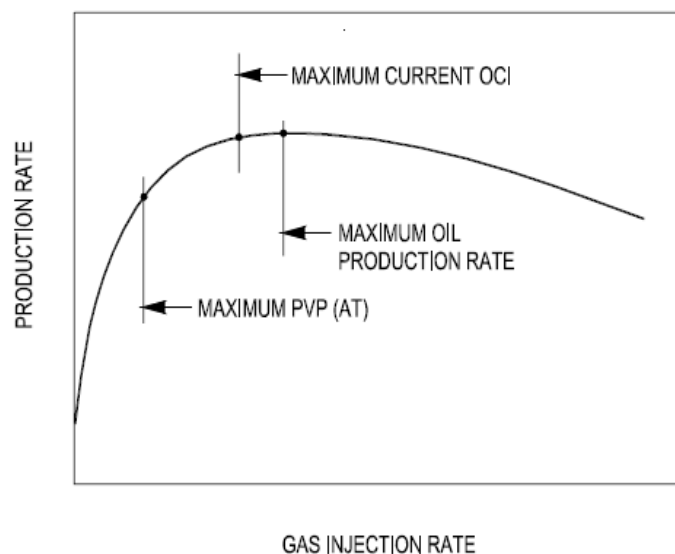
Figure 2-19: Gas lift performance curve (Hu, 2005).

Gas-lift optimisation principles were developed in the oil industry during the early 1950s by establishing the relationships between gas injection rate, gas injection pressure, the most efficient injection point, and the production rate from a particular well. These relationships enabled the creation of technical procedures, applications and standards for gas-lift design

methods. However these design methods need to be optimised and developed for further studies, especially in gas-lift design performance, to maximise oil production and to solve undesired flow instability problems that still occur in gas lift systems (Asheim, 1988).

Optimising gas-lift systems is crucial in order to obtain the optimum production rate that can be achieved by a certain amount of gas injected into the system. This requires a better understanding of two-phase flow behaviours in production tubing (Yasin *et al.*, 2014). The gas lift system operation conditions should be taken into account in any optimisation process. Figure 2.18 illustrates the bottom-hole pressure against the production rate of a typical gas lift in which the production rate increases greatly as the gas injection rate increases, then tends to stabilise before reaching a peak. The operating conditions can be classified into three ranges, when gas is injected into the well: an unstable, optimum (stable) and normal gas lift operation according to gas injection pressure as shown in Figure 2.20. The unstable region is where there are wide variations in injection pressure due to two mix phases of gas and liquid mixing with each other, and normally the stable region is subject to higher injection rates. The optimum gas lift region is when there is minimum a slippage of the gas phase. If there is an increase in injected gas, the production rate steadily decreases because the reduced hydrostatic pressure drop cannot compensate for the increased friction loss induced by the gas flow rate (Hatton and Potter, 2011).
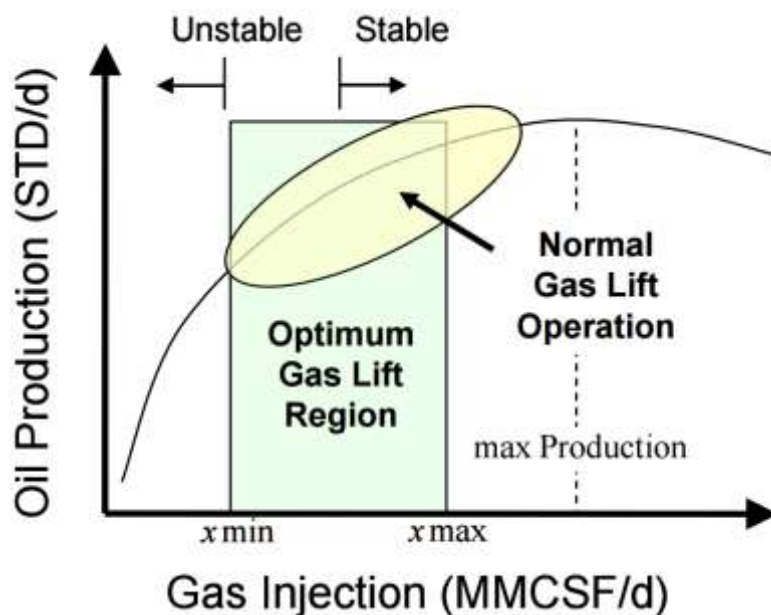
Figure 2-20: The effect of injection pressure on production rate using optimisation curve (Hatton and Potter, 2011)

40

Furthermore, the gas lift valve performance is crucial in any optimisation protocol. Elldakli *et al*. (2014) and Decker (1993) investigated gas lift valve performance under different operating conditions and how this affected the overall unloading gas lift performance. The authors' results indicated that the gas lift valves do not open fully during the lifting process and have certain restrictions in flow path due to the valve stem. This is because of lack of valve performance data and understanding the reaction of the valve with operating pressures considering load rate, stem travel, flow coefficient (Cv) and differential pressure ratio (xt) across the orifice inside the valve as shown in Figure 2.21. Therefore, the design and calculations of available gas lift valves must be developed in such a way that any restrictions that may affect the flow rate through the valve are avoided, and also static force balance equations are not applicable for this case. In addition to that, the stability of set pressure, vibration suppression and the overall stability that reduces total production from gas lifted wells must be considered.
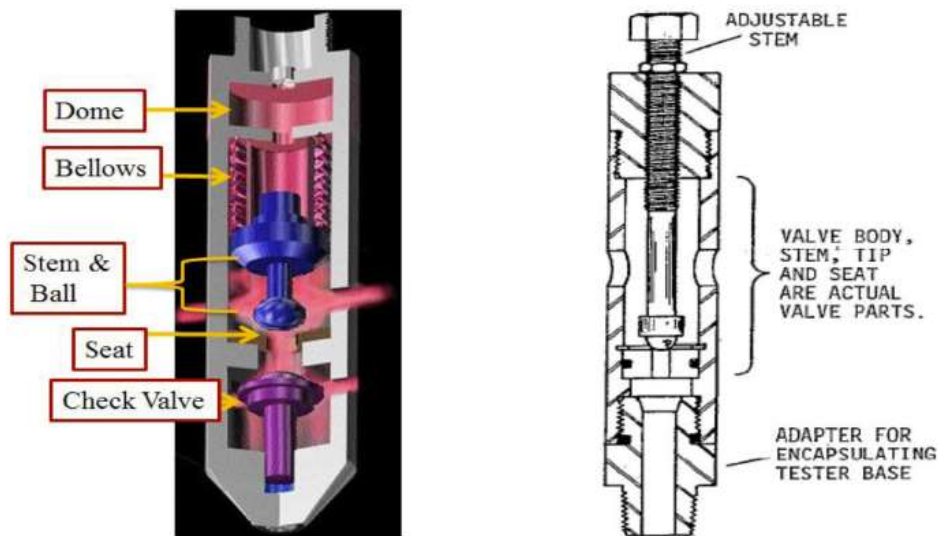
Figure 2-21: Components of gas lift valve (Elldakli *et al.*, 2014)

Fairuzov and Guerrero-Sarabia (2005) studied the effect of operating valve characteristics on the stability of gas lift systems for four different injection valve designs with fixed port sizes. The injection valves that were investigated were a square-edged orifice valve, a nozzle venturi valve, a fully open conventional gas lift valve and a gas lift valve operated in throttling range. The results showed that the first three mentioned valves had almost the same stability map regions and performance. In addition, the casing heading reduced partially at

any gas rate when the gas lift valves were operated in the throttling range. However, this required high casing pressure. In addition, it was difficult to achieve stability at low injection rates when the venturi valve was used. This was good evidence that the existing gas lift valves have limitations and should be developed.

Furthermore, Rilian *et al.* (2012) investigated the performance of venturi and square edge orifice gas lift valves in two gas lifted wells. The aim of these investigations was to reduce the differential pressure between casing and tubing pressures to allow a greater amount of gas to flow from upstream to downstream as shown in Figure 2.22. As a result of this, the performances of both valves were different. In addition to that, the results showed that oil production increased partially. However, at the same time, gas injection rate rose considerably until it reached a point that affected the gas supply availability when the venturi valve was used. Therefore, the distribution of gas to other gas lift wells in the field must be taken into account when the venturi valve is used.
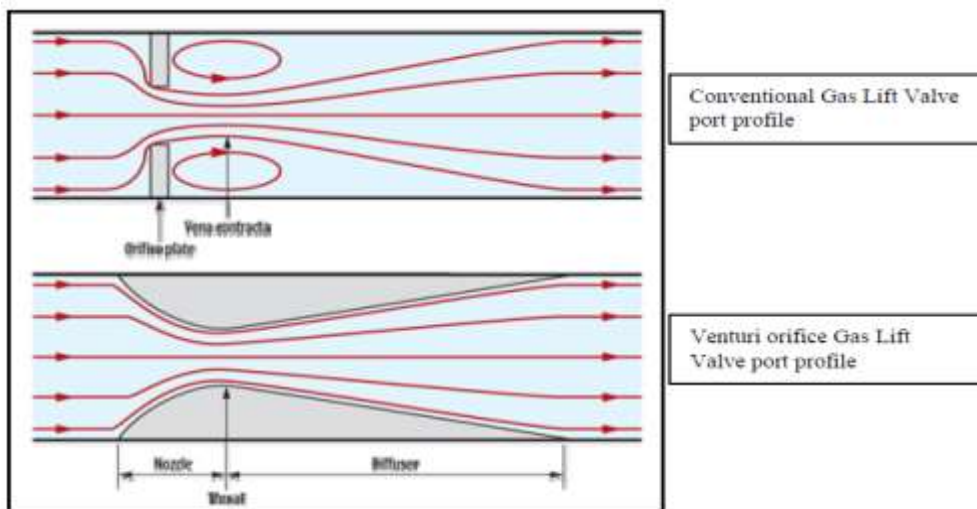
Figure 2-22: Port profile of an orifice and venturi gas lift valve (Rilian *et al.*, 2012)

Another previous attempt by Elldakli *et al.* (2014) developed the design of a conversational orifice gas lift valve (GLV) by modifying the (GLV) seat. This modification was achieved by changing the angle of the taper valve seat, as illustrated in Figure (2.23). Consequence, this seat modification reduced the required stem travel to allow a flow area equal to the port area. The results indicated that the modified design improved stem travel compared with

42

conversational gas lift valves and also increased the volumetric gas flow rate through the valve. However, the ability of the modified design to stabilise the gas lift system was not mentioned during this experimental study. The stem travel can be calculated from port bottom radius (r_p) and port top radius (r_T).
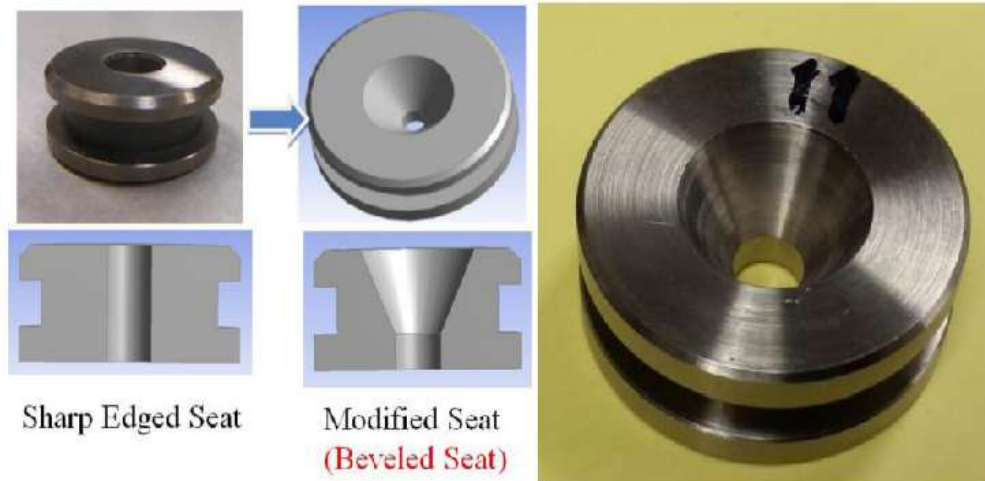
Figure 2-23: Comparison of sharp edged seat and modified (Elldakli *et al.*, 2014).

On the other hand, Chia and Hussain (1999) investigated gas lift systems with dual gas lift completion wells using the gas lift optimisation allocation model (GOAL), nodal analysis, gas lift databases and gas lift monitoring system (GLMS), also involving a modified wireline fishing technique for retrievable gas lift valves as shown in Figure 2.24 to maximise oil production from gas lifted wells. However, the authors' optimisation processes encountered a number of problems related to emulsion, sand and multi-phase flow fluid behaviours. The authors highlighted the flow stream countercurrent to the formation of liquid stream. This action can create significant turbulence, which reduces gas lift efficiency. Furthermore, Mahdiani and Khamehchi (2015) investigated gas lift flow instability in several gas lift wells in the early stage of gas allocation optimisation and put it as a constraint or limit in injecting gas, considering the amount of available gas and the oil production rate in the field. The authors indicated that it was not necessary to stabilise gas lift wells by increasing the gas injection rate or even doubling it, because there are still some wells that have flow instability phenomena, even when gas injection rates are doubled. Therefore, other techniques should be developed to minimise this problem and optimise the multiphase flow behaviours.
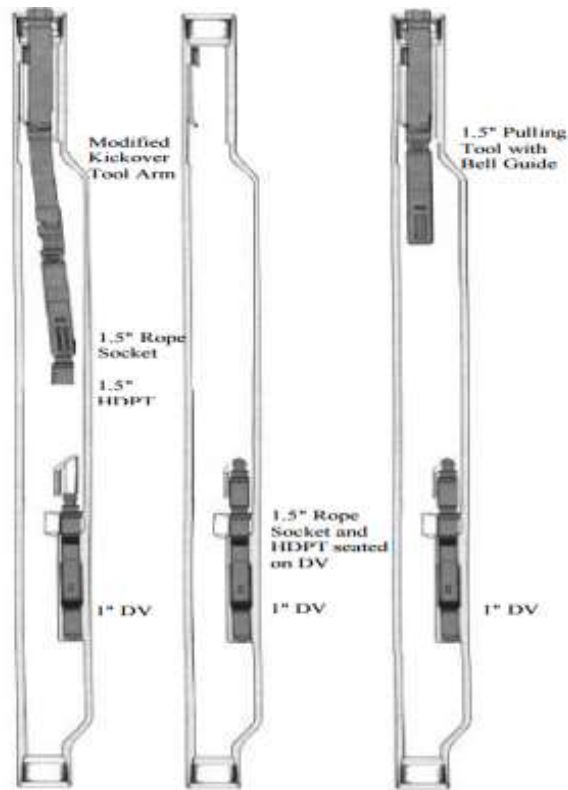
Figure 2-24: The modified fishing technique was designed to tackle the tight dummy valve problem(Chia and Hussain, 1999)

In addition, Mahmudi and Sadeghi (2013) developed a mathematical model to track the variation of several parameters during gas lift operations in different vessels. These stages began from the oil reservoir, gas lift valve, surface choke valve at the wellhead, and production separators and ended in the crude oil store tanks as shown in Figure 2.25. This model is connected with the Marquardt optimisation method and genetic algorithm to optimise the long-term economic return of the oil field. The results showed that when production lifetime is divided into consecutive intervals with gas injection rate, tubing diameter and separator pressures, the maximum net present volume increased.
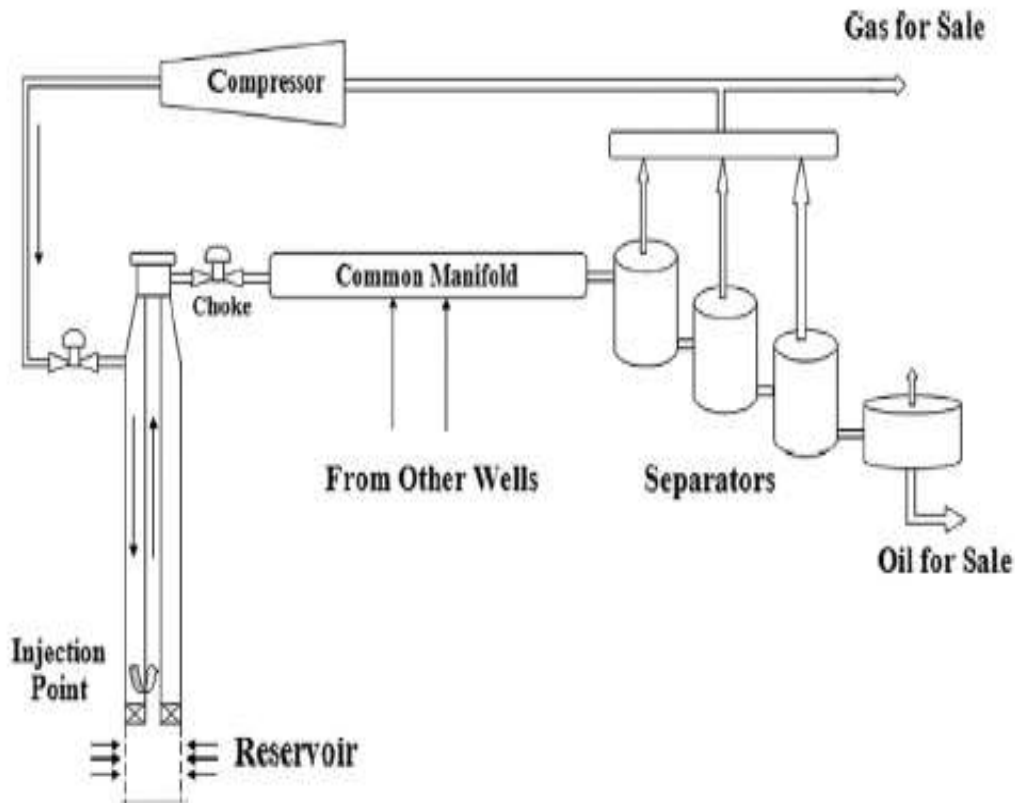
Figure 2-25: The differential liberation continuous gases lift process (Mahmudi and Sadeghi, 2013).

2.8 Gas Lift Feedback Control Systems

The multi-phase flow behaviours (oil, water and gas) can be changed when transported upward in a vertical pipe, especially gas lift methods in the oil industry where this type of flow causes a reduction in the total oil production rate and serious operational problems in surface production facilities due to its flow instability. Therefore, there are several conventional approaches to manage these flow instabilities in oil wells, such as choking the flow in the wellhead, increasing the gas lift injection rate or changing the surface production facilities capacity to accommodate gas and liquid slugs that are produced from gas lifted wells. However, all these practical attempts are inefficient or expensive in over-design. In most cases, increasing the backpressure to the system from the surface is partially effective in minimising flow oscillations and reduces the oil production rate from the gas lift method (Forero *et al.,* 1993).

In recent years, active feedback control systems have been introduced in the oil industry. A feedback control system is defined as a special control system for the inlet and outlet of the system. This can be achieved by either opening or closing surface valves, for example, inlet and outlet choke valves in the wellhead. The feedback control systems are based on certain settings and measurements of pressure, temperature, level or flow. Furthermore, these feedback control systems can be operated manually by setting certain points, or automatically. In addition, the automatic feedback can be controlled mechanically, electrically, hydraulically and electronically (Dalsmo *et al.,* 2002).

In addition, (Eikrem *et al.,* 2002) developed two realistic gas lift systems models using the multi-phase flow simulator OLGA 2000. These control structure models were based on controlling input and output pressures on the gas lift systems. The first control structure model relied on measurements of the down-hole pressure and the second used the measurements of pressure at the top of the annulus. Despite both control structures being able to slightly increase oil production, these control structures increase the backpressure to the system, which consequently necessitates more horsepower compressors and down-hole pressure measurements, and is not reliable because of harsh operating conditions in the well bore. Furthermore, these structures do not consider fluid behaviours in production tubing due to flowing of fluid with different densities upward of the vertical column.

Furthermore, Eikrem (2006a) investigated different types of control structures for single gas-lift wells. The author stated that all these control structures were examined by using simulation studies and verified by laboratory experiments; moreover, the author developed two control structure models for open-loop and closed-loop. The open-loop control structure controls the pressure drop across the upstream of the production choke by adjusting the opening of the well head production choke; and the closed-loop control structure controls an estimate of down-hole pressure of the well by adjusting the opening of the production choke by using an extended Kalman filter. In addition, the author presented another control structure for different gas lift completion, which is a dual gas lift to distribute gas between two tubing strings in the same well. Although these control structures can maintain the cyclic heading pressure in a gas lift well automatically. However, these feedback control systems increase the backpressure to the well. This leads to decreased oil production from gas lifted wells, as there are several parameters that affect flow instability, such as the development of two-phase flow and its density-wave along the vertical column.

Evers *et al*. (2009) constructed a laboratory experiment and used the OLGA simulator to investigate the effect of density wave instability in a continuous gas lift. The authors used a Smart choke algorithm in their experiment, which was developed by the Shell Oil Company to control the volumetric flow rate to reduce the density wave instability that occurs in the tubing column during the lifting process, thereby optimising oil production from the well. The Smart choke algorithm is an active control technique used to maintain a fixed total volumetric flow rate to a certain set point.

The authors mentioned that the performance curves are used only for steady state conditions. Therefore, initial indications of oscillations and perturbation can be obtained from the curves, but not for fully developed flow behaviours. The authors reported that the density wave is distinguished clearly at low gas injection rates. OLGA simulation results showed that the small scale of frequency and cyclic flow behaviour caused density wave instability. As the flow rate increased, the fluctuations disappeared and the system stabilised slightly. The authors concluded that low bottom-hole pressure is recommended to prevent any possible damage to reservoir formation and to increase the ultimate recovery of the reservoir. Although the Smart choke algorithm increased the volumetric flow, this happens only when the pressure drop is measurable and the Smart choke algorithm could not be tested in their gas lift experiment because the downstream of the valve was opened to atmospheric pressure.

In addition, Plucenio *et al.* (2012) have proposed a feedback control technique to suppress the oscillations during gas lift operations due to the casing heading and density wave phenomena. Even though the technique optimises the opening of the choke valve and gas injection rate to the casing annulus space by using a control algorithm, this technique increases the backpressure to the well bore, which restrict the reservoir's natural flow. This restriction reduces total oil production from the well and there is a limitation in this technique's reaction with downhole pressure during operation. This present study will develop new technique stabilize fluid behaviours by reducing bubble sizes .This leads to increase oil production from gas lifted wells without increasing backpressure or changing the gas compressors in the oil fields.

2.9 Summary

This chapter provides a detailed description of the concept of the gas lift method for both continuous and intermittent methods. In addition, literature reviews of two-phase and multi-phase flow in a vertical pipe show the development of the research over the years. This includes types of flow regime that may occur due to the development of this type of flow, and other attempts for modelling the flow patterns. This chapter also presents a clear explanation of the flow instability and its types within two-phase flow in the gas lift method and what has been done in the gas lift industry to optimise or improve gas lift valve performance. Finally, chapter two describes previous attempts and techniques that have been used to overcome the research problem. The present study aims to critically investigate the cause of the flow instability within two-phase flow in gas lifted wells. In addition, developing new technique to stabilise flow behaviours thus increase total oil production without increasing backpressure to the system or change the surface production facilities.

CHAPTER 3

EXPERIMENTAL APPARATUS, SET-UP AND METHOD OF DATA PROCESSING

3.1 Introduction

This Chapter presents consequent of the designs, apparatus and set-up of the two-phase flow experiment. In addition, measurement techniques, procedure of rig operation and the experimental data processing have been descried. Furthermore, the upward two-phase flow behaviours, such as measuring the sizes of air bubbles and their velocities have been explained. These aimed at understanding the physics behind the fluid behaviours and to unravel the main cause of the flow instability occurrence.

3.2 Experimental Apparatus Designs

The real design of the gas lift method depends on several factors such as productivity index of the oil reservoir, depth of the well, the design settings and the accumulation of crude oil in the production tubing. The gas injection point (gas lift valve) can be located at the bottom of the production tubing up to 1000 m or more in some designs. This is based on the level of crude oil in the vertical production tubing and productivity index of the reservoir as shown in Figure 3.1. The vertical production tubing was simulated in 2 m long with a 66 mm ID to understand the fluid behaviours and the main cause of the flow instability within two-phase flow as these fluid behaviours repetitively occur along the vertical column.
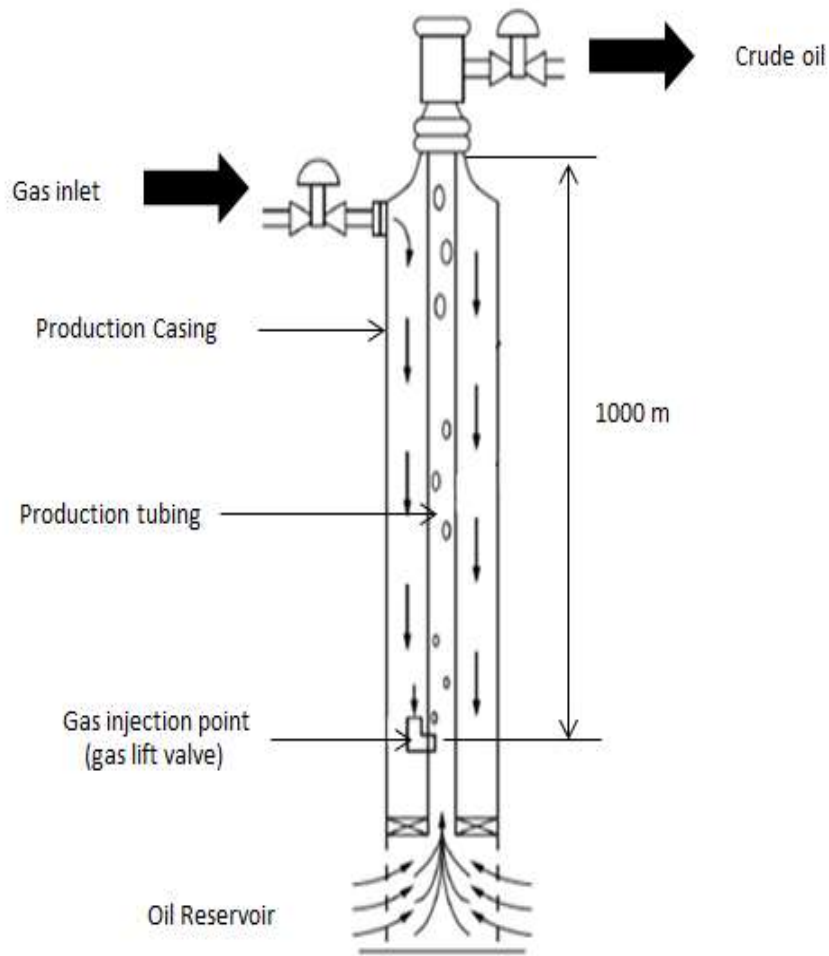
Figure 3-1: the real design of gas lift method

Under laboratory conditions this system was simulated by scaled down to 2 m and operated at different operating conditions to allowed the two-phase flow to develop and obtained the main fluid behaviours which causing the flow instability within the gas lift column. The following provides the apparatus that used during this investigation. Two experiments were therefore designed in this research investigation ; the first design was a small-scale experiment for visualization of fluid flow, as shown in Figure 3.2 and the second design presented in Section 3.3.2 was used for the main two-phase flow experiment, as shown Figure 3.3.
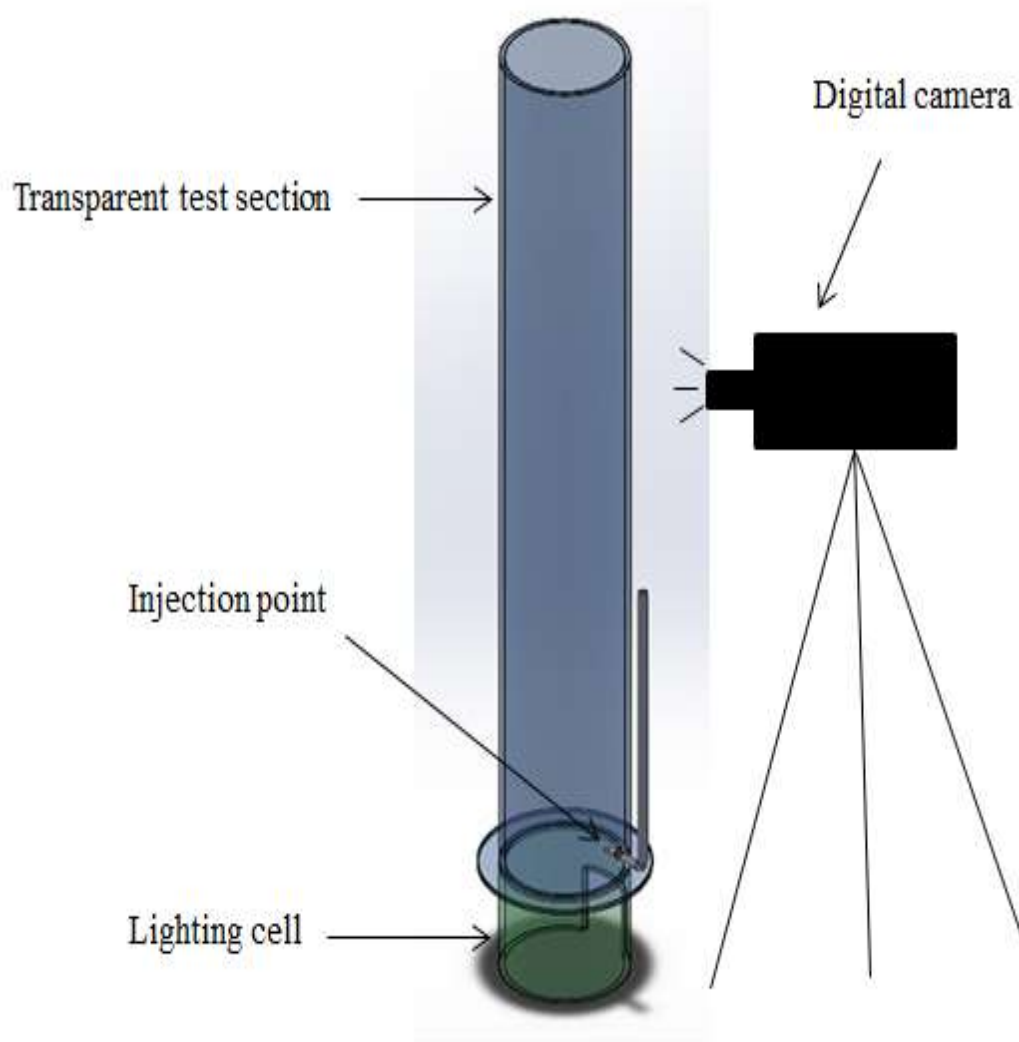
Figure 3-2: Small-scale fluid visualization design
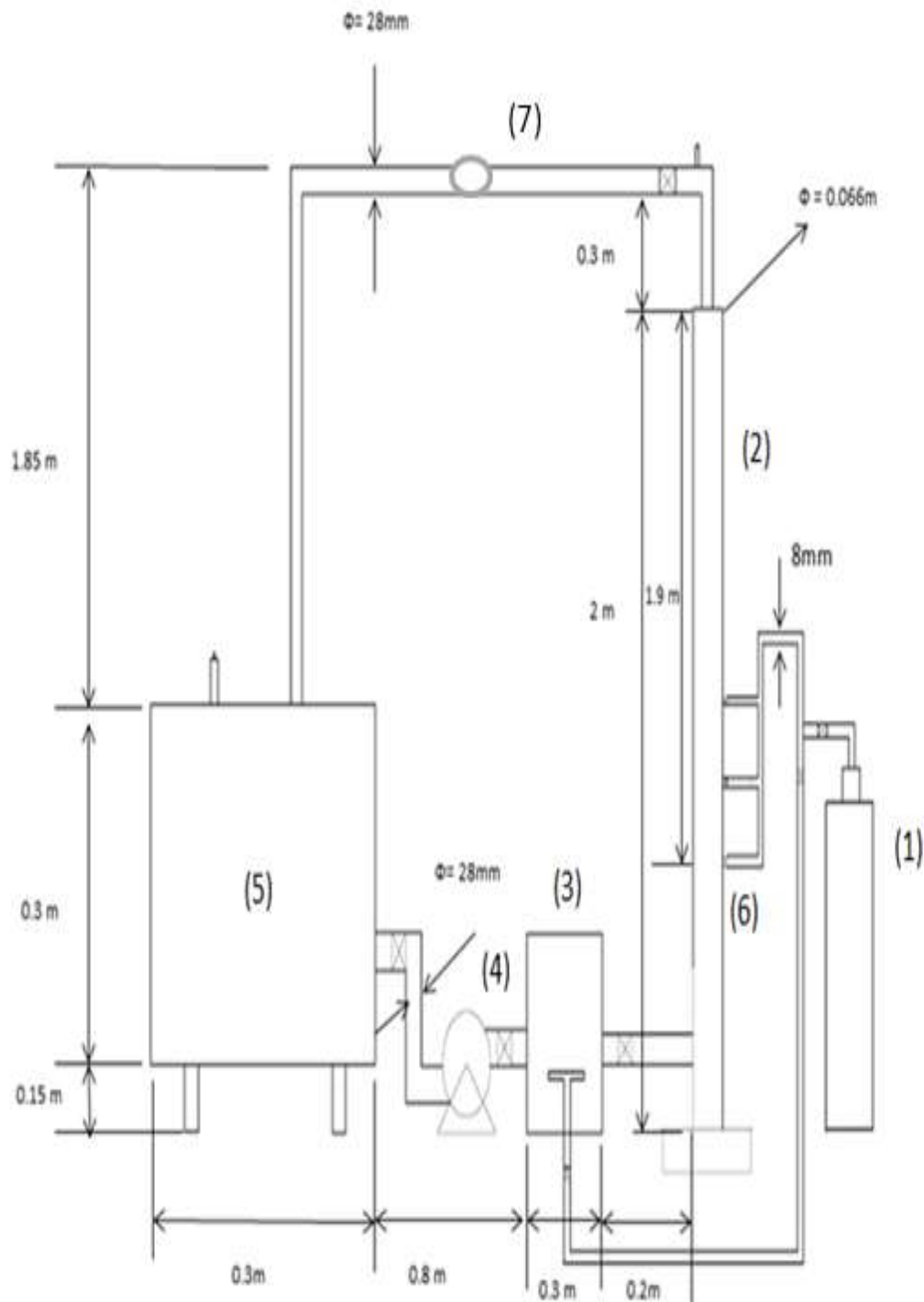
(1) Gas cylinder (gas source), (2) transparent test section, (3) fluid mixer, (4) centrifugal pump, (5) liquid tank (6) Injection point, (7) Turbine meter

Figure 3-3: Schematic design of two-phase flow apparatus

3.3   Experimental Apparatus and Set up

3.3.1   Small Scale Visualisation Experiment: Design-1

The purpose of the small-scale visualisation experiment was to determine the best visualise way to the fluid behaviour inside a PVC transparent pipe. This involved using different coloured lighting techniques to visualise the air bubbles in stagnant water by applying different lights colours (blue, green and white) under the test section before designing the large-scale two-phase flow experiment. This test was conducted to achieve the best and clearest view of air bubbles shapes and edges within the two-phase flow in the transparent PVC pipe and to avoid any light reflections from the surroundings. The small-scale visualisation experiment as shown Figure 3.4 consisted of a transparent PVC pipe (1) with an injection point (2), a small lighting cell (3) which was powered by batteries (4) and changeable small lamp (5) which was protected by a lighting cell housing (6) and a digital camera. The transparent pipe was 0.9 m long with a 66 mm ID and had an injection point of 0.11m from the base of the pipe with a port size of 4 mm. The injection point was attached with a needle valve to enable the manual adjustment of the air flow rate to the transparent test section.
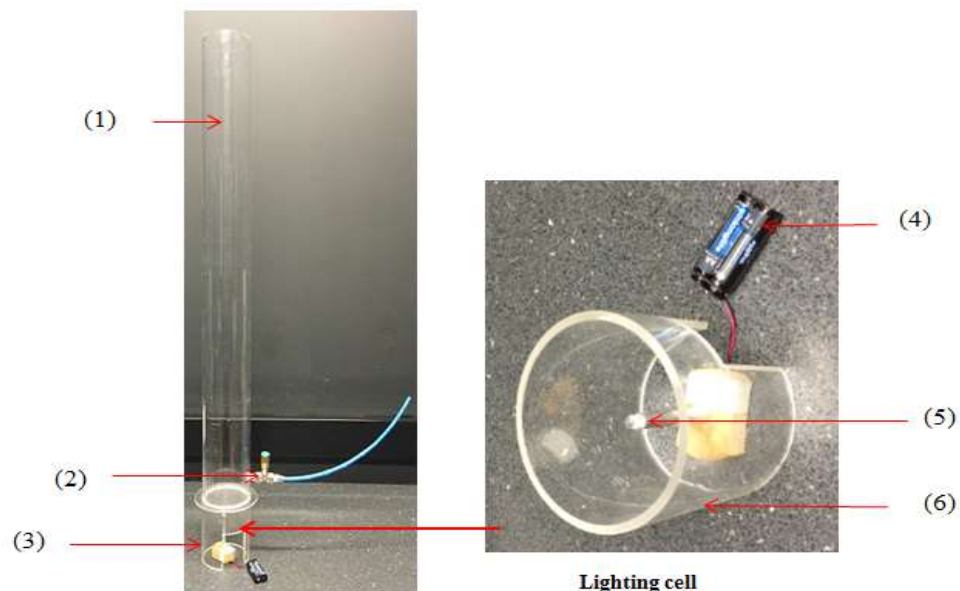
(1) Transparent pipe, (2) injection point, (3) Lighting cell, (4) battery, (5) lamp, (6) lighting cell housing

Figure 3-4: Small-scale visualisation experiment setup

53

3.3.2   Two-Phase Flow Apparatus: Design-2

The two-phase flow experiment rig as shown in Figure 3.5 consists of a 2 m long transparent PVC (Polyvinyl chloride) pipe (13) with an internal diameter of 66 mm and 76 mm external diameter. The transparent PVC pipe (13) also highlighted in Figure 3.6 was the test section for the two-phase flow investigation. As shown in Figure 3.5, the transparent PVC pipe was connected to the pipework in the loop by upper flange (12) with 120 mm OD and sealed with soft rubber. The air injection point (18) and its holder are designed to permit an easy change between the Multiple Nozzles Injection Technique (MNIT) and Single Nozzle Injection Technique (SNIT) as illustrated in Figure 3.7 by inserting them inside the injection point holder which is then closed by the other isolation valve. The liquid tank (1) was used to store water and as separator for separating air from water. Furthermore, the liquid phase (water) from the liquid tank (1) was circulated continuously and intermittently in this experiment loop by a 0.5 horse power (HP) centrifugal pump (17). It should be noted that throughout this investigation water was used as working fluid since the column of corresponding water in the petroleum production tubing has the highest hydrostatic pressure compared with crude oil. Therefore, lifting process of the crude oil column will be easier. As the density of crude oil is less than density of water. In addition, as the difference in density between the reservoir fluid and injected gas increases, the fluid behaviours become chaotic and unstable. This allows the researcher to investigate distinctly into this flow instability phenomenon. In comparison with using crude oil. Moreover, the health and safety issues in using flammable liquid are considered.

The liquid flow rate was measured using digital flow rate meters in the inlet (8) and outlet pipe section (5). The inlet digital flow meter (8) was installed at the outlet of the pump after the bypass line (2). The outlet digital flow meter (5) was installed at the outlet line of the transparent PVC pipe (13) after the choke valve (9) at the top of the rig. Each flow rate meter consists of two parts: the meter and mount device and both flow rate meters. The flow rate of the inlet digital flow meter (8) and outlet digital flow meters (5) are ranged from 3 l/min to 100 l/min and an accuracy of +/- 5%. The two pressure gauges used in the two-phase flow experiment ranged from 0 to 60 psi. The inlet pressure gauge (14) was connected to the inlet pressure sensor (19) while the outlet pressure gauge (6) was connected to the outlet pressure sensor (11). The inlet temperature sensor (20) measured the initial temperature of the two-phase flow before entering the transparent PVC pipe (13) while the outlet temperature sensor measured (10). The inlet and outlet temperature sensors were connected to a digital

thermometer (4), installed in the front panel of the two-phase flow rig. A Cannon Eon high-speed digital camera (16) with 18-551:3.5-5.6 IS zoom lens was used to capture the fluid behaviours in the transparent PVC pipe (13). The Cannon Eon high-speed digital camera (16) had a resolution of 3456 x 2304, and frame rate of 60 frames per second.
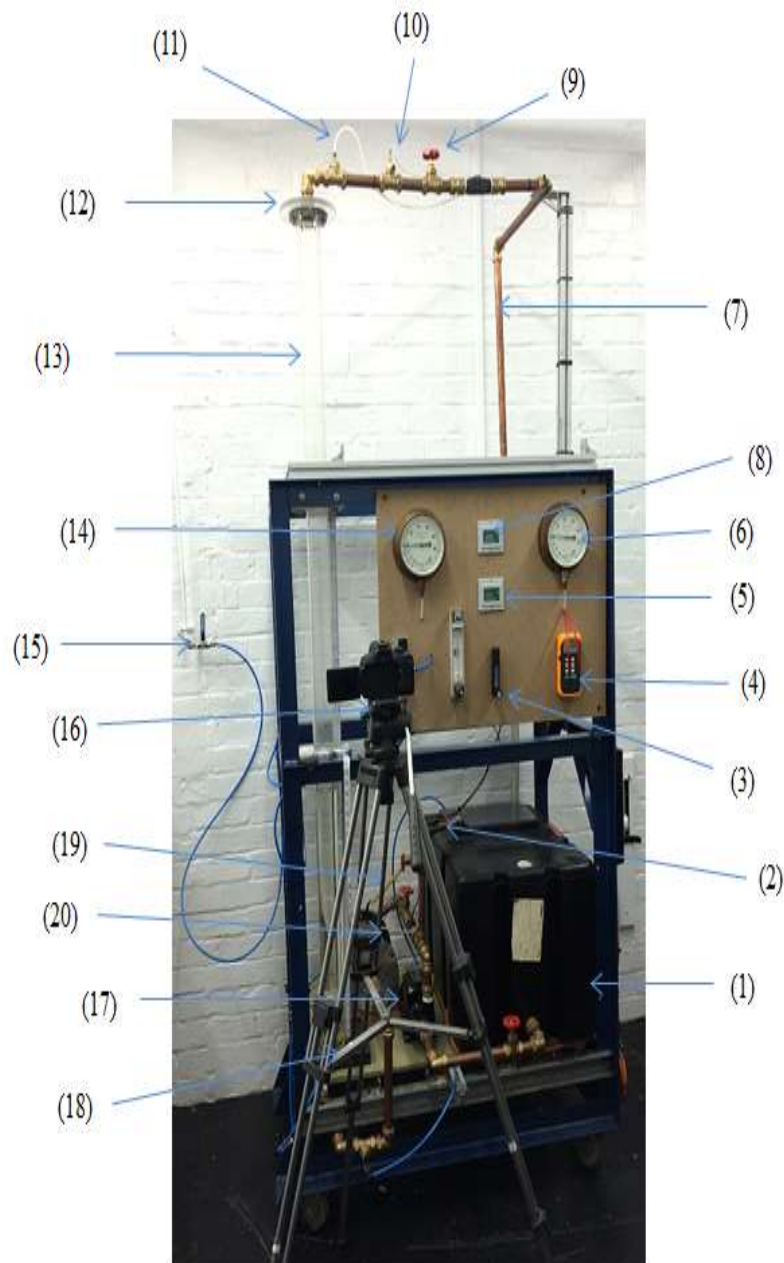
(1) Liquid tank, (2) bypass line, (3) air flow meter, (4) thermometer, (5) outlet digital flow rate meter, (6) outlet pressure gauge, (7) return line to tank, (8) inlet digital flow meter, (9) choke valve, (10) outlet temperature sensor, (11) outlet pressure sensor, (12) upper flange, (13) transparent PVC pipe, (14) inlet pressure gauge, (15) air supply, (16) digital camera, (17) centrifugal pump, (18) air injection point, (19) inlet pressure sensor, (20) inlet temperature sensor.

Figure 3-5: Two-phase flow apparatus simulating gas lift system
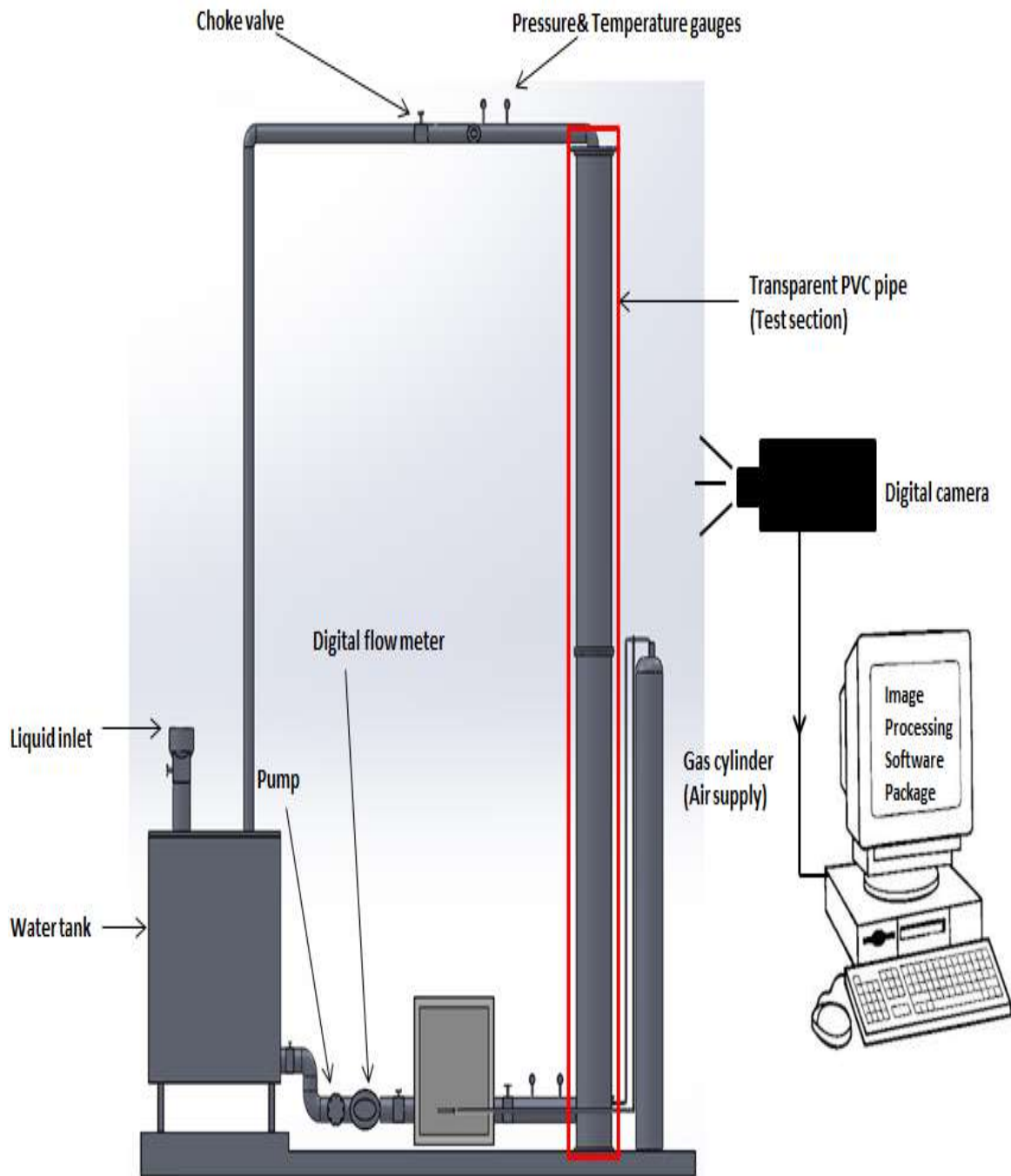
Figure 3-6: Schematic diagram of transparent PVC simulated the gas lift column
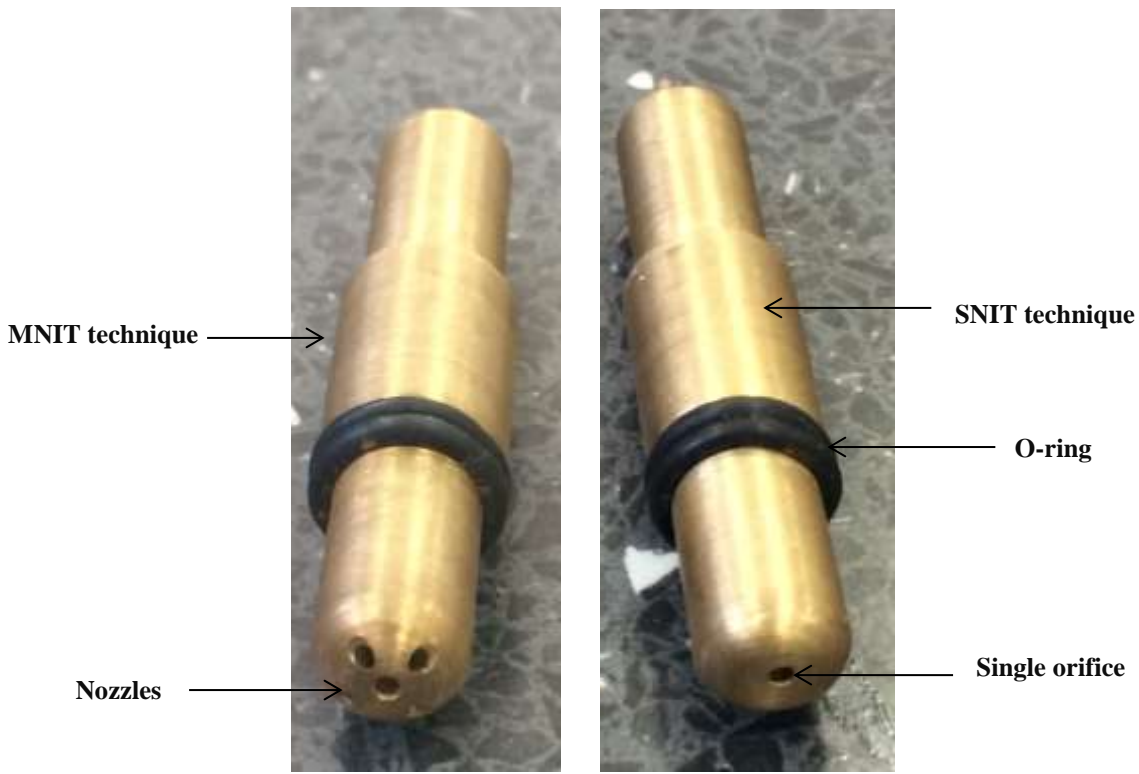
Figure 3-7: Multiple nozzles injection technique (MNIT) and single nozzle injection technique (SNIT)

3.4 Design of Multiple Nozzles Injection Technique (MNIT)

As shown previously in Figure 3.7, is essential part of this investigation since the determination of the diameter and distribution of orifices in the head of the gas lift valve is critical. This could affect the behaviours of the upward two-phase flow, gas injection rate and gas injection pressure considerably. It should be thus estimated as accurate as possible and compared with the design of previous investigators (Faustinelli *et al.*, 1999) that used they used the sharp edge orifice valve, which uses a Single Nozzle Injection Technique (SNIT). In addition, both these techniques must have the same geometrical dimensions in terms of diameter and total area to achieve a reduction of two-phase flow instability, which still occurs even when the orifice valve is used. The nozzle diameter used in the multiple nozzles injection technique in this work was 1 mm, giving a geometric area shown in Table 3.1:

Table 3-1: Geometrical dimensions of each orifice

Geometric parameter	Single orifice (SNIT)	Multiple nozzles (MNIT)
No. of orifice	1	5
Total Diameter (mm)	2.24	2.24
Total area (mm^2)	3.93	3.93

The following sections provide the procedures that were used in operating the two apparatus: Design-1 and design – 2.

3.5   Procedure of Rig Operation

3.5.1   Small-Scale Visualisation Rig: Design-1

The procedure was followed systemically utilising the set-up rig shown in Figure 3.4, in order to find the white lighting source was the best lighting colour in terms of enabling a clear view of the bubble shapes and their edges when recorded with a digital camera. Additionally, light reflection was avoided when recording videos in a dark room in the university laboratory by the use of a black background. Light reflection is one of most common problems in achieving good image quality, because it may hide very important characteristics of the flow in the test section. The light reflection can also cause errors in the image processing measurements, because the bright reflection can be wrongly identified as bubbles, which can negatively affect the accuracy of readings. Therefore, all these troubleshooting problems were avoided and considered in the large-scale experiment. Finally, the decision was made to construct a large-scale two-phase flow experiment and avoid anything that affected the accuracy of the measurement of the fluid behaviours.

3.5.2 Two-Phase Flow Apparatus: Design-2

The experimental procedure of the two-phase flow apparatus are summarised in the following:

1. Fill up the rig tank with approximately 50 litres of tap water. This gives approximately 45% of the tank level and the remaining space is for the separation of air from water, when the fluid mixture is returned from the test section.

2. Ensure that the water level is higher than the heater inside the water tank, if the heater is used.

3. Make sure that the valves are fully open, except the air valves to the injection point, which are set to closed.

4. Start the centrifugal pump and adjust the water flow rate to a minimum to check there is no leakage in the experiment loop.

5. Adjust the choke valve at 20%. This gives the lowest backpressure to the system and permits the flow to develop in the test section.

6. Place the black background behind and around the transparent test section in order to avoid any light reflections.

7. Attach the measuring tape along the pipe vertically to measure the length of each segment and is also used for calculating the velocity of the bubbles with the image processing software.

8. Place the portable white lamps at the bottom of the vertical column to obtain the best visualisation of the fluid.

9. Set up the digital camera in front of the test section at the required height depending on the segment level (starting from the injection point to the top of the test column) being observed.

10. Open the air supply valve to the air regulator and adjust the air pressure to the required pressure, which must not exceed the maximum pressure (5 bar) when the choke valve is opened at 20%.

11. Adjust the water flow rate by using the bypass line and inlet flow rate digital meter.

12. Switch on the thermometers to measure temperature for both the inlet and outlet.

13. Switch on the digital camera and then start recording videos of fluid behaviours at different operating conditions for single orifice technique and multiple nozzles injection techniques.

3.6 Method of Processing and Acquisition

3.6.1 Method of Data Processing

This Chapter provide the details of data processing and acquisition using simulated two-phase flow gas lift rig design that previously shown in Figure 3.5. These include:

a) Two-phase flow gas lift rig (§ 3.6.1.1)
b) Practical sizing and bubble velocity (§ 3.6.2)

3.6.1.1 Two-phase flow gas lift rig

The flow structure and fluid behaviours of two-phase flow have been investigated experimentally in a vertical transparent pipe (ID: 66 mm, Length: 2 m) using an image processing package called DynamicStudio 2015a. The test column is divided into five segments, starting from the injection point from the bottom to the top of the column. The first segment was 0.38 m in length and was 0.1 m upward from the injection point and then the remaining segments have the same lengths up to the end of the column, at two metres length as shown in Figure 3.8. The test section is attached with a measuring tape to provide a length scale so that the velocity of the bubbles can be calculated. Each segment was operated under different operating conditions and the flow recorded by the digital camera in front of the column and at different levels, with each recording being for 30 seconds for each operating scenario. Data was recorded for different variables such as sizes, velocities and shapes of bubbles.
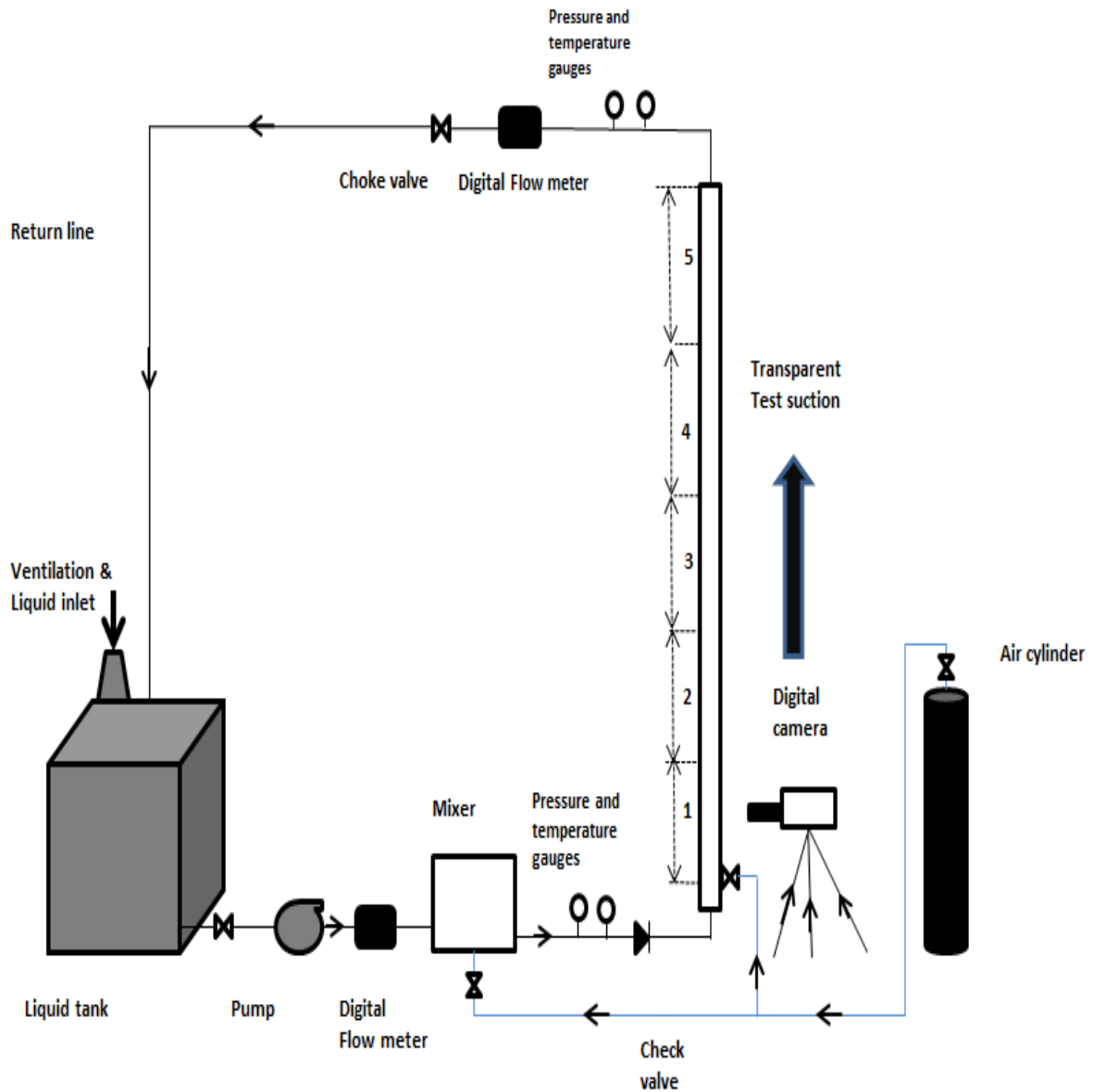
Figure 3-8: The flow diagram of simulated vertical column apparatus for the gas lift optimisation

The videos were recorded by using a digital camera respectively from segment 1 to segment 5, and were converted to single frames by using the Free Video to JPG converter software, V.5.0.61 build 805. The frame rate was 0.016 ms. These frames were checked to make sure they were all clear, after which, these frames were imported to the image processing package DynamicStudio 2015a.

3.6.1.2 Data Acquisition of Bubble Velocity and Bubble Sizing

The bubble sizes and velocity data obtained from segment 1 to segment 5 of the transparent PVC test pipe respectively as shown in Figure 3.8 are summarised in Tables in the appendix A for both techniques. For example, Table 3.4 represents experiment data sheet for measurement of bubble sizes and velocities for segment one when the single orifice technique while Table 3.5 represents experiment data sheet for measurement of bubbles sizes and velocities for (MNIT) technique. There are some definitions and measurement used in this experiment as the following:

The equivalent bubble diameter is an irregularly shaped air bubble is the diameter of a sphere of equivalent area.

The average bubble diameter is the average sizes of air bubbles including small and large bubbles in each frame.

The minimum bubble size is the size of the smallest air bubble in each frame.

The maximum bubble size is the size of the large bubble in each frame.

Bubble velocity is the velocity of the bubbles between two point located in each measured segment along the test section.

The bubble account is the number of air bubbles measured in each frame.

3.6.2   Practical sizing and bubble velocity processing

Commercial DynamicStudio software package was used for image acquisition and analysis for Particle Image Velocimetry (PIV) and particle sizing. The software also has tools for acquisition, configuration, analysis, and post processing of acquired data. This software has been used for detecting and measuring particle sizing but in this investigation, it was used to measure bubble sizes and velocities within two-phase flow in the simulated gas lift column.

The software can provide information about fluid behaviours, such as bubble sizes (average, maximum, minimum and equivalent bubble diameters), velocity of bubbles, bubble area and bubble count, which are important for the distribution of bubbles. In addition, this package has an interesting feature known as shadow processing. It is capable of detecting bubbles' shapes and edges and has an adaptive PIV function to show bubbles' velocity profiles. This

feature captured and showed details and observations about the interactions between bubbles, especially when bubbles were forming and collapsing. This fluid dynamic process was achieved statically and dynamically. This means, the software allows the user to capture bubble sizes and their velocities in one frame and double frames. This feature allow the user to connect all frames together to give continuous flow. Finally, there are several steps that must be followed to distinguish between gas phase (air bubbles) and liquid phase (water) and capture bubble sizes and their velocities in the simulated test section. These steps are summarised and shown in Figure 3.9.

(a) Model Calibration

 (b) Image min/max

 (c) Image arithmetic Image

(d) Image masking

(e) Image processing library & double frame

(F) Shadow processing & sizing
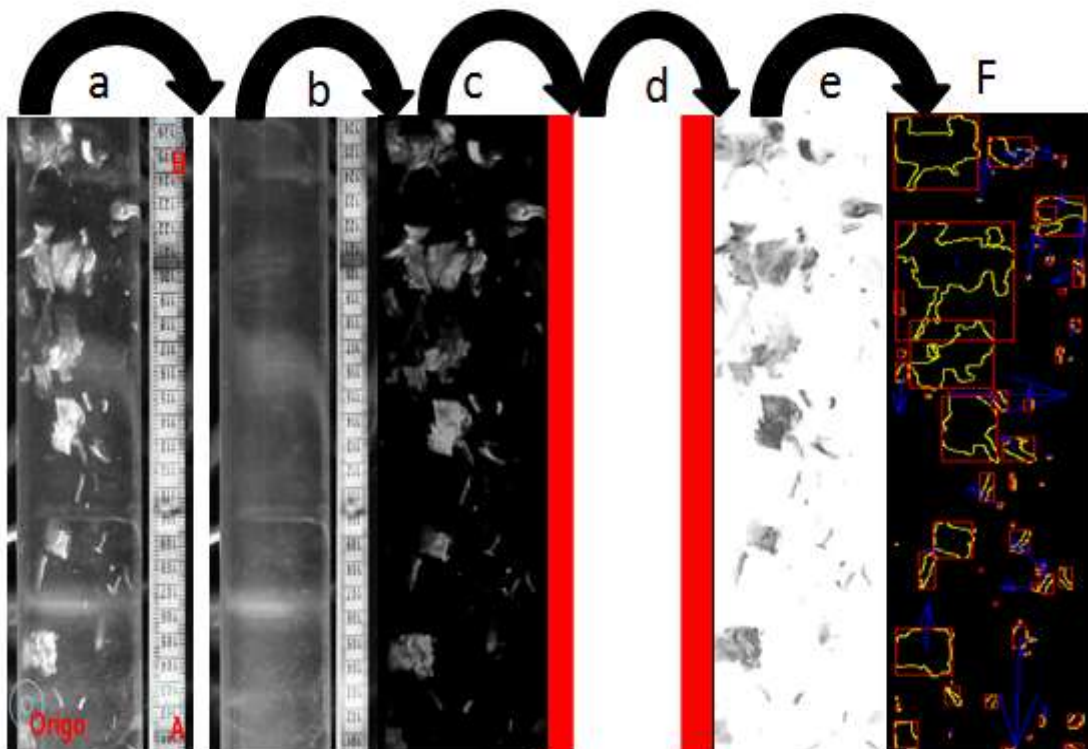
Figure 3-9: Advanced image-processing procedure of Dynamic studio2015a

The following briefly describes these steps:

a) Model calibration

The calibration of the model is an important step, because the conditions of recording videos and digital camera positions can be changed from time to time during the experiment. Therefore, when frames are imported to the model, the first frame can be used as a starting point for other remaining frames. Thus, the calibration of this frame and measuring its scale factor are essential, and subsequently these calibration settings can be applied for the remaining frames. For velocity measurements, the scale factor has to be determined. This can be achieved by using the calibrated first frame then duplicating to locate two points – A for the starting point and B for ending point – located at the measuring tape, and then the program will calibrate and calculate the measure scale factor for the remaining frames. Therefore, the velocity can be calculated for every bubble flowing from point A to point B. In addition, dewarping method is also useful to validate and/or verify the parameters, since dewarping one or more of the calibration images should produce a de-warped image where calibration markers are well aligned.

b) Image Min/ Mean/Max

This feature is useful to distinguish between phases (air and water). The 'Image Min/Mean/Max' method is located in the "Image Processing" category in the software settings. It is used to compute power mean greyscale values from a series of images. The Power Mean (or generalised mean) M_P with exponent 'p' of the positive real numbers $x_1, \ldots, x_n$ is defined as:

$$M_P = \left(x_{1,\ldots\ldots}x_n\right) = \left(\frac{1}{n}\sum_{i=1}^{n} x_i^p\right)^{\frac{1}{p}} \qquad (3.1)$$

Where

P = approaching minus infinity will return the minimum of all x-values and for p approaching plus infinity will return the maximum.

M1 (p=1) is the conventional (arithmetic) mean, and in the limit of p approaching 0 we get the geometric mean:

64

$$M_0\left(x_{1,\ldots\ldots,}x_n\right) = \sqrt[n]{\prod_{i=1}^{n} x_i} \hspace{3cm} (3.2)$$

The recipe supports already known p-values of:

$P = +\infty$ (Maximum) ,$P = 2$ (Quadratic Mean), $P = 1$ (Arithmetic Mean), $P = 0$ (Geometric Mean), $P = -1$ (Harmonic Mean), $P = -\infty$ (Minimum).

The Power means for a given series of values can be ordered as follows: Maximum $> =$ Quadratic $> =$ Arithmetic $> =$ Geometric $>=$ Harmonic $> =$ Minimum The formula for power mean is defined with positive x-values in mind, but Maximum, Quadratic, Arithmetic and Minimum can be computed for negative values as well. The Geometric and Harmonic mean has been designed to return zero if just a single non-positive grey value is found among the input grey values.

c) Image arithmetic

As the name implies, this method enables arithmetic on pixel values and it can be performed on any type of image (for example 8-, 10- or 12-bit images) as well as floating point images, and can be applied to both single- and double-frame images.

There are four types of operation that can be performed in this method:
  i.   Addition and subtraction
  ii.   Multiplication and division
        And the two operand types:
  iii. Image as operand
  iv.   Constant value as operand

It is possible to combine the two operands, so for example subtract another image and then add the constant value. Finally, there is an option to perform data clamping on the result. This is useful to limit the output to a certain range.

d) Define mask

Define mask enables the user to define a mask for regions or areas of specific interest on the frame and avoid any regions not required for these investigations, which may affect the analysis and results.

e) Image masking

This method is used to mask images by assigning specific grey-values in regions defined by the software user as being of no interest. In order to apply this function, a mask has to be defined using the analysis method "Define Mask". The mask ensemble must contain either one static mask or N dynamic masks, where N equals the number of images.

f) Image processing library (IPL)

The filters featured in the IPL module can be used to smooth images (Low-pass), detect the bubbles' edges (High-pass), and enhance image contrast (Low-pass & Morphology) as well as for non-linear calculations (Signal processing). It also includes various image-processing tools (Utility and Threshold). Finally, a Custom filter is available to allow filtering with user-defined filter kernels. The following are brief descriptions of some filters available in the image processing library:

i. Low pass filter

This filter is the simplest linear, local filter used to smooth images. This filter does not take spatial gradients inside the kernel into consideration, as shown in Figure 3.10. Thus, for applications related to fluid mechanics, kernel sizes of (3x3) or (5x5) are recommended. Larger kernel sizes may significantly increase numerical diffusion.
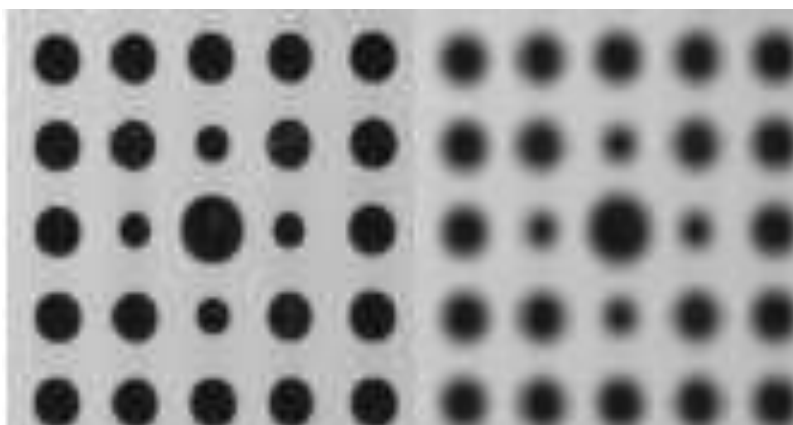
Figure 3-10: Low pass filter

The NxN mean filters use very simple convolution kernels:

3x3

1	1	1	
1	1	1	/9
1	1	1	

5x5

1	1	1	1	1	
1	1	1	1	1	
1	1	1	1	1	/25
1	1	1	1	1	
1	1	1	1	1	

ii. **Morphology filters**

Morphology filters are a class of nonlinear filters, which in their most basic form correspond to the minimum and maximum filters as shown in Figure 3.11. Combining these in different ways can however produce results that are more advanced.

- Dilation & erosion filters
- Opening & closing filters
- Tophat & blackhat filters
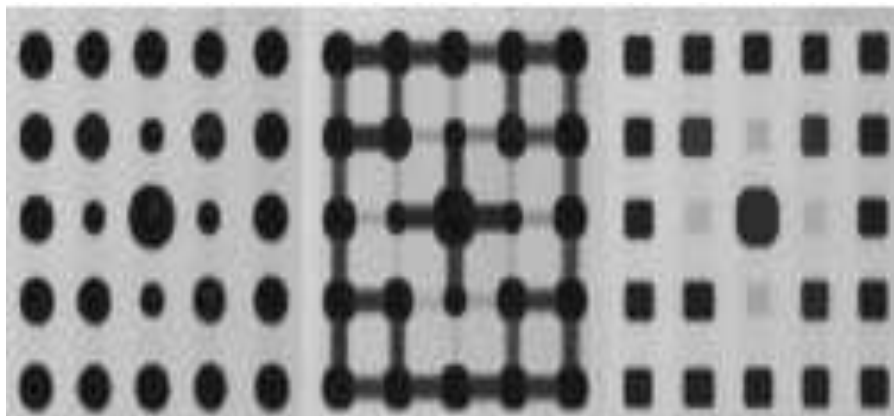
Figure 3-11: Opening & closing filters

g) Shadow size processing

The package also includes the Shadow Sizing Processing as well as various filtering procedure that described above. The shadow size processing is a method where bubbles' edges are detected and measured as shown in Figure 3.12. This feature provides detailed measurements, such as different bubble sizes, the bubbles' positions, the shape of bubbles and the velocity of bubbles. According to Dentec Company 2015, this technique has no limitations in measuring sizes and shapes of bubbles or droplets, and it can be used both with transparent and opaque bubbles, as well as droplets.
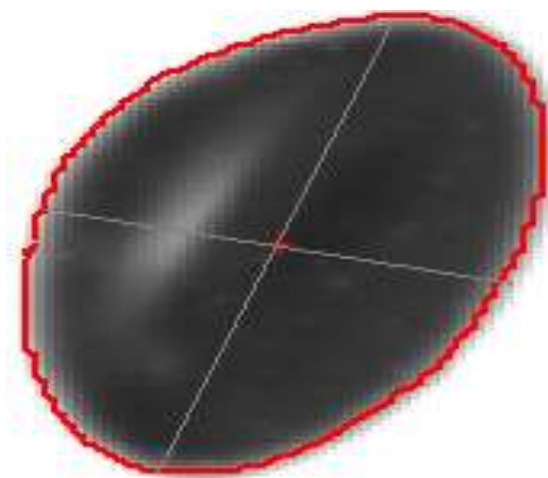
Figure 3-12: Shadow-sizing technique

3.7   Errors and Accuracy

The accuracy of devices and instruments used in this two-phase flow experiments could be affected by water and air flow rates, pressure and temperature measurements. The water digital flow meter had of accuracy of: +/- 5% and repeatability: +/- 1%.

The accuracy of pressure gauges was +/- 1.6 %.

The digital thermometer with 2 external K-type thermocouples was up to 0.1 C / 0.1 F in accuracy.

The temperature calibration can be achieved before every run of the experiment by using the self-calibration function and restoring factory settings on the device. The overall accuracy of

air bubble sizes measurements using the shadow processing technique (DynamicStudio2015a software) was ± 0.0006 pixels.

All tests were repeated at least 3 times ensuring the consistency and confidence in the acquire data

3.8   Summary

This Chapter presents the experimental apparatus, set up and method of data processing and acquisition for this investigation. The software used to investigate the two-phase flow in simulated gas lift rig using recorded videos commercial package, DynamicStudio 2015a. The software provides detail of fluid behaviours such as bubble sizes (average, maximum, minimum and equivalent bubble diameters), velocity of bubbles, bubble area and bubble count. In addition, this Chapter proposes new technique for gas lift methods called multiple nozzles injection technique (MNIT) to stabilise the system during operations without increasing the backpressure to the system. Instead of the existing gas lift valves, which have single (sharp edge) orifice technique (SNIT).

CHAPTER 4

RESULTS AND DISCUSSION

4.1 Introduction

This Chapter discuss the results of gas lift optimisation and flow instability utilising the apparatus and procedure that already described in Chapter-3. Especially the Chapter presents the results using:

- Single Nozzle Injection technique (SNIT) (§ 4.2)
- Multiple Nozzle Injection Technique (MNIT) (§ 4.3)

The SNIT results demonstrates the following prior to use of MNIT. The use of SNIT also provides the benchmark comparison on fluid behaviours, as currently used on gas lift operation, with MNIT proposed tested and presented in this investigation.

i. *Factors affecting the behaviours of bubbles using SNIT (§ 4.2)*
 a) Effect of injection pressure on bubble sizes (§ 4.2.1)
- Effect of injection pressure on average bubble sizes (§ 4.2.1.1)
- Effect of injection pressure on small bubble sizes (§ 4.2.1.2)
- Effect of Injection pressure on large bubble sizes (§ 4.2.1.3)

 b) *Effect of bubble velocity on the development of bubble sizes (§ 4.2.2)*
 c) *Effect of port size on bubble sizes (§ 4.2.3)*
 d) *Bubble coalescence and development (§ 4.2.4)*

ii. *Optimisation of two-phase flow behaviours using MNIT (§ 4.3)*
- Reducing initial bubble sizes within two-phase flow (§ 4.3.1)
- Reducing initial average bubble sizes (§ 4.3.1.1)
- Reducing initial average small bubble sizes (§ 4.3.1.2)

- Reducing initial average large bubble sizes (§ 4.3.1.3)

- Effect of gas injection rate on outlet liquid flow rate (§ 4.3.2)

- Effect of velocity of liquid-phase on average bubble sizes (§ 4.3.3)

- Comparison between distribution of bubbles for both techniques (§ 4.3.4)

- Confirmation and observation of the growth rate of bubble sizes (§ 4.3.5)

- Distribution of bubbles at 1m above injection point (§ 4.3.5.1)

- Effect of Reducing initial Bubble Size on Production Rate (§ 4.3.6)

4.2   Factors Affecting the Behaviours of Bubbles Using SNIT

There are a number of variables that can effect bubble sizes and thus lead to flow instability within upward two-phase flow in a vertical pipe during gas lifting. The main variables that have been considered are the coalescence process among bubbles, injection pressure, injection rate, port size, and velocity of bubbles, velocity of liquid-phase, and distribution of bubbles across the test section and the performance of each technique in increasing outlet flow rate (oil production rate). Table 4.1 shows the operating conditions that were used throughout all the trials utilising SNIT as shown in Figure 3.7.

Table 4-1: The single nozzle injection technique (SNIT) operating conditions

Liquid flow rate l/min	Air Injection Pressure (bar)*	Air flow rate l/min	Inlet pressure (Psi)	Outlet pressure (Psi)	Inlet Temp C^o	Outlet Temp C^o	Outlet flow rate l/min
5 l/min	0.5	1	3	0.5	17.3	17.7	5.88
	1	3	3.2	0.7	17.3	17.7	7.24
	2	5	3.3	0.7	17.3	17.7	11.83
	3	6.4	3.4	0.8	17.3	17.7	12.89
	4	8	3.5	1	17.3	17.7	15.53
	5	9	3.8	1	17.3	17.7	16.30
10 l/min	0.5	1	3.4	1	17.3	17.7	12.90
	1	2.8	3.5	1	17.3	17.7	13.97
	2	5	3.7	1	17.3	17.7	15.40
	3	6	3.8	1	17.3	17.7	16.6
	4	8	3.8	1.4	17.3	17.8	18.69
	5	9	3.9	1.4	17.4	17.8	20.70
20 l/min	0.5	1	4.2	1.8	17.4	17.8	23.4
	1	2.8	4.2	1.8	17.4	17.8	25.3
	2	4.8	4	1	17.4	17.8	27.0
	3	6	4	1.5	17.4	17.8	29.7
	4	7.8	4	1.5	17.4	17.8	31.92
	5	9	4	1.6	17.4	17.8	34.5
30 l/min	0.5	1	4	0.8	17.4	17.8	34.8
	1	2.8	4.5	1	17.4	17.8	36.10
	2	4.8	5	1.8	17.4	17.8	38.6
	3	6	5.2	2	17.4	17.8	40.7
	4	7.8	5.8	2	17.4	17.8	43.2
	5	9	6	2.1	17.4	17.8	46.6

Note (*): 1 bar = 14.5 psi

4.2.1 Effect of Injection Pressure on Bubble Sizes

4.2.1.1 Effect of Injection Pressure on Average Bubble Sizes

The increase in injection pressure has a considerable effect on the two-phase flow behaviour. Figure 4.1 illustrates the relationship between air injection pressure and average bubble sizes using Single Nozzle Injection Technique (SNIT) with port size of 2.24 mm, which was shown previously in Figure 3.7. This effect was investigated at constant liquid phase (water) velocity of 2.4 cm/s and at different air injection pressures from 0.5 bar to 5.0 bar. Overall, the most significant feature shown in Figure 4.1 is that as the injection pressure increases the average bubble sizes decrease, as highlighted by Descamps *et al.,* 2007 that injection pressure effect on the bubble sizes. Because the water is about 1000 times denser then air and both (air and water) have different bulk elastic properties. In addition, the air is a homogenous scattering of many types of molecules, meaning it has a huge potential for compression and its composition is mainly N2 and O2, which have very weak forces between them. Moreover, the molecules have low enough kinetic energy that, due to intermolecular forces. Therefore, as injection pressure increases, the fractional volume "bulk modulus" of air bubbles reduces.

The present results, however, shows that there was a steep reduction in the average bubble size from 9.75 to 6.80 mm when the injection pressure increased from 0.5 to 1 bar see Figure 4.1. Thereafter, it reduces to 6.2 mm at 3 bar, followed by a marked decline in average bubble size ending at 5.06 mm when the injection presure was increased to 5 bar. In addition, the total number of bubbles measured was 14850 bubbles and the mean and standard deviation was 0.8.
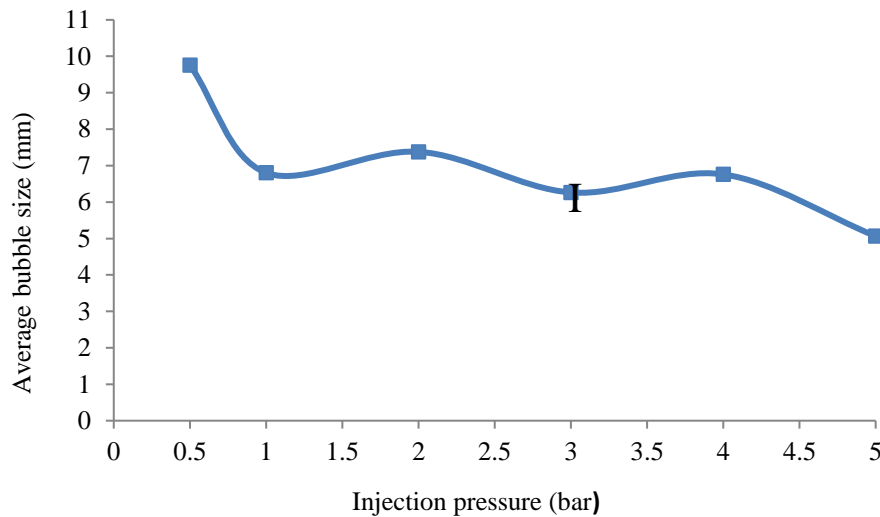
Figure 4-1: The effect of injection pressure on average bubble size at constant liquid velocity 2.4 cm/s

The increase in the injection pressure provides evidence that the injection pressure has a large effect on the behaviours of the two-phase flow in the gas lifted systems, as shown in Figure 4.2. This is due to the increase in the backpressure to the test section and reduces in the pressure drop along due to the bubble sizes were shrunk. This shrinkage in bubbles sizes is because of the density of water is approximately $1000 \, \text{kg/m}^3$. The average density of air is about $1 \, \text{kg/m}^3$. Thus, liquid water is about 1000 times denser then air and both have different bulk elastic properties. In addition, the air is a homogenous scattering of many types of molecules, meaning it has a huge potential for compression and its composition is mainly N2 and O2,which have very weak forces between them. Moreover, the molecules have low enough kinetic energy that, due to intermolecular forces. Therefore, as injection pressure increases, the fractional volume "bulk modulus" of air bubbles reduces.

Furthermore, high turbulence at low injection pressure because of the diameter of bubbles was quite a large. This has relationship and impact on the development of flow patterns (bubbly, slug, churn and annular) and their behaviours within the two-phase flow as observed by (Alamu and Azzopardi, 2011) that there was a link between bubble sizes and turbulent diffusion. Consequently, the injection pressure plays an important role in decreasing bubbles size gradually and stabilises the upward flow. This would restrict the development of flow. However, the increase in the injection pressure is limited, as it requires large capacity gas compression units (gas compressors) with financial impact. Thus, the evidence from the results show that as injection pressure increases, the average bubble size decreases in the

vertical test section. Furthermore, the bubble sizes must be reduced to minimise the number of bubbles reaching a certain diameter (maturation) and then collapsing, thus causing turbulence and flow instability.
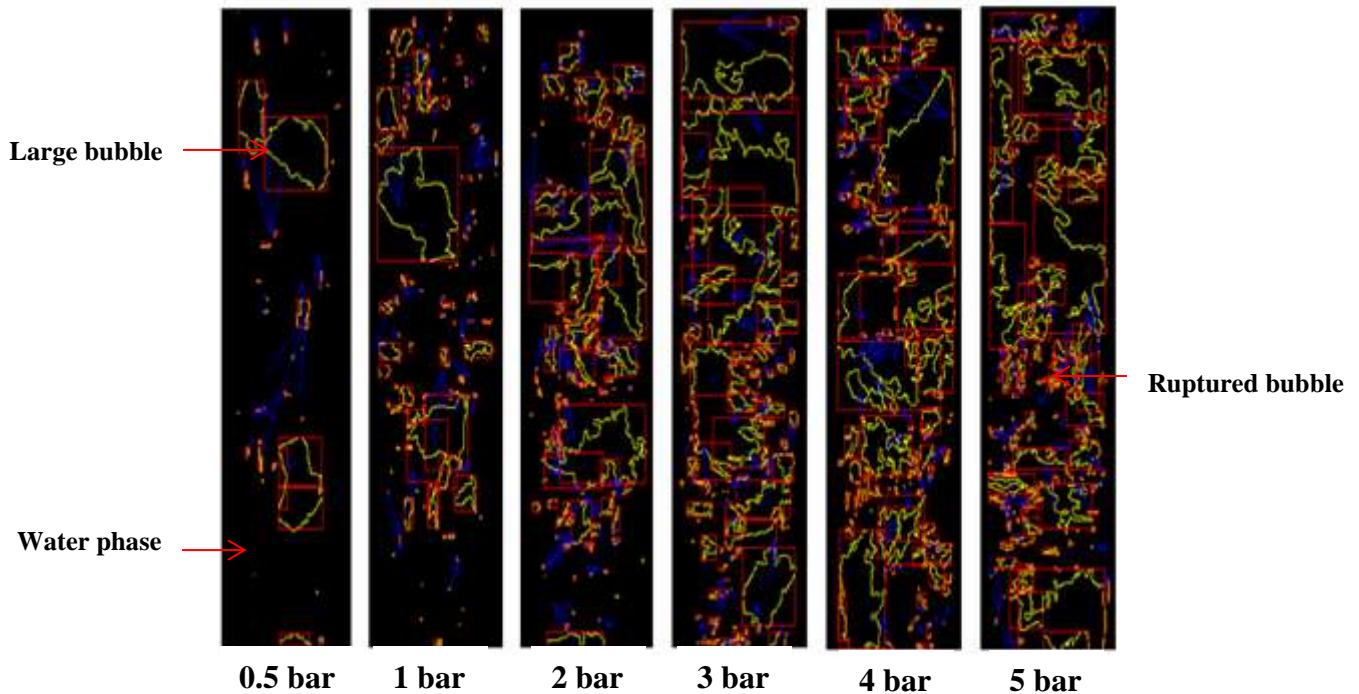
Figure 4-2: The effect of injection pressure on average bubble size using shadow sizing for SNIT at constant liquid phase velocity 2.4cm/s

4.2.1.2 Effect of Injection Pressure on Average Small Bubble Sizes

The effect of injection pressure was investigated for minimum (small) and large bubbles depending on their sizes to understand which bubbles were collapsing and causing the flow instability in the vertical test section. Figure 4.3 demonstrates the relationship between the injection pressure and small bubble sizes at different injection pressures. Overall, the average minimum bubble size was very sensitive and decreased dramatically, especially at low injection pressures. The results show that there was a sharp decline in minimum average bubble size from 1.37 to 1.16 mm when the injection pressure is increased from 0.5 to 2 bar, and thereafter it increased slightly to 1.22 mm, then remained stable, ending at 1.2 mm when injection pressure is increased to 5 bar. It was observed experimentally that the small bubbles did not collapse due to their tiny sizes. However, there were a number of bubbles coalescing with other neighbouring bubbles due to collision and eddies created within the flow, especially at low pressure. The average standard deviation between measured bubbles sizes

75

was 0.12. In addition, the small bubble sizes are required for the gas lift process, but with a good distribution.
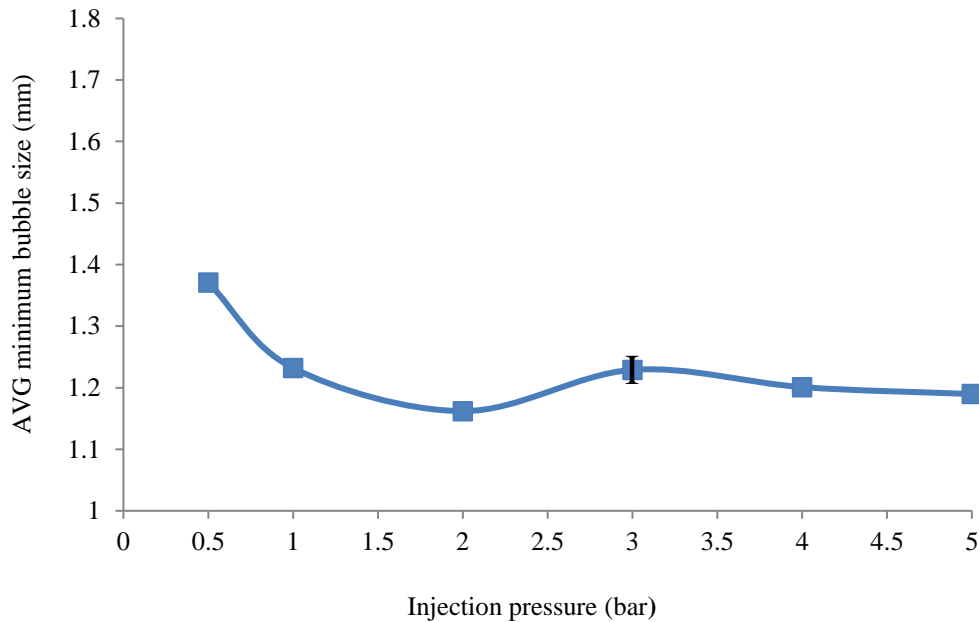
Figure 4-3: The influence of injection pressure on the average minimum (small) bubble sizes at constant liquid phase velocity 2.4 cm/s

4.2.1.3 Effect of Injection Pressure on Large Bubble Size

The influence of injection pressure even reaches mature large bubbles (Taylor bubbles) travelling in the centre of the test section. This is due to the reduction in the pressure drop along test section when the injection pressure is increased. Figure 4.4 illustrates the relationship between air injection pressure and the average maximum (large) bubble size at a constant water velocity of 2.4 cm/s. The results showed that there was a marked increase in the average large bubble size from 34 to 50.36 mm when the pressure was increased from 0.5 to 3 bar. Nevertheless, the average maximum bubble size declined gradually from 48.94 mm to 43.33 mm when the injection pressure reached 5 bar. This means that there were two different effects of injection pressure on large bubble sizes. Furthermore, the effects are positive because the average bubble size was reduced at higher pressure. In addition, it was observed that a number of large bubbles collapsed when the injection pressure was 3 bar at 1.5 m pipe length, this a greed with study of the critical value of (Taylor) bubbles by (Waltrich *et al.*, 2013, Azzopardi *et al*., 2015) as shown previously in Figure 2.11-12 causing

76

large oscillations and pressure drop within the two-phase flow. Figure 4.5 also shows qualitatively the collapse of Taylor bubbles in the present study similar to that of Waltrich *et al*., 2013. Therefore, this observation of large bubble ruptures is critical and one of the main aims of this research work, as the collapse of these bubbles is the main cause of the pressure drop and turbulence and flow instability within the upward flow and also caused the collision with other neighbouring bubbles as shown in Figure 4.6. These behaviours are the main cause of flow instability during upward flow. Thus, the bubble sizes must be reduced in order to minimise this fluid flow phenomenon.
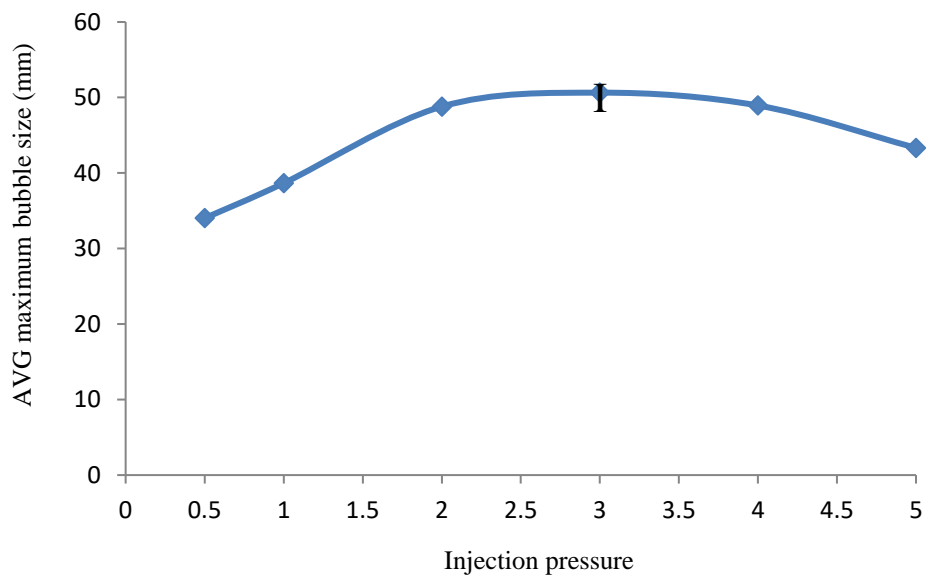
Figure 4-4: The effect of injection pressure on maximum (large) bubble size at constant liquid phase velocity 2.4 cm/s
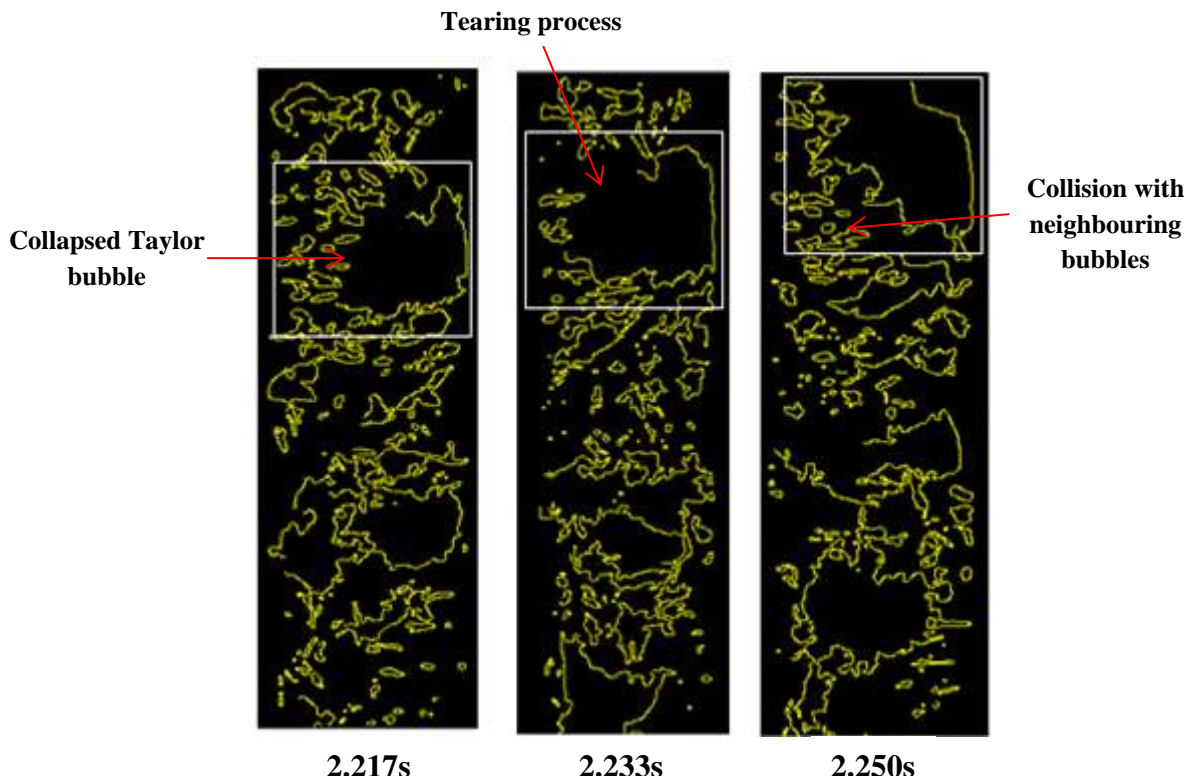
Figure 4-5: collapse and collision of the (Taylor) bubble captured by shadow sizing technique at 3 bar injection pressure

Therefore, a new approach or technique should be developed to reduce the initial bubble sizes and at the same time distribute them across the entire pipe area. This transformation will change the structure of the two-phase flow, minimise the development of upward two-phase flow, and prevent the bubbles from reaching critical sizes large bubbles collapse and maintain the flow regime in bubbly flow pattern as much as possible. In order, not reaching the transitional flow regions such as bubbly to slug, slug to churn and churn to annular. This will increase the lifting performance, reduce the collapse of bubbles, and increase the productivity of the gas lift method.
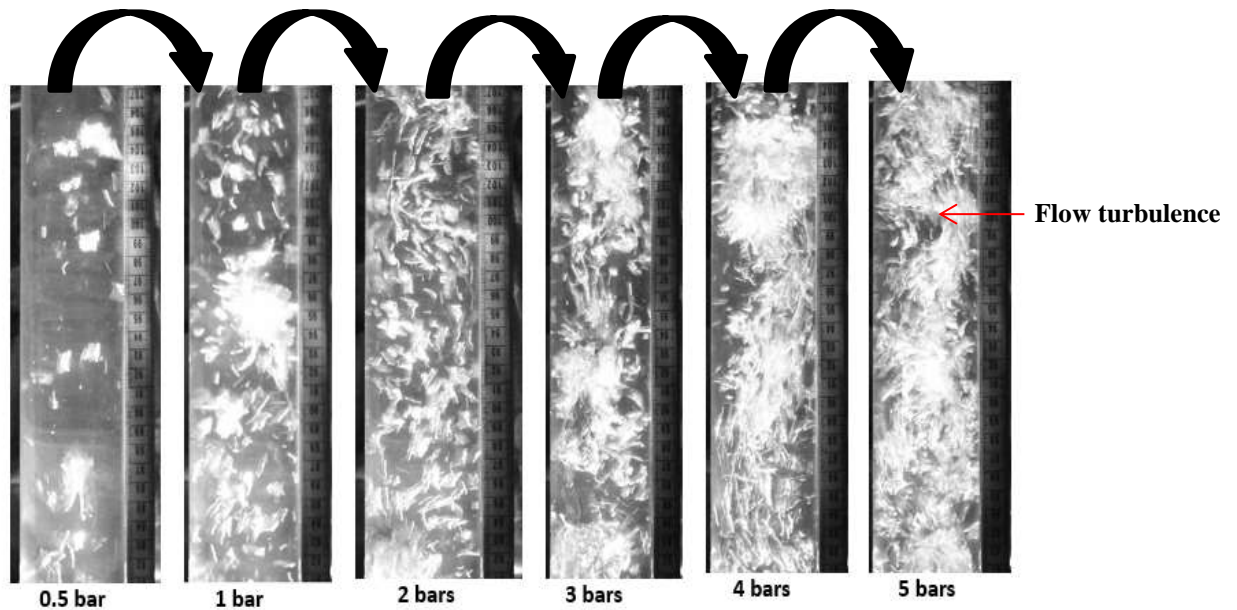
Figure 4-6: The effect of injection pressure on the bubbles' behaviours

4.2.2   Effect of Reynolds number on the development of bubble sizes

It is essential to consider the bubbles' movements, velocities and their Reynolds number in this case to investigate whether Reynolds number is one of the variables causing bubbles to grow. Figure 4.7 demonstrates the relationship between the Reynolds number of bubbles and bubble sizes at a constant liquid phase velocity of 2.4 cm/s and at different injection pressures. In general, the increasing in Reynold number has a great impact on bubble size. The results showed that as Reynold number increases, the bubble sizes rise, and this agrees with the results obtained by Liu *et al.,* 2016, and Guet, 2004. It should also be noted that this effect was observed for all injection pressures. The maximum bubble size measured at 3 and 4 bar. In addition, it was found that the velocity of bubbles was strongly dependent on bubble sizes and the large bubbles had higher velocities compared with smaller bubbles and these results matched with observations by Acuña and Finch, 2010 that found that large bubbles are faster than bubbles with diameter less than 2.5 mm. This was very clear from the velocity profiles and data. However, there was a slight a reduction in Reynold number of bubbles when injection pressure increased to 5 bar due to reduction in bubble sizes and their velocities at higher pressure at these operating conditions. Therefore, if the bubble sizes were reduced, then the Reynolds number of bubbles would decrease and then the development of two-phase flow would be optimised and postponed, and would not reach the higher Reynolds number where bubbles start to collapse and cause oscillations and turbulence within vertical flow.
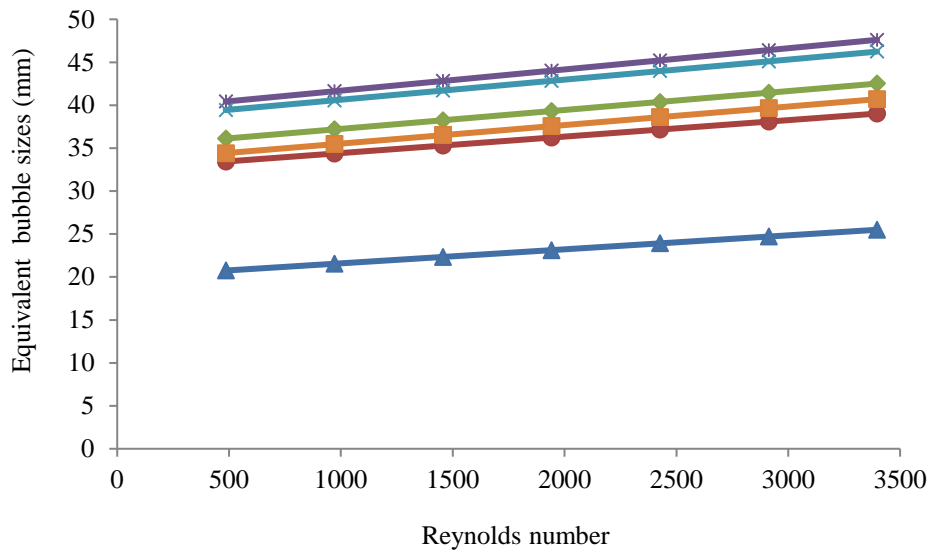
Figure 4-7 The relationship between the gas phase Reynolds number and bubble size at constant liquid velocity 2.4 cm/s.

Furthermore, the measurements of bubble velocities during the upward flow gave very interesting and clear evidence that there were fluctuations within the two-phase flow due to rupture and collapse of bubbles. This happens when bubbles reach critical sizes at specific velocity. Therefore, it is necessary to reduce the average flowing bubble sizes to minimise the development of two-phase flow. During the oil production process, any restrictions to flow within production tubing in the gas lift method are not recommended, because there are other operations undertaken during the lifting process such as wireline operation Therefore, there should be a new technique to change the initial fluid behaviours during the lifting process and prevent bubbles reaching these critical sizes, especially when bubbles collapse and collide with neighbouring flowing bubbles. These regions are known as the transitional flow regions, where the flow behaviour is critical and depending on interfacial forces between phases.

There is another type of velocity that must be considered in two-phase flow in the gas lift method. It is known as the liquid phase velocity and in the oil industry it is referred to as the reservoir response (PI) (Asheim, 1988). It is the ability of fluid to flow though reservoir rocks to the wellbore when gas is injected through gas lift valves to the production tubing. Figure 4.8 illustrates the effect of liquid-phase velocity (water) on average bubble size. The results showed that the average bubble size remained stable at 10 mm at low liquid phase velocity

from 2.4 cm/s to 4.8 cm/s, then it rose gradually ending at 14.02 mm when the liquid phase velocity increased from 4.8 to 14.6 cm, as shown in Figure 4.9. This confirms that the effect productivity index of the reservoir (PI) should be considered in any gas lift flow instability criteria, because as the liquid-phase velocity increases, so to do the bubble sizes. This is supporting the unified criteria for continuous gas lift instabilities by Alhanati *et al*, 1993 which was neglected by Asheim,1988. Thus, the flow oscillations within the two-phase flow increase. Therefore, average bubble size within the two-phase flow must be reduced to reduce these fluctuations and to achieve better stability.
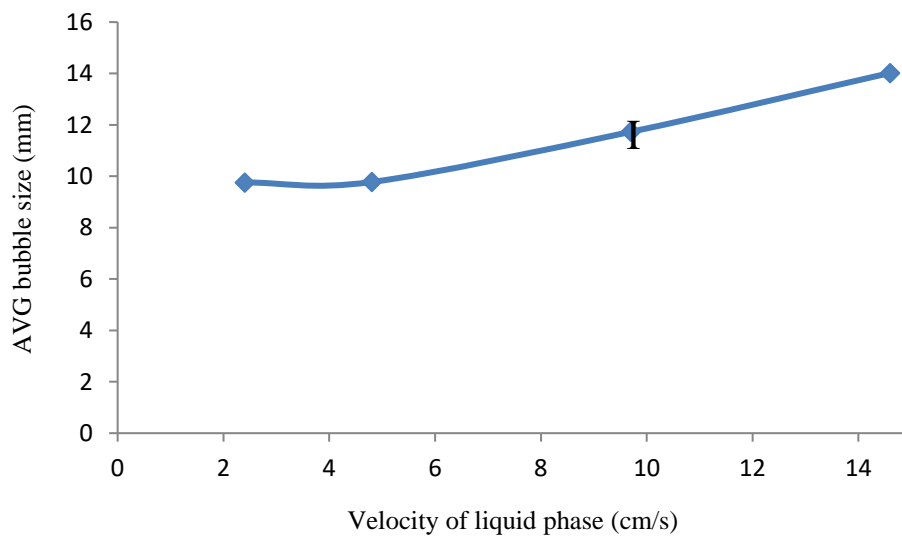
Figure 4-8: The effect of liquid phase velocity on average bubble size
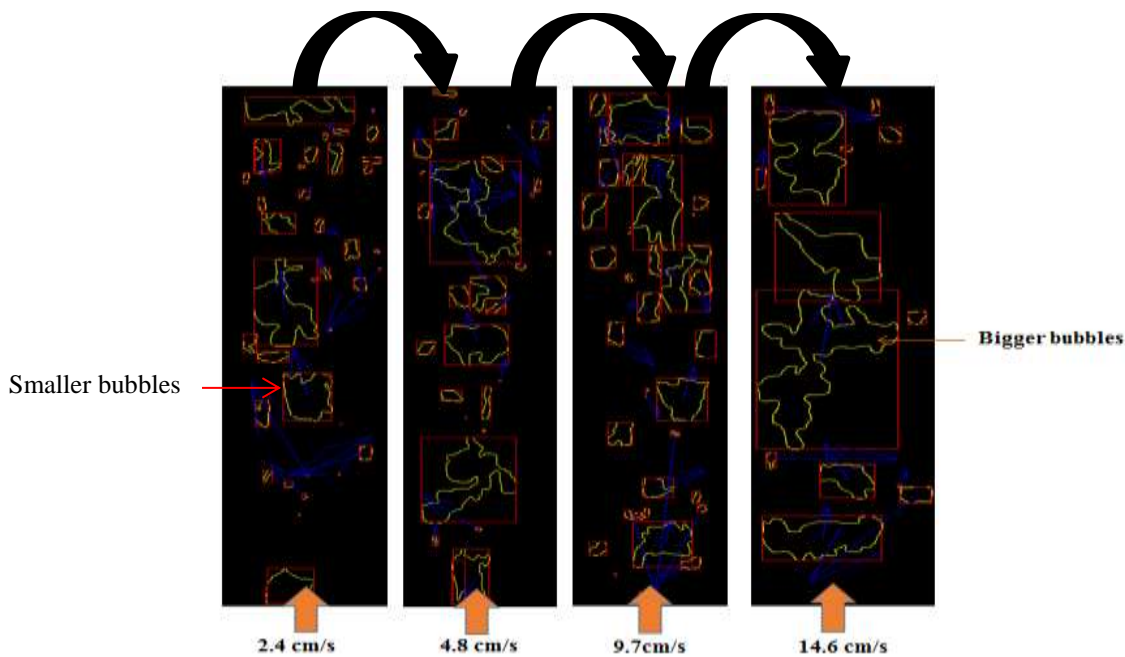
Figure 4-9: The effect of liquid phase velocity on average bubble size at 1m length

81

The large bubbles (Taylor bubbles) flowing in the centre of the pipe have the highest velocities. This is due to their large size and buoyancy as highlighted by Acuña and Finch, 2010 and shown in Figure 2.12. The results showed that the maximum bubble size increased gradually from 34 mm to 37 mm when the liquid phase velocity was increased from 2.4 cm/s to 14.6 cm/s when the injection pressure was 0.5 bar, as shown in Figure 4.10. This is evidence that the velocity of the liquid phase has a slight effect in contributing to large bubble sizes. As the flow develops downstream these bubbles collapse along the test section. These fluctuations could be reduced if the bubble sizes were reduced slightly.
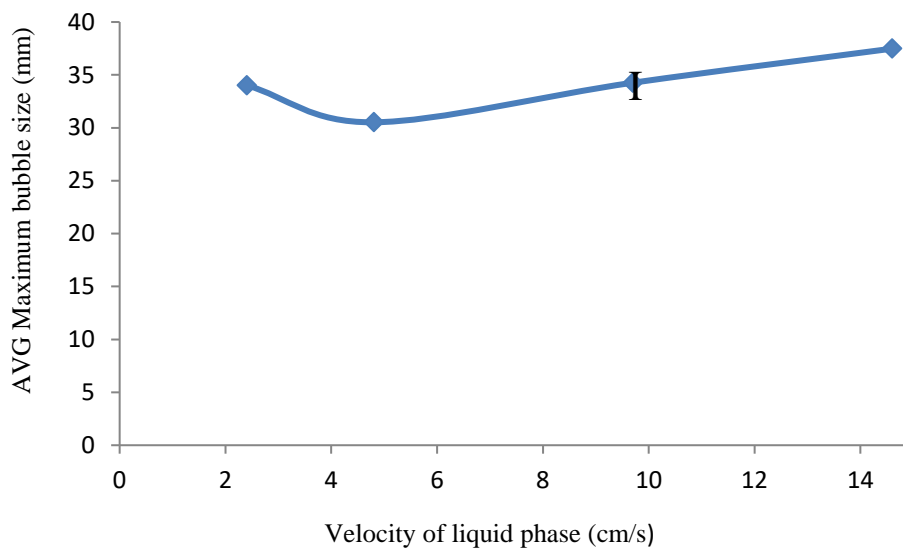
Figure 4-10: The influence of liquid phase velocity on maximum bubble size

4.2.3   Effect of port size on bubble size

The port size has a significant effect on the upward two-phase behaviours and this agrees with results obtained by (Ter Avest and Oudeman, 1995, Faustinelli *et al.,* 1999) that using single orifice causes subcritical flow conditions at the injection point. Overall, there was a sharp increase in the average bubble size when the single port size was increased. Figure 4.11 demonstrates the effect of increasing port size on average bubble size at a constant liquid flowrate of 5 l/min and injection pressure of 1 bar. The results showed that as port size increases, the average equivalent bubble size increases. The graph indicated that there was a

slight increase in the bubble sizes from 30.42 to 32.11 mm when the port size was increased from 0.2 to 0.7 mm. Thereafter, it dropped slightly from 32.11 to 31.50 mm when port size was 0.9 mm, followed by a sharp increase in the average equivalent bubble size ending at 34.44 mm when the port size increased to 1.2 mm. In addition, it was found that a higher jet velocity produced from a smaller diameter orifice shows higher breakup frequency of the bubbles at 6.6 m/s in the plunging zone and consequently smaller bubbles are observed throughout the column with a smaller diameter orifice. This means that there was high air velocity in front of the injection point which causing large flow fluctuations and turbulence in the vertical test section. This is due to subcritical flow conditions at the injection point such as sonic velocity, critical pressure and critical temperature due to interaction between injected air and liquid –phase (water) as this supported by (Faustinelli *et al.,* 1999) .
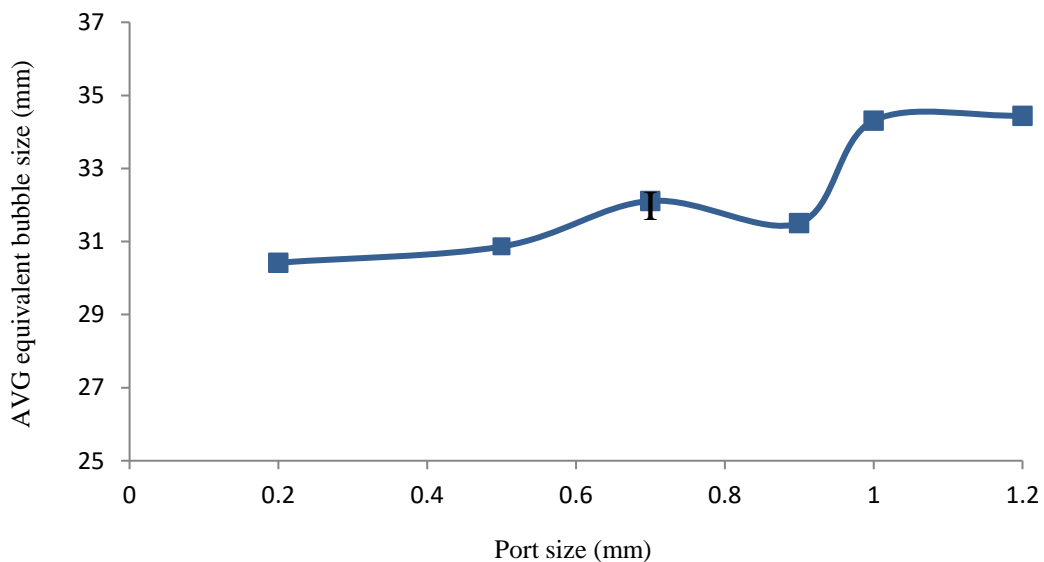
Figure 4-11: The effect of port size on bubble size at constant flow rate 5 l/min and pressure 1 bar

In addition, the increase in the orifice port size of the gas lift valve has a negative effect on the stability of upward two-phase flow. This was clear from the relationship between the increase in the port size and the bubble sizes in the vertical column. These fluctuations in the average bubble size continued to occur as port size increased. Therefore, the increase in port size leads the overall average bubble size to oscillate, even under constant operating conditions. It can be concluded that the increase in port size has a destabilising effect and causes an increase in the bubble size. Moreover, the smaller port sizes cause an increase in

the air velocity in front of the injection point. This led to an undesired situation when the large bubbles in the centre of pipe started to collapse and caused a large amount of turbulence and eddies in the pipe. This is one of the causes of two-phase flow instability and reduction in outlet flow rate and lifting performance in the vertical test section (Guet and Ooms, 2006). Therefore, there should be an alternative orifice shape for injecting air into the system.

4.2.4 Bubble coalescence and development

When the SNIT was used, it was observed at the air injection point that the initial bubble size was approximately equivalent to the size of the orifice and as soon as these bubbles left the orifice port size directly, they went to the centre of the vertical test section and then started to coalesce together depending on the mixture velocity. This process causes bubble sizes to increase and flow to develop quickly via the creation of large bubbles in the centre of the pipe. This also reported in the work by Zhang and Fan, 2003 and Tan *et al*., 2013. This fluid behaviour was investigated by analysing the recorded videos frame by frame as shown in Figure 4.12. Subsequently, these large bubbles collapse when they reach mature sizes. Wu et al., 1998, also mentioned this observation. This size depends on port size, pipe diameter and operating conditions. Moreover, it was observed that the distances between the bubbles were very small, and this aids the possibility of speedy coalescence.

Therefore, the distribution of bubbles in the pipe needs to be changed to a better distribution to keep sufficient distance between the flowing bubbles and to distribute them from the centre of the pipe to the rest of the pipe area close to the pipe wall. This will minimise bubble coalescence and delay the development of two-phase flow as much as possible. Furthermore, the initial two-phase flow behaviours at the injection point are crucial, because the first interaction between phases with different densities (gas and liquid) at the injection point has a large impact on and relation to other upward two-phase flow behaviours in the vertical column. For example, if the distribution of bubbles changes directly once they leave the injection point, this will change many behaviours of the upward two-phase flow, especially if the sizes of the bubbles have been reduced at the same time. This will maintain a bubbly flow regime as much as possible along the pipe, with smaller bubbles travelling smoothly with good distribution and approximately the same mixture velocity. Thus, this minimises the coalescence process among air bubbles in the test section. This is therefore increase the

lifting performance and total oil production rate from the gas lift method by minimising the flow instability with upward two-phase flow along the pipe.
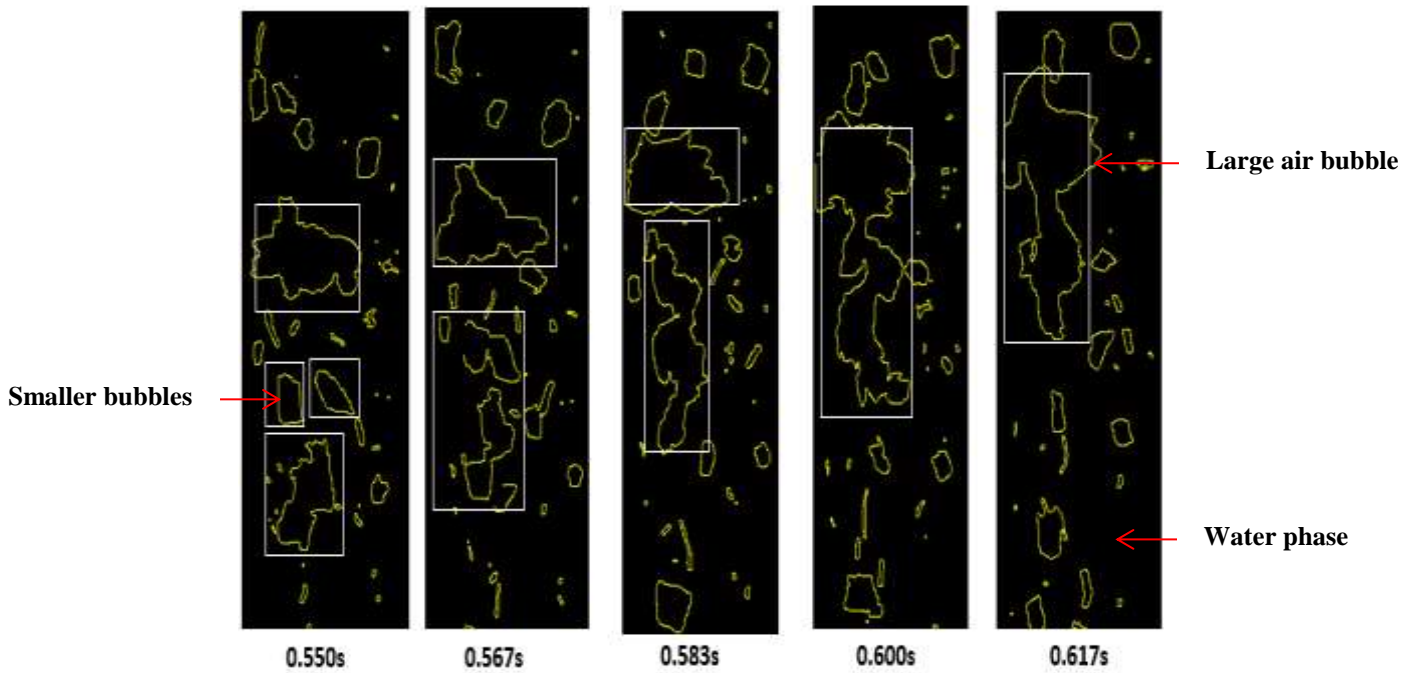
Figure 4-12: The bubble coalescence process at low liquid-phase velocity 2.4 cm/s and 0.5 bar

4.3 Optimisation of the two phase-flow behaviours using MNIT

Table 4.2 shows the operating parametric conditions that were used in this phase of the experiments using MNIT, which was shown in Figure 3.7. The fluid behaviour in the vertical column during oil production using gas lift methods are very challenging due to the complex multi-phase behaviours, which can cause a reduction in the total oil production. Therefore, there should be a new way or technique to reduce and optimise these chaotic fluid behaviours during the lifting process, without increasing backpressure by choking the gas lifted wells or using the conventional feedback control systems, which are only partially effective. This new technique would reduce the flow instability within the two-phase flow, resulting in an increase in the total oil production from the gas lift method.

Table 4-2: The multiple nozzles injection technique (MNIT) operating conditions

Liquid flow rate l/min	Air Injection Pressure (bar)	Air flow rate l/min	Inlet pressure (Psi)	Outlet pressure (Psi)	Inlet Temp C^o	Outlet Temp C^o	Outlet flow rate l/min
5 l/min	0.5	1	2.9	0.5	17.1	17.6	6.6
	1	3	3	0.5	17.1	17.6	7.8
	2	4.8	3	0.5	17.1	17.6	9.6
	3	6	3	0.5	17.1	17.6	13
	4	8	3.1	1	17.1	17.6	15
	5	9	3.2	1	17.1	17.6	16.6
10 l/min	0.5	1	3	1	17.1	17.6	12.9
	1	2.9	3.2	1	17.1	17.6	14.1
	2	4.8	3.5	1	17.1	17.6	16.4
	3	6	3.6	1	17.1	17.6	19
	4	7.8	3.7	1	17.1	17.6	20.6
	5	9	3.8	1	17.1	17.6	23.9
20 l/min	0.5	1	4.2	1.6	17.1	17.6	24
	1	3	4	1	17.1	17.6	26.2
	2	4.5	4	1.2	17.1	17.6	28.84
	3	6	4	1.4	17.1	17.6	31.4
	4	8	4	1.7	17.2	17.7	36.4
	5	9	4.1	2	17.2	17.7	39.4
30 l/min	0.5	1	5	1	17.2	17.7	36.6
	1	2.8	5.3	1.2	17.2	17.7	38.2
	2	4.5	5.7	2	17.2	17.7	41.2
	3	6	5.9	2	17.2	17.7	45.3
	4	7.8	6	2	17.2	17.7	47
	5	9	6	2.8	17.2	17.7	50.1

Note (*): 1 bar = 14.5 psi

A new modified gas lift valve with multiple nozzles injection technique (MNIT) also shown in Figure 3.7 is designed and introduced for the first time in the gas lift method in the oil industry instead of the single (sharp edge) orifice gas lift valve and other existing valves. The purpose of the valve is to reduce initial bubble sizes and to distribute the smaller bubbles from the centre of the pipe (core peaking) to the rest of the pipe area (wall peaking). Consequently, there will be an increase in the gas lifting performance and total oil production and also stabilisation of the multi-phase flow behaviours. This can be achieved by maintaining better bubble distribution by keeping sufficient distance among these small bubbles to reduce the coalescence process between flowing bubbles. As result of this, reduces initial bubble sizes and also minimises further interaction between phases and the collapse process between the travelling bubble sizes.

The design of small nozzles in the new technique as shown in Table 3.1 depends on the gas injection flow rate required for that particular oil well. The total area of these nozzles gives an equivalent or less gas injection rate compared with the same geometrical area of single orifice technique. This was considered in the design of nozzles in the head of multiple nozzles injection technique. The new technique (MNIT) gave acceptable results compared with the single orifice technique in terms of reducing initial bubble sizes, and distribution of bubbles in the vertical test section. In addition, it increased the production and performance of the gas lift method. The results obtained from the multiple nozzles injection technique will be presented successively in the following sections and compared with SNIT results where appropriate.

4.3.1   Reducing Bubble Sizes within Two-Phase Flow

4.3.1.1   Reducing Initial Average Bubble Sizes

Reducing the initial bubble sizes has a major impact on the stability of two-phase flow in the vertical column in the gas lift method, especially if these bubble sizes were reduced and have a better distribution across the entire pipe area. Figure 4.13 illustrates a comparison between the performances of the new multiple nozzles injection technique (MNIT) and the single orifice gas lift valves in reducing the initial average bubble sizes at different injection pressures and a constant liquid flow rate of 5 l/min. Overall, the most significant features of the line graph are: the average bubble sizes generated by the new technique (MNIT) were

lower than the average bubble sizes produced by the SNIT at different injection pressures. This is due to smaller diameter of each nozzle in the new technique, which creates higher jet velocity at the injection point. Figure 4.13 shows there is a steep decrease in the initial average bubble sizes from 9.76 to 7.23 mm at 0.5 bar, when the new multiple nozzles injection technique was used, representing a 25% reduction in the average initial bubble sizes. Then the size declined considerably to 4.42 mm at 4 bars, which represented a 34% reduction compared with an orifice valve. Subsequently, a rapid drop in the average bubble sizes ending at 3.89mm, when injection pressure was 5 bars. Moreover, there was a 23% decline in average bubble size between the two systems. As a result of this, the average overall reduction between the two techniques was 22% at different injection pressures with the same port size dimensions of 2.24 mm.
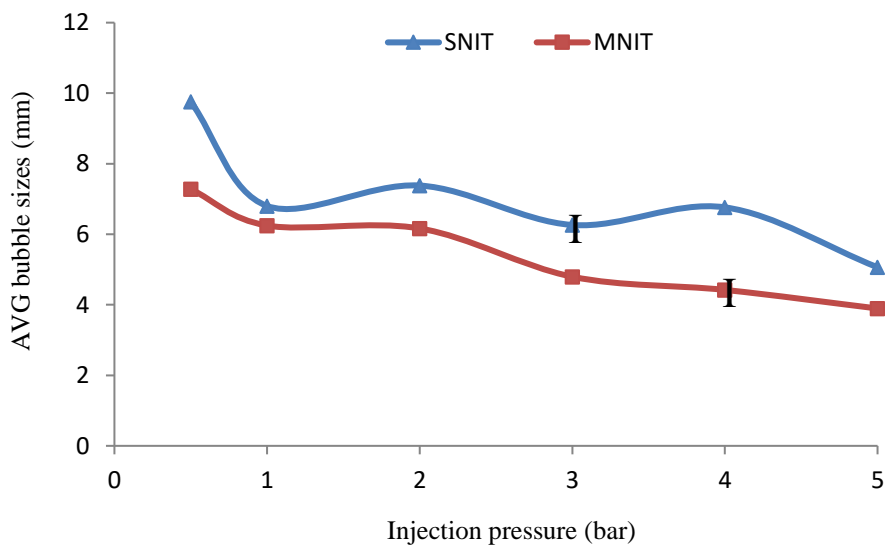
Figure 4-13: Comparison between the new MNIT and the SNIT for gas lift optimisation at a constant flow rate 5 l/min.

4.3.1.2   Reducing Initial Average Minimum (small) Bubble Sizes

Furthermore, there was confirmation of the performance of the new multiple nozzles injection technique (MNIT) in reducing all different bubbles sizes including the small flowing bubble sizes in the vertical test section. Further investigations were carried out to ensure that the small bubble sizes were reduced likewise. Figure 4.14 demonstrates a comparison between using the new multiple nozzles injection technique and the SNIT in

reducing small bubble sizes at different air injection pressures during the upward two-phase flow in the test section. In gerenal, the results showed that the average minumum bubble size produced from the MNIT was lower than the SNIT under the same operating conditions. There was a gradual reduction in minimum average bubbles size to 1.17 mm when the new technique was used, compared with the single orifice technique was 1.37 mm at 0.5 bar injection pressure. Thus, the reduction in average small bubble size was 14.54% at this point, and reduced to 0.99 mm at 3 bars. The sharp edge orifice valve was 1.23 mm under the same operating conditions. Moreover, the reduction in the small bubble sizes was 19% at this point between both techniques, and then there was a regular reduction ending at 0.96 mm when the injection pressure was 5 bar, compared with the single orifice, which was 1.19 mm. In addition, the average overall reduction in the small bubble sizes between both gas lift valves was 16.1% at different injection pressures. Therefore, the new technique is effective in reducing bubble sizes, including the small sizes.
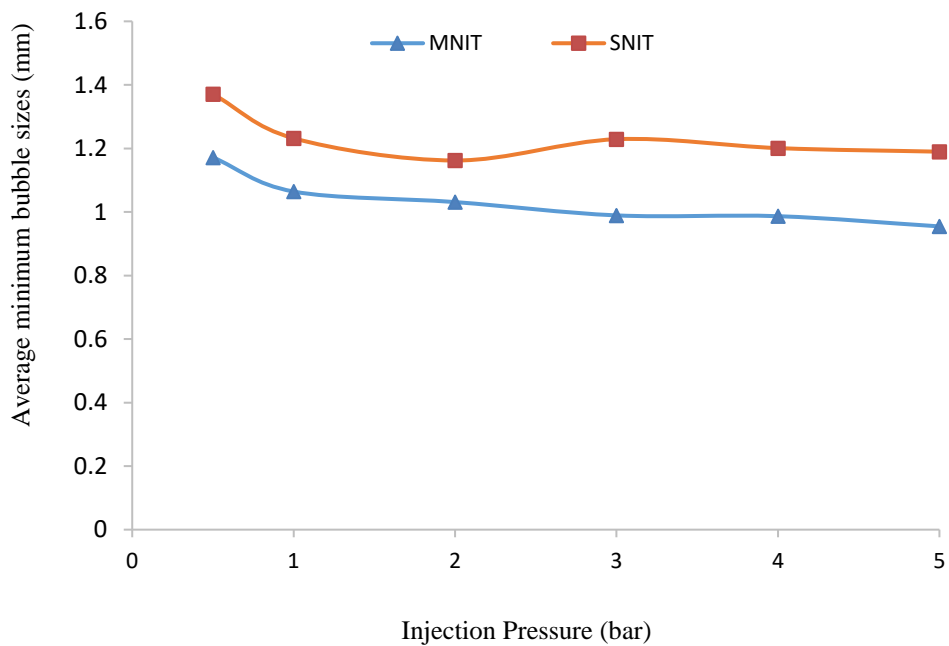
Figure 4-14: Comparison between the new MNIT and the SNIT for gas lift optimisation at constant flow rate 5 l/min

4.3.1.3   Reducing Initial Average Maximum (large) Bubble Sizes

In addition, large bubbles (Taylor bubbles) flowing in the middle of the pipe have a great influence on the stability of two-phase flow in the gas lifted wells. This is due to their sizes being critical and close to the collapse region of bubbles. Therefore, it is very important to reduce the sizes of large bubbles to avoid the rupture of these large bubbles and their collision with other nearby bubbles. This is one of the main causes of the flow instability phenomenon. Figure 4.15 demonstrates a comparison between the performances of the MNIT and SNIT in decreasing the average large bubble sizes flowing in the centre of the test section. The results showed that at the first injection pressures, the average large bubble sizes produced from the new multiple nozzles injection technique were higher than for the orifice valve. Because of at the low injection pressure less than 1.3 bar, the velocity of the air was slightly low through the nozzles of the MNIT to shear the air bubbles. However, after 1.3 bar injection pressure, the trend in average large bubble sizes from the single orifice became higher than for the multiple nozzles. This means, at this intersection point and operating conditions the average bubble size of air bubbles are the same sizes. Furthermore, the average large bubble sizes started to decline gradually after the injection pressure reached 1.5 bar, followed by a slight decline to 43.49 mm when the injection pressure was 2 bar when the multiple nozzles was used. In comparison, the single nozzle valve was 48.8 mm at the same pressure, and thereafter descended moderately to 42.09 mm at 3 bar. In comparison with the single nozzle orifice average bubble size was 50.64 mm, then there was a sharp drop in the average large bubble sizes ending at 38.30 mm when the new MNIT was used, at 5 bar injection pressure, which was 43.33 mm at the same injection pressure. The overall reduction in the average large bubble sizes between both techniques at different injection pressures was 8.22%. It can be concluded that Multiple Nozzle Injection Technique is capable in reducing large bubble sizes in the test section compared with Single Nozzle Injection Technique with the same geometrical dimensions and operating conditions especially at higher injection pressures.
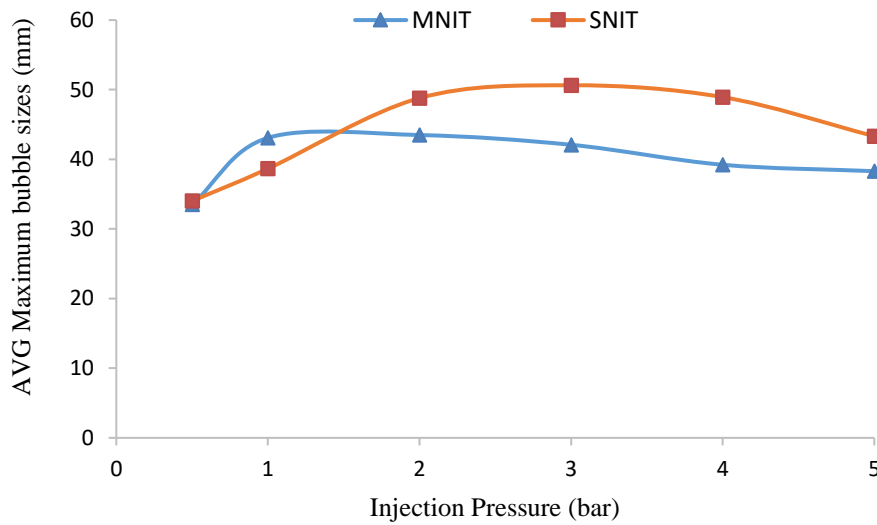
Figure 4-15: Comparison between the MNIT and SNIT for gas lift optimisation at a constant flow rate 5 l/min

4.3.2 Effect of gas injection rate on outlet liquid flow rate

The gas injection rate is an important parameter that has a major impact in any gas lift operation. Therefore, it is essential to investigate and optimise the gas injection rate. Figure 4.16 illustrates the effect of the gas injection rate on the outlet flow rate using the new multiple nozzles injection technique and single nozzle injection technique at different air injection flow rates. Overall, the results showed that as the gas injection rate increases, the outlet flow rate rises. The flow rate is measured by a digital flow meter at the experiment outlet lines. These digital flow meters measure the volumetric flow rate not mass flow rate. As result of this, there are small differences between inflow and out flow figures. This is due to the complexity of measurement of multiphase flow. In addition, the injected air was ventilated to the atmosphere through a ventilation point. This could lead to an increase in the production rate when the new multiple nozzles injection technique is used. Figure 4.16 reveals that there was a marked increase in the outlet flow rate to 36.6 l/min when the new multiple nozzles injection technique was used, compared with the SNIT which was 34.8 l/min at the same gas injection rate of 1 l/min. Thereafter, there was a sharp increase to 45.2 l/min when the gas injection rate increased to 6 l/min using the MNIT. However, it was only 40.7 l/min when the SNIT was used under the same operating conditions. Furthermore, when the gas injection rate was raised to 9 l /min, the outlet flow rate was 50.1 l/min using the MNIT, which was higher than the outlet flow rate from the SNIT, which was 46.6 l/min.

91

It can be concluded that the performance of the new multiple nozzle injection technique was better than the single nozzle orifice at the same air injection rates. This is due to reduction of the initial bubble sizes and improved distribution of bubbles as shown in (§ 4.3.1) and (§4.3.1.6). In addition, the design of the new technique gave equivalent or lower air injection flow rate. In comparison with the single nozzle orifice.
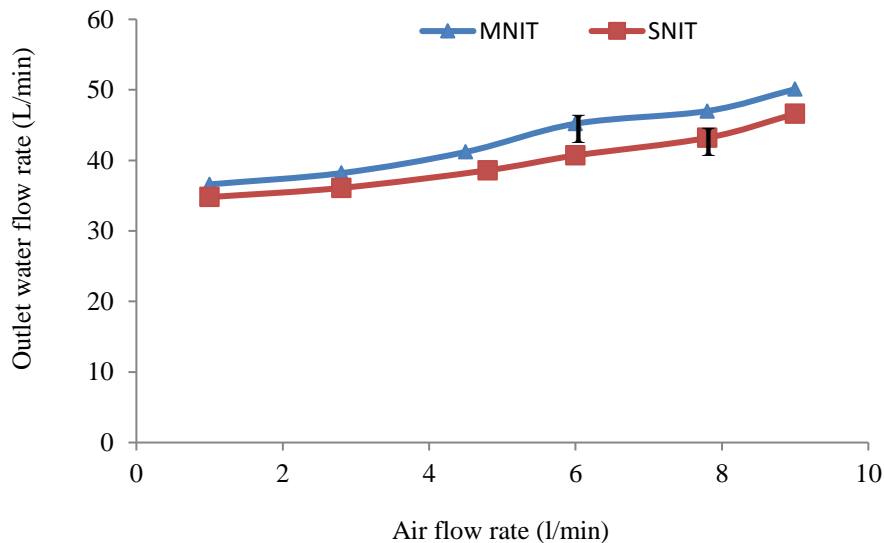
Figure 4-16: The performance of the MNIT and the SNIT for gas lift optimisation at different air injection rates.

4.3.3   Effect of velocity of liquid-phase on average bubble sizes

The velocity of liquid-phase (water) is one of the variables that have a slight effect on the average bubble sizes. Therefore, it is important to ensure that the average bubble sizes in the test column were reduced and maintained even if the velocity of the liquid-phase increased. Figure 4.17 demonstrates a comparison between the new multiple nozzles injection technique and single nozzle orifice at different liquid-phase velocities and a constant pressure of 0.5 bar. In gerenal, the results showed that the average bubble size produced from the multiple nozzles injection technique was still lower than the single (sharp edge) technique under different liquid –phase velocilties.. The results showed that there was a gradual increase in the average bubble sizes as the velocity of the liquid-phase was increased. This is due to the liquid-phase velocity is low at these ranges and it did not shear bubble sizes at the injection point as can be seen in Figure 4.17. The graph showed that the average bubble sizes were reduced to 7.27 mm when the new multiple nozzles injection technique was used at a liquid

phase velocity of 2.4 cm/s compared with the orifice valve was 9.75 mm. This gives an overall reduction in the average bubble sizes of 25% at this liquid velocity. Furthermore, at a high liquid phase velocity of 14.6 cm/s, the average bubble sizes reached 14mm using the orifice valve. Nevertheless, when the new technique was installed, the average bubble sizes were reduced to 13mm, even though the velocity of the liquid-phase had increased. However, the average bubble sizes produced from the new multiple nozzles injection technique were still smaller than the average bubble sizes created by the conventional orifice valve under different liquid-phase velocities.
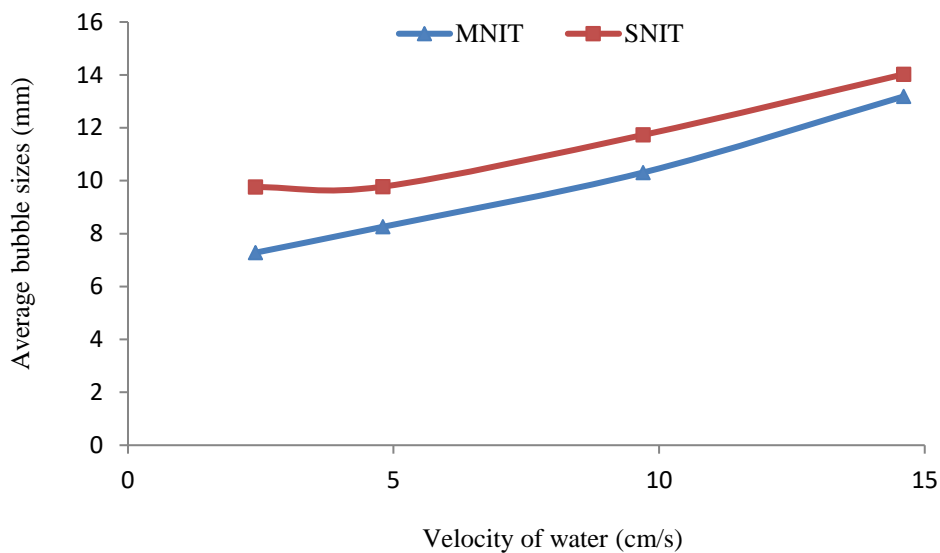
Figure 4-17: Comparison between the MNIT and SNIT at constant injection pressure 0.5 bar.

It is recommended to increase the number of small bubbles above the injection point in the vertical column in the gas lift method with the same amount of gas injection rate. Because of maintaining smaller bubbles and bubbly flow regime in gas lifting process will increase total oil production and bring the stability to the system. In addition, prevents from reaching to the transitional regions when the flow developed. Figure 4.18 illustrates a comparison between the new multiple nozzles injection technique and a single nozzle orifice in increasing the number of smaller bubbles under the same operating conditions. The results showed that the number of detected bubbles increased considerably when the new technique was used compared with the normal single nozzle orifice. As shown in Figure 4.18 there is a steep increase in the number of detected bubbles to 39 bubbles when the pressure was 0.5 bar when

the new multiple nozzles injection technique was used compared with the single nozzle orifice valve, where there were 25 bubbles above the injection point. This gave an increase in the number of bubbles of 56%. Thereafter, the number of bubbles rises to 104 bubbles when the injection pressure was increased to 2 bars while using the multiple nozzle injection technique. In comparison with the single nozzle orifice there were 63 bubbles. The increment in the number of bubbles was 65% under these operating conditions.

Furthermore, at a higher injection pressure of 4 bar using the new multiple nozzles injection technique, the average number of bubbles increased to 200 bubbles compared with the single nozzle orifice were 105 bubbles. The increase in the number of bubbles was 90.5% at this injection pressure. It can be concluded that the new multiple nozzle caused a significant increase in the number of smaller bubbles in the test column of about 60.2% compared with the orifice valve at different injection pressures. Therefore, this led to improved distribution of bubbles and lifting performance in the test section.
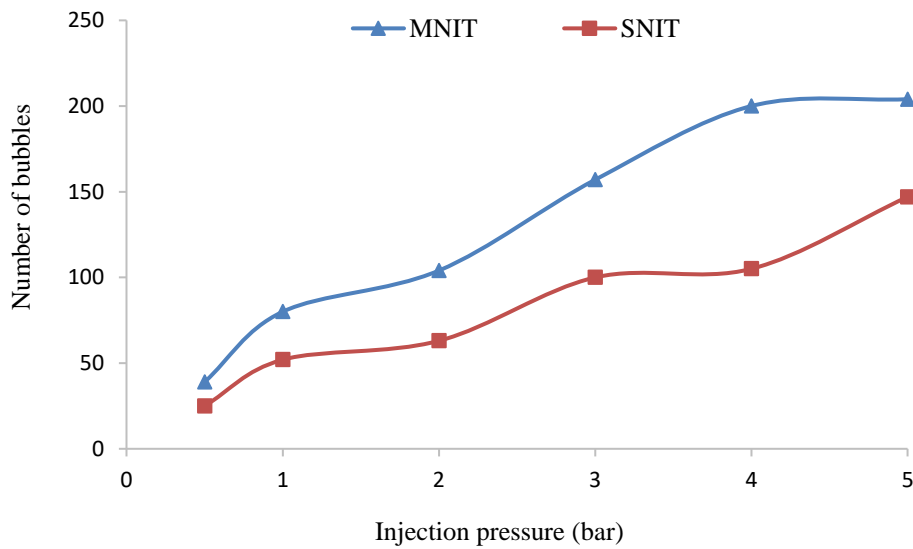
Figure 4-18: Comparison between the MNIT and SNIT under the same operating conditions

4.3.4   Comparison between distribution of bubbles for: MNIT Versus SNIT

The distribution of air bubbles has a major impact on the lifting performance and the stability of two-phase flow in the gas lift method in the oil industry. Therefore, the path of moving air

bubbles should be changed from the middle of the vertical pipe to across the entire pipe area. This will reduce the possibility of the coalescence process among air bubbles, avoid the creation of large bubbles in the test section, and thus delay the development of two-phase flow regimes. This agrees with distribution of air void fraction reported by (Szalinski *et al.,* 2010).

Figure 4.19 demonstrates a comparison between the performances of the new Multiple Nozzles Injection Technique and the Single Nozzle Injection Technique in distributing initial bubbles at 0.5 bar injection pressure.

Figure 4.19 shows that there is a considerable increase in smaller bubble frequency of bubbles sizes between 6.5 and 7 mm when the MNIT is used, compared with the SNIT, which had a frequency of 11 with larger bubbles between 9 to 9.5 mm at 0.5 bar injection pressure. This is because MNIT creates a large number of smaller bubbles via its small orifices.

In addition to that, when these small bubbles enter the test column they spread across the pipe area and even close to the pipe wall. This is perceived to be due to the high bubble velocities' penetration in the liquid phase across the pipe area at the injection point and the smaller orifice sizes in the new technique. This type of bubble distribution is called *wall peaking*, as typified in Figure 4.20. This type of distribution increases the liquid phase lifting performance. On the contrary, the path of bubbles which exit port-size of the single orifice valve moves directly to the centre of pipe and then they rapidly coalesce with neighbouring bubbles. This is called *core peaking* and it is one of main reasons for the development and instability of the two-phase flow in a vertical pipe, as this type of bubble distribution gives a high possibility for bubbles to coalesce and develop in the middle of the vertical column.
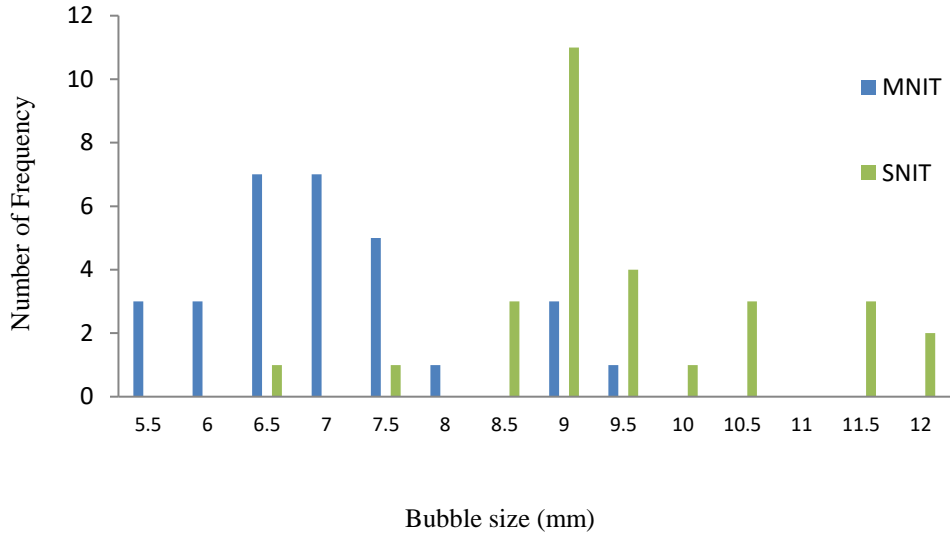
Figure 4-19: Comparison between the distribution of air bubbles using the MNIT and SNIT at 0.5 bar; with S.D =1.01
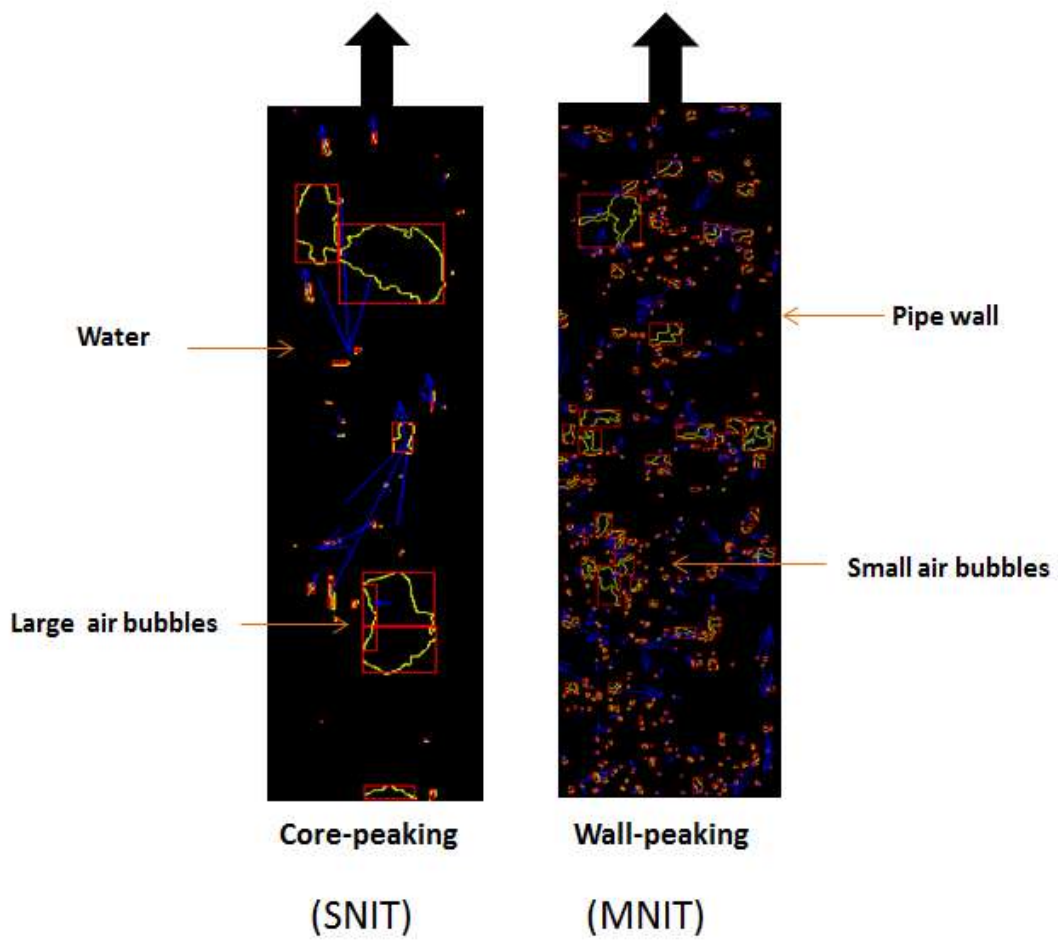
Figure 4-20: Changing bubble distribution from core peaking to wall peaking using the MNIT

Moreover, when both techniques were investigated at higher injection pressures, it was found that as the injection pressure increases, the distribution of bubbles improved significantly, especially when the new multiple nozzle injection technique was used, due to the increase in the number of smaller bubbles occupying the entire area of the pipe, including in the vicinity of the pipe wall. There was sufficient distance between the upward flowing bubbles to minimise the collision and coalescence processes between neighbouring bubbles when the superficial velocity increased and with the development of the flow patterns (bubbly, slug, churn and annular). Therefore, this two-phase flow development can be controlled by reducing the initial air bubble sizes and changing the distribution of bubbles in the column. Furthermore, this has the potential to increase the total oil production from the gas lift method in the oil industry because the performance is improved, as shown in Figure 4.16.

Figure 4.21 demonstrates the comparison between the bubble distributions of the new multiple nozzle injection technique and a single nozzle injection technique at 5 bar injection pressure. As can be seen in Figure 4.21 there was a sharp increase in the frequency of bubbles with sizes between 3 to 3.5 mm when comparing the two techniques. There was peak frequency of bubble sizes between 5.25 to 5.5 mm with SNIT. Figure 4.21 also indicates that the bubble distribution shifted to smaller bubble sizes with better distribution when MNIT was used. In addition, the air injection rates were the same for both cases. Finally, could be concluded that the distribution of initial small bubble sizes has a major effect on the stability of two-phase flow behaviours and increases the performance of the gas lifting process. Thus, the growth rate of bubble sizes generated by the new technique along the vertical pipe makes it impossible for the bubbles to reach the size of the large bubbles produced from the SNIT, even if the flow is developed. This is because the type of bubble distribution from the new technique is maintained wall peaking. This means that the possibility of smaller bubbles coalescing and developing is lower and is due to these smaller bubbles travelling along the pipe with almost the same size and mixture velocity. In comparison, the bubbles produced from the SNIT have a greater opportunity to grow and coalesce with other bubbles, creating large bubble sizes then collapsing when they reach their critical size. This is one of the main reasons for the pressure fluctuations and two-phase flow instability along the test section.
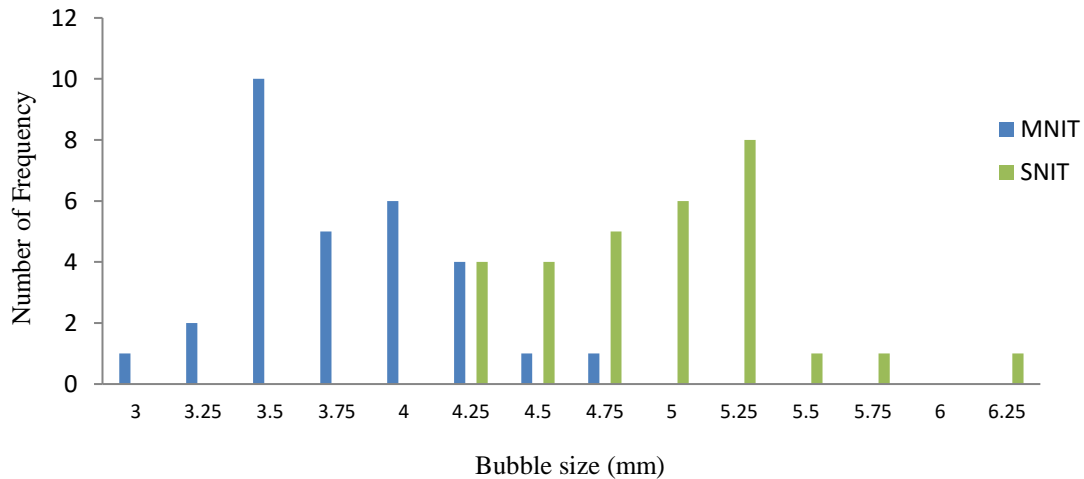
Figure 4-21: Comparison between the bubble distribution of the two techniques at 5 bar injection pressure

4.3.5   Confirmation and observation of the growth rate of bubble sizes

Reducing the initial bubble sizes is essential and should be observed and maintained along the test section to ensure that the smaller bubble sizes generated from the MNIT are still smaller than the bubble sizes produced from the SNIT, which is widely used in the oil industry. Therefore, the bubble sizes were measured at the middle of the transparent test section 1 metre above the injection point when both valves were used to confirm that the bubble sizes produced from the new technique were still smaller than those bubble sizes created from the single nozzle orifice. Figure 4.22 demonstrates the performances of the two techniques in reducing the average bubble sizes at different injection pressures at the middle of the test section. Overall, the results showed that the average flowing bubble sizes produced from the multiple nozzle were still smaller than those generated by the single orifice nozzle.

Figure 4.22 shows that there is a gradual decline in the average bubble sizes when the MNIT and SNIT was used at the initial injection pressure and the difference between both is slightly small. This is due to the air injection velocity was low to shear the air bubbles. However, then there is a steep reduction in the average bubble size to 2.50 mm when the injection pressure was increased to 2 bar using the new multiple nozzle injection technique. In comparison, the average size with the single orifice was 2.9 mm. Thereafter, the average bubble size declined sharply to 2.17 mm with the multiple nozzle when the injection pressure was increased to 3 bar. The average bubble size produced from the single orifice was 2.76 mm under the same operating conditions. The reduction in the average bubble size between both techniques was

21% at this point. Furthermore, when the injection pressure reached 4 bar, the average bubble size decreased moderately to 2 mm when the multiple nozzle was used in comparison with the single orifice nozzle, where the size was 2.46 mm. The reduction in average bubble size was 15% under these operating conditions. When the injection pressure reached 5 bar, the average bubble size reduced regularly to 1.96 mm, compared with 2.43 mm with the single orifice. The overall reduction in the average bubble size between both techniques was 11% at different injection pressures.
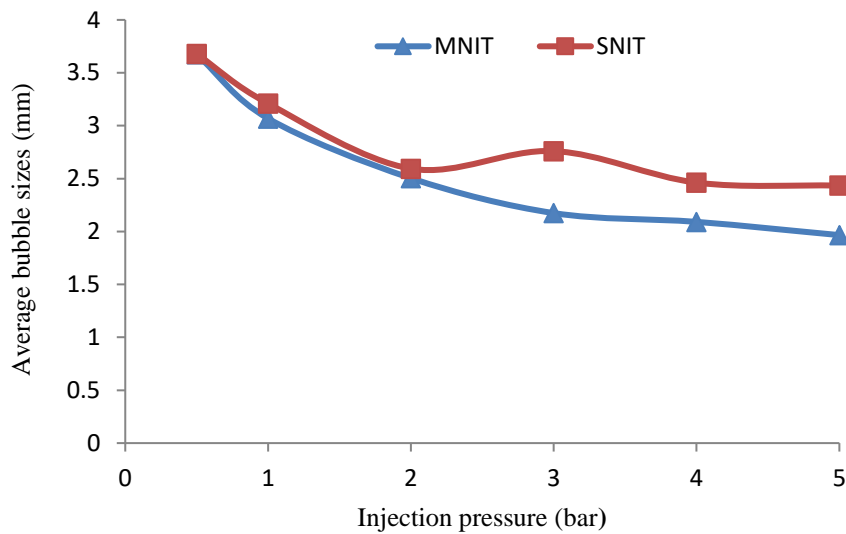
Figure 4-22: The relationship between the average bubbles size and injection pressure for both nozzle configurations at the middle region of the test section

Investigations were also carried out to ensure that large bubble sizes (Taylor bubbles) were reduced and did not develop after 1 metre above the injection point. Figure 4.23 illustrates the comparison between both techniques in reducing large bubble sizes at the middle of the pipe at different injection pressures. In general, the results showed that there was a fluctuation in the average large bubble sizes when the single orifice nozzle was used. In addition, it is noted that the decline in the average maximum bubble sizes was almost the same sizes at the initial injection pressures for both techniques between 0.5 to 1 bar. This is because the air velocity at the injection point was slightly low to shear the air bubbles through the orifices. However, there was a steep reduction to 15.29 mm in the average large bubble sizes when the injection pressure was increased to 2 bar when the new multiple nozzle was used at the region in the

middle of the pipe. In comparison, with the single orifice nozzle the average size was 20.93 mm.

In addition, the reduction in the average bubble sizes was 27% at this point, and then it rises slightly to 15.59 mm when the injection pressure is increased to 3 bar when the MNIT was used, compared with the single orifice nozzle, where it was 24.08 mm. The difference between both techniques was 35.26% in the middle of the test section at 3 bar. As a final point, the average maximum bubble size reduces to 14.63 mm when the injection pressure reached 5 bar with multiple orifices compared to 25.99 mm using single nozzle orifice. It can be concluded that the bubble sizes produced from the multiple orifices are still smaller than with the single orifice even at different heights of the simulated column, due to consistant bubble distribution. The overall reduction in the bubble sizes between both techniques was 21% at different injection pressures.
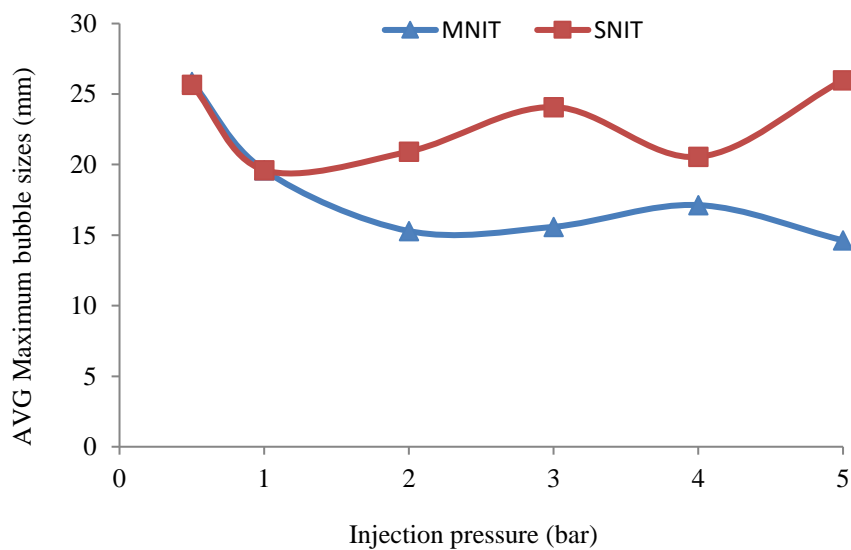
Figure 4-23: Comparison between the two nozzle configurations, 1m above the injection point

Even small bubble sizes were measured at the middle region of the simulated column of the apparatus to ensure that their smaller size compared to the single orifice was maintained. Figure 4.25 illustrates a comparison between the two nozzles in reducing the average small bubble sizes. Overall, the most significant feature shown in Figure 4.25 is that there was a sharp decrease in the small bubble sizes when the injection pressure was increased from 0.5

to 5 bar when the multiple orifices was used in comparison to a gradual reduction in the average minimum bubble sizes when the single orifice nozzle was installed. In addition, at the first injection pressures, the average small bubble sizes produced from the SNIT were smaller than the new multiple nozzles injection technique. Because of at the low injection pressure less than 1.5 bar, the velocity of the air was slightly low through all nozzles of the MNIT to shear the air bubbles compare with SNIT. However, after 1.5 bar injection pressure, the trend in average small bubble sizes from the single orifice became higher than for the multiple nozzles. This means, at this intersection point and operating conditions the average bubble size of air bubbles are the same sizes.

Furthermore, the results also shows that there is a steep decline in the average minimum bubble sizes to 0.92 mm, compared with the average minimum bubble size of 0.93 mm using the single orifice at 2 bar injection pressure. Afterward, it dropped to 0.91 mm when the injection pressure increased to 3 bar using the new multiple orifices, the average size of 0.93 mm. There then followed a moderate reduction to 0.91 mm in the average minimum bubble size once the injection pressure reached 5 bar, compared with the single orifice where the average size was 0.92 mm under the same operating conditions.
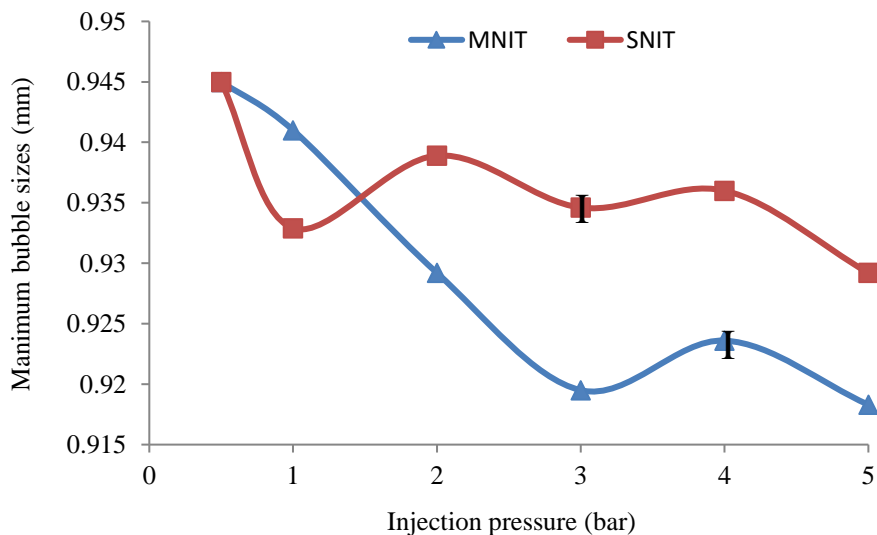
Figure 4-24: Comparison of two nozzle configurations in reducing the average minimum bubble sizes at the middle of the region of simulated column of apparatus

The effect of the velocity of the liquid phase was checked at the middle of the simulated column of the apparatus to ensure that the average bubble sizes produced from the multiple orifices were not affected by this velocity and that the bubble sizes were still smaller than those created from the single orifice. Figure 4.25 demonstrates the effect of the liquid phase velocity on the average bubble sizes at the middle region of the simulated column of the apparatus. In general, the most significant feature on Figure 4.25 is that the average bubble sizes generated from the multiple orifices are still lower than using the single orifice, even if the velocity of the liquid phase was increased.

The results show that as the velocity of the liquid phase rises, the average bubble sizes increase. There is a slight increase in the average bubble sizes to 3.67 mm when the liquid phase velocity was 2.4 cm/s by comparison, where the average size was 4.14 mm. The difference between both techniques was 11.3% at this velocity. Subsequently, the bubble sizes rises moderately to 3.8 mm when the liquid phase velocity is increased to 4.8 cm/s, compared with the single orifice, where the size was 4.85 mm. The reduction in the average bubble sizes between both techniques was 21.64% at this point. Subsequently there was growth in the average bubble size to 4.98 mm at 14.6 cm/s liquid phase velocity. In comparison, the average bubble size was 5.51 mm between two techniques. It can be concluded that the multiple orifices is still capable of reducing the average bubble size at different pipe lengths and different liquid phase velocities.
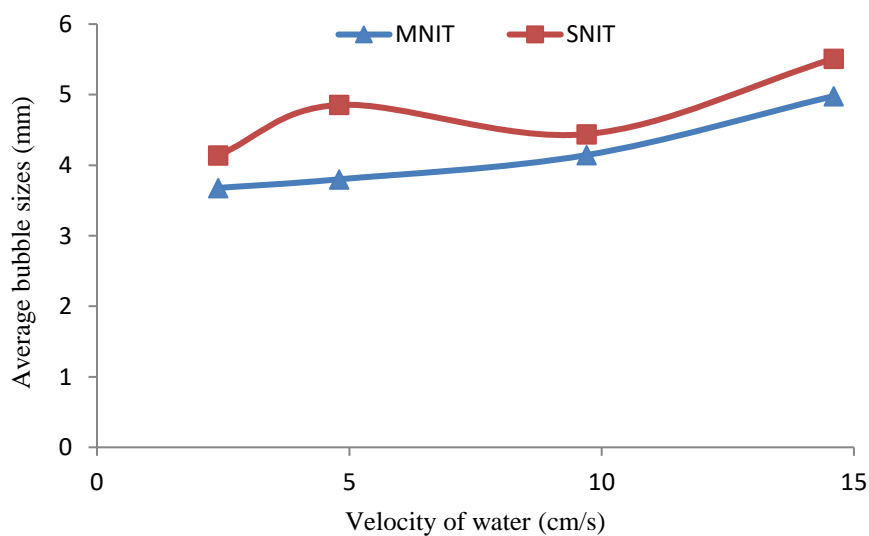
Figure 4-25: The effect of velocity of the liquid phase on the average bubble size for both nozzle configurations at the middle region of the simulated column apparatus

It is essential to track and observe the number and sizes of small bubbles, which are generated from the multiple orifices along the simulated column of the apparatus to ensure that the number of these small bubbles is still higher than with the single nozzle orifice and that the bubbles do not exhibit considerable coalescence. Figure 4.26 illustrates the number of detected bubbles at 1 m above the injection point at different injection pressures using both techniques.

The results show that the number of bubbles produced from the new multiple orifice nozzle is more than the number produced from the single orifice, especially when the injection pressure is increased above 2 bar. As can be seen there is a steep increase in the number of air bubbles to 262 bubbles at 4 bar injection pressure. When both configurations compared together the number is 208 for single orifice. The increment in the number of bubbles was 20.60 % under these operating conditions. Thereafter, it grew sharply, ending at 294 bubbles when the multiple orifices are used at 5 bar and 211 bubbles with single orifice. It can be concluded that the number of small bubbles produced from the MNIT was still higher than the number produced with the SNIT, even at the middle region of the pipe, due to their improved initial distribution of small sizes. It seems that the coalescence rate was reduced when the distribution of bubbles changed from core peaking to wall peaking. This is because these small bubbles travel at almost the same velocity, and thus the chance to coalesce and develop is lower.
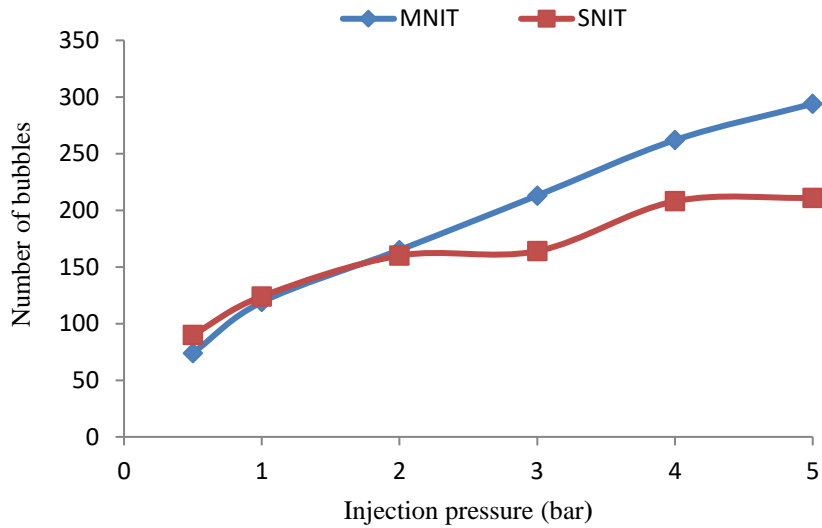
Figure 4-26: The number of bubbles at 1m above the injection point using both techniques at different injection pressures

4.3.5.1 Distribution of bubbles at 1m above injection point

The distribution of air bubbles above the middle of the simulated column of the apparatus found to have the distribution that to be still normal and spread across the entire pipe area (wall peaking). Figure 4.27 demonstrates a comparison between the nozzle configurations in the distribution of air bubbles at 1m above the injection point at 4 bar injection pressure.

The most significant features shows the distribution of air bubbles using the MNIT typified in Figure 4.27 that is still normal and better than the distribution of bubbles when the single orifice is used. It note that the performance of the MNIT in distributing air bubbles increases as the injection pressure increases to 5 bar, and also air bubble sizes are reduced, as shown in Figure 4.28. The results shows that there is a sharp increase in the frequency of smaller air bubbles between 2 and 2.15 mm bubble sizes when the multiple orifices are used compared with the single orifice, where the peak frequency is between 2.47 and 2.56 mm in size. It was found that the bubble distribution of the multiple orifice was across the entire the simulated column with smaller bubble sizes. It can be concluded that the MNIT tends to be more reliable in distributing air bubbles, especially at higher injection pressures, when compared with the single orifice.
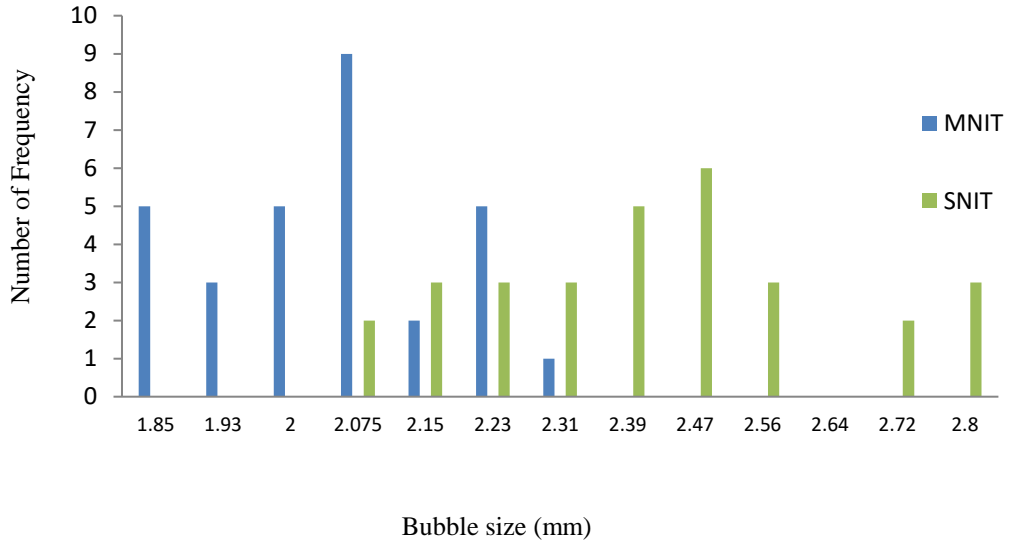
Figure 4-27: Comparison between the distribution of bubbles for both configurations at 1m above the injection point at 4 bar
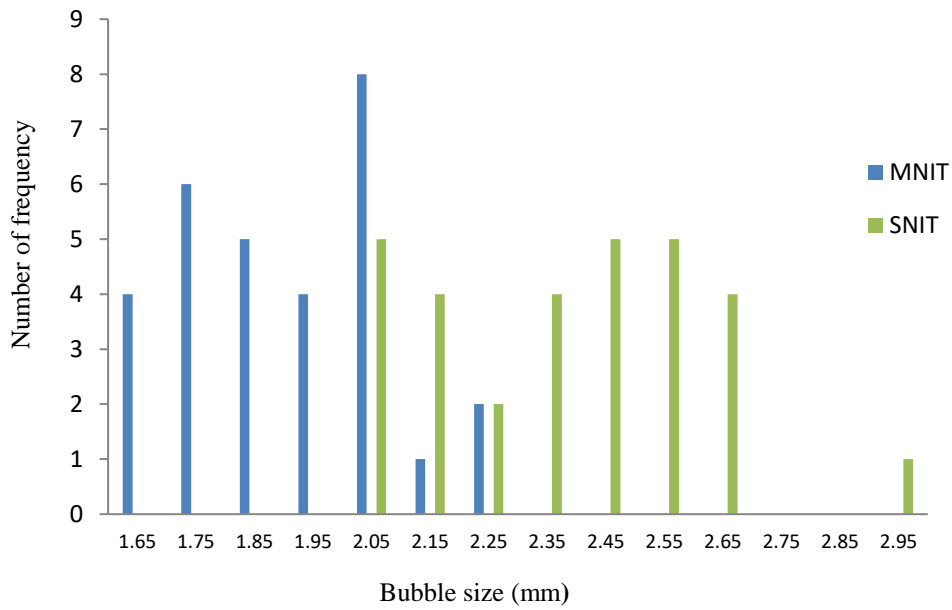
Figure 4-28: Comparison between the distribution of bubbles for both configurations at 1 m above the injection point at 5 bar

4.3.6   Effect of reducing initial bubble size on production rate

The new the multiple orifice nozzle was installed at the injection point, the initial bubble sizes were reduced as discussed in the previous sections, and the distribution of air bubbles improved significantly. As a result of this, the systemic instability within two-phase flow was reduced, the vertical lifting performance was increased and gas lift system became more stable in comparison with the single sharp edge orifice. This was reported by (Hu, 2005) that the systematic flow instability can cause serious flow oscillations within the system. In most cases, these oscillations are a major cause of production losses and are harmful to operational smoothness, safety and efficiency. Figure 4.29 illustrates the performance of the multiple nozzle injection technique and single (conventional) orifice valve in increasing the outlet flow rate (oil production rate) at different injection pressures and a constant inlet flow rate 30 l/min. The flow rate is measured by a digital flow meter at the experiment outlet lines. This digital flow meter measures the volumetric flow rate not mass flow rate. As result of this, there are small differences between inflow and out flow figures. This is due to the complexity of measurement of multiphase flow and it's behaviours within vertical test section.

Overall, the most significant feature shown in Figure 4.29 is the outlet liquid flow rate (production rate): that tends to be higher with the multiple orifice nozzle than with the single orifice nozzle. The results shows that there is an increase to 36.6 l/min when the multiple orifice nozzle injection technique was used at 0.5 bar injection pressure, compared with the single orifice nozzle of 34.8 l/min. The increment in the outlet production rate was 5.2% at low pressure. Afterwards, it rises sharply to 41.2 l/min when the MNIT was used in comparison with the SNIT, which is only 38.6 l/min at 2 bar injection pressure. The difference between both techniques at these operating conditions was 6.7%. Subsequently there was a rapid growth ending at 50.10 l/min at 5 bar injection pressure, compared with the single orifice nozzle, which is 46.6 l/min. Finally, it is concluded that the new multiple orifice injection technique increased the average lifting performance and production rate by 7.5% at different injection pressures compared with the conventional single orifice gas lift.
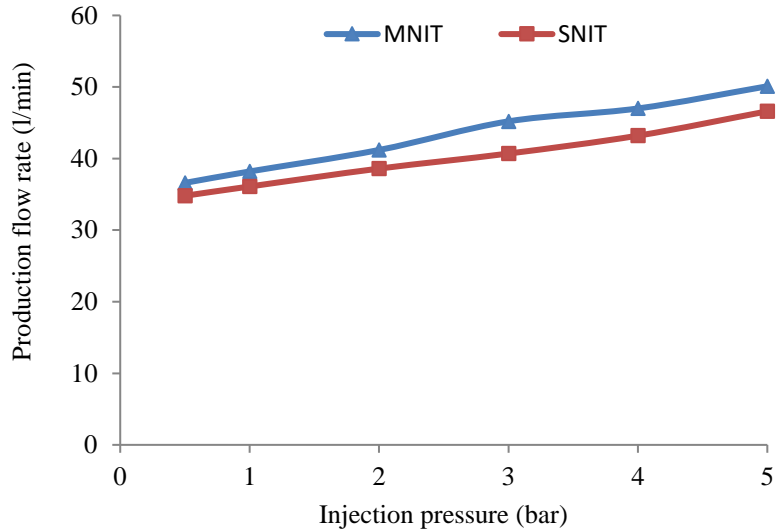
Figure 4-29: Comparison between the performance of the two techniques in increasing (production rate) at a constant inlet liquid flow rate 30 l/min.

4.4 Summary

This Chapter presents the experimental results and discussions of the variables that can affect the growth of bubble sizes within upward two-phase flow and lead to flow instability in gas lift system. The two design configurations that were used Single Nozzle Injection Technique (SNIT) and Multiple Nozzle Injection Technique (MNIT) on a simulated column apparatus for gas lift optimisation were compared against each other. The summary of the findings are as following:

a) § 4.2.1 showed that when the air injection pressure was increased from 0.5 to 5 bars, the average air bubble sizes reduced from 9.75 to 5.06 mm at contant liquid phase velocity 2.4 cm/s.

b) § 4.2.2 indicated that as bubble velocity increases, the bubble sizes increases. However the velocity of bubbles reduced at 5 bar injection pressure.

c) § 4.2.3 showed that as port size increases, the bubble sizes increases and have a negative effect on the stabiltiy of the two-phase flow.

d) § 4.2.4 presented the mechanism of bubble coalescence and development at the middle of the test section when the single orifice technique was used.

e) § 4.3.1.1 showed the MNIT reduced the initial bubble sizes by 22%.

107

f) § 4.3.1.2 showed that the MNIT decreased the average small bubble within two-phase flow by 16%.

g) § 4.3.1.3 indicated that the MNIT is capable in reducing large bubble sizes (Taylor bubbles) by 8%.

h) § 4.3.3 indicated that the MNIT is cable of changing the distribution of bubbles in the simulated column apparatus from the core peaking to wall peaking.

i) § 4.3.5 confirmed that the average bubbles sizes generated from the MNIT are smaller than using the SNIT, even at different length of the test section.

j) § 4.3.6 showed that the lifting performance was increased by 7.5% when the MNIT was used compared with SNIT

The overall effect of parameters on the stability of two-phase flow in gas lifted well can also be summarised in Table 4.3.

Table 4-3: Summary of the effect of parameters on the stability of two-phase flow

Parameters	Stability of Two-phase flow	Lifting performance	Production rate
Port size	The increase of port size has destabilising effect	The increase of port size decrease the lifting performance of gas lifted system	Reduce the production rate because it cause flow instability
Injection rate	At high rate stabilising effect but at low rate destabilising	Increase partially	Increase partially
Injection pressure	Increase has stabilising effect because it reduces bubble sizes	Increase partially	Increase partially
Distribution of gas bubbles	Core peaking distribution has destabilising effect ,however, wall peaking stabilising effect	Core peaking decreasing and wall peaking increasing	Both effects
Reducing bubble sizes	Stabilising effect	Increase	Increase
Single nozzle (SNIT)	Destabilising effect	Reducing	Reducing
Multiple orifice nozzle (MNIT)	Stabilising effect	increase	increase

CHAPTER 5

Two-phase Flow Modelling using Computational Fluid Dynamics

5.1 Introduction

A huge amount of oil and gas are consumed every day and the slightest enhancement in extraction efficiency will have a substantial influence on profits for companies in the oil and gas industry. Therefore, solving the flow instabilities of multiphase flow in gas lift systems is the priority for oil companies. One of the methods used to understand fluid behaviours and optimise multi-phase flow is computational fluid dynamics (CFD) (Çengel and Cimbala, 2014).

The aim of this chapter is to use ANSYS Fluent computational fluid dynamics to simulate and validate the experimental results data. The research will investigate the reasons for flow instabilities and aspects of optimising gas-lift effectively and efficiently. This will be achieved by assessing the effects of operating conditions of flow formation, bubble behaviours, pressure drop, gas void fraction and the interactions between phases. In addition, a novel technique will be introduced to stabilise gas lift systems with potential increase the total oil production rate by replacing SNIT by the MNIT to reduce the initial gas bubble sizes and improve the distribution of gas bubbles in the column. Therefore, a comprehensive three-dimensional gas-lift model was developed to simulate the gas-liquid flow consists of a 66 mm wide and 2 m high gas-lift system, and it will be presented in this chapter.

5.2 Computational Fluid Dynamics (CFD)

CFD is a numerical method in which applied mathematics, physics and commercial computational software are used to visualise fluid flows (gas and/or liquid). The governing equation for CFD is based on the Navier-Stokes equations. CFD can obtain details about the flow field that experiments cannot achieve, such as shear stress, velocity, pressure profiles and flow streamlines. Engineers compare both experimental and numerical data analyses in order to validate their results (Çengel and Cimbala, 2014).

Numerical methods can give initial good predictions of fluid flow in different scenarios before building any experiment, and also they can be used to calculate certain parameters that

cannot be measured in the experiments. The simulation software also allows the user to change variables such as the velocity of oil or gas and pressure outlet. In the last decades, the improvement in computer and chemical technologies has contributed to an increase in research to optimise gas-lift systems using computational fluid dynamics (CFD). There is much literature studying different aspects of fluid behaviours along a vertical pipe (Morel *et al.,* 2010, Ohnuki and Akimoto, 1996, Dai *et al.*, 2013). However, there are not many topics of research on the effect of reducing bubble sizes and bubble formation in gas-lift systems. The following are definitions of common terms that one might come across in this section:

5.2.1   Finite Volume Method (FVM)

The discretisation technique method that is most commonly used in CFD is the finite volume method (FVM). FVM allows the computational domain to divide the domain into control volumes where the variable is located at the centre of the control volume. It integrates the differential form of the governing equations over each control volume using interpolation. This is an advantage for FVM where it ensures conservation: in the cells and globally in the domain. It also allows unstructured mesh or grids, which decreases the computational time. However, the discretised equations also include the values for the cell faces (Stenmark, 2013). Therefore, the interpolation methods are used to obtain approximate values at certain positions. This method affects the numerical stability, convergence rate and accuracy. In the vertex-centred method, the control volumes are constructed around each mesh vertex. The control volume lies within several mesh elements, the discretisation is carried out within each element, and the properties are distributed to the corresponding control volume. The appearance of the shape functions depends on the element type. Figure 5.1 illustrates the two mesh element methods (Stenmark, 2014).
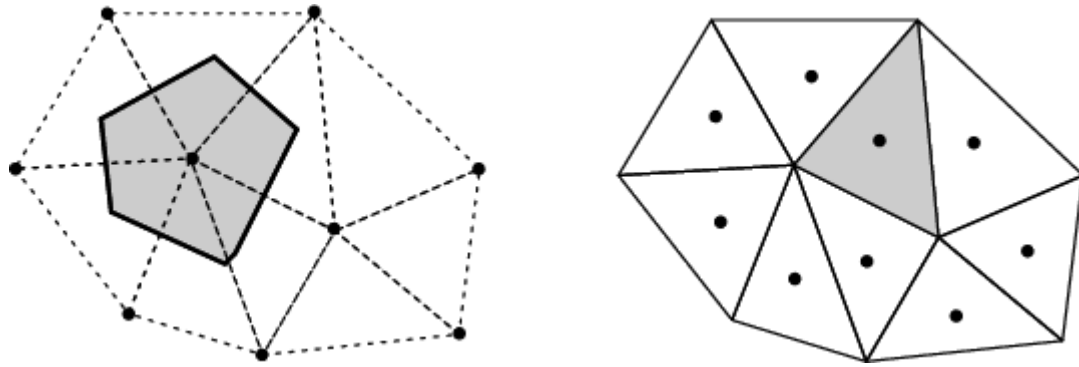
Figure 5-1: The cell-centred (left) and the vertex-centred (right) method (Stenmark, 2013)

5.3   Multi-phase Numerical Modelling Approaches

Models are used in order to describe and predict the fluid flow. As mentioned earlier, modelling a multiphase flow is very difficult due to its complexity and limitations. For example, the procedure is time consuming and the capacity of the computer is not sufficient to cope. This has led scientists to develop models that can be applied to different multiphase flow applications. There are two main types of modelling; Eulerian-Lagrange and Eulerian-Eulerian.

5.3.1   Euler-Lagrange Model

The Lagrangian method is tracking an object to determine its properties. The method is used when a fluid particle is being followed at each point. The fluid properties are then determined as the fluid particles move around. The method does not have a specific boundary layer and it can track fluid movement, direction and location wherever it moves. The method can obtain information by simply following an object's movement (Stenmark, 2013).

5.3.2   Euler-Euler Model

The Eulerian method is observing fluid properties as a function of time and space. The phases in the method are assumed to be continuous. Multi-fluid models are suitable for two-phase gas-liquid flows as both phases are treated as a continuum. Imagine a container where fluid particles can flow in and out. The method can observe and monitor the particles inside the container. However, outside the container the method is not able to monitor the fluid

particles. The model can also be used to simulate a dispersed flow where the overall flow interest area can track every individual particles. The volume fraction should be high in order to describe the dispersed phase is continuum. Each phase is calculated independently and a set of conservation equations is solved for each phase. The model coupled pressure and interphase exchange coefficients need to be modelled. The user must have knowledge of this and it is up to the user which model to include for their simulation. A number of models are suitable for different flow types and this is all based on empirical evidence and developed from other literature. The mixture model is another Eulerian method where the phases are treated as interpenetrating continua. However, in the mixture model the transport equations are based on mixture properties, such as mixture velocity or mixture viscosity. It also solves the mixture momentum equation and can also be used without relative velocities for the dispersed phases to model a homogeneous multiphase flow (Stenmark, 2013).

5.3.3 Volume of Fluid Model

The volume of fluid (VOF) model solves for two or more immiscible fluids, where the interest is the location of the boundary between the fluids. The momentum equations shared by the fluids and the volume fraction of each fluid in each cell are calculated throughout the domain. It solves using a single set of momentum equations and tracking the volume fraction of each of the fluids in the domain.

The transport equations solve the mixture properties, which means the variables are presumed to be shared between the phases. The VOF model tracks the interface between two or more phases, and is suitable for flows with sharp interfaces. In order to obtain a sharp interface the discretisation of the equation is crucial (Stenmark, 2013).

5.4 Modelling Two-phase Flow

5.4.1 Multi-Fluid Modelling

In a gas-lift system a turbulence model will be used in bubbly flow and slug flow regimes. The way to model a multiphase flow is to model one flow regime at a time. It is not always possible to predict the flow transition from one flow regime to another using the same model. Common approaches for a gas-lift system for modelling two-phase flow are the Eulerian-

Eulerian, Eulerian-Lagrange and direct numerical solution (DNS) (Sattar *et al.,* 2013, Dai *et al.*, 2013, Behbahani *et al.,* 2012). The Eulerian-Lagrangian approach uses the discrete bubble model where all particles or bubbles in the gas phase are tracked individually. This approach needs high computational cost and time (Sattar *et al.,* 2013). There are various Euler-Euler models that can be used, for example the mixture model, the Volume of Fluid (VOF) model and the Euler model.

The model proposed by Dai *et al.* (2013) for modelling all flow regimes (bubbly, slug, annular, etc.) in a 3 m long and 189mm wide vertical pipe of Euler-Euler coupled with the multi-fluid VOF approach is the most suitable to implement in CFD. Bubble sizes were on average from 5-15mm, where larger bubbles (>10mm) have more inertia and tend to separate from the incoming liquid. This area of interest is important because they create pockets of high gas volume fraction at the top section of pipe. Through this study, the authors concluded that the pressure gradient and other transport characteristics such as mass and heat transfer are closely related to the flow regimes in the pipe. Most of the numerical models used flow regime to recognise the flow and applied the experimental results to develop empirical correlations to calculate the void fraction, gas-liquid hold-up and pressure drop (Dai *et al*., 2013).

Harasek *et al*. (2010) performed transient ab initio simulations using OpenFOAM-1.6 and implemented a volume of fluid (VOF) model to describe the immiscible gas and liquid phase in a bubble column of Nakao (1983) at very high grid densities (173 million). The VOF model was chosen because the model assumes two or more immiscible fluids in which water and air were used in this paper. The superficial gas velocity was set to V=0.04m/s and a constant pressure of gas inlet was injected into a 1000 mm column filled with water for six seconds in real time. However in this case, they did not use any turbulence model due to the unphysically slow rise of the air bubbles and assumed that the turbulence model was giving unphysical results. Harasek *et al.* concluded that the simulation produced a good agreement with the experimental results, showing good gas hold-up results in the bubble column.

Further studies made by Yasin *et al.* (2014) proposed a two-phase CFD simulation using an Euler-Euler model with a mixture model to calculate the gas-liquid flow in the pipe, varying the injection depth on vertical upward flow and the effect of the gas injection rate. This paper focused on velocity as the main variable of the flowing fluids. Three different depths of injection rate of 5, 15 and 25 metres from the casing shoe were studied. From the literature, it

was found that the gas-lift system was installed as deep as possible. The results determined that the lowest injected point had the highest velocity of 3.02 m/s. Furthermore, the effect of the gas injection rate was further developed and it was shown that the gas injection rate significantly increased the oil production rate because the density and the hydrostatic pressure in the column are reduced. Thus, the velocity increases, flowing vertically upward. because the total pressure depends on the static pressure losses, which is a function of the fluid density, and the dynamic pressure losses, which are due to the flow regime in the column. In a gas-lift system, static pressure has a constant gravity and height. Thus, the only variable that can be changed is the density of the fluid. Conversely, the introduction of a gas phase to the flow is crucial because the gas is less dense than the liquid. However, fluid instabilities known as slippage can occur during the flow. Thus, the gas phase will move faster than the liquid phase, consequently reducing the production rate, and it would be economically inefficient. Additional research of economic analysis needs to be performed in order to determine the optimum gas injection rate for certain wells. The author concluded that the lower the gas injected, the higher the velocity of flowing fluid in the gas-lift system. The CFD model showed that when the gas injection rate was increased by 20%, the velocity of flowing fluid increased by 1.7%.

Guet *et al.* (2004) developed a numerical model based on the Euler-Euler modelling approach for predicting the radial profile of the void fraction and velocity due to bubble size changes. The results obtained were compared with the experimental results shown in the literature. Furthermore, the model was used to conclude the bubble size effect on the gravitational pressure gradient by calculating the drift-flux distribution parameter depending on the bubble size and liquid input. Other studies carried out by Behbahani *et al.* (2012) reported that the radial profiles were affected by forces from turbulent dispersion, lift and the wall. They learned that to predict the correct value of peak void fraction they had to reduce the standard Tomiyama lift and wall forces.

Stenmark (2013) compared multiphase flow in a vertical T-junction using ANSYS Fluent and CFX. The numerical model was validated using an experimental model of air-water mixtures in a T-junction with a horizontal branch. The focus of this paper is to predict the flow phenomenon and investigate the effect accurately using different settings of the numerical solver. The Euler-Euler model and the gas dispersed phase diameter were chosen. Stenmark concluded that the predicted volume fraction was in good agreement, however the velocity

was in low agreement. Thus, additional models were added for polydispersed flow to increase the agreement for velocity.

Tabib *et al.* (2008) modelled 3D transient CFD simulations of a bubble column using three different turbulence closures of $k - \varepsilon$, RSM and LES models and implemented a sensitivity study of different interphase forces (drag, lift, turbulent dispersion and added mass). The purpose of this paper was to compare the turbulence models that could predict the experiment carried out by (Bhole *et al.,* 2006, Kulkarni *et al.,* 2007). They concluded that the RSM model was in better agreement than the $k - \varepsilon$ in predicting the turbulent kinetic profiles, whereas the LES model performed well at predicting the average behaviour of the flow. Conversely, they determined that the LES model was best at simulating flow structures and instantaneous flow profiles. In the interphase forces, the drag law of (Zhang and Vanderheyden, 2002) was the best; and the lift coefficient by Kulkarni (2003) was found to give better predictions. Turbulent dispersion is concluded to be intuitive and for the added mass there are no significant contributions.

Behbahani *et al.* (2012) explored a multi-fluid Euler-Euler model with the standard $k - \varepsilon$ to predict bubbly flow in an 80D air-water vertical pipe simulation. The models were tuned with the help of direct numerical solution (DNS) and experimental data. They used many experimental studies conducted by other researchers (Prasser *et al.*, 2003, Lucas *et al.,* 2005, Liu, 1998, Wang *et al.,* 1987) and compared the results to different numerical studies. The multiphase flow in the well is assumed to be isothermally incompressible, with no mass transfer, in one continuous phase and one or more dispersed phases. The authors also tuned the proposed model to simulate gas lift in an oil reservoir of 20 m height, 73 mm diameter and 8mm gas diameter. Four different bubble sizes (2, 3, 4.5, 5.5 mm) were used and for each size, four gas superficial velocities (0.05, 0.1, 0.2, 0.3 m/s) were simulated. The multi-fluid model was validated and plotted on a graph with eight other correlations for the bubble flow regime carried out by the researchers. (Guet, 2004) had the most accurate results predicted in all ranges of bubble diameter.

Deen *et al.* (2001) compared the LES and $k - \varepsilon$ turbulence models in modelling a bubble column reactor. Previous studyies considered the lift and virtual mass force, however the result showed no influence on the study. The LES was able to capture the transient movement of the bubble plume significantly compared to the $k - \varepsilon$ turbulence models. The results

concluded that the velocity and velocity fluctuations showed quantitative agreement with the experimental results.

5.4.1.1 Bubble Coalescence and Break up

Morel *et al.* (2010) modelled a numerical simulation of isothermal bubbly flows with different bubble sizes using the Multi-Size-Group (MUSIG) approach. They tested four different approaches and used isothermal flows without phase change as a first stage. The approaches were: single approach for bubbly flows (Wu *et al.,* 1998b), first moment density approach using a bubble diameter distribution function represented by a log-normal law, second moment density approach using a bubble diameter distribution function represented by a quadratic law and multi-field (MUSIG) approach. (Lucas *et al.,* 2005). They took into account the bubble coalescence and break-up phenomena, as well as the gas expansion due to compressibility. The first method chosen by Wu *et al.* (1998b) was the single approach for the bubble coalescence and break-up. It gave reasonable results in the experimental case. The first method of the moment density approach based on log-normal law was able to model the bubble coalesce but not the bubble break-up due to the divergence of the log-normal law. The second method of the moment density approach assumed the quadratic law parabolic shaped function; due to this, it was not able to reproduce the bubble coalescence and break-up. The multi-field approach was tested using the CFD simulation to model bubble coalescence and break-up. Morel recommended further investigations into the effect of bubble diameter range, model discretisation, and bubble coalescence mass exchange.

Sattar *et al.* (2013) developed the population balance modelling approach, where the author predicted and tracked the number density of different bubble classes ranging from $1.57 - 12.56$ mm. The model illustrated an improved bubble break-up and bubble coalescence based on work undertaken by Hagesaether *et al.* (2002) and also concluded that the Sauter mean diameter increased as the height increased. The paper used the Euler-Euler model, as the liquid is considered as the continua and the gas (bubbles) is considered as the dispersed phase. The simulation was carried out in a cylindrical bubble column. The bubble column was 4,600 mm high, with 78 mm internal diameter and an inlet diameter of 2.34 mm. The stationary liquid in the model was filled in the column and gas was injected at the bottom with a gas superficial velocity of 0.01, 0.02 and 0.06m/s. The momentum interfacial exchanges are also important. They take into account the effect between the gas phase and

liquid phase interaction by using the interfacial momentum source. The turbulence k-e model was used and the momentum and turbulence were classed as first order upwind. The results showed good agreement with the experimental results.

Pourtousi *et al.* (2015) implemented sensitivity analysis to determine the effect of bubble size at different superficial gas velocities and illustrate the bubble formation and flow regime inside the bubble column.

It is assumed that in the column, the interaction between the dispersed gas and the liquid affects the interphase forces (drag, lift, and so on), turbulence and bubble diameter. Thus, the correct selection of numerical settings is needed to simulate an accurate model.

The Ansys CFX 13 solver was used to simulate the numerical model using an Euler-Euler model with the SIMPLEC procedure to calculate the equation coupled with the total variation diminishing (TVD) method and the maximum Courant-Friedrichs-Lewy (CFL) number must be less than one to improve the accuracy and use less computational effort in comparison with other methods. The operational conditions, gas-liquid properties and flow regimes depend on bubble shape and diameter. Therefore, experimental observation and a sensitivity study of bubble diameters on the accuracy of flow patterns are needed. One bubble size can be used for the numerical study to lower computational cost. The Schiller-Naumann drag model is appropriate for spherical bubble shape. The results shown in the numerical model were computed for 1400s for various bubble sizes (3-5.5mm). The paper established that the 3mm bubble is in good agreement with the experimental data for superficial gas velocities ranging from 0.0015 to 0.025m/s. However, these numerical settings are used for low gas velocities.

Deju *et al.* (2013) assessed the gas-liquid flow using population balance modelling (PBM) to capture bubble coalescence and break-up. The authors uses two particular PBE methods; namely the direct quadrature method of moment (DQMOM) and the Multi-Size-Group (MUSIG) model. The computational fluid dynamics ANSYS CFX 11 was used and the average bubble number density was added to capture the flow. The DQMOM was observed to be closer to the measurements compared with the MUSIG. This emphasised the key parameters of coalescence and break-up kernels have a vital role in predicting the physical behaviour of bubble size evolution for different PBE methods. The assumption of a spherical bubble will work in a bubbly flow, however in the case of slug flow or Taylor bubbles, the wake entrainment and surface instability could become significant. Thus, there is greater

118

emphasis on improving the interfacial force model, including other possible bubble mechanisms.

Further studies by Khan *et al.* (2015) proposed a signal processing based technique to calculate and classify bubble size. The numerical model is run using ANSYS Fluent and the volume of fluid model was used. The captured data are analysed using signal processing. Signal processing is a scheme to classify and determine the size of bubbles with a short-time Fourier transform base. A cylindrical vessel was filled with water to a height of 40mm. Tetrahedral elements was used to refine the grid at the air inlet. Air was injected at the bottom of the tube with a radius of 1mm at four different velocities of 0.02, 0.05, 0.2 and 0.4m/s. A SIMPLEC algorithm is used for pressure-velocity coupling and a first-order implicit time scheme with convergence criteria of 0.001 was used. The results showed that the proposed technique is able to predict the bubble size with information from bubbles passing through a single sensor point.

Taha and Cui (2006) assessed the motion of single Taylor bubbles in vertical tubes. The authors also investigated the Taylor bubbles in stagnant and flowing fluids to obtain the complete bubble formation. The volume of fluid (VOF) model was implemented to capture the shape, velocity magnitude and velocity distribution of the slug flow and was compared with experimental findings. It was found that the Taylor bubbles had a cylindrical body with a spherical nose and fluctuating tail.

5.4.1.2 Turbulence Model

Turbulent flow is much more difficult to solve than laminar flow. The flow field is always unsteady and turbulent eddies occur in three dimensions where random, swirling and vortical structures take place. Turbulence models are to solve turbulent flow solutions. The turbulent flow simulation needs a fine and quality grid to resolve all the unsteady three- dimensional turbulent eddies. The models have additional transport equations that enhance mixing and diffusion of turbulence that must be solved along with the mass and momentum equations (Çengel and Cimbala, 2014).

For a gas-liquid flow, there is no standard turbulence model (LES, DNS, $k - \varepsilon$, $k - \omega$, etc.) specifically used for this case. From numerical investigation, one turbulence model that is widely used for gas-liquid bubbly flow in a vertical pipe is the two transport equation model; the $k - \varepsilon$ model. The model is preferred to predict the liquid flow pattern and gas hold-up because of its lower computational cost, and it provides good results and the simplest algorithm (Sattar *et al.,* 2013, Pourtousi *et al.,* 2015, Behbahani *et al.,* 2012).

For the disperse bubbly phase, a zero equation turbulence model is used while the standard $k - \varepsilon$ model is applied for the continuous phase. These two turbulence methods have better performance when the coalescence and break-up occur under higher superficial gas velocity, hence the $k - \varepsilon$ model is commonly used for simulating 3D gas-liquid flow (Pourtousi *et al.,* 2015), where k is the kinetic energy and ε is the turbulent dissipation. Turbulent dissipation is the rate at which velocity fluctuations dissipate. The equations are solved simultaneously with the equations of mass and momentum. However, the variables are not necessarily known, and instead it is used for specifying turbulence intensity and turbulent length scale (hydraulic diameter). Turbulent models are heavily reliant on the approximations of empirical constants for mathematical closure of the equations (Behbahani *et al.,* 2012). Furthermore, two new equations will add two additional boundary conditions specific to the turbulence properties at inlets and outlets. Most of the literature uses the standard $k - \varepsilon$ model, which is suitable for the turbulence model to capture the flow inside the column, especially when the Reynolds number is low (Çengel and Cimbala, 2014).

5.5   Numerical Simulation Methodology

5.5.1   Introduction

Fluid flow in a gas-lift system is extremely complex and the user needs to have a well-rounded knowledge in a multiphase flow and computational fluid dynamics (CFD) background in order to design and simulate the fluid behaviours in a gas-lift system. This system is a widely used technique that uses high-pressure gas to lift reservoir fluid to the surface artificially. In simple terms, the principle of gas-lift is that the gas is injected down into the well to reduce the density of the reservoir fluid, which then decreases the flowing pressure gradient and then the bottom-hole pressure so that it is lower than the static pressure,

thus allowing the fluid to flow in the wellbore and to the surface facilities. There are many advantages of gas-lift, such as outstanding flexibility with wide ranges of depth, especially for offshore oil wells as well as low maintenance and operating costs. Gas-lift optimisation is an important process to achieve optimum design and efficient operation, and thus the operating parameters must be understood.

Furthermore, the relationship between the development of flow regimes and design assumptions must be considered, as it will influence significantly the total production rate from this method. The gas-lift method undergoes a huge pressure drop, turbulence of flow and mixing of fluids with different densities along the production tubing. Computational fluid dynamics (CFD) has developed into a powerful tool to simulate the operating parameters in a gas-lift system in different scenarios. The CFD software enables the user to incorporate a multiphase model with turbulence and a discrete model to capture or emulate a real-world gas-lift. In addition to solving the mass and continuity equations for the continuous phase, the discrete phase model (DPM) allows simulation of a discrete phase (spherical bubbles) dispersed in the continuous phase (liquid). This will help to gain exceptional knowledge of the factors affecting the flow instability, which influence total production flow rates and cause operational problems such as gas compressor shutdown in this system. The discrete phase model will provide further insights into the dynamics of multiphase flows. It also predicts the trajectory and interaction among the gas bubbles in dispersed flow (discrete phase particle). Thus, the discrete phase model is very important for reasonable predictions of bubble formation.

The objectives of this simulation study are:

(i)   To investigate the upward two-phase flow behaviours that are capable of causing flow instability in a vertical column, using a multi-fluid Volume of fluid (VOF) model, and assess their applicability in predicting the local dynamic flowing fluid behaviours, such as pressure, pressure drop, void fraction and velocity, which are relevant in a gas-lift system.

(ii)   To reduce the initial bubble sizes and improve the distribution of flowing air bubbles by replacing the conventional single orifice gas lift valve (SNIT) by a new gas lift valve with the multiple nozzles injection technique (MNIT) at the injection point at the bottom of the vertical column.

(iii)   To enhance the lifting performance and increase the total oil production rate from gas lifted wells by stabilising the upward two-phase flow behaviours using a gas injection rate that is the same as or lower than other existing techniques.

This section presents the simulation design steps that were used in the study: the computer-aided tool (CAD), the design stages of the new technique, boundary conditions and flow parameters for the numerical simulations.

5.5.2   Numerical Simulation (CFD)

The research focuses on understanding the main cause of the flow instability in gas-lift systems using numerical methods. This will give more details about upward two-phase flow behaviours in the vertical column in this system. Moreover, the results obtained from these numerical simulation methods will be benchmarked with experimental results. Hence it was important to learn about different multi-fluid modelling methods to capture the two-phase flow behaviours concerning bubble breakup and bubble coalescence. The software used will be presented in this section. The fluid flow in the gas-lift system will be simulated in three dimensions. It is important to have some background in computer aided design (CAD) software that will be used in order to build a comprehensive 3D model. There will be a brief description of (CAD) software, Rhinoceros 5 and ICEM CFD (Integrated Computer Engineering and Manufacturing) used for geometry and mesh generation respectively. Also, the commercial computational fluid dynamics (CFD) programme, ANSYS (Analysis System) Fluent, will be introduced.

5.5.3   Computer Aided Design (CAD)

5.5.3.1   Rhinoceros software

Rhinoceros, also known as Rhino or Rhino 3D, is a versatile 3D CAD modeller that allows a detailed and accurate model design. A 3D gas lift model will be constructed consisting of a 2 m long vertical pipe with an injection point 0.1m from the base of pipe using the NURBS (Non-Uniform B-Spline Surface) curves and surfaces, a feature in the Rhinoceros Computer Aided Design (CAD) tool. This design tool is very accurate as it supports scalable geometrical entities having parametric curves and surfaces up to 3-5 degrees (Rhino,

2016)(Rhino 3D, 2015). These gas lift 3D models are constructed in different scenarios, then imported to CFD software to investigate the fluid behaviours. The properties and accuracy of the 3D models' geometries are summarised in Table 5.1:

Table 5-1: Properties and accuracy of 3D models

Grid properties	Units (layouts and models)
• Grid count = 200 • Minor grid line every 0.05 metres • Major lines every 10 minor grid lines	• Absolute tolerance $(1e^{-10})$ • Relative tolerance $(1e^{-10})$ • Angle tolerance $(1e^{-2})$ • Unit is metres

5.5.4 ICEM CFD (Grid Generation)

ICEM CFD is a meshing software that can produce high quality volume or surface meshes with minimal effort. In ICEM CFD, structured and unstructured mesh blocking approaches can be applied for tetrahedral or hexahedral meshes in a simple and complex geometry (Ansys Inc., 2016b). According to Çengel and Cimbala (2014), generating the grid on a model is one of the most important steps in CFD, as it has a great influence on the solver convergence and solution. The flow domains are split into smaller cells and the grid designates the cells on which the flow is solved. Factors that can affect the mesh quality for a good solution are skewness, mesh refinements, grid density, element quality, aspect ratio, and so on. Those factors were carefully treated and checked within the model to ensure quick convergence and accuracy in the numerical solution. Sattar *et al.* (2013) generated two different meshes of the model with a total number of elements of 148,127 and 293,307 respectively. Both models were run identically and when compared, the results showed no significant differences, and thus the 148,127 mesh was used. Furthermore, Pourtousi *et al.* (2015) also did a mesh sensitivity study where three different qualities of mesh were generated of 40,500, 59,000 and 82,320 elements. The grid proved that the denser or more closely compacted grid increased the accuracy of the results.

5.5.5   Fluent

Computational Fluid Dynamics Fluent software is a product by ANSYS. The Fluent software contains a comprehensive suite and it is widely used for modelling fluid flow and other related engineering applications. It has the ability to simulate a wide range of phenomena: mixtures of liquids and gas, turbulence, heat transfer, and reactions for industrial applications and the transient flow phenomena are quickly solved (Ansys Inc., 2016a). It provides the tools needed to investigate two-phase flow instabilities.

Fluent software will solve conservation equations for mass and momentum and for flows involving turbulence, and an additional equation for viscous and transport equation is solved. Fluent is based on the robust finite volume method (FVM) discretisation technique and it allows the user to use segregated and coupled solution methods. As mentioned in the previous section, the FVM method divides the domain into small control volumes where the choice of discretisation method will also dictate the results in other multiphase models. Hence, the volume of fluid (VOF) method interface is retained as dispersed. Furthermore, Fluent contains a number of discretisation techniques. To model the interfacial momentum forces, the equations of drag, lift and wall forces can also be solved (Stenmark, 2013).

In a gas-lift system, to model the dispersed phases with two-phase gas-liquid flow, there are three main approaches. The default settings will assume the dispersed phase has a constant diameter defined by a user-defined function (hydraulic diameter). However, bubble coalescence and bubble breakup are not considered. To investigate the dispersed phase, the population balance modelling (PBM) or the interfacial area concentration (IAC) settings can be used. The IAC is the interfacial area between the two phases and the approach is a more simple technique than the PBM in which only one additional transport equation is solved per secondary phase. Furthermore, the IAC model can simulate the bubble coalescence and bubble breakup. However, it cannot predict the distribution of particle sizes. The PBM method in Fluent as described in the previous sections allows three methods to solve: the discretised population balance, the Standard Method of Moments (SMM) and the Quadrature Method of Moments (QMOM) (Ansys Inc., 2013). In discrete methods, the particles are individually separated by a finite number of size intervals.

This approach is really appropriate to use when the size is known and assumed to be constant throughout the domain. However, the computational effort can be heavy if the number of intervals is excessive. In the SMM method, the population balance modelling is converted to

a set of transport equations for moments of the distribution, however this may reduce the number of equations to be solved significantly compared to the discrete method. SMM is very useful when the overall quantities and average are sufficient to represent the particle distribution. The QMOM is implemented in a wide range of flow cases, and exchanges any closure required compared to the SMM. Please see the ANSYS Fluent Population Balance Module Manual for a more detailed description (2013).

5.5.5.1   Numerical CFD Modelling

A typical CFD analysis will be broken down into three main stages: pre-processor, solver, and post-processor.

Pre-processor:

1. Create a gas-lift design on Rhinoceros 5; export the design using a STEP file.
2. Create a quality grid on ICEM CFD 17.1 and list the boundary conditions. Export the grid using an Unstructured Mesh file and read the mesh on Fluent;

Solver:

3. Apply the settings and boundary conditions and then solve the numerical problem on Fluent 17.1 by using a turbulence model and multiphase model; Grid Independency test.
4. Monitor the convergence of the model;

Post-processor:

5. Visualise and analyse the CFD results on CFD-Post 17.1. Validate the model using the experimental results;
6. Further analysis on the validated numerical model. Figure 5.3 describes the computational fluid dynamic simulation method that will be followed in this research.
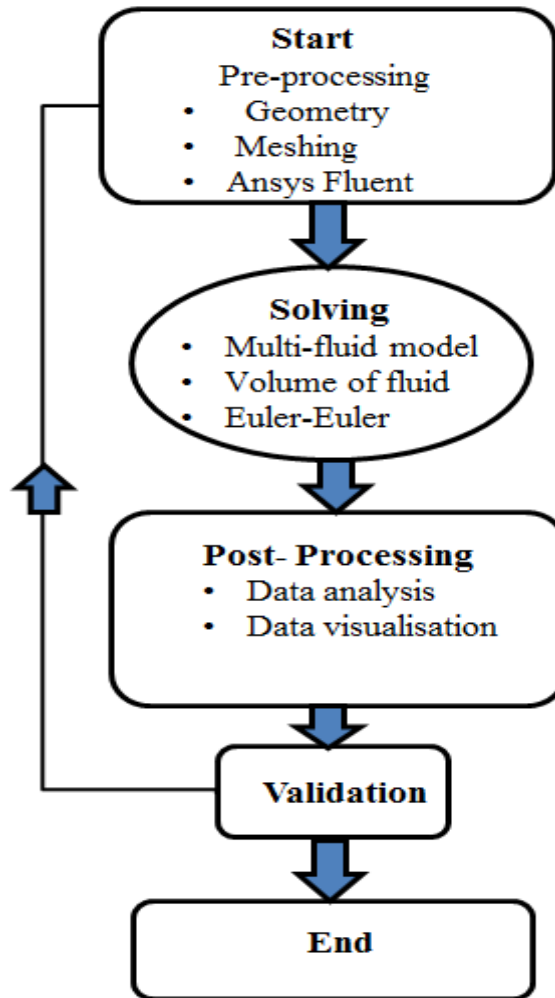
Figure 5-2: Computational fluid dynamics (CFD) simulation flow chart

5.5.6   The Numerical Design of the Gas Lift Model

The gas lift simulation model was simplified as much as possible to concentrate on the area where the flow instability phenomenon occurs within the simulated column of the apparatus, starting from the gas injection point at the bottom of the test section, and also to avoid complication in the construction of the model. The geometry dimensions of the model are shown in Figure 5.4. The gas lift model consists of 2000 mm high, 66 mm internal diameter with an injection point 0.1 m from the base of the pipe as shown in Figure 5.3. The gas injection point was changed for the first scenario for the different port sizes of 0.2, 1, 2, and 4 mm when the orifice valve was used as shown in Figure 5.5, to investigate the effect of varying the port size on the stability of upward two-phase behaviours, and also to compare with the new technique with multiple nozzles injection (MNIT). The MNIT consists of five

small nozzles, each of 1 mm diameter, as shown in Figure 5.6. In addition, the total diameter of the five nozzles was calculated as 2.24 mm as shown in Table 3.1, and then this new technique was compared with the single (sharp edge) orifice technique (SNIT) with the same port size of 2.24 mm. Furthermore, the lifting performance and distribution of the void fraction in the column of both valves were investigated to ascertain which one of them was better to stabilise the system and thus increase the oil production rate of the gas lift method. The parameters of the gas lift geometry model are listed in Table 5.2. The model design was created in Rhino 3D and saved as a STEP file in order that it would be recognised by ICEM CFD. In this case, the simulation type is a turbulent two-phase flow. The parameters defining the flow in the domain taken from the experimental study are listed.
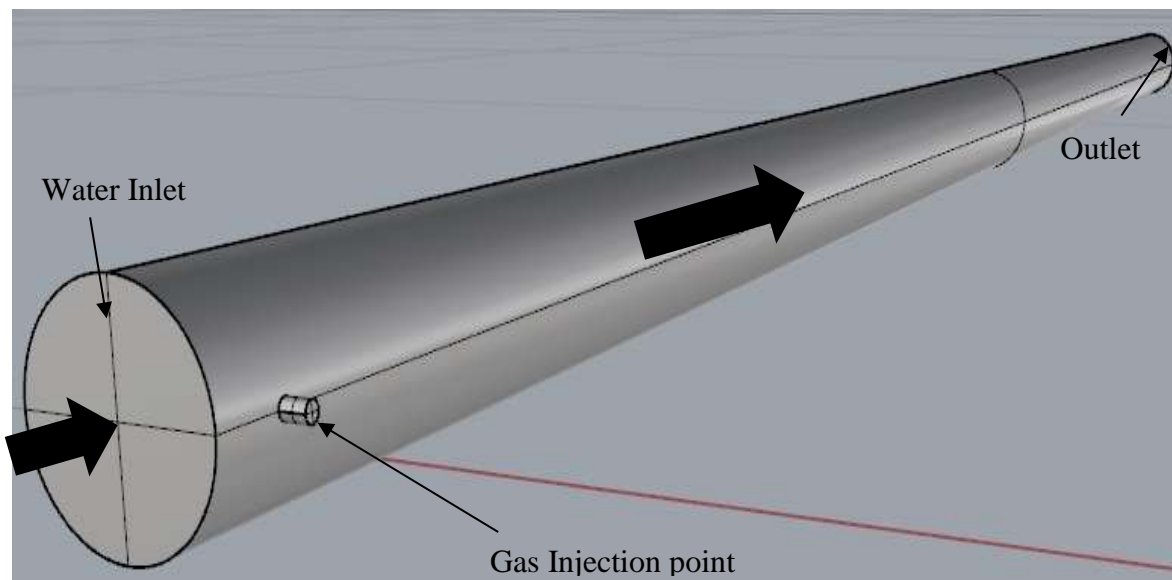
Figure 5-3: Gas lift simulation CAD model
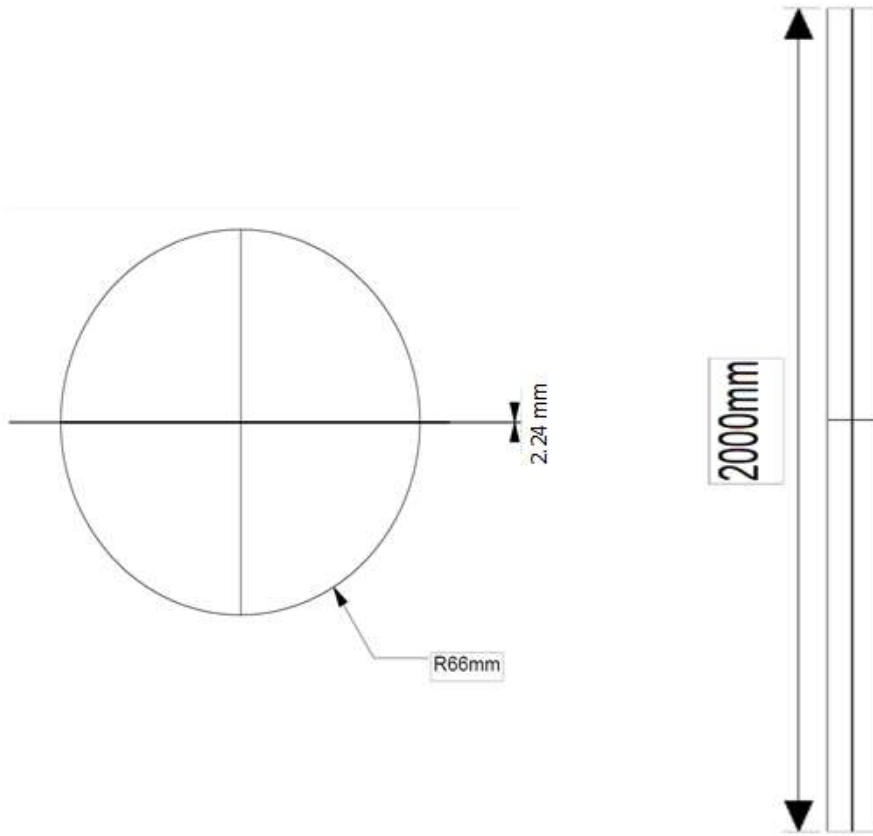
Figure 5-4: Dimensions of gas lift geometry simulation model
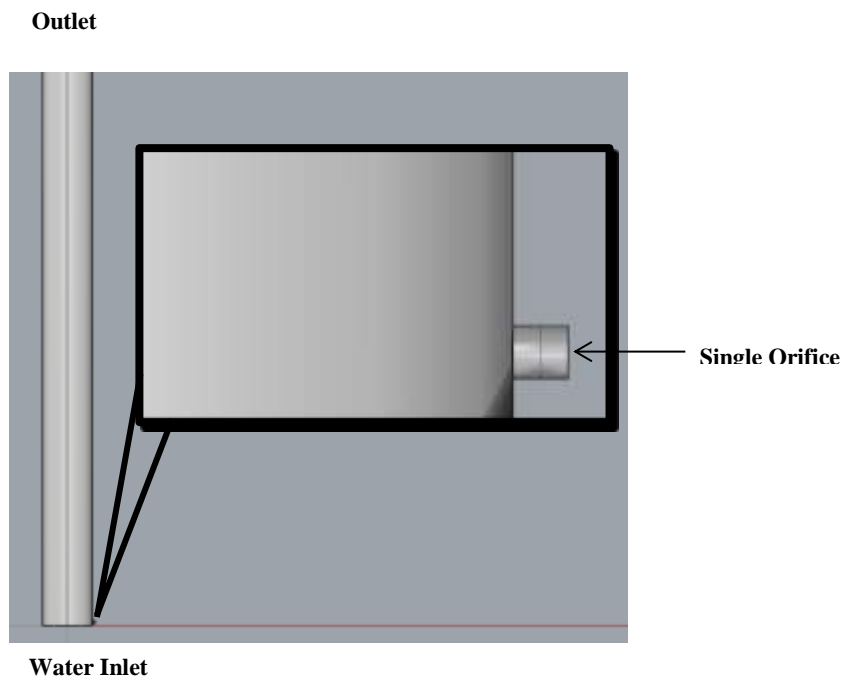
Figure 5-5: Gas injection point with an orifice of 2.24 mm

128
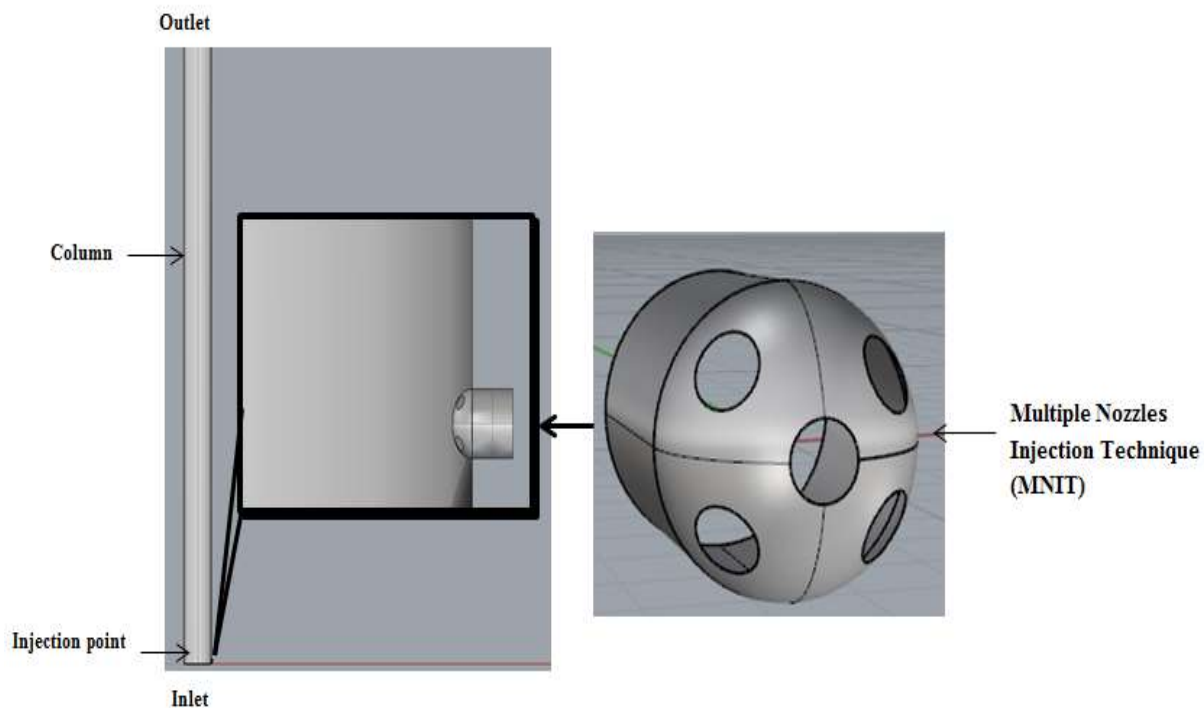
Figure 5-6: Gas injection point with 2.24mm (MNIT) (Each nozzle diameter is 1mm)

Table 5-2: Parameters of gas lift geometry model

Parameter	Value	Units
Length of pipe	2000	mm
Internal diameter of pipe	66	mm
Orifice Diameter	0.2, 1, 2 , 4	mm
Diameter of each nozzle of (MNIT)	1	mm

5.5.7 Mesh Generation

The grid domain of the gas lift column was created using ANSYS ICEM CFD 17.1. During modelling and mesh generation, simplification of complex shapes was taken into consideration, as the production tube and gas injection pipe were assumed to be cylindrical with a smooth surface. An unstructured meshing approach was used to create the mesh with only tetrahedral cells. Refinements of 0.05 mm were added near the junction of the gas inlet. The distribution of cells at the inlet and near the connection can be seen in Figure 5.7. Furthermore, two different grids of the models was generated – 448,044 elements for the model with the orifice valve and 547,090 elements for the model with the multiple nozzles injection (MNIT).

Table 5.3 lists the properties for the mesh generated. Furthermore, the hexahedral mesh may perhaps be employed in the geometry, however due to time constraints, the geometry grid volume near the junction is unstructured. Therefore, the tetrahedral mesh was selected for the gas-lift model. The junction is the main area of interest where fluid instabilities begin to occur, and thus refinements were made. The mesh statistics of the grid are shown in Table 5.3.

5.5.7.1 ICEM Interactive Mesh

1. Start by opening Workbench and double click the Fluid Flow (Fluent) project.
2. Upload or import geometry of the step file (Rhino) in the DesignModeler.
3. Generate the uploaded geometry to the project and create the named selection that has two inlets and one outlet.
4. Launch the ANSYS meshing application and edit the mesh by assigning a tetrahedron mesh, set on patch independent with Interactive ICEM CFD.
5. Additional settings applied before generating mesh.
6. Create a refined mesh by applying edge sizing to the junction of the pipe and alter the global mesh sizing by changing the minimum and maximum element sizes.
7. Once done with the alteration, generate mesh and save the unstructured mesh file (MSH).
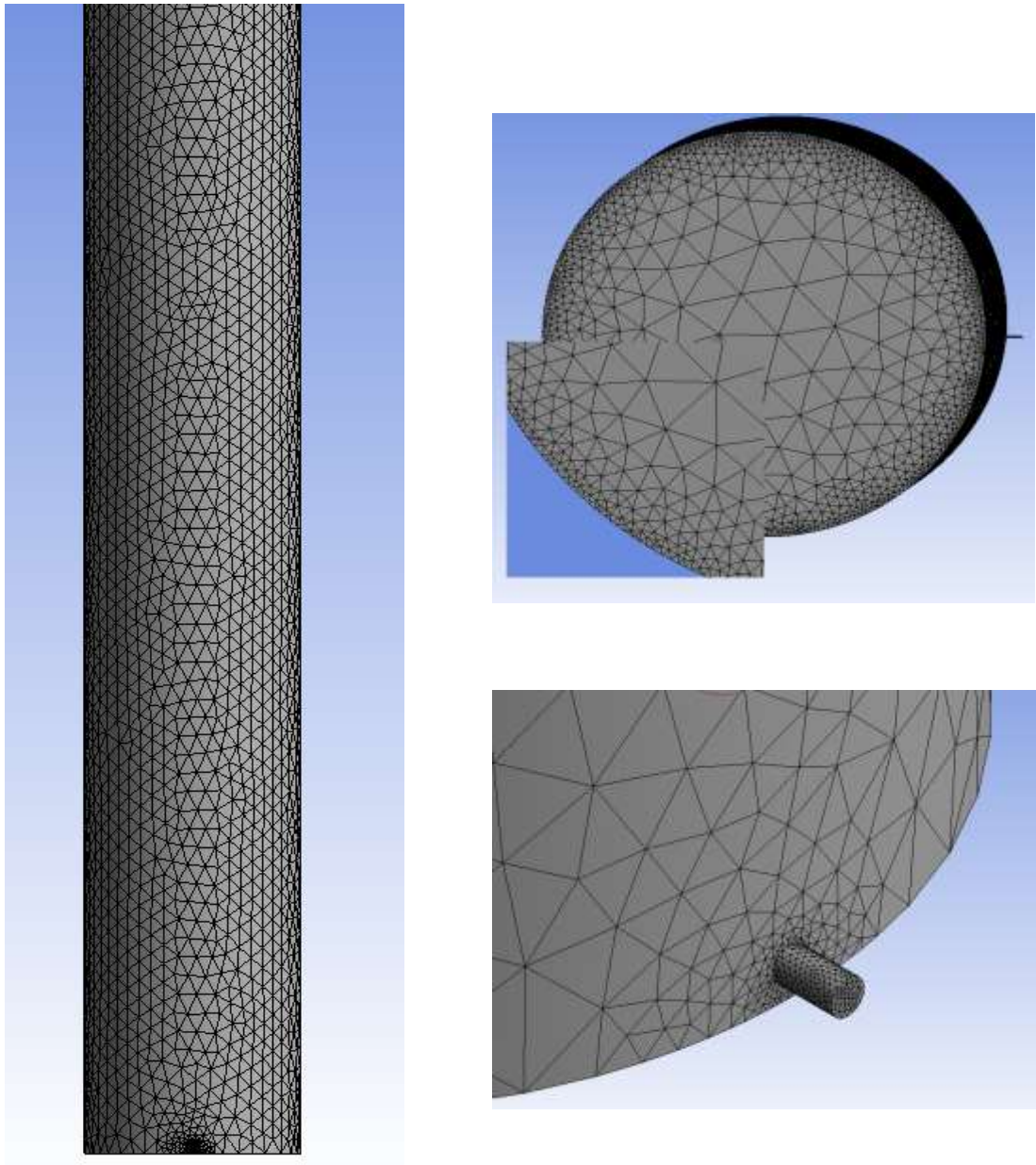
Figure 5-7: The mesh of the gas lift model

Table 5-3: The mesh statistics & quality

Mesh	No. of elements	Skewness	Aspect ratio	Element quality
Orifice	448,044	0.11653	1.6495	0.90071
MNIT	547,090	0.88675	1.6914	0.88675

5.5.8   Numerical Simulation Settings

The simulation model consists of a vertical column and gas injection point into which water and air enter respectively at a specific flowrate and injection pressure. The height of the gas injection point is 10 mm above the base of the column domain. The water is the primary phase (continuous) and the air was set as the secondary phase due to gas being a discrete phase. The air is injected at a specified velocity at the initial simulation; the model was filled with water. The water is introduced from the bottom of the column at a certain pressure, known as the bottom-hole pressure (BHP). Table 5.4 presents the relevant information and properties of the fluids used. In addition, assumptions were made that the water and air were well mixed in front of the injection point before reaching the top of the column. The parameters defining the flow in the domain and the known initial conditions are taken from the experimental data and listed in Table 5.5.

Table 5-4 : Fluid properties

Fluid Properties	Density (kg m^{-3})	Viscosity (Pa.s)
Water	998.2	0.001
Air	1.225	1.7894e-5

Table 5-5: The boundary conditions for the model

Boundary conditions	Pressure	Velocity (l/min)
Water Inlet	0.21 bar	5
Gas Inlet	0.5, 1, 2, 3, 4 bar	N/A
Mixture Outlet	0.070 bar	6.6

In this section, the multi-fluid volume of fluid (VOF) is used to simulate the gas lift system. The computational domain and boundary conditions are demonstrated in the previous section. The gas is injected into the three-dimensional domain. The governing equation is solved using the finite volume based discretisation and the $k - \varepsilon$ model was added for the turbulence model. The pressure and velocity coupling were set in SIMPLE and the terms were discretised by the highest order upwind scheme. The no slip boundary conditions with

standard wall functions for the turbulence model were applied at the pipe wall. The boundary conditions of the velocity inlet and pressure outlet were observed to be working well in the gas-lift system compared to other boundary conditions. The discrete phase model was combined in which the fluid phase is treated as the continuum while the dispersed phase is solved by tracking a large number of bubbles through the domain. This is used because the dispersed phase can exchange momentum, mass and energy with the fluid phase. There were several simulations conducted in this research investigation using the VOF model in the simulated gas lift system models and Table 5.6 shows the implemented settings for all scenarios:

Table 5-6: Scenarios of numerical simulations

Parameter	Case 1 Orifice valve	Case 2 Orifice valve	MNIT valve	Units
Port size	0.2, 1, 2, 4	2.24	2.24	mm
Air pressure	0.5, 1, 2, 3, 4, 5	0.5, 1, 2, 3, 4, 5	0.5, 1, 2, 3, 4, 5	bar
Water flow rate	5, 10, 20, 30	5,10,20,30	5, 10, 20, 30	l/min

Case one reports the effect of different port sizes (0.2, 1, 2 and 4 mm) on upward two-phase flow behaviours in the model under operating conditions of 0.5 bar air pressure and 5 l/m water flow rate. Moreover, the effect of air injection pressure was investigated for 0.5, 1, 2, 3, 4, and 5 bar using 0.2 mm port size at 5 l/m water flow rate. Furthermore, the effect of varying the water flow rate to 5, 10, 20 and 30 l/m has been studied at 0.2 mm port size and 0.5 bar air pressure.

Furthermore, case 2 studies the performance of the single orifice with 2.25 mm port size and is compared with the new multiple nozzles injection technique (MNIT). Each nozzle diameter is 1 mm, which gives the same total diameter of single orifice of 2.24 mm as shown in Table 3.1. The comparison of both techniques under the same operating conditions and gas injection rates is presented in the next chapter.

CHAPTER 6

NUMERICAL RESULTS, ANALYSIS AND DISCUSSION

This Chapter presents the basis for CFD qualitative results, analysis and discussions from a comprehensive three-dimensional CFD multi-fluid volume of fluid (VOF) gas-lift simulation developed model to predict the two-phase flow behaviours in the simulated column of the apparatus and compared with experimental results and observations when it is appropriate. In addition, the numerical simulation results obtained from the new multiple nozzles injection technique MNIT were modelled and the results compared with the SNIT at the same operating conditions and dimensions.

The presentation and discussions of the numerical simulation results that were performed in chapter 5 are shown below:

1) *Single Nozzle Injection Technique (SNIT) (§ 6.1)*

   a) Effect of port size on the upward tow-phase flow behaviours (§ 6.1.1)

   b) Effect of pressure drop on two-phase flow behaviours (§ 6.1.2)

   c) Effect of gas injection rate on two-phase flow behaviours (§ 6.1.3)

   d) Effect of mixture velocity on two-phase flow behaviours (§ 6.1.4)

   e) Effect of air injection pressure on distribution of air bubbles (§ 6.1.5)

2) *Multiple Nozzles Injection Technique (MNIT) (§ 6.2)*

   a) Pressure Drop along Test Section Pipe (§ 6.2.1)

   b) Effect of mixture velocity on two-phase flow behaviours (§ 6.2.2)

   c) Distribution of the air void fraction (§ 6.2.3)

3) *Comparison between the performance of the multiple nozzle technique and single orifice technique (§ 6.3)*

6.1 SNIT Gas Lift Technique

6.1.1 Effect of Port size on the Upward Two-phase Flow Behaviours

The gas-lift simulation model was undertaken with different port sizes of 0.2 mm, 1 mm, 2 mm and 4 mm to understand the effect of varying port size on the upward flow stability in gas lift methods. Further, it was found that every port size produces a different initial velocity and allows a certain air injection rate at a specific air injection pressure. The gas port size is certainly one of the important variables that needs to be determined as it would affect the fluid flow behaviours in a gas-lift system (Ter Avest and Oudeman, 1995). T the port size is capable of changing the initial flow behaviours and creating huge differential pressure between upstream and downstream in front of the injection point at the bottom of the column, this leads to the fluid flow behaviours being affected over the entire length of the column.

Figure 6.1 illustrates the void fraction of injected air in flowing water at different port sizes (Q_w = 5 l/m and air pressure, P_a = 5 bar), measured by percentage. Overall, the results showed that as port size increases, the air void fraction increases along the column to the outlet. This is due to the greater mass flow through port size, which permits larger initial bubbles to the column. This was expected, as the bubbles would coalescence with one another, creating larger (Taylor) bubbles, as this was demonstrated at different time steps in Figure 4.12 and also matched the experimental investigations. From observation, the contour and graph showed a gradual increase in void fraction near the gas inlet, which indicates bubbly flow at 0.5 m high and then the coalescence process started within the air bubbles, creating bubbly/slug flow at 1 m height, when the 0.2 mm port size was used.

The 0.2 mm port size has been observed to have the higher void fraction, which means that the injected bubbles coalesced quicker, and bubble diameters increased dramatically, compared with other orifice port sizes. This is because the jet velocity at the injection point was higher with smaller port sizes. On other hand, the 1 mm port size created the lowest void fraction throughout the simulation even though at 1.5 m there was a large gas pocket, but it decreased again at 1.7 m along the column. In addition, the 4 mm port size produced the highest air void fraction, especially at 1.5 m length from the downstream.

It was noted that the increase in orifice valve port size has a destabilising effect on the stability of the upward two-phase flow. This was due to increased air injection rate, and larger initial bubble sizes in the column. Therefore, this leads to bubbles coalescing together quickly in the middle of the pipe, creating bigger bubbles, which then ultimately collapse. These cause serious oscillations within the two-phase flow and reduce the lifting performance of the gas lift systems. Thus, there should be a new technique to reduce the initial bubble sizes and at the same time distribute bubbles in such a way as to minimise the coalescence process within the flow by increasing the distance between flowing bubbles. If there is sufficient distance between the flowing bubbles and they are travelling with the same fluid mixture velocity, then the coalesce rate will decrease. As a result of this, the gas lift system and surface facilities become more stable and the oil production rate from this method increases at the outlet.
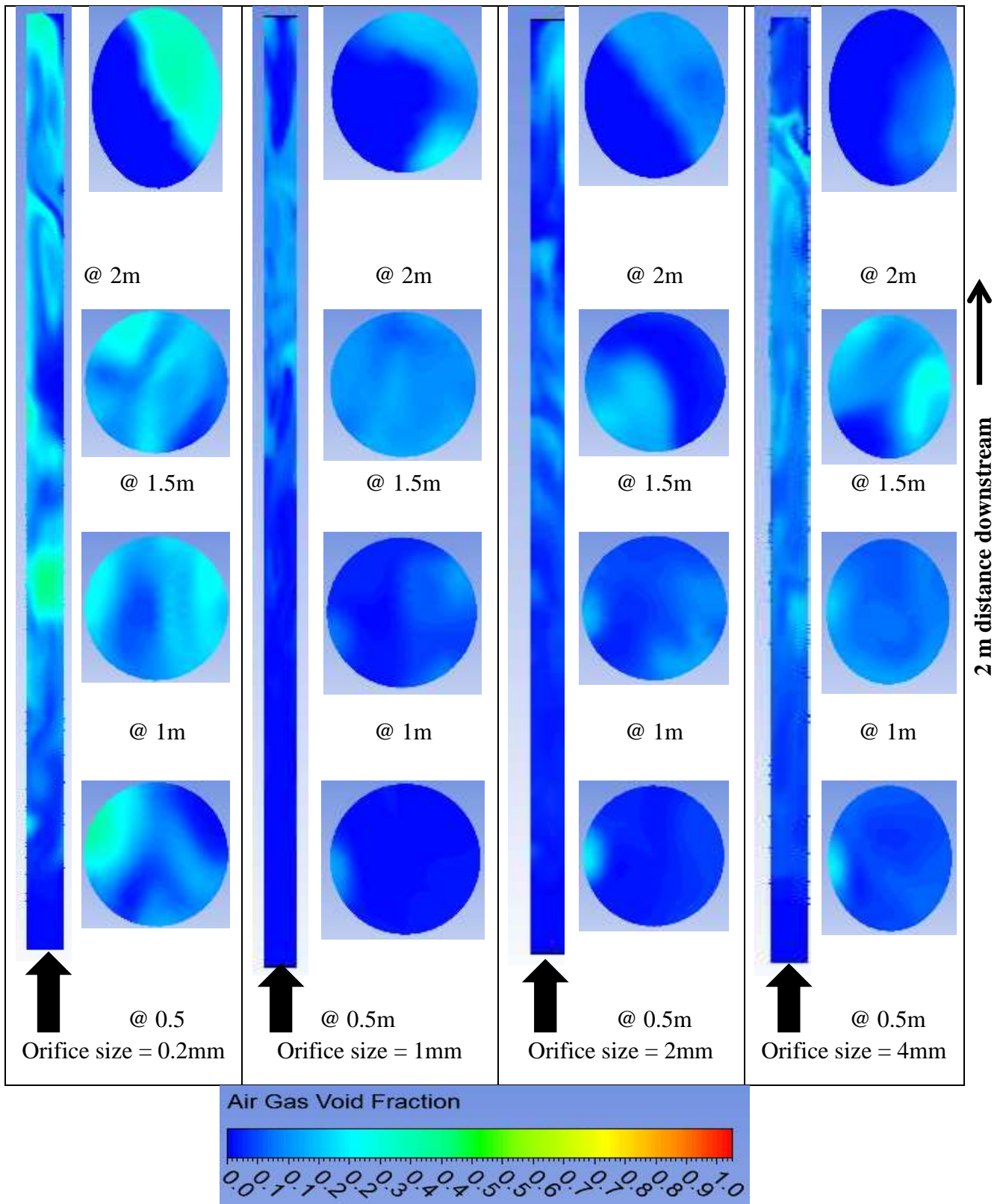
Figure 6-1: Contours of the horizontal and vertical gas void fraction of 0.2mm, 1mm, 2mm and 4mm port size.

6.1.2 Effect of Pressure Drop on Two-phase Flow Behaviours

The pressure drop plays a major role in liberating the air bubbles from the liquid phase within upward two-phase flow along the vertical pipe. Figure 6.2 shows the relationship between the pressure drop and 2 m distance downstream at different injection pressures with the same port size of 2.24 mm. The pressure drop was calculated in the developed simulation model at different points along the test section, starting from 0.02 m and ending at the top of the pipe at 2 m, as shown in appendix 7.5. In general, the results showed that as the length of the pipe increased, the pressure drop increases. Moreover, the graph showed that the maximum pressure was at the bottom of the column, as a result of the hydrostatic pressure of the water in the vertical pipe.

This pressure was decreased gradually as soon as the air was injected into the bottom of the column. This led to a reduction in the density of the liquid phase (water). Thus, as the pressure drop increases, the bubble sizes, the air void fraction and velocity increase along the pipe. There was a sharp decrease in pressure between the inlet and outlet from 34,772 to 17,231 Pa along the vertical pipe, when the air injection pressure was 0.5 bar. In this case, the maximum pressure drop was $0.18 \, \text{bar} \, (\Delta P = 17{,}541 \, \text{Pa})$. compared with other injection pressure scenarios. This is because the air bubbles were larger at low injection pressures, which created the highest air void fraction across the pipe. However, when the injection pressure was increased in the other scenarios (1, 2, 3, 4 and 5 bar), it was noticed that the pressure drop decreased as the injection pressure increased. For example, when the air injection pressure was 5 bar, the pressure drop decreased considerably to 0.11 bar, from $28{,}411$ to $17{,}220 \, \text{Pa} \, (\Delta P = 11{,}191 \, \text{Pa})$. Therefore, when the injection pressure was increased, the bubble sizes decreased and this caused the pressure drop to decrease along the pipe length. Thus, the smaller air bubbles have the lower air void fraction within the two-phase flow.

Finally, it was concluded that as the pressure drop increases, the bubble sizes increase and this leads the bubbles to coalesce together and grow until they reach the critical bubble size, at which point these large bubbles collapse. This is the main reason for fluctuations and development of the upwards two-phase flow along the pipe. Therefore, the pressure drop must be minimised within the two-phase flow by reducing the flowing bubble sizes and distributing the air bubbles through the whole pipe area instead of having them flowing only

in the centre of the column. This will reduce the oscillations within the two-phase flow (gas and liquid) and minimise the flow instability that occurs in gas lifted wells.
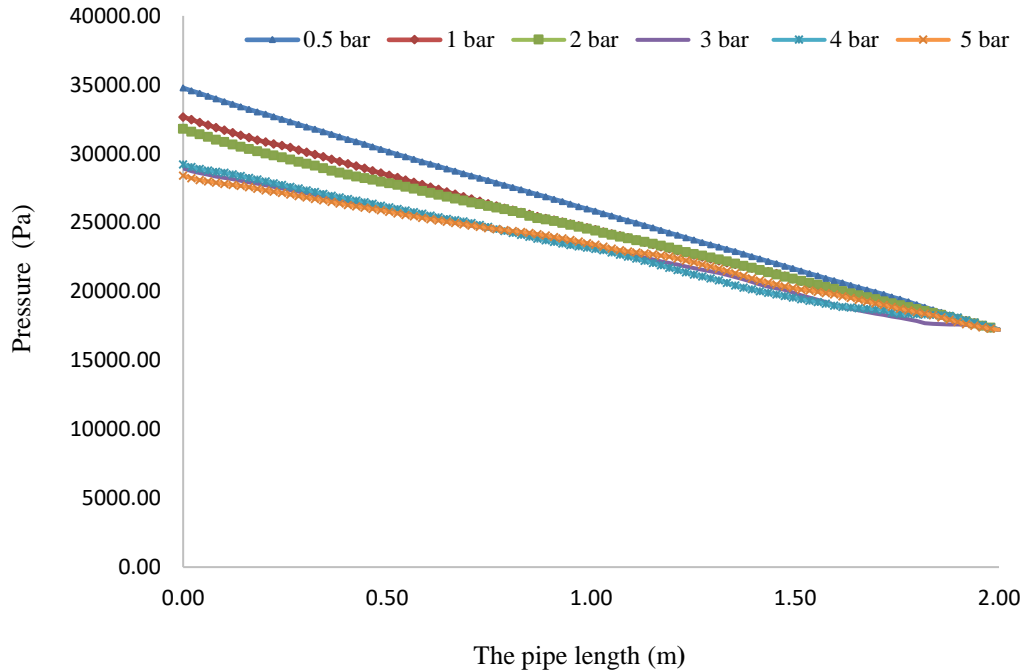
Figure 6-2: Pressure-drop along the pipe at different injection pressures using orifice port size of 2.24mm

6.1.3   Effect of Gas Injection Rate on Two-Phase flow Behaviours

Gas injection rate is an important aspect in gas-lift systems and distribution of gas to other gas lift wells in the field. Therefore, the gas injection rate must be optimised to maximise the production rate and enhance the well performance without causing any large flow oscillations within the upward two-phase flow. Figure 6-3 demonstrates the effect of air injection rates on the void fraction along the vertical pipe using an orifice valve with 2.24 mm port size.

Overall, there was a direct relationship between the air injection rate and void fraction within the flow. The results showed that as the air injection rate increased, the void fraction also increased. Furthermore, there were fluctuations in the air void fraction along the pipe, especially at high air injection rates. Figure 6-3 shows that the void fraction was less than 22 percentage long the simulated test section, when the air injection rate was 1 l/min. However, it reached 45 percentage especially at the first half metre of the column then started fluctuating until the end of the test section at air injection rate 3-5 l/min. Thereafter, the air

void fraction reached 60 percentage particularly at the bottom of the test section and reached a peak at 90 percentage at the end of the simulated test section when air injection rate was 6.4 l/min. Then it fluctuated sharply when the air injection rate increased to 8 l/min. In addition, the graph showed that there was a gradual reduction in the void fraction, when the air injection rate was 9 l/min, especially after the middle of the test section. These oscillations occur due to the frequent collapse of the large bubbles in the middle of the pipe.

The relationship between the air injection pressure and the flow rate is directly proportional. As a result of this, as the injection pressure increases, the air mass flow rate increases through the port size. This is the main reason for the decrease in the void fraction at high flow rates. As the air flow rate increases, the injection pressure also increases. This leads to a reduction in the bubble sizes along the pipe, and reduces the oscillations slightly. It can be concluded that the increase in the gas injection rate has a stabilising effect on the upward two-phase flow behaviours, especially at high flow rates.
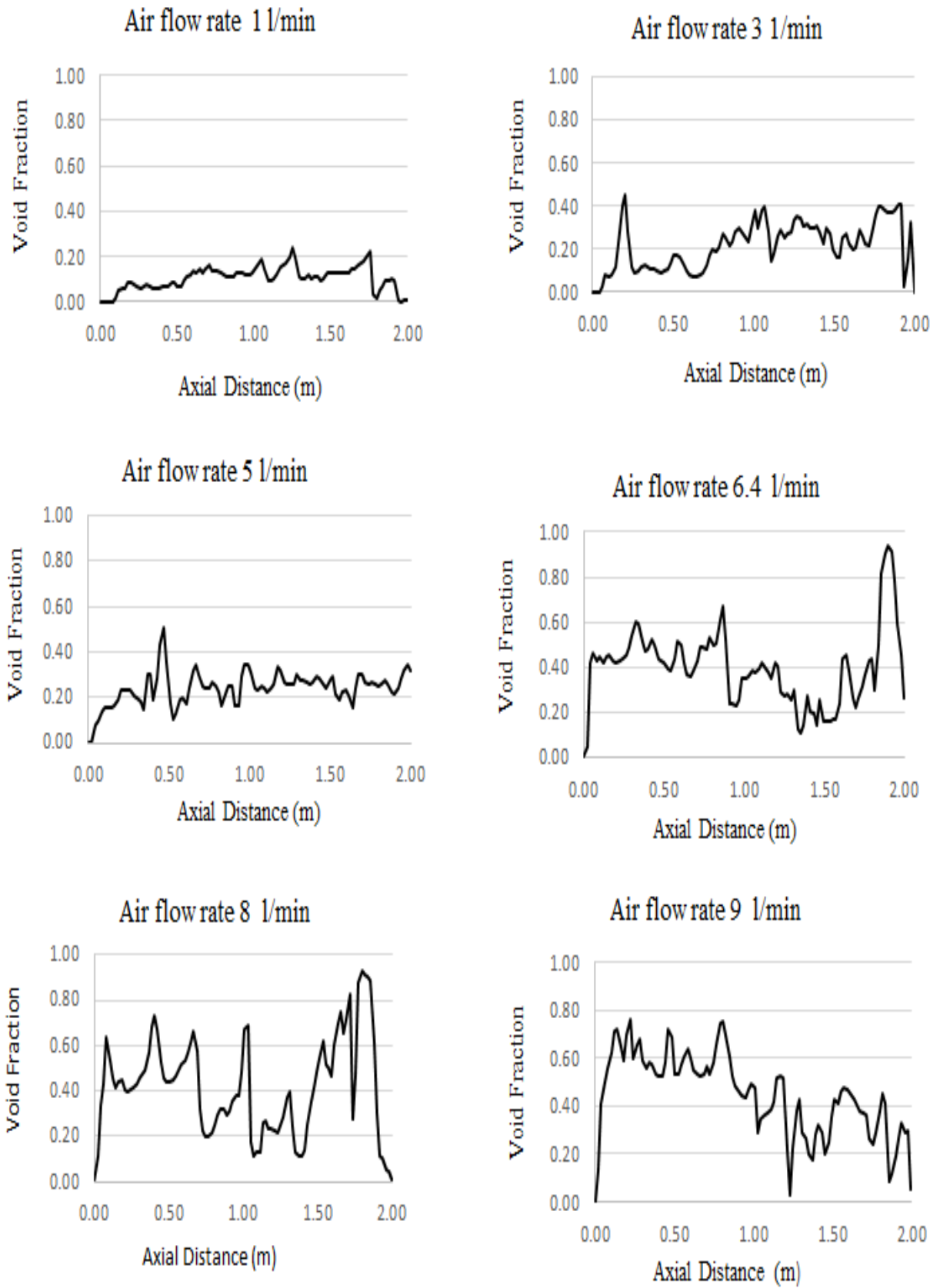
Figure 6-3: The effect of air injection rate on void fraction long the vertical column using 2.24 mm single orifice port size

6.1.4   Effect of Mixture Velocity on Two-Phase Flow Behaviours

The velocity has a major effect on the development of upward two-phase flow, because as the velocity increases, the bubble sizes increase within the flow. However, this increase in bubble size must be minimised to reduce the mixture velocity. The experimental results showed that the larger bubble sizes have higher velocity than the small bubble sizes due to greater buoyancy, the action of gravity and the difference between the density of the air and water phases. The results from the CFD simulation volume of fluid (VOF) models give a prediction of the mixture velocity profiles at different injection pressures along the test section. Figure 6.4 illustrates the mixture velocity at different injection pressures using a sharp edge orifice port size of 2.24 mm at the injection point. The results show that there was a steep fluctuation in the mixture velocity, especially when the injection pressures were 2, 3 and 4 bar. However, the mixture velocity declined when the injection pressure was increased to 5 bar. This might be a result of the decrease in bubble sizes at high injection pressures.

Therefore, there should be a new technique to reduce the bubble sizes during the flow and minimise the mixture velocity. This will reduce the development of flow regimes and make the system more stable.
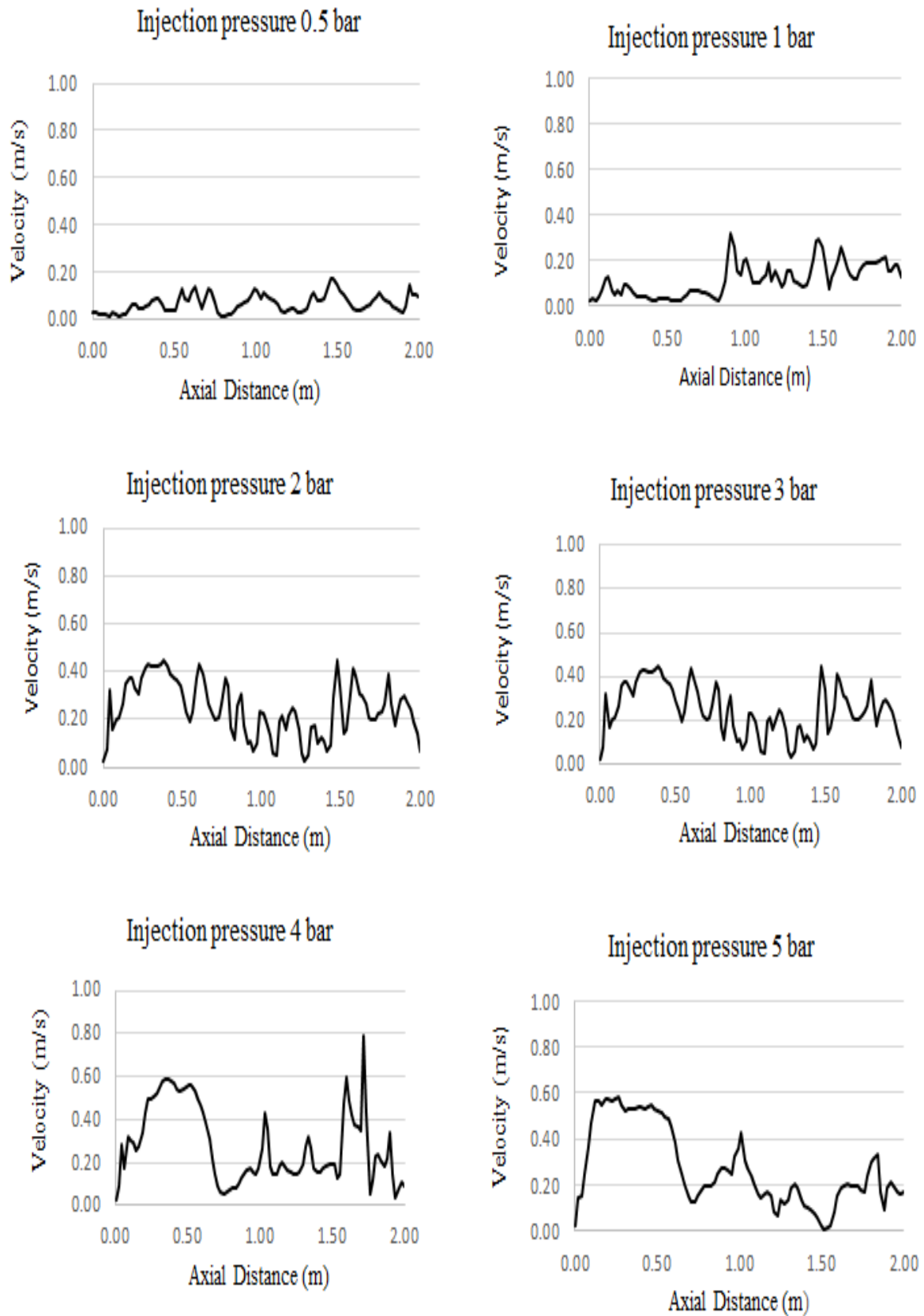
Figure 6-4: The mixture velocity at different injection pressures using orifice port size 2.24mm

6.1.5 Effect of Air Injection Pressure on Distribution of Air Bubbles

The increase in injection pressure has a considerable effect on the distribution and behaviours of bubbles within the upward two-phase flow in gas lifted wells. Overall, the distribution of air bubbles was poor when the orifice valve was used and there were still large slugs of air along the vertical column. Figure 6-5 demonstrates the effect of injection pressures on the air bubbles' void fraction using the single orifice gas lift valve with a port size of 2.24 mm at the injection point. The results showed that there were still large pockets of air (Taylor bubbles) with approximately the same diameter of the pipe travelling along the column, especially when the injection pressures were 3 and 4 bars as shown in Figure 6.5. Furthermore, these large bubbles with high void fraction ratio collapsed when they reached the critical bubble diameter (maturation), as the superficial velocity increased and the flow was fully developed. Thus, the distribution of void fraction results agreed with results obtained by (Azzopardi *et al.,* 2015). In addition, the distribution of air bubbles is still in the middle of the pipe and not spreading throughout the entire pipe area. This leads bubbles to coalesce together, rapidly creating bigger bubbles. At 5 bars injection pressure, there were few Taylor bubbles detected. This is due to the slight decrease in bubble sizes when injection pressure increases.

This collapse of large bubbles causes serious pressure fluctuations and backflow and creates a large pressure drop within the flow. This is the main cause of the flow instability within two-phase flow and the reduction in total oil production from gas lifted wells. Therefore, there should be a new method to reduce air bubble sizes and at the same time distribute them from core-peaking to wall-peaking to enhance lifting performance and to increase oil production from gas lifted wells in the oil industry.
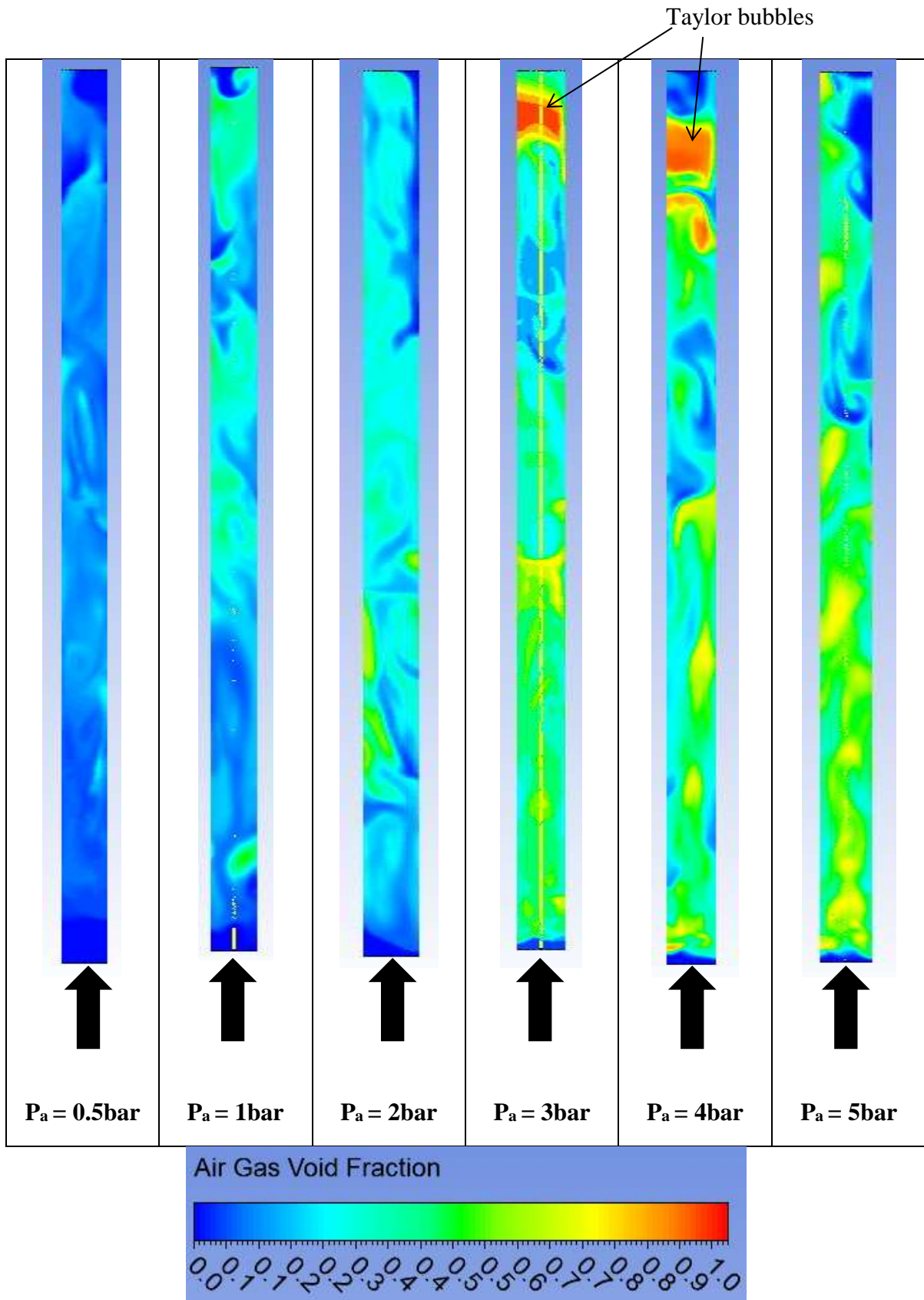
Figure 6-5: The effect of injection pressures on air void fraction along the simulated column apparatus using single orifice technique (SNIT) with port size 2.24 mm

6.2   Multiple Nozzles Injection Technique (MNIT)

It was very clear from the experimental and numerical simulation results obtained for the orifice valve with 2.24 mm port size that the upward two-phase flow developed quickly and flow oscillations (due to bubbles collapsing) and flow instability still occurred along the vertical test section. This is because the air bubbles injected from the single orifice valve (initial bubble sizes) is reasonably large and as soon as these bubbles depart from the port, the bubbles moved toward the centre of the pipe and then coalesced directly with each other. In addition, it was observed that the distribution of air bubbles was very poor and the distances between the bubbles were small. Therefore, this led bubbles to coalesce together very quickly, thus creating big bubbles (Taylor bubbles) which then collapsed along the pipe. This is the main reason for the two-phase flow instability, which results in a reduction in oil production in the gas lift system in the oil industry or any other similar applications using gas to lift liquid.

Therefore, a new technique was developed to reduce the bubble sizes within the two-phase flow and improve the distribution of the bubbles across the entire pipe area via changing the flow path of the smaller bubbles with the use of the multiple nozzles technique from the centre of the pipe to rest of the area. The new technique is called the multiple nozzles injection technique (MNIT) and consists of a gas lift valve without an orifice or a venturi and multiple nozzles technique at the outlet of the valve. The multiple nozzles injection technique is comprised of a number of nozzles as shown in Figure 3.5 in chapter 3. The design and diameter of nozzles depend on the gas injection rate required for that particular gas lift well. The results obtained from this new technique are presented in the following section.

6.2.1   Pressure Drop along Test Section Pipe

The pressure drop plays an important role in the development and behaviours of air bubbles within the upward two-phase flow along the vertical pipe. Therefore, the MNIT and SNIT were tested under the same operating conditions in order to be able to compare the performances of both valves. Figure 6-6 shows the relationship between the pressure drop and the length of pipe at different injection pressures using the new multiple nozzles injection technique. In general, the most significant feature of the line graph is that the pressure drop rises as the pipe length increases. The pressure drop was calculated in the simulation model

every 0.02 m along the pipe, as shown in appendix B. The results showed that there was a marked decrease in the pressure drop along the pipe when the multiple nozzles injection technique was used at different injection pressures compared with the pressure drop along the pipe when an orifice valve was used.

Furthermore, when the injection pressure was 0.5 bar, the pressure drop between the inlet and the outlet of the simulated column of the apparatus was 0.11 bar, (31,539-20,684 =($\Delta P =$ 10,855 Pa)) when the MNIT was used. In comparison, the SNIT pressure drop was 0.18 bar ($\Delta P =$17,541 Pa) (Sardeshpande *et al.*, 2015). This indicated that the Multiple Nozzles Injection Technique produced smaller air bubbles and these bubbles had smaller void fractions along the pipe. The void fraction of small bubbles creates less pressure drop along the pipe. Therefore, reducing the pressure drop within two-phase flow minimises the coalescence process among air bubbles, because the bubble growth is restricted within the flow when the pressure drop is reduced gradually and there is no huge flowing differential pressure due to the dispersal of large bubbles, such as Taylor bubbles. This leads to a reduction in the development of two-phase flow and flow instability, which happens due to the collapse of large bubbles.
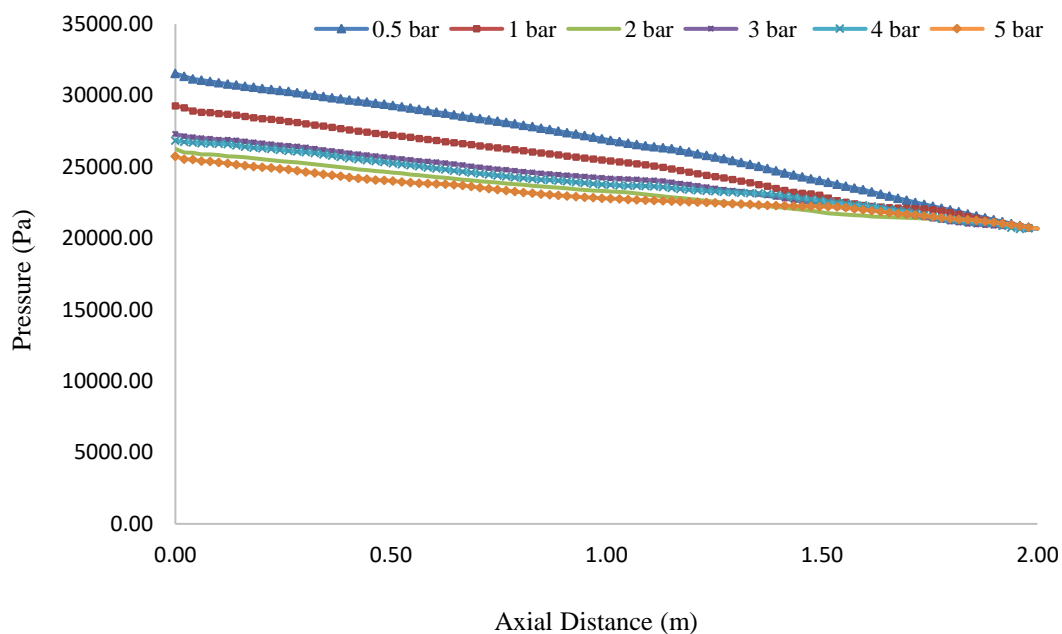
Figure 6-6: The relationship between pressure drop and the length of pipe at different injection pressures using the MNIT with port size of 2.24 mm.

In addition, the pressure drop was compared for both valves at a high injection pressure. At a high injection pressure, the performance of the new multiple nozzles injection technique is better in terms of reducing bubble sizes and improving the distribution of bubbles inside the column. Figure 6-7 illustrates the comparison of the pressure drop between the MNIT and the SNIT at 5 bar injection pressure. The results showed that in the first pipe length, the pressure drop of the sharp edge orifice valve was higher than the new multiple nozzles injection technique. However, after 1.2 m pipe length, the multiple nozzles injection technique's pressure drop trend became higher than the orifice valve's trend. There was a gradual decrease in the pressure drop along the vertical column when the multiple nozzles injection technique was used (Orkiszewski, 1967). It was only 0.05 bar (25,739-20,684 =($\Delta P =$ 5,055 Pa)) between the inlet and the outlet of the test section. This means that there is no large pocket of air (Taylor bubbles) along the pipe.

In comparison with the orifice valve, there was a steep decrease in the pressure drop when the orifice valve was used and the pressure drop was 0.11 bar (28,411-17,220 = ($\Delta P =$ 11,191 Pa)) at the same injection pressure and under the same operating conditions. This is good evidence that reducing bubble sizes has a major effect on pressure drop. This is due to the air void fraction being distributed equally in the form of small bubbles along the column. Therefore, minimising the pressure drop within two-phase flow reduces the coalescence process and restricts bubble size growth rate along the vertical pipe. This will diminish the fluctuations within the two-phase flow due to the collapse of big bubbles. It can be concluded that the new MNIT reduces the pressure drop within the two-phase flow by decreasing the flowing bubble sizes and distributing them throughout the entire pipe area. This stabilises the upward two-phase flow better than the SNIT.
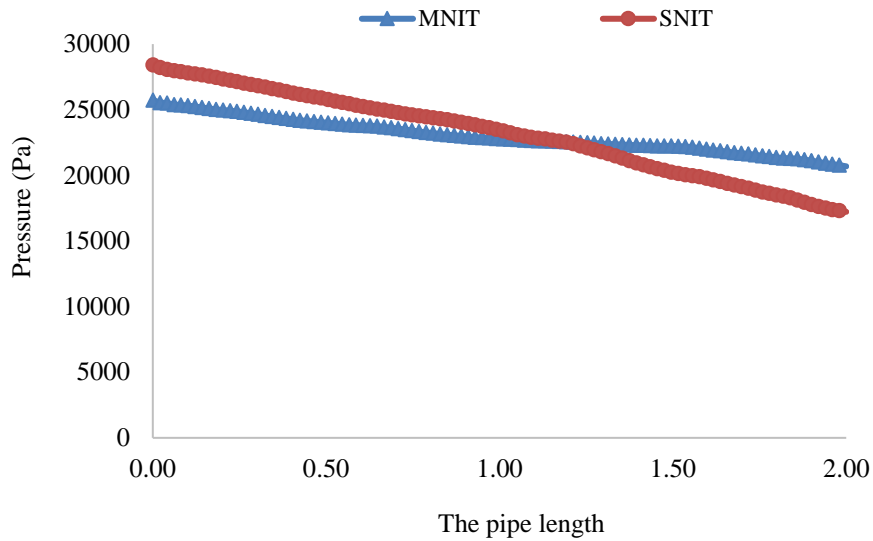
Figure 6-7: Comparison of the pressure drop between the MNIT technique and the single orifice valve at 5 bar injection pressure.

6.2.2 Effect of Mixture Velocity on Two-phase Flow

The mixture velocity has a negative effect on the stability of two-phase flow, because as the velocity of bubbles and mixture increases, the bubble sizes also increase. However, when the MNIT was used, the bubble sizes were reduced. The mixture velocity profile was very different and steady compared with the SNIT. Figure 6-8 demonstrates the mixture velocity along the test section using the multiple nozzles injection technique at different air injection pressures. The results showed that the mixture velocity was stable and did not fluctuate in comparison with the orifice valve's mixture velocity, as discussed in the previous section and as shown in Figure 6-4.

Because the air bubbles produced from the multiple nozzles injection technique are small in size and travelling with approximately the same average mixture velocity and are also well distributed throughout the whole pipe area, this prevents the creation of large bubbles which have higher velocities that cause oscillations when these bubbles collapse within the upward two-phase flow.
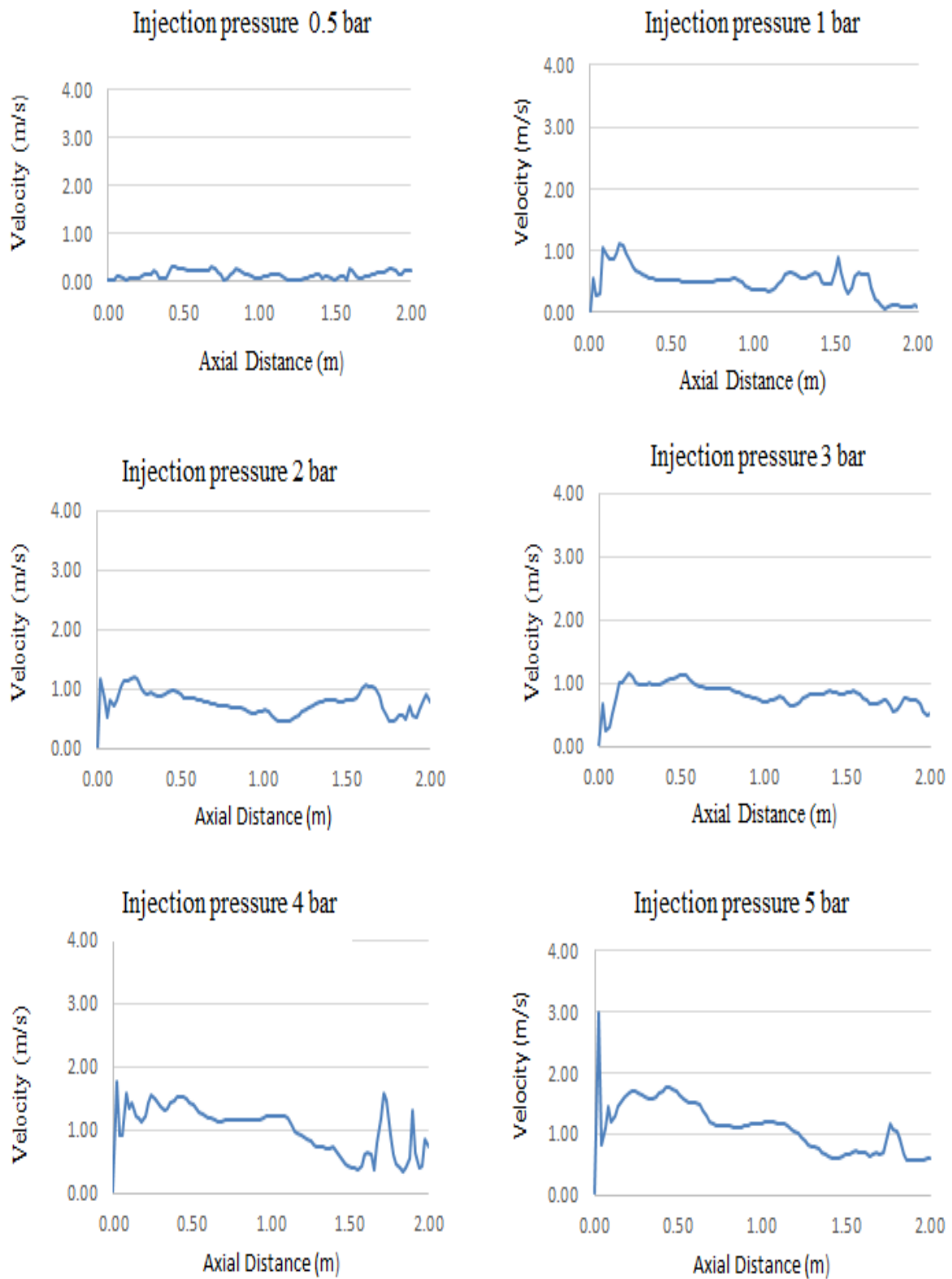
Figure 6-8: The mixture velocity along the simulated column apparatus using the MNIT at different injection pressures.

6.2.3 Distribution of the Air Void Fraction

It is clear from the different numerical simulation scenario results that reducing bubble sizes and distribution of these smaller air bubbles throughout the entire pipe area have a major effect on the stability and lifting performance of upward two-phase flow in the gas lift method. Figure 6-9 shows the distribution of the air void fraction along the vertical pipe using the MNIT at different air injection pressures. The results showed that the MNIT is capable of changing the distribution of air bubbles within the two-phase flow along the vertical test section. The graph showed that as the injection pressure increases, the performance of the MNIT in distributing the air bubbles within two-phase flow improves. The distribution of flowing air bubbles was changed from core-peaking in the middle of the pipe to wall-peaking near to the pipe wall when the new technique was used. This means that the air bubble coalescence process has been reduced and this is achieved by decreasing the pressure drop and distributing the smaller bubbles within the two-phase flow along the vertical pipe. The small flowing bubbles were evenly distributed and it was observed that the dominant flow pattern was bubbly flow pattern, and that bubbles had approximately the same flowing velocities and sizes.

Furthermore, when the MNIT was used, there was no large air pocket flowing along the test section that would cause a large pressure drop within the flow. Moreover, it was observed that the best wall-peaking distribution was achieved when the air injection pressure was 5 bar and the air void fraction was distributed throughout the entire pipe area (Azzopardi *et al.,* 2014). This reduces the fluctuations and stabilises the upward two-phase flow in the test section. Hence, the lifting performance and production rate were increased markedly in the outlet flow meter (Guet and Ooms, 2006). These simulation results matched the experimental results in terms of distribution of bubbles, increasing the lifting performance and production rate in the outlet of the column. In comparison with the SNIT, there were large air pockets occupying the entire pipe diameter, especially when the injected air pressure was 3 and 4 bar. In addition, these large pockets (Taylor bubbles) frequently occur along the vertical pipe, because the initial bubble sizes were quite large and coalescing in the middle of the pipe. However, these fluid behaviours were changed when the MNIT was used and the initial bubble sizes were reduced, and the distribution was changed from core-peaking to wall-peaking throughout the entire pipe area. This was achieved without increasing the backpressure to the system or putting any flow restrictions in the pipe.
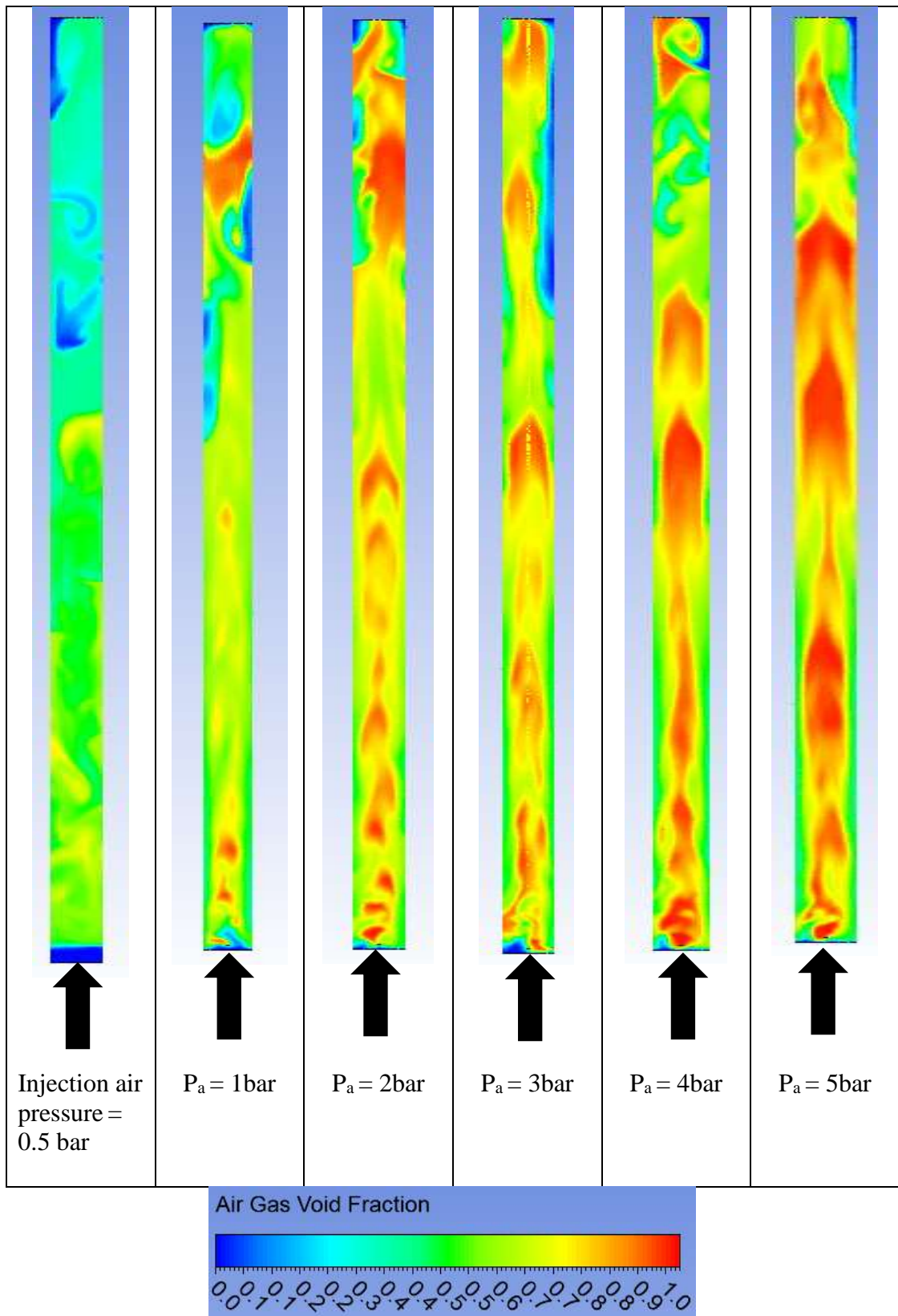
Figure 6-9: The distribution of air void fraction along the vertical simulated column apparatus using the MNIT at different air injection pressures.

The stability in distributing the air bubbles void fraction within the two-phase flow is crucial. Figure 6-10 illustrates the air void fraction along the test section at different injection pressures, measured by percentage. The results showed that there were smaller fluctuations in the air void fractions along the pipe when the MNIT was used compared with the orifice valve under the same operating conditions. This is good evidence that air bubbles were distributed perfectly along the vertical column and the variations in air void fraction had been reduced. The injected bubbles have small sizes and flow at the same mixture velocity and there is no large difference between their velocities because of their equal sizes upward of the vertical column. Therefore, the air void fraction was steady and stable during the lifting process, and this reduces the chaotic and turbulent flow behaviours within the two-phase flow due to the collapse of large flowing bubbles. It can be concluded from the air void fraction results along the test pipe that the reduction in size and improved distribution of air bubbles play an important role in the stability of two-phase flow in the gas lift method.
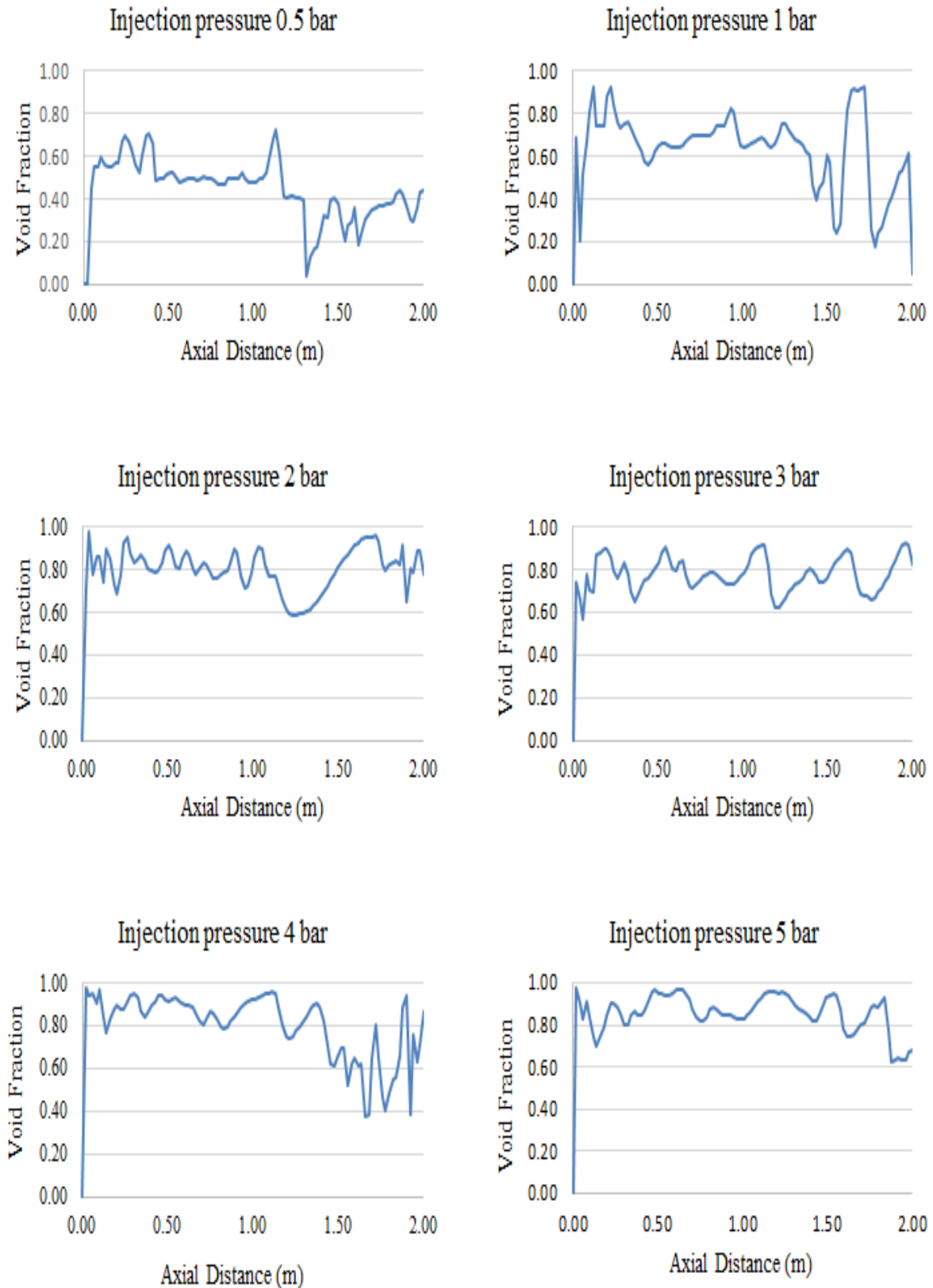
Figure 6-10: The stability of the air void fraction along the simulated column apparatus at different injection pressures using the MNIT with port size of 2.24 mm.

154

6.3 Comparison between the Performance of the Multiple Nozzles Injection Technique (MNIT) and Single Nozzle Injection Technique (SNIT)

The simulation results that were obtained from the new multiple nozzles injection technique at different scenarios and under different operating conditions were better than for the normal orifice valve in terms of reducing bubble sizes and improving the distribution of smaller bubbles along the vertical test section. Therefore, reducing the bubble sizes decreases the pressure drop along the vertical column. This confines the development of the flow because most of the bubbles are small. Thus, the velocity of bubbles and the mixture will be minimised due to the bubbles' small sizes and buoyancy. In addition, distributing smaller bubbles throughout the entire pipe area (wall-peaking) reduces the coalescence process that happens between neighbouring bubbles as shown in Figure 6.11. This was clear from the air void fraction distribution results along the test section. This leads to a decrease in the bubble size growth rate along the pipe. As a result of this, the lifting performance and production rate were increased. Furthermore, the flow instability within the upward two-phase flow was minimised to the lowest point in the vertical column.

On the other hand, when the SNIT simulated, the bubble sizes increased rapidly, because the initial bubble sizes were large and at the same time flowing in the middle of the pipe very close to each other. This leads bubbles to coalesce faster and thus creates large bubbles (Taylor bubbles) as shown in Figure 6.11. As soon as these large bubbles reach maturity and a critical size, they collapse, causing collisions with neighbouring bubbles as shown previously in Figure 4.5. Thereafter, this causes serious oscillations and flow instability within the flow. In addition, it was observed that distribution of the air void fraction was poor and core-peaking. The pressure fluctuations due to bubbles collapsing were dominant and this process was repeated frequently. Therefore, the multiple nozzles injection technique is a good choice for gas lifted wells suffering from flow instability and any other application using gas to lift liquid in a vertical column. It is evident that Figure 6.11, the flow instability occurs with SNIT which are also supported by the experimental finding shown previously 4.29 in which the production rate can be improved using the Multiple Nozzle Injection Technique compared to current Single Nozzle Injection Technique.
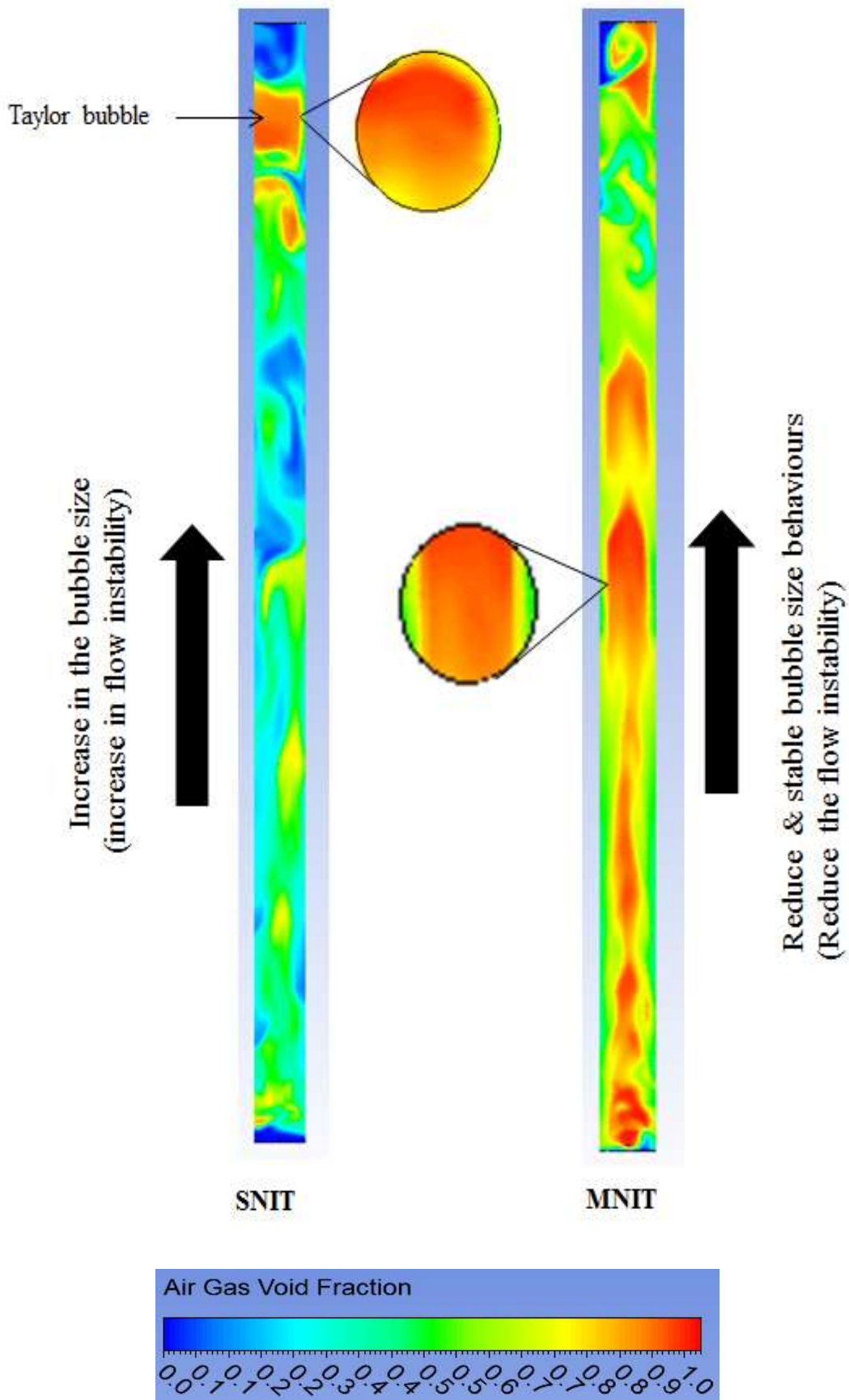
Figure 6-11 Comparison between both techniques in distributing air bubbles in the simulated column apparatus at 4 bar injection pressure.

6.4 Proposed MNIT from Present Study

Figure 6.12, shows the proposed MNIT which is capable in reducing the initial bubble sizes and changing the distribution of the gas bubbles from middle of the production tubing core peaking to across the entire pipe area wall peaking. This minimise the two-phase flow instability within the gas lift operation. The systematic flow instability can cause serious flow oscillations within the system. In most cases, these oscillations are a major cause of production losses and are harmful to operational smoothness, safety and efficiency. These are some advantages of MNIT as following:

1. Stabilise the gas lift system by reducing the initial bubble sizes and distributing the gas bubbles across the entire pipe area. This leads to increase gas lifting performance.
2. This technique has potential to improve the total oil production rate from the gas lifted wells.
3. It does not create any restriction inside the production tubing which may affect the other operation such as wireline operations.
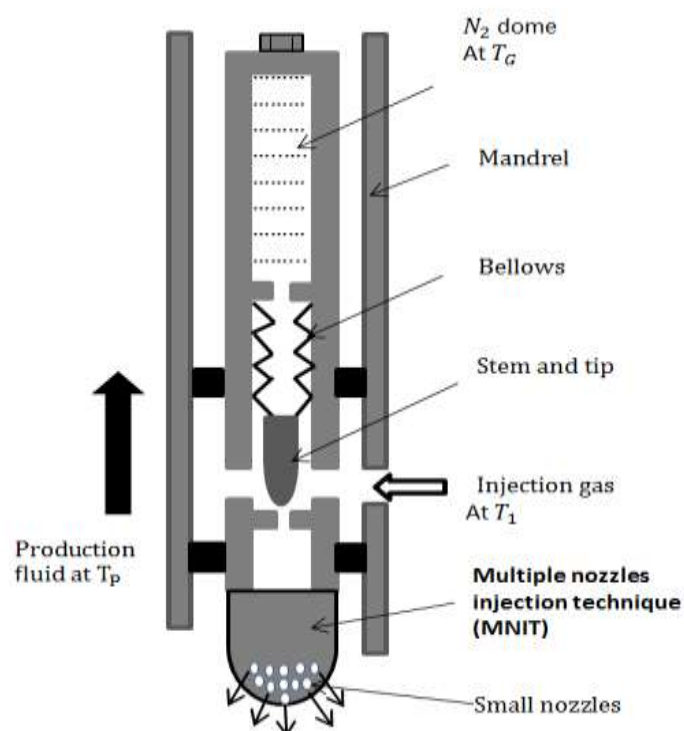
Figure 6-12: The proposed MNIT from the present study

6.5 Limitations

The VOF model considers the interfacial forces and the superficial velocities for gas and liquid were assumed. However, the model only gave overall predictions about fluid behaviours in the test section and the model is not capable of giving more details such as bubble sizes, bubble formation and bubble collapse, as these have not been modelled. Also considered were the transitional regions between each flow pattern when the flow developed. Thus, developing a robust gas lift model mimicing the behaviours of multi-phase flow in a vertical pipe is complex.

6.6 Summary

This chapter presents the numerical simulation results and discussions of the variables that can affect behaviours of the two-phase flow and lead to flow instability phenomenon .These findings can be summarised as following:

Section 6.1.3 showed that the increase in the port size has negative effect on the stability of two-phase flow and the distribution of air void fraction the test section.

Section 6.1.2 indicated that the single orifice technique cause large pressure drop along the test section from 34,772 to 17,231 Pa between the inlet and outlet, when the air injection pressure was 0.5 bar. In this case, the maximum pressure drop was $0.18\,\text{bar}\,(\Delta P = 17{,}541\,\text{Pa})$.

Section 6.2.1 indicated that the multiple nozzles injection technique (MNIT) reduced the pressure drop between the inlet and outlet of the test section to 0.11 bar and the overall reduction by 50% compared with single orifice technique.

Section 6.2.3 showed that the multiple nozzles injection technique (MNIT) changed the air void fraction from the centre of the test section cross the entire pipe area even near to the wall of the pipe. This reduced the air slug travelling the middle of pipe.

CHAPTER 7

CONCLUSIONS AND FUTURE WORKS

7.1 CONCLUSIONS

The flow structure, behaviours and instability of two-phase flow (air and water) have been investigated experimentally in simulated gas lift column with a vertical transparent pipe (ID: 66 mm, Length: 2 m) using an image processing package (DynamicStudio 2015a) and numerically using a computational fluid dynamic (CFD) model. The experimental investigations were carried out with two different techniques: Single Nozzle Injection Technique (MNIT) and Multiple Nozzle Injection Technique (SNIT) focusing on the behaviours of air bubbles within two-phase flow. The two types of gas injection with single orifice (SNIT) that are used in the existing gas lift systems in the oil fields and MNIT as proposed as alternative method. This was investigated in order to assess the suitability of the two methods for the gas lift method. The lifting performance of this proposed system tends to reduce the flow instability within upward two-phase flow. The following conclusions can be drawn from this research study:

<u>Single Nozzle Injection Orifice (Sharp Edge) (SNIT)</u>

An experiment were carried out using the SNIT at different port sizes to mimic the reality of upward fluid behaviours in gas lifts and to understand the effect of all variables that are capable of causing the flow instability phenomenon in gas lift systems. The following concluding remarks are derived from this study:

1. The bubbly and slug flow patterns were observed in the simulated column made of PVC material, and the axial distribution of bubbles at different operating conditions showed an interesting observation on the air bubbles' coalescence and collision mechanisms, both statically and dynamically. Furthermore, it has been found that bubble size had a significant effect on the stability of the axial structure of two-phase flow, especially when bubbles reached a critical size (maturation) and then collapsed. This behaviour causes the pressure drop and vacuum and backflow in that particular region of collapsed bubbles, which leads to collision with some bubbles nearby. Thus, this collision causes disturbances and small waves within the flow in the vertical pipe.

159

This process will be repeated simultaneously depending on the velocities of bubbles flowing upward in the pipe (Section 4.2.1) and (Section 4.2.4).

2. The velocity of air bubbles had a considerable impact on fluctuations, structure and the development of two-phase flow. It provides evidence that air bubbles under the same operating conditions have different velocities depending on their sizes. Therefore, as air bubble velocity increases, the bubble sizes increase due to their buoyancy (Section 4.2.2).

3. Port size diameter has a major effect on bubble sizes and the gas injection rate, as a higher breakup frequency was anticipated at smaller diameters of the injection point, resulting in lower bubble sizes being observed. The sensitivity analysis of the effect of port size on the bubble sizes within two-phase flow showed that port size has a destabilising effect on the stability of the upward two-phase flow because it increases bubble size with poor bubble distribution in the column. This develops upward two-phase flow regimes and results in flow instability along the production tubing. Accordingly, there must be an alternative to the (sharp edge) single orifice injection technique (SNIT), as it operates on throttling range and creates large differential pressure between upstream and downstream pressure. This causes the casing heading phenomenon between the casing and production tubing in gas lift systems (Section 4.2.3).

4. The increase in injection pressure has a positive effect on the stability of upward two-phase flow in a vertical column in gas lifted systems. As the injection pressure increases, the bubble sizes decrease. In addition, it was observed that large bubbles decrease in size at high pressures (Section 4.2.1).

5. The velocity and flowrate of the liquid phase have a positive and stabilising effect on two-phase flow, because when inlet flow rate (reservoir response) increases in the test section, it compensates for the vacuum pressure caused by the gas lifting process (Section 4.2.2)

It can be concluded that the increase in bubble sizes plays a major role in the rapid development and instability of upward two-phase flow when the normal orifice gas lift valve

is used. The initial bubble sizes were significantly large when bubbles departed the port, and grew speedily due to their poor distribution (core-peaking) when bubbles were flowing in the middle of the pipe. This resulted in the bubbles coalescing quickly, creating large bubbles. Subsequently, these bubbles collapse within the flow, causing collisions with neighbouring bubbles, large pressure drop along the pipe, pressure fluctuations and also flow instability within the two-phase flow. Therefore, the initial bubble sizes should be reduced and the distribution should be extended throughout the entire pipe area (wall- peaking) to stabilise the two-phase flow, as this would improve the lifting performance and total oil production rate from gas lifted wells.

Multiple Nozzles Injection Technique (MNIT)

When the orifice was replaced with the new Multiple Nozzles Injection Technique at the injection point at the bottom of the vertical column, the behaviours of the upward flowing two-phase flow structure were modified in terms of the bubble sizes, pressure drop and distribution. From the comparison of results obtained from both gas lift valves with the same dimensions (2.24 mm), the following conclusions can be drawn:

1- The average overall bubble sizes were reduced from 7.01 to 5.47 mm. The reduction was 22% when the new multiple nozzles injection technique was used compared with the normal orifice valve at different injection pressures (Section 4.3.1.1).

2- In addition, the average overall minimum bubbles sizes were decreased from 1.23 to 1.03 mm, areduction of 16.1% when the new technique was applied (Section 4.3.1.2).

3- The average large bubble sizes (Taylor bubbles) reduced from 44.07 to 39.95 mm with an the overall average reduction of 8.22% in the test section under different operating conditions (Section 4.3.1.3).

4- It was found that the new multiple nozzles injection technique resulted in a significant increase (60.2%) in the number of detected bubbles in the column in comparison with the orifice valve under the same operating conditions.

5- The lifting performance improved and the average production rate was increased to 7.5% when the multiple nozzles injection technique was used in comparison with the conventional orifice gas lift valve under the same operating conditions (Section 4.3.3).

6- It was found that when the multiple nozzles injection technique was used and the velocity of the liquid phase was increased, the bubble sizes were 14.75% less than those produced from the orifice valve under the same operating conditions.

7- The distribution of air bubbles was improved and changed from the middle of the vertical pipe (core-peaking) to the entire pipe area (wall-peaking) the SNIT was poor and air bubbles were flowing in the centre of the pipe. This assisted the two-phase flow to develop quickly and then caused the flow instability, which is the main reason for the reduction in the total oil production in gas lifted wells (Section 4.3.4).

In conclusion, the new MNIT is capable of reducing initial flowing gas bubble sizes and changing the distribution of gas bubbles throughout the entire pipe area (wall-peaking). This leads to a stabilised flow within the upward two-phase flow, which therefore has the potential to increase the lifting performance and thus the total production rate of gas lifted wells.

Conclusion: Numerical Simulations

Finally, the three-dimensional numerical simulation results closely agreed with the experimental results, and the following conclusions can be drawn:

1. The pressure drop calculations provided stronger evidence of the effect of the pressure drop in the development of the upward two-phase flow. Therefore, as the pressure drop increases, the bubble sizes increase, which then leads to the creation of large bubbles which then coalesce together until they reach a critical size and collapse. This is one of the main reasons for fluctuations, backflow and development of the upward two-phase flow along the pipe. Therefore, the pressure drop must be minimised within the two-phase flow by reducing the flowing bubble sizes and distributing the air bubbles throughout the whole pipe area instead of just flowing in the centre of the

column. This will reduce the oscillations within the two-phase flow (gas and liquid) and minimise the flow instability that occurs in gas lifted wells (§6.2.1).

2. It was found that the MNIT is capable of reducing the pressure drop from 0.18 to 0.05 bar. The overall average reduction was to just above 50% within two-phase flow by decreasing the sizes of the flowing bubbles and distributing them across the entire pipe area, especially at high-pressure. This stabilises the upward two-phase flow better than the SNIT (Section 6.2.1).

3. The sensitivity analysis of increasing the orifice valve port size pointed out that this has a destabilising effect on the upward two-phase flow. This is because it increases the air injection rate, and produces larger initial bubble sizes in the column, especially with large port sizes. These cause faster development of two-phase flow, serious oscillations within two-phase flow and a reduction in the total production rate in gas lift systems (Section 6.1.1).

4. The relationship between the air injection pressure and air flow rate is directly proportional. Thus, as the injection pressure increases, the air flow rate also increases.

5. The air void fraction results showed that the new multiple nozzles injection technique changed the distribution of air bubbles in the simulated PVC vertical column from the centre of pipe (core-peaking) to the entire pipe area (wall-peaking). In addition, this void fraction was stable in different scenarios due to the bubble sizes being small and the bubbles being well distributed. This stabilised the two-phase flow, resulting in the lifting performance and the outlet flow rate by 8%, in comparison with the normal orifice gas lift valve (Section 6.2.3).

7.2 RECOMMENDATIONS FOR FUTURE WORK

The following recommendations for future work and development of the new technique are suggested:

- The author suggests adding mineral oil to the experimental working fluids (air, oil and water) in the experiment tank to investigate the multi-phase flow behaviours.

- The design of the new technique's nozzles can be developed with different angles and smaller orifice sizes in the head of the Multiple Nozzles Injection Technique.

- The three-dimensional gas-lift simulation model should be developed to simulate a long vertical test section up to 1000 m.

- The numerical model can integrate the population balance equations (PBE) along with the Euler-Euler model. This can be implemented to allow a better insight into the factors affecting the bubble size and their distribution in the column. The inclusion can also assist the interaction among bubbles in dispersed flow. PBE allows the bubble break-up and coalescence phenomena to be modelled. These phenomena are key parameters in predicting reasonable results for bubble size and distribution.

- Investigate the bubble formation using advanced multi-phase models such as the Mixture and Eulerian models. The models solve a larger set of momentum and continuity equations for each phase. In addition to predict the actual flow in the column. The model will solve the equations for each phase (gas-liquid), which can give better qualitative results.

REFERENCES

Abdulkadir, M., Azzi, A., Zhao, D., Lowndes, I. & Azzopardi, B. 2014a. Liquid film thickness behaviour within a large diameter vertical 180° return bend. *Chemical Engineering Science,* 107**,** 137-148.

Abdulkadir, M., Hernandez-Perez, V., Lowndes, I. S., Azzopardi, B. J. & Dzomeku, S. 2014b. Experimental study of the hydrodynamic behaviour of slug flow in a vertical riser. *Chemical Engineering Science,* 106**,** 60-75.

Acuña, C. A. & Finch, J. A. 2010. Tracking velocity of multiple bubbles in a swarm. *International Journal of Mineral Processing,* 94**,** 147-158.

Alamu, M. B. 2010. *Investigation of Periodic Structures in Gas-Liquid Flow.* PhD Thesis, University of Nottingham.

Alamu, M. B. & Azzopardi, B. J. 2011. Wave and drop periodicity in transient annular flow. *Nuclear Engineering and Design,* 241**,** 5079-5092.

Alhanati, F. J. S., Schmidt, Z., Doty, D. R. & Lagerlef, D. D. 1993. Continuous Gas-Lift Instability: Diagnosis, Criteria, and Solutions. Society of Petroleum Engineers.

Ansari, M. R. & Azadi, R. 2016. Effect of diameter and axial location on upward gas–liquid two-phase flow patterns in intermediate-scale vertical tubes. *Annals of Nuclear Energy,* 94**,** 530-540.

Ansys Inc. 2013. Fluent Population Balance Modul.

Ansys Inc. 2016a. *Fluent* [Online]. Available: https://caeai.com/ansys-software-support/ansys-software/computational-fluid-dynamics-ansys-cfx-and-fluent-cfd-software.

Ansys Inc. 2016b. *ICEM CFD* [Online]. Available: http://resource.ansys.com/Products/Other+Products/ANSYS+ICEM+CFD.

Asheim, H. 1988. Criteria for Gas-Lift Stability.

Asheim, H. 1999. Verification of Transient, Multi-Phase Flow Simulation for Gas Lift Applications. Society of Petroleum Engineers.

Azzopardi, B. J., Do, H. K., Azzi, A. & Hernandez Perez, V. 2015. Characteristics of air/water slug flow in an intermediate diameter pipe. *Experimental Thermal and Fluid Science,* 60**,** 1-8.

Azzopardi, B. J., Pioli, L. & Abdulkareem, L. A. 2014. The properties of large bubbles rising in very viscous liquids in vertical columns. *International Journal of Multiphase Flow,* 67**,** 160-173.

Behbahani, M., Edrisi, M., Rashidi, F. & Amani, E. 2012. Tuning a multi-fluid model for gas lift simulations in wells. *Chemical Engineering Research and Design,* 90**,** 471-486.

Bellarby, J. 2009. *Well completion design*, Elsevier.

Bertuzzi, A. F., Welchon, J. K. & Poettman, F. H. 1953. Description and Analysis of an Efficient Continuous-Flow Gas-Lift Installation.

Bhole, M. R., Roy, S. & Joshi, J. B. 2006. Laser doppler anemometer measurements in bubble column: effect of sparger. *Industrial & engineering chemistry research,* 45**,** 9201-9207.

Bordalo, S. N. & Gaspari, E. F. 1997. Stability Parameter for Two-Phase Vertical Annular Flow. Society of Petroleum Engineers.

Brill, J. P. 1987. Multiphase Flow in Wells. *Journal of Petroleum Technology,* 39.

Çengel, Y. A. & Cimbala, J. M. 2014. *Fluid mechanics fundamentals and applications.* , McGraw-Hill Higher Education.

Cheng, H., Hills, J. & Azzorpardi, B. 1998. A study of the bubble-to-slug transition in vertical gas-liquid flow in columns of different diameter. *International Journal of Multiphase Flow,* 24**,** 431-452.

Chia, Y. C. & Hussain, S. 1999. Gas Lift Optimization Efforts and Challenges. Society of Petroleum Engineers.

Da Hlaing, N., Sirivat, A., Siemanond, K. & Wilkes, J. O. 2007. Vertical two-phase flow regimes and pressure gradients: Effect of viscosity. *Experimental Thermal and Fluid Science,* 31**,** 567-577.

Dai, Y., Dakshinammorthy, D. & Agrawal, M. CFD Modeling of Bubbly, Slug and Annular Flow Regimes in Vertical Pipelines. Offshore Technology Conference, 2013. Offshore Technology Conference.

Dalsmo, M., Halvorsen, E. & Slupphaug, O. 2002. Active Feedback Control of Unstable Wells at the Brage Field. Society of Petroleum Engineers.

Decker, K. L. 1993. Gas-Lift Valve Performance Testing. Society of Petroleum Engineers.

Deen, N. G., Solberg, T. & Hjertager, B. R. H. 2001. Large eddy simulation of the gas–liquid flow in a square cross-sectioned bubble column. *Chemical Engineering Science,* 56**,** 6341-6349.

Deju, L., Cheung, S. C. P., Yeoh, G. H. & Tu, J. Y. 2013. Capturing coalescence and break-up processes in vertical gas–liquid flows: Assessment of population balance methods. *Applied Mathematical Modelling,* 37**,** 8557-8577.

Descamps, M. N., Oliemans, R. V. A., Ooms, G. & Mudde, R. F. 2007. Experimental investigation of three-phase flow in a vertical pipe: Local characteristics of the gas phase for gas-lift conditions. *International Journal of Multiphase Flow,* 33**,** 1205-1221.

Duns Jr, H. & Ros, N. Vertical flow of gas and liquid mixtures in wells. 6th World Petroleum Congress, 1963. World Petroleum Congress.

E.Brown, K. & Beggs, H. D. 1977. The technology of artificial lift methods. *Book,* Volume 1 inflow performance multiphase flow in pipes the flowing well.

Ebrahimi, M. 2010. Gas Lift Optimization in One of Iranian South Western Oil Fields. Society of Petroleum Engineers.

Eikrem, G. O. 2006a. *Stabilization of gas-lift wells by feedback control.* Citeseer.

Eikrem, G. O. 2006b. Stabilization of Gas-Lift Wells by

Feedback Control.

Eikrem, G. O., Foss, B., Imsland, L., Hu, B. & Golan, M. 2002. Stabilization of gas lifted wells. *IFAC Proceedings Volumes,* 35**,** 139-144.

Elldakli, F., Soliman, M. Y., Shahri, M., Winkler, H. W. & Gamadi, T. D. 2014. Improved Gas Lift Valve Performance Using a Modified Design for GLV Seat. Society of Petroleum Engineers.

Evers, M. G. L., Van Beusekom, V. L. & Henkes, R. a. W. M. 2009. Appearance and Mitigation of Density Waves in Continuously Gas-Lifted Oil Wells. BHR Group.

Fairuzov, Y. V. & Guerrero-Sarabia, I. 2005. Effect of Operating Valve Performance on Stability of Gas-Lift Wells. Society of Petroleum Engineers.

Faustinelli, J., Cuauro, A. & Bermúdez, G. 1999. A Solution to Instability Problems in Continuous Gas-Lift Wells Offshore Lake Maracaibo. Society of Petroleum Engineers.

Forero, G., Mcfadyen, K., Turner, R., Waring, B. & Steenken, E. 1993. Artificial lift manual part 2a.

Gilbert, W. E. 1954. Flowing and Gas-lift well Performance. American Petroleum Institute.

Grimstad, B. & Foss, B. 2014. A nonlinear, adaptive observer for gas-lift wells operating under slowly varying reservoir pressure. *IFAC Proceedings Volumes,* 47**,** 2824-2829.

Guerrero-Sarabia, I. & Fairuzov, Y. V. 2013. Linear and non-linear analysis of flow instability in gas-lift wells. *Journal of Petroleum Science and Engineering,* 108**,** 162-171.

Guet, S. & Ooms, G. 2006. Fluid mechanical aspects of the gas-lift technique. *Annu. Rev. Fluid Mech.,* 38**,** 225-249.

Guet, S., Ooms, G., Oliemans, R. & Mudde, R. 2004. Bubble size effect on low liquid input drift–flux parameters. *Chemical engineering science,* 59**,** 3315-3329.

Guet, S. C. L. 2004. *Bubble size effect on the gas-lift technique*, TU Delft, Delft University of Technology.

Hagedorn, A. R. & Brown, K. E. 1964. The Effect of Liquid Viscosity in Two-Phase Vertical Flow.

Hagesaether, L., Jakobsen, H. A. & Svendsen, H. F. 2002. A model for turbulent binary breakup of dispersed fluid particles. *Chemical Engineering Science,* 57**,** 3251-3267.

Harasek, M., Horvath, A., Jordan, C. & Kuttner, C. 2010. *CFD simulation of bubble columns using a VOF model*, na.

Hasan, A. R. & Kabir, C. S. 1988. A Study of Multiphase Flow Behavior in Vertical Wells.

Hatton, R. N. & Potter, K. 2011. Optimization of gas-injected oil wells. *Science Applications International Corporation (SAIC)*, 1-4.

Hu, B. 2005. *Characterization of gas-lift instabilities.* PhD Thesis, Norwegian University of Science and Technology.

Isao, K. & Mamoru, I. 1987. Drift flux model for large diameter pipe and new correlation for pool void fraction. *International Journal of Heat and Mass Transfer,* 30, 1927-1939.

Kaji, R. & Azzopardi, B. J. 2010. The effect of pipe diameter on the structure of gas/liquid flow in vertical pipes. *International Journal of Multiphase Flow,* 36, 303-313.

Kaji, R., Azzopardi, B. J. & Lucas, D. 2009. Investigation of flow development of co-current gas–liquid vertical slug flow. *International Journal of Multiphase Flow,* 35, 335-348.

Koide, K., Kato, S., Tanaka, Y. & Kubota, H. 1968. Bubbles generated from porous plate. *Journal of Chemical Engineering of Japan,* 1, 51-56.

Krishna, R., Urseanu, M. I., Van Baten, J. M. & Ellenberger, J. 1999. Rise velocity of a swarm of large gas bubbles in liquids. *Chemical Engineering Science,* 54, 171-183.

Kulkarni, A., Ekambara, K. & Joshi, J. 2007. On the development of flow pattern in a bubble column reactor: experiments and CFD. *Chemical engineering science,* 62, 1049-1072.

Kulkarni, A. A. 2003. *Transport phenomena and non-linear dynamics in multiphase systems.* Ph. D. Thesis, University of Mumbai, India.

Levich, V. & Krylov, V. 1969. Surface-tension-driven phenomena. *Annual Review of Fluid Mechanics,* 1, 293-316.

Liu, L., Yan, H., Zhao, G. & Zhuang, J. 2016. Experimental studies on the terminal velocity of air bubbles in water and glycerol aqueous solution. *Experimental Thermal and Fluid Science,* 78, 254-265.

Liu, T.-J. 1997. Investigation of the wall shear stress in vertical bubbly flow under different bubble size conditions. *International journal of multiphase flow,* 23, 1085-1109.

Liu, T. The role of bubble size on liquid phase turbulent structure in two-phase bubbly flow. Proc. Third International Congress on Multiphase Flow ICMF, 1998. 8-12.

Lucas, D., Krepper, E. & Prasser, H.-M. 2005. Development of co-current air–water flow in a vertical pipe. *International Journal of Multiphase Flow,* 31**,** 1304-1328.

Mahdiani, M. R. & Khamehchi, E. 2015. Stabilizing gas lift optimization with different amounts of available lift gas. *Journal of Natural Gas Science and Engineering,* 26**,** 18-27.

Mahmudi, M. & Sadeghi, M. T. 2013. The optimization of continuous gas lift process using an integrated compositional model. *Journal of Petroleum Science and Engineering,* 108**,** 321-327.

Mantecon, J. C. 1993. Gas-Lift Optimisation on Barrow Island, Western Australia. Society of Petroleum Engineers.

Morel, C., Ruyer, P., Seiler, N. & Laviéville, J. M. 2010. Comparison of several models for multi-size bubbly flows on an adiabatic experiment. *International Journal of Multiphase Flow,* 36**,** 25-39.

Ohnuki, A. & Akimoto, H. 1996. An experimental study on developing air-water two-phase flow along a large vertical pipe: effect of air injection method. *International journal of multiphase flow,* 22**,** 1143-1154.

Omebere-Iyari, N. K. & Azzopardi, B. J. 2007. A Study of Flow Patterns for Gas/Liquid Flow in Small Diameter Tubes. *Chemical Engineering Research and Design,* 85**,** 180-192.

Orkiszewski, J. 1967. Predicting Two-Phase Pressure Drops in Vertical Pipe.

Pan, L.-M., Zhang, M., Ju, P., He, H. & Ishii, M. 2016. Vertical co-current two-phase flow regime identification using fuzzy C-means clustering algorithm and ReliefF attribute weighting technique. *International Journal of Heat and Mass Transfer,* 95**,** 393-404.

Plucenio, A., Ganzaroli, C. A. & Pagano, D. J. 2012. Stabilizing gas-lift well dynamics with free operating point. *IFAC Proceedings Volumes,* 45**,** 95-100.

Poettman, F. H. & Carpenter, P. G. 1952. The Multiphase Flow of Gas, Oil, and Water Through Vertical Flow Strings with Application to the Design of Gas-lift Installations. American Petroleum Institute.

Posenato, A. & Rosa, V. R. 2012. Unload Procedure With Control of Liquid Flow Rate Through Gas Lift Valve. Society of Petroleum Engineers.

Pourtousi, M., Ganesan, P. & Sahu, J. 2015. Effect of bubble diameter size on prediction of flow pattern in Euler–Euler simulation of homogeneous bubble column regime. *Measurement,* 76**,** 255-270.

Prasser, H., Lucas, D., Krepper, E., Baldauf, D., Böttger, A. & Rohde, U. 2003. Strömungskarten und Modelle für transiente Zweiphasenströmungen Forschungszentrum *FZR-379***,** 183.

Pringle, C. C. T., Ambrose, S., Azzopardi, B. J. & Rust, A. C. 2015. The existence and behaviour of large diameter Taylor bubbles. *International Journal of Multiphase Flow,* 72**,** 318-323.

Rhino, D. 2016. *Rhinoceros 5 features* [Online]. Available: http://resource.ansys.com/Products/Other+Products/ANSYS+ICEM+CFD.

Rilian, N. A., Rohman, A. F., Hamzah, K., Arseto, Y. I., Narso, N. & Kurniawan, C. 2012. Successful Application of Venturi Orifice Gas Lift Valve in Kaji-Semoga Field, South Sumatra: A Case Study. Society of Petroleum Engineers.

Sanderford & W, D. 1981. Method and apparatus for optimizing production in a continuous or intermittent gas-lift well. Google Patents.

Sardeshpande, M. V., Shastri, P. & Ranade, V. V. 2015. Two Phase Flow Boiling Pressure Drop in Small Channels. *Procedia IUTAM,* 15**,** 313-320.

Sattar, M., Naser, J. & Brooks, G. 2013. Numerical simulation of two-phase flow with bubble break-up and coalescence coupled with population balance modeling. *Chemical Engineering and Processing: Process Intensification,* 70**,** 66-76.

Schlumberger 1999. Gas lift design and technology.

Stenmark, E. 2013. On multiphase flow models in ANSYS CFD software. *Chalmers Universiy of Technology, Sweden*.

Sun, B., Yan, D. & Zhang, Z. 1999. The instability of void fraction waves in vertical gas-liquid two-phase flow. *Communications in Nonlinear Science and Numerical Simulation,* 4**,** 181-186.

Szalinski, L., Abdulkareem, L. A., Da Silva, M. J., Thiele, S., Beyer, M., Lucas, D., Hernandez Perez, V., Hampel, U. & Azzopardi, B. J. 2010. Comparative study of gas–oil and gas–water two-phase flow in a vertical pipe. *Chemical Engineering Science,* 65**,** 3836-3848.

Tabib, M. V., Roy, S. A. & Joshi, J. B. 2008. CFD simulation of bubble column—an analysis of interphase forces and turbulence models. *Chemical Engineering Journal,* 139**,** 589-614.

Taha, T. & Cui, Z. 2006. CFD modelling of slug flow in vertical tubes. *Chemical Engineering Science,* 61**,** 676-687.

Taitel, Y., Bornea, D. & Dukler, A. 1980. Modelling flow pattern transitions for steady upward gas-liquid flow in vertical tubes. *AIChE Journal,* 26**,** 345-354.

Taitel, Y., Lee, N. & Dukler, A. 1978. Transient gas-liquid flow in horizontal pipes: Modeling the flow pattern transitions. *AIChE Journal,* 24**,** 920-934.

Tan, Y. H., Rafiei, A. A., Elmahdy, A. & Finch, J. A. 2013. Bubble size, gas holdup and bubble velocity profile of some alcohols and commercial frothers. *International Journal of Mineral Processing,* 119**,** 1-5.

Ter Avest, D. & Oudeman, P. 1995. A Dynamic Simulator to Analyse and Remedy Gas Lift Problems. Society of Petroleum Engineers.

Torre, A. J., Schmidt, Z., Blais, R. N., Doty, D. R. & Brill, J. P. 1987. Casing Heading in Flowing Oil Wells.

Waltrich, P. J. & Barbosa, J. R. 2011. Performance of Vertical Transient Two-Phase Flow Models Applied to Liquid Loading in Gas Wells. Society of Petroleum Engineers.

Waltrich, P. J., Falcone, G. & Barbosa Jr, J. R. 2013. Axial development of annular, churn and slug flows in a long vertical tube. *International Journal of Multiphase Flow,* 57**,** 38-48.

Wang, S., Lee, S., Jones, O. & Lahey, R. 1987. 3-D turbulence structure and phase distribution measurements in bubbly two-phase flows. *International Journal of multiphase flow,* 13**,** 327-343.

Wu, Q., Kim, S., Ishii, M. & Beus, S. 1998a. One-group interfacial area transport in vertical bubbly flow. *International Journal of Heat and Mass Transfer,* 41**,** 1103-1112.

Wu, Q., Kim, S., Ishii, M. & Beus, S. G. 1998b. One-group interfacial area transport in vertical bubbly flow. *International Journal of Heat and Mass Transfer,* 41**,** 1103-1112.

Xu, J.-Y., Zhang, J., Liu, H.-F. & Wu, Y.-X. 2012. Oil–gas–water three-phase upward flow through a vertical pipe: Influence of gas injection on the pressure gradient. *International Journal of Multiphase Flow,* 46**,** 1-8.

Yasin, S. S. M., Aziz, N. M. a. N., Zakaria, Z. & Samsuri, A. 2014. A Study of Continuous Flow Gas Lift System Using CFD. *Journal of Applied Sciences,* 14**,** 1265.

Zabaras, G. J. 1994. Physical Modelling Of Vertical Multiphase Flow: Prediction Of Pressure Gradients In Oil And Gas Wells. Offshore Technology Conference.

Zhang, D. & Vanderheyden, W. 2002. The effects of mesoscale structures on the disperse two-phase flows and their closures for dilute suspensions. *Int. J. Multiph. Flow,* 28**,** 805-822.

Zhang, J. & Fan, L.-S. 2003. On the rise velocity of an interactive bubble in liquids. *Chemical Engineering Journal,* 92**,** 169-176.

APPENDICES

This appendices comprises of the following:

A. *Appendix A: Experimental Data for both techniques*

B. *Pressure-drop along the test section for both techniques*

C. *List of publications*

8.1 Appendix -A

Experimental data sheet that were used to record the operating conditions during each run for both SNIT and MNIT trials.

Liquid flow rate l/min	Air Injection Pressure (bar)*	Air flow rate l/min	Inlet pressure (Psi)	Outlet pressure (Psi)	Inlet Temp C^o	Outlet Temp C^o	Outlet flow rate l/min
5 l/min	0.5	1	3	0.5	17.3	17.7	5.88
	5	9	3.8	1	17.3	17.7	16.30
10 l/min							
20 l/min							
30 l/min							

Typical data sheet for bubble sizes and velocities for each segment

	P etroleum T echnology R esearch G roup	SEGMENT :1 Video- 8775 Single Nozzle Injection Technique (SNIT) Operating conditions: P = 0.5 bar Liquid Flow rate = 5 l/min, Date: 15/04/2016	University of Salford MANCHESTER

Bubble Diameter (mm)	Bubble Velocity (m/s)	Equivalent Bubble Diameter (mm)	Average Bubble Diameter (mm)	Minimum Bubble size (mm)	Maximum Bubble size (mm)	Bubbles accounts per frame
0	-8.497	0.966	9.14	1.15	34.5	28
		Average	**Average**	**Average**		

Experimental Data for MNIT

		SEGMENT :1	Video- 8655	University of Salford MANCHESTER		
		Operating conditions: P = 0.5 bar Liquid Flow rate =5 l/min				
Bubble Diameter (mm)	Bubble Velocity (m/s)	Equivalent Bubble Diameter (mm)	Average Bubble Diameter (mm)	Minimum Bubble size (mm)	Maximum Bubble size (mm)	Bubbles accounts
0	-7.11	0.809	7.22	1.14	32	40
1320	-6.884	1.685	7.22	1.14	30.2	39
2640	-6.657	2.561	6.8	1.36	28.6	35
3960	-6.43	3.436	6.84	1.14	27.4	41
5280	-6.203	4.312	7.84	1.32	43.9	29
6600	-5.976	5.188	6.89	1.14	28.9	33
7920	-5.75	6.064	5.97	1.14	35.9	36
9240	-5.523	6.939	6	1.14	32.2	37
10560	-5.296	7.815	6.04	1.14	26.5	43
11880	-5.069	8.691	6.41	1.14	34.2	34
13200	-4.842	9.567	6.83	1.14	38.2	36
14520	-4.616	10.443	6.79	1.14	40.5	32
15840	-4.389	11.318	7.2	1.14	35.8	35
17160	-4.162	12.194	5.22	0.991	39.3	49
18480	-3.935	13.07	6.47	1.32	40.8	39
19800	-3.708	13.946	7.12	1.14	44.6	27
21120	-3.482	14.821	7.32	1.14	41.3	39
22440	-3.255	15.697	7.21	1.32	28.9	40
23760	-3.028	16.573	6.61	1.1	30.4	40
25080	-2.801	17.449	7.63	1.62	30.2	39
26400	-2.574	18.324	7.22	1.14	31	40
27720	-2.348	19.2	9.01	1.14	30.1	35
29040	-2.121	20.076	7.62	1.14	32.7	42
30360	-1.894	20.952	9.11	1.14	28	39
31680	-1.667	21.828	9.29	1.14	27.8	44
33000	-1.44	22.703	7.62	1.04	27.2	44
34320	-1.214	23.579	7.98	1.14	31.6	40
35640	-0.987	24.455	6.86	1.14	41	50
36960	-0.76	25.331	8.38	1.14	31.9	41
38280	-0.533	26.206	9.65	1.14	33.9	45
39600	-0.306	27.082	Average 7.279	Average 1.1717	Average 33.5	42
40920	-0.08	27.958				36

42240	0.147	28.834				36
43560	0.374	29.71				41
44880	0.601	30.585				39
46200	0.828	31.461				38
47520	1.055	32.337				37
48840	1.281	33.213				37
50160	1.508	34.088				38
51480	1.735	34.964				35
52800	1.962	35.84				35
54120	2.189	36.716				36
55440	2.415	37.591				40
56760	2.642	38.467				31
58080	2.869	39.343				31
59400	3.096	40.219				34
60720	3.323	41.095				40
62040	3.549	41.97				39
63360	3.776	42.846				31
64680	4.003	43.722				26
	4.23	44.598				34
	4.457	45.473				36
	4.683	46.349				31
	4.91	47.225				27
	5.137	48.101				30
	5.364	48.977				44
	5.591	49.852				32
	5.817	50.728				42
	6.044	51.604				44
	6.271	52.48				37
	6.498	53.355				33
	6.725	54.231				32
	6.951	55.107				31
	7.178	55.983				26
	7.405	56.859				37
	7.632	57.734				21

Bubble Diameter (mm)	Bubble Velocity (m/s)	Equivalent Bubble Diameter (mm)	Average Bubble Diameter (mm)	Minimum Bubble size (mm)	Maximum Bubble size (mm)	Bubbles accounts
		SEGMENT :1 — Video- 8656 — Operating conditions: P = 1 bar — Liquid Flow rate =5 l/min				
0	-7.572	0.808	8.27	1.14	46.6	48
1320	-7.343	1.77	7.73	1.14	40.2	71
2640	-7.114	2.732	6.91	1.14	42.1	73
3960	-6.885	3.694	6.46	1.4	41.2	76
5280	-6.656	4.657	7.18	1.09	44.7	64
6600	-6.428	5.619	6.94	1.14	48.3	64
7920	-6.199	6.581	5.58	0.989	55.3	74
9240	-5.97	7.544	6.91	0.989	50.1	73
10560	-5.741	8.506	7.25	0.932	61.5	44
11880	-5.512	9.468	6.41	0.989	41.6	76
13200	-5.283	10.43	7	0.872	61.1	71
14520	-5.054	11.393	6.94	1.14	43.5	71
15840	-4.825	12.355	5.97	0.989	33	89
17160	-4.596	13.317	7.77	1.04	50.4	64
18480	-4.367	14.279	5.01	1.14	30.6	99
19800	-4.139	15.242	5.47	1.09	36.6	100
21120	-3.91	16.204	6.87	1.14	50.7	75
22440	-3.681	17.166	4.99	1.14	29	107
23760	-3.452	18.129	5	1.14	37.6	107
25080	-3.223	19.091	5.74	1.14	30.1	97
26400	-2.994	20.053	5.49	0.932	52	91
27720	-2.765	21.015	5.58	0.932	37.6	84
29040	-2.536	21.978	5.49	0.989	40.1	94
30360	-2.307	22.94	5.97	0.808	31.1	93
31680	-2.078	23.902	5.36	0.989	55.4	96
33000	-1.85	24.865	5.77	1.14	42.6	88
34320	-1.621	25.827	5.62	1.14	46	90
35640	-1.392	26.789	6.02	1.04	45.1	96
36960	-1.163	27.751	5.51	1.09	30.7	104
38280	-0.934	28.714	6.21	1.09	37.8	81
39600	-0.705	29.676	Average 6.247	Average 1.064	Average 43.086	82
40920	-0.476	30.638				77

42240	-0.247	31.601				80
43560	-0.018	32.563				83
44880	0.211	33.525				82
46200	0.44	34.487				88
47520	0.668	35.45				98
48840	0.897	36.412				71
50160	1.126	37.374				73
51480	1.355	38.337				72
52800	1.584	39.299				94
54120	1.813	40.261				85
55440	2.042	41.223				84
56760	2.271	42.186				67
58080	2.5	43.148				62
59400	2.729	44.11				86
60720	2.957	45.073				61
62040	3.186	46.035				75
63360	3.415	46.997				54
64680	3.644	47.959				84
	3.873	48.922				94
	4.102	49.884				68
	4.331	50.846				91
	4.56	51.809				78
	4.789	52.771				81
	5.018	53.733				66
	5.246	54.695				58
	5.475	55.658				58
	5.704	56.62				49
	5.933	57.582				44
	6.162	58.545				66
	6.391	59.507				53
	6.62	60.469				66
	6.849	61.431				53
	7.078	62.394				66
	7.307	63.356				68

Bubble Diameter (mm)	Bubble Velocity (m/s)	Equivalent Bubble Diameter (mm)	Average Bubble Diameter (mm)	Minimum Bubble size (mm)	Maximum Bubble size (mm)	Bubbles accounts
0	-7.707	0.807	5.62	1.04	38.4	92
1320	-7.472	1.746	5.3	1.09	61.8	93
2640	-7.238	2.685	6	0.807	45.4	88
3960	-7.003	3.624	6.09	1.09	48.1	98
5280	-6.769	4.563	5.98	0.988	46.4	101
6600	-6.535	5.502	5.72	1.09	38.8	96
7920	-6.3	6.442	5.83	1.04	48.6	116
9240	-6.066	7.381	6.2	1.09	48.9	97
10560	-5.831	8.32	6.31	1.04	45.8	110
11880	-5.597	9.259	6.17	0.988	35	113
13200	-5.362	10.198	5.43	1.14	39	127
14520	-5.128	11.137	5.75	1.14	45.4	120
15840	-4.893	12.076	5.77	0.872	36.8	146
17160	-4.659	13.015	6.48	0.932	50.2	99
18480	-4.425	13.954	6.58	1.14	42.7	99
19800	-4.19	14.894	6.29	0.932	41.9	88
21120	-3.956	15.833	6.1	1.14	50.5	71
22440	-3.721	16.772	5.02	1.04	30.5	134
23760	-3.487	17.711	5.77	0.807	36.8	132
25080	-3.252	18.65	8.3	1.14	36	66
26400	-3.018	19.589	7.14	1.14	57.8	81
27720	-2.783	20.528	6.03	0.988	39.3	121
29040	-2.549	21.467	6.84	1.09	46.3	90
30360	-2.315	22.406	5.83	0.807	33.2	135
31680	-2.08	23.346	8.04	1.14	50.8	74
33000	-1.846	24.285	5.59	0.932	35.5	142
34320	-1.611	25.224	6.82	1.14	39.8	87
35640	-1.377	26.163	5.93	1.14	39.5	84
36960	-1.142	27.102	6.26	0.872	47.3	99
38280	-0.908	28.041	5.77	1.14	48.3	106
39600	-0.673	28.98	Average 6.165	Average 1.031	Average 43.493	116

40920	-0.439	29.919				122
42240	-0.205	30.858				117
43560	0.03	31.798				106
44880	0.264	32.737				137
46200	0.499	33.676				136
47520	0.733	34.615				155
48840	0.968	35.554				146
50160	1.202	36.493				97
51480	1.437	37.432				95
52800	1.671	38.371				90
54120	1.905	39.31				94
55440	2.14	40.25				116
56760	2.374	41.189				112
58080	2.609	42.128				144
59400	2.843	43.067				123
60720	3.078	44.006				121
62040	3.312	44.945				123
63360	3.547	45.884				111
64680	3.781	46.823				106
	4.015	47.763				132
	4.25	48.702				111
	4.484	49.641				96
	4.719	50.58				113
	4.953	51.519				119
	5.188	52.458				121
	5.422	53.397				103
	5.657	54.336				124
	5.891	55.275				93
	6.125	56.215				162
	6.36	57.154				95
	6.594	58.093				114
	6.829	59.032				157
	7.063	59.971				110
	7.298	60.91				133
	7.532	61.849				95

		SEGMENT :1　　　　　　Video- 8658　　　University of Salford MANCHESTER Operating conditions: P = 3 bar Liquid Flow rate =5 l/min				
Bubble Diameter (mm)	Bubble Velocity (m/s)	Equivalent Bubble Diameter (mm)	Average Bubble Diameter (mm)	Minimum Bubble size (mm)	Maximum Bubble size (mm)	Bubbles accounts
0	-7.674	0.807	4.34	0.807	33.4	176
1320	-7.439	2.119	4.3	0.989	50.1	191
2640	-7.203	3.43	4.05	1.04	38.1	173
3960	-6.967	4.741	4.72	0.872	59.2	156
5280	-6.732	6.053	4.53	1.04	36.1	181
6600	-6.496	7.364	5.39	1.09	42.5	150
7920	-6.261	8.675	4.56	0.932	31.2	187
9240	-6.025	9.986	3.93	0.989	26.2	211
10560	-5.789	11.298	4.97	1.04	31	150
11880	-5.554	12.609	4.3	0.982	48.8	192
13200	-5.318	13.92	4.47	0.932	44.1	174
14520	-5.082	15.232	4.32	0.872	43.2	159
15840	-4.847	16.543	5.48	1.14	59.2	132
17160	-4.611	17.854	4.92	0.932	36	145
18480	-4.375	19.166	5.28	0.932	55.1	105
19800	-4.14	20.477	4.68	0.932	50.3	156
21120	-3.904	21.788	5.11	1.04	56.2	123
22440	-3.668	23.099	4.11	0.932	38.2	153
23760	-3.433	24.411	5.16	0.989	45.5	136
25080	-3.197	25.722	4.28	0.872	40	170
26400	-2.961	27.033	5.2	1.04	39.4	147
27720	-2.726	28.345	5.13	0.989	32.4	146
29040	-2.49	29.656	5.17	1.14	48.9	138
30360	-2.254	30.967	5	0.932	39.6	140
31680	-2.019	32.279	5.49	1.09	59.1	138
33000	-1.783	33.59	5.71	1.14	36.1	131
34320	-1.548	34.901	5.01	0.932	39.7	164
35640	-1.312	36.213	5.1	1.14	34.5	144
36960	-1.076	37.524	5.03	0.932	33.2	143
38280	-0.841	38.835	4.14	0.989	35.6	186
39600	-0.605	40.146	Average 4.796	Average 0.9892	Average 42.096	210

40920	-0.369	41.458				210
42240	-0.134	42.769				199
43560	0.102	44.08				184
44880	0.338	45.392				179
46200	0.573	46.703				141
47520	0.809	48.014				146
48840	1.045	49.326				195
50160	1.28	50.637				157
51480	1.516	51.948				164
52800	1.752	53.259				139
54120	1.987	54.571				167
55440	2.223	55.882				170
56760	2.459	57.193				180
58080	2.694	58.505				160
59400	2.93	59.816				168
60720	3.166	61.127				162
62040	3.401	62.439				188
63360	3.637	63.75				158
64680	3.872	65.061				149
	4.108	66.373				123
	4.344	67.684				167
	4.579	68.995				152
	4.815	70.306				122
	5.051	71.618				141
	5.286	72.929				145
	5.522	74.24				130
	5.758	75.552				176
	5.993	76.863				132
	6.229	78.174				110
	6.465	79.486				123
	6.7	80.797				154
	6.936	82.108				153
	7.172	83.42				185
	7.407	84.731				185
	7.643	86.042				161

	SEGMENT :1 Video- 8659	University of Salford MANCHESTER
	Operating conditions: P = 4 bar Liquid Flow rate =5 l/min	

Bubble Diameter (mm)	Bubble Velocity (m/s)	Equivalent Bubble Diameter (mm)	Average Bubble Diameter (mm)	Minimum Bubble size (mm)	Maximum Bubble size (mm)	Bubbles accounts
0	-7.207	0.808	4.71	1.03	34.9	215
1320	-6.985	2.046	4.4	0.933	36	215
2640	-6.762	3.284	4.75	1.04	37.5	179
3960	-6.54	4.521	3.86	0.873	35.5	237
5280	-6.318	5.759	4.29	0.933	36.1	212
6600	-6.095	6.997	4.17	0.873	34.7	201
7920	-5.873	8.235	4.14	0.933	29	213
9240	-5.651	9.472	4.01	0.99	31	210
10560	-5.428	10.71	3.42	0.933	51.7	246
11880	-5.206	11.948	3.92	0.99	37.1	228
13200	-4.984	13.185	4.3	1.14	31.4	189
14520	-4.761	14.423	4.46	0.933	38.5	167
15840	-4.539	15.661	3.97	0.933	31	221
17160	-4.317	16.899	4.44	1.09	39	193
18480	-4.094	18.136	4.26	0.99	30.9	192
19800	-3.872	19.374	4.89	1.09	43.4	206
21120	-3.649	20.612	4.74	0.873	51.9	181
22440	-3.427	21.85	4.53	1.09	29.2	211
23760	-3.205	23.087	5.98	0.933	38.9	138
25080	-2.982	24.325	4.65	1.09	42.5	154
26400	-2.76	25.563	5.01	0.873	32.3	182
27720	-2.538	26.801	4.69	0.933	39.2	193
29040	-2.315	28.038	4.75	1.09	54.1	157
30360	-2.093	29.276	4.36	0.933	50.6	194
31680	-1.871	30.514	4.38	1.04	50.2	192
33000	-1.648	31.752	4.58	0.99	34.8	222
34320	-1.426	32.989	4.17	1.04	33.6	222
35640	-1.204	34.227	4.38	1.09	31.1	201
36960	-0.981	35.465	4.25	0.99	52.9	206
38280	-0.759	36.703	4.19	0.933	57.6	216
39600	-0.537	37.94	Average 4.421	Average 0.9867	Average 39.22	220

40920	-0.314	39.178				260
42240	-0.092	40.416	187			189
43560	0.13	41.653				195
44880	0.353	42.891				214
46200	0.575	44.129				183
47520	0.797	45.367				221
48840	1.02	46.604				235
50160	1.242	47.842				213
51480	1.464	49.08				236
52800	1.687	50.318				240
54120	1.909	51.555				225
55440	2.132	52.793				244
56760	2.354	54.031				202
58080	2.576	55.269				226
59400	2.799	56.506				229
60720	3.021	57.744				215
62040	3.243	58.982				217
63360	3.466	60.22				219
64680	3.688	61.457				208
	3.91	62.695				217
	4.133	63.933				170
	4.355	65.171				194
	4.577	66.408				197
	4.8	67.646				203
	5.022	68.884				175
	5.244	70.121				187
	5.467	71.359				173
	5.689	72.597				199
	5.911	73.835				179
	6.134	75.072				228
	6.356	76.31				193
	6.578	77.548				169
	6.801	78.786				155
	7.023	80.023				178
	7.245	81.261				190

Bubble Diameter (mm)	Bubble Velocity (m/s)	Equivalent Bubble Diameter (mm)	Average Bubble Diameter (mm)	Minimum Bubble size (mm)	Maximum Bubble size (mm)	Bubbles accounts
0	-7.568	0.806	3.74	1.04	28.4	236
1320	-7.341	1.999	4.44	1.09	35.6	157
2640	-7.114	3.192	3.39	0.988	31	261
3960	-6.888	4.385	3.72	0.871	51.1	211
5280	-6.661	5.578	3.89	0.871	37.9	202
6600	-6.435	6.77	3.76	0.871	44.2	196
7920	-6.208	7.963	3.67	0.931	32.3	259
9240	-5.981	9.156	4.64	1.04	78.3	128
10560	-5.755	10.349	4.27	0.931	54.6	193
11880	-5.528	11.542	3.78	0.931	37.9	229
13200	-5.302	12.734	3.81	0.871	35.5	214
14520	-5.075	13.927	3.66	0.931	54.2	190
15840	-4.848	15.12	3.22	0.871	27.5	280
17160	-4.622	16.313	3.57	0.988	23.3	253
18480	-4.395	17.506	3.67	0.988	42.1	214
19800	-4.169	18.698	3.33	0.931	40.1	241
21120	-3.942	19.891	3.59	0.871	31.9	242
22440	-3.715	21.084	3.7	0.871	26.6	241
23760	-3.489	22.277	3.61	0.988	34.3	191
25080	-3.262	23.47	4.07	0.988	43.1	170
26400	-3.036	24.663	4.01	1.09	28.2	218
27720	-2.809	25.855	3.85	0.988	26.8	221
29040	-2.582	27.048	4.76	1.09	31.3	173
30360	-2.356	28.241	4.1	0.931	39.7	198
31680	-2.129	29.434	4.26	0.988	33.4	217
33000	-1.903	30.627	4.16	0.931	46.6	211
34320	-1.676	31.819	3.62	1.09	43.3	189
35640	-1.449	33.012	4.05	0.931	32.7	225
36960	-1.223	34.205	4.12	0.806	35.3	212
38280	-0.996	35.398	4.39	0.931	42	185
39600	-0.77	36.591	Average 3.895	Average 0.9546	Average 38.31	273
40920	-0.543	37.783				196

188

42240	-0.317	38.976				195
43560	-0.09	40.169	189			232
44880	0.137	41.362				239
46200	0.363	42.555				273
47520	0.59	43.747				255
48840	0.816	44.94				254
50160	1.043	46.133				284
51480	1.27	47.326				234
52800	1.496	48.519				248
54120	1.723	49.712				261
55440	1.949	50.904				226
56760	2.176	52.097				231
58080	2.403	53.29				205
59400	2.629	54.483				178
60720	2.856	55.676				219
62040	3.082	56.868				210
63360	3.309	58.061				216
64680	3.536	59.254				266
	3.762	60.447				238
	3.989	61.64				219
	4.215	62.832				225
	4.442	64.025				294
	4.669	65.218				281
	4.895	66.411				206
	5.122	67.604				223
	5.348	68.796				235
	5.575	69.989				262
	5.801	71.182				216
	6.028	72.375				219
	6.255	73.568				260
	6.481	74.761				258
	6.708	75.953				260
	6.934	77.146				243
	7.161	78.339				236

	P(etroleum) T(echnology) R(esearch) G(roup)	SEGMENT :1 Video- 8662 Operating conditions: P = 0.5 bar Liquid Flow rate =10 l/min		University of Salford MANCHESTER		
Bubble Diameter (mm)	Bubble Velocity (m/s)	Equivalent Bubble Diameter (mm)	Average Bubble Diameter (mm)	Minimum Bubble size (mm)	Maximum Bubble size (mm)	Bubbles accounts
0	-6.702	0.871	8.46	0.988	36.8	32
1320	-6.484	1.853	8.81	1.14	37.6	35
2640	-6.267	2.835	9.61	1.14	33	31
3960	-6.05	3.817	8.72	1.09	41.6	34
5280	-5.833	4.799	8.68	1.14	33.7	40
6600	-5.616	5.781	10.4	1.47	40	25
7920	-5.398	6.763	7.63	0.871	45.6	33
9240	-5.181	7.745	8.34	1.14	33.4	30
10560	-4.964	8.727	7.91	1.14	32.4	33
11880	-4.747	9.709	10.2	1.14	35.2	21
13200	-4.529	10.691	9.14	1.14	25.7	29
14520	-4.312	11.673	7.94	1.14	34	32
15840	-4.095	12.655	9.41	1.14	33.8	30
17160	-3.878	13.637	9.51	0.931	38.1	22
18480	-3.661	14.619	8.61	1.14	38.5	29
19800	-3.443	15.601	8.08	1.14	35.1	30
21120	-3.226	16.583	9.61	1.47	41	30
22440	-3.009	17.565	8.2	1.14	36.1	32
23760	-2.792	18.547	6.59	1.14	33.6	48
25080	-2.575	19.529	8.05	1.14	38.9	34
26400	-2.357	20.511	7.04	1.32	40.4	33
27720	-2.14	21.493	8.84	1.14	35.6	30
29040	-1.923	22.475	7.74	1.14	38.6	27
30360	-1.706	23.457	7.28	1.14	32.3	37
31680	-1.488	24.439	6.49	1.14	32.7	45
33000	-1.271	25.421	7.49	1.09	32.4	36
34320	-1.054	26.403	5.88	1.17	33.3	47
35640	-0.837	27.385	7.99	1.14	26.7	38
36960	-0.62	28.367	7.39	1.14	34.1	41
38280	-0.402	29.349	7.69	1.14	34	42
39600	-0.185	30.331	Average 8.257	Average 1.144	Average 35.47	38
40920	0.032	31.313				33

42240	0.249	32.295				35
43560	0.467	33.277				36
44880	0.684	34.259				37
46200	0.901	35.241				36
47520	1.118	36.223				35
48840	1.335	37.205				25
50160	1.553	38.187				25
51480	1.77	39.169				24
52800	1.987	40.151				23
54120	2.204	41.133				31
55440	2.421	42.115				43
56760	2.639	43.097				35
58080	2.856	44.079				31
59400	3.073	45.061				25
60720	3.29	46.043				39
62040	3.508	47.025				33
63360	3.725	48.007				40
64680	3.942	48.989				35
	4.159	49.971				32
	4.376	50.953				24
	4.594	51.935				26
	4.811	52.917				36
	5.028	53.899				51
	5.245	54.881				41
	5.462	55.863				37
	5.68	56.845				29
	5.897	57.827				30
	6.114	58.809				26
	6.331	59.791				31
	6.549	60.773				34
	6.766	61.755				37
	6.983	62.737				41
	7.2	63.719				30
	7.417	64.701				26

	Petroleum Technology Research Group	SEGMENT :1 Video- 8668 Operating conditions: P = 0.5 bar Liquid Flow rate =20 l/min	University of Salford MANCHESTER			
Bubble Diameter (mm)	Bubble Velocity (m/s)	Equivalent Bubble Diameter (mm)	Average Bubble Diameter (mm)	Minimum Bubble size (mm)	Maximum Bubble size (mm)	Bubbles accounts
0	-7.414	0.873	8.75	1.14	29.8	40
1320	-7.181	1.765	9.89	1.36	28.5	33
2640	-6.949	2.657	8.83	1.09	22	43
3960	-6.716	3.548	8.93	1.14	30.7	34
5280	-6.484	4.44	9.36	1.14	43.8	28
6600	-6.251	5.332	10.5	2.09	41.1	25
7920	-6.018	6.224	10.2	1.28	34.1	24
9240	-5.786	7.116	9.26	1.14	37.2	31
10560	-5.553	8.008	9.24	1.09	27.2	33
11880	-5.321	8.9	8.85	1.14	37.1	35
13200	-5.088	9.792	11.5	1.14	39	22
14520	-4.856	10.684	10.4	1.32	37.7	28
15840	-4.623	11.576	11.5	1.36	44.6	21
17160	-4.39	12.468	11.5	1.23	36.9	21
18480	-4.158	13.36	10.5	1.48	37.9	23
19800	-3.925	14.252	13	1.32	44.6	20
21120	-3.693	15.144	9.67	1.04	32.8	30
22440	-3.46	16.036	12.7	1.14	35.5	20
23760	-3.228	16.927	10	1.14	41.2	32
25080	-2.995	17.819	11.6	1.14	36.4	24
26400	-2.762	18.711	10.2	1.36	30	31
27720	-2.53	19.603	8.5	1.14	32.9	31
29040	-2.297	20.495	9.87	1.14	31.4	29
30360	-2.065	21.387	9.69	1.14	33.1	23
31680	-1.832	22.279	11.6	1.14	38.6	23
33000	-1.6	23.171	9.18	1.14	38.4	27
34320	-1.367	24.063	11.8	1.32	27.2	26
35640	-1.134	24.955	12	1.32	47	17
36960	-0.902	25.847	11.6	1.36	45.4	18
38280	-0.669	26.739	8.6	1.14	35.8	32
39600	-0.437	27.631	Average 10.307	Average 1.2373	Average 35.93	30
40920	-0.204	28.523				31
42240	0.028	29.414				19
43560	0.261	30.306				29
44880	0.494	31.198				22

46200	0.726	32.09				24
47520	0.959	32.982	193			20
48840	1.191	33.874				24
50160	1.424	34.766				24
51480	1.656	35.658				23
52800	1.889	36.55				30
54120	2.122	37.442				29
55440	2.354	38.334				25
56760	2.587	39.226				23
58080	2.819	40.118				27
59400	3.052	41.01				26
60720	3.284	41.901				28
62040	3.517	42.793				23
63360	3.75	43.685				28
64680	3.982	44.577				28
	4.215	45.469				34
	4.447	46.361				26
	4.68	47.253				38
	4.912	48.145				24
	5.145	49.037				31
	5.378	49.929				35
	5.61	50.821				24
	5.843	51.713				30
	6.075	52.605				28
	6.308	53.497				29
	6.54	54.388				28
	6.773	55.28				36
	7.006	56.172				37
	7.238	57.064				24
	7.471	57.956				30
	7.703	58.848				31

Bubble Diameter (mm)	Bubble Velocity (m/s)	Equivalent Bubble Diameter (mm)	Average Bubble Diameter (mm)	Minimum Bubble size (mm)	Maximum Bubble size (mm)	Bubbles accounts
0	-7.678	1.147	13.4	2.09	51.1	14
2	-7.373	2.565	10.1	1.55	60.2	12
4	-7.068	3.984	12.3	3.14	50.1	20
6	-6.763	5.403	9.29	1.36	17.9	15
8	-6.458	6.822	12.7	1.15	46.2	17
10	-6.153	8.241	12.7	2.34	40.4	16
12	-5.848	9.66	11.7	1.15	35.3	27
14	-5.544	11.078	11.7	1.48	41.6	21
16	-5.239	12.497	11.5	2.32	43.6	18
18	-4.934	13.916	12.2	3.23	42.5	19
20	-4.629	15.335	14.7	1.84	42.7	22
22	-4.324	16.754	14.3	3.89	40.2	15
24	-4.019	18.173	15.9	1.15	29	23
26	-3.714	19.591	14	1.32	46.5	21
28	-3.409	21.01	16.1	1.15	45.2	22
30	-3.104	22.429	14.9	1.32	47.2	17
32	-2.799	23.848	12.8	1.65	54.8	11
34	-2.494	25.267	12.4	1.48	37.7	14
36	-2.19	26.686	14.2	1.55	35.2	21
38	-1.885	28.104	10.7	2.77	34.1	18
40	-1.58	29.523	14.6	1.15	33.3	22
42	-1.275	30.942	16.6	3.23	39	13
44	-0.97	32.361	13.7	1.65	44	12
46	-0.665	33.78	13.2	1.32	37.5	16
48	-0.36	35.199	13.3	3.12	41.8	11
50	-0.055	36.617	13.7	1.69	38.6	19
52	0.25	38.036	14.9	2.89	31.1	19
54	0.555	39.455	13.9	1.48	42.1	13
56	0.86	40.874	11.1	4.19	39.3	15
58	1.165	42.293	12.9	1.48	51.2	19
60	1.469	43.712	13.183	2.004333	41.31333	12
62	1.774	45.13				22
64	2.079	46.549				18
66	2.384	47.968				18
68	2.689	49.387				16

70	2.994	50.806				24
72	3.299	52.225	195			25
74	3.604	53.643				12
76	3.909	55.062				19
78	4.214	56.481				22
80	4.519	57.9				25
82	4.823	59.319				22
84	5.128	60.738				19
86	5.433	62.156				23
88	5.738	63.575				23
90	6.043	64.994				16
92	6.348	66.413				18
94	6.653	67.832				23
96	6.958	69.251				24
98	7.263	70.669				23

8.2   Appendix –A

Experimental Data for SNIT

University of
Salford
MANCHESTER

P etroleum
T echnology
R esearch
G roup

Bubble Diameter (mm)	Bubble Velocity (m/s)	Equivalent Bubble Diameter (mm)	Average Bubble Diameter (mm)	Minimum Bubble size (mm)	Maximum Bubble size (mm)	Bubbles accounts
0	-8.497	0.966	9.14	1.15	34.5	28
1320	-8.24	1.758	11.9	1.46	35.9	20
2640	-7.983	2.549	10.9	1.27	39	25
3960	-7.726	3.34	11	1.27	42.1	21
5280	-7.468	4.131	9.25	1.51	41	23
6600	-7.211	4.923	8.89	1.27	28.6	20
7920	-6.954	5.714	9.04	1.27	32.6	27
9240	-6.697	6.505	6.55	1.27	35.2	33
10560	-6.44	7.297	9.11	1.41	32.2	23
11880	-6.182	8.088	9.71	1.27	30.5	24
13200	-5.925	8.879	8.92	1.21	30.9	28
14520	-5.668	9.671	9.72	1.27	30.5	30
15840	-5.411	10.462	9.22	1.27	26	28
17160	-5.154	11.253	9.49	1.27	25.2	28
18480	-4.896	12.044	7.78	1.27	26.9	34
19800	-4.639	12.836	9.25	1.46	30.6	29
21120	-4.382	13.627	10.3	1.27	29.3	27
22440	-4.125	14.418	9.38	1.27	38.3	29
23760	-3.868	15.21	9.15	1.27	33.8	35
25080	-3.61	16.001	12.4	1.63	32.5	19
26400	-3.353	16.792	9.28	1.63	38.1	25
27720	-3.096	17.583	7.89	1.27	30.6	33
29040	-2.839	18.375	9.76	1.46	31.6	27
30360	-2.582	19.166	8.91	1.37	29	32
31680	-2.324	19.957	12.1	1.27	38.8	22
33000	-2.067	20.749	9.45	1.27	37.1	25
34320	-1.81	21.54	11.9	1.27	46.2	17
35640	-1.553	22.331	9.68	1.46	43.3	24
36960	-1.296	23.123	11.7	1.27	28.3	20
38280	-1.038	23.914	11	2.53	42.1	23

197

39600	-0.781	24.705	9.759	1.371333	34.02333	18
40920	-0.524	25.496				18
42240	-0.267	26.288				18
43560	-0.01	27.079				19
44880	0.248	27.87				25
46200	0.505	28.662				25
47520	0.762	29.453				26
48840	1.019	30.244				26
50160	1.276	31.036				28
51480	1.534	31.827				21
52800	1.791	32.618				24
54120	2.048	33.409				23
55440	2.305	34.201				21
56760	2.562	34.992				26
58080	2.82	35.783				24
59400	3.077	36.575				16
60720	3.334	37.366				27
62040	3.591	38.157				32
63360	3.848	38.949				24
64680	4.106	39.74				23
	4.363	40.531				29
	4.62	41.322				33
	4.877	42.114				30
	5.134	42.905				27
	5.392	43.696				26
	5.649	44.488				36
	5.906	45.279				19
	6.163	46.07				29
	6.42	46.862				34
	6.678	47.653				32
	6.935	48.444				31
	7.192	49.235				30
	7.449	50.027				27
	7.706	50.818				26
	7.964	51.609				28
	8.221	52.401				25
	4.23421	26.6834				23

		SEGMENT :1	Video- 8776		University of SALFORD MANCHESTER	
		Operating conditions: P = 1 bar Liquid Flow rate = 5 l/min				
Bubble Diameter (mm)	Bubble Velocity (m/s)	Equivalent Bubble Diameter (mm)	Average Bubble Diameter (mm)	Minimum Bubble size (mm)	Maximum Bubble size (mm)	Bubbles accounts
0	-8.126	0.896	7.33	0.967	45.4	50
1320	-7.887	1.826	7.15	1.27	37.8	50
2640	-7.648	2.755	6.75	1.27	36.6	46
3960	-7.409	3.685	7.34	1.27	30.3	52
5280	-7.17	4.615	6.17	1.27	32.4	62
6600	-6.931	5.545	7.09	1.27	30.7	55
7920	-6.693	6.475	7.24	1.27	32.9	51
9240	-6.454	7.405	6.66	1.27	37.2	52
10560	-6.215	8.335	7.22	1.27	40	55
11880	-5.976	9.265	6.76	1.27	30.7	52
13200	-5.737	10.195	7.23	1.27	37.4	50
14520	-5.498	11.125	6.76	1.27	32.6	61
15840	-5.259	12.055	6.24	1.27	34.5	64
17160	-5.02	12.984	6.09	1.27	32.9	57
18480	-4.781	13.914	5.75	1.27	35.8	57
19800	-4.543	14.844	6.14	1.27	38	57
21120	-4.304	15.774	6.58	1.27	47.5	46
22440	-4.065	16.704	6.17	1.27	39.3	55
23760	-3.826	17.634	5.91	1.03	43.5	54
25080	-3.587	18.564	5.97	1.27	43.7	50
26400	-3.348	19.494	6.54	1.27	37.1	52
27720	-3.109	20.424	7.39	1.27	31.7	48
29040	-2.87	21.354	6.61	1.27	39	58
30360	-2.631	22.284	7.21	0.896	32.4	54
31680	-2.393	23.214	7.21	1.27	31.4	57
33000	-2.154	24.143	6.89	1.16	48.3	54
34320	-1.915	25.073	7.5	1.16	47.4	41
35640	-1.676	26.003	7.25	1.27	52.3	41
36960	-1.437	26.933	8.28	1.27	41.4	45

38280	-1.198	27.863	6.66	1.27	59.7	44
39600	-0.959	28.793	6.803	1.2321	38.66333	54
40920	-0.72	29.723				67
42240	-0.481	30.653				65
43560	-0.243	31.583				60
44880	-0.004	32.513				46
46200	0.235	33.443				51
47520	0.474	34.372				73
48840	0.713	35.302				67
50160	0.952	36.232				59
51480	1.191	37.162				71
52800	1.43	38.092				45
54120	1.669	39.022				61
55440	1.907	39.952				63
56760	2.146	40.882				51
58080	2.385	41.812				58
59400	2.624	42.742				78
60720	2.863	43.672				72
62040	3.102	44.601				53
63360	3.341	45.531				71
64680	3.58	46.461				51
	3.819	47.391				41
	4.057	48.321				67
	4.296	49.251				57
	4.535	50.181				65
	4.774	51.111				56
	5.013	52.041				45
	5.252	52.971				50
	5.491	53.901				49
	5.73	54.83				54
	5.969	55.76				34
	6.207	56.69				65
	6.446	57.62				66
	6.685	58.55				56
	6.924	59.48				61
	7.163	60.41				61

Bubble Diameter (mm)	Bubble Velocity (m/s)	Equivalent Bubble Diameter (mm)	Average Bubble Diameter (mm)	Minimum Bubble size (mm)	Maximum Bubble size (mm)	Bubbles accounts
0	-7.782	0.908	6.03	1.19	55.5	76
1320	-7.541	1.974	5.69	1.19	49.5	74
2640	-7.299	3.041	7.14	1.19	58.2	62
3960	-7.058	4.108	9.72	1.14	53	40
5280	-6.817	5.175	6.46	1.19	46.5	74
6600	-6.575	6.242	7.96	1.19	48.2	61
7920	-6.334	7.309	6.33	1.19	39.7	80
9240	-6.093	8.376	6.26	1.19	37.6	77
10560	-5.851	9.443	6.71	1.19	39.6	74
11880	-5.61	10.509	7.35	0.97	47.8	70
13200	-5.369	11.576	6.67	1.19	38	75
14520	-5.127	12.643	6.16	0.97	50	72
15840	-4.886	13.71	7.51	1.37	58.8	60
17160	-4.644	14.777	8.1	1.19	45.8	59
18480	-4.403	15.844	9.34	1.19	46.9	43
19800	-4.162	16.911	7.18	1.19	55.5	56
21120	-3.92	17.977	7.97	1.19	50.9	55
22440	-3.679	19.044	7.96	1.19	44.3	64
23760	-3.438	20.111	6.68	1.14	61.1	75
25080	-3.196	21.178	7.88	1.19	52.1	66
26400	-2.955	22.245	9.87	1.19	49.8	41
27720	-2.714	23.312	6.81	1.03	59.6	64
29040	-2.472	24.379	8.06	1.19	51.3	54
30360	-2.231	25.446	8.47	1.19	40.3	45
31680	-1.99	26.512	7.33	1.19	46.9	59
33000	-1.748	27.579	6.78	1.19	44.6	71
34320	-1.507	28.646	6.69	1.19	37.3	76
35640	-1.266	29.713	7.17	1.03	55.8	52
36960	-1.024	30.78	7.9	1.19	48.2	50
38280	-0.783	31.847	7.27	1.03	51.4	66
39600	-0.542	32.914	7.381667	1.162	48.80667	51
40920	-0.3	33.98				62
42240	-0.059	35.047				60
43560	0.182	36.114				48

44880	0.424	37.181				62
46200	0.665	38.248				40
47520	0.906	39.315				71
48840	1.148	40.382				69
50160	1.389	41.449				56
51480	1.63	42.515				75
52800	1.872	43.582				61
54120	2.113	44.649				76
55440	2.354	45.716				90
56760	2.596	46.783				80
58080	2.837	47.85				85
59400	3.078	48.917				90
60720	3.32	49.983				64
62040	3.561	51.05				76
63360	3.802	52.117				80
64680	4.044	53.184				63
	4.285	54.251				67
	4.526	55.318				71
	4.768	56.385				70
	5.009	57.452				79
	5.25	58.518				82
	5.492	59.585				84
	5.733	60.652				67
	5.975	61.719				80
	6.216	62.786				66
	6.457	63.853				81
	6.699	64.92				104
	6.94	65.986				78
	7.181	67.053				65
	7.423	68.12				80
	7.664	69.187				77
	7.905	70.254				81
	4.043757576	35.5807				55

University of
Salford
MANCHESTER

Bubble Diameter (mm)	Bubble Velocity (m/s)	Equivalent Bubble Diameter (mm)	Average Bubble Diameter (mm)	Minimum Bubble size (mm)	Maximum Bubble size (mm)	Bubbles accounts
0	-8.03	0.896	6.23	1.27	54.1	102
1320	-7.783	2.094	5.81	1.27	53.5	127
2640	-7.535	3.292	6.95	1.27	46.2	80
3960	-7.287	4.49	5.98	1.27	54.3	109
5280	-7.04	5.687	5.26	1.27	50.3	138
6600	-6.792	6.885	6.16	1.27	49.6	104
7920	-6.544	8.083	6.92	1.16	51.6	77
9240	-6.297	9.281	7.01	1.27	48.1	96
10560	-6.049	10.479	6.23	1.16	78.8	75
11880	-5.802	11.676	7.03	1.27	49.9	93
13200	-5.554	12.874	6.6	1.27	32.7	105
14520	-5.306	14.072	7.47	1.21	53.4	84
15840	-5.059	15.27	6.29	1.27	46.4	92
17160	-4.811	16.468	6.52	1.1	46.8	96
18480	-4.564	17.666	7.15	1.21	47.6	59
19800	-4.316	18.863	6.2	1.27	46.9	91
21120	-4.068	20.061	6.83	1.27	47.6	95
22440	-3.821	21.259	6.06	1.27	54.5	106
23760	-3.573	22.457	5.55	1.21	59.3	135
25080	-3.325	23.655	4.72	1.27	52.7	156
26400	-3.078	24.853	5.13	1.27	55.3	105
27720	-2.83	26.05	5.89	1.27	42.8	105
29040	-2.583	27.248	5.96	1.27	62.6	99
30360	-2.335	28.446	5.71	1.27	49.3	117
31680	-2.087	29.644	5.86	1.16	49.4	119
33000	-1.84	30.842	5.87	1.27	62.4	96
34320	-1.592	32.04	7.03	1.27	42.4	77
35640	-1.345	33.237	6.73	1.27	44.5	85
36960	-1.097	34.435	6.26	0.968	42.5	74

38280	-0.849	35.633	6.49	1.03	43.8	107
39600	-0.602	36.831	6.263333	1.229267	50.64333	113
40920	-0.354	38.029				65
42240	-0.107	39.227				87
43560	0.141	40.424				101
44880	0.389	41.622				101
46200	0.636	42.82				72
47520	0.884	44.018				85
48840	1.132	45.216				105
50160	1.379	46.414				105
51480	1.627	47.611				102
52800	1.874	48.809				82
54120	2.122	50.007				102
55440	2.37	51.205				88
56760	2.617	52.403				99
58080	2.865	53.601				108
59400	3.112	54.798				105
60720	3.36	55.996				63
62040	3.608	57.194				85
63360	3.855	58.392				91
64680	4.103	59.59				208
	4.351	60.788				117
	4.598	61.985				130
	4.846	63.183				129
	5.093	64.381				84
	5.341	65.579				118
	5.589	66.777				118
	5.836	67.975				107
	6.084	69.172				99
	6.331	70.37				114
	6.579	71.568				85
	6.827	72.766				104
	7.074	73.964				98
	7.322	75.162				95
	7.569	76.359				92
	7.817	77.557				112

		SEGMENT :1 Video- 8779 Operating conditions: P = 4 bar Liquid Flow rate = 5 l/min				University of Salford MANCHESTER

Bubble Diameter (mm)	Bubble Velocity (m/s)	Equivalent Bubble Diameter (mm)	Average Bubble Diameter (mm)	Minimum Bubble size (mm)	Maximum Bubble size (mm)	Bubbles accounts
0	-8.275	0.896	5.21	1.16	27.8	175
1320	-8.027	2.03	6.01	1.27	37.3	126
2640	-7.779	3.163	7.97	1.27	49.6	92
3960	-7.531	4.297	6.52	1.27	61.3	107
5280	-7.283	5.43	7.25	1.27	43.3	105
6600	-7.035	6.564	6.43	1.27	38.1	120
7920	-6.787	7.698	7.44	1.27	50.1	99
9240	-6.539	8.831	7.09	1.27	53.4	97
10560	-6.29	9.965	6.39	1.27	52.5	96
11880	-6.042	11.098	7.07	1.27	51.9	98
13200	-5.794	12.232	6.2	1.27	74.3	67
14520	-5.546	13.365	7.92	1.27	48.9	74
15840	-5.298	14.499	6.38	1.04	46.6	115
17160	-5.05	15.632	9.3	1.27	51.8	78
18480	-4.802	16.766	7.3	1.04	54.5	87
19800	-4.554	17.899	7.85	1.16	43.7	98
21120	-4.306	19.033	7.43	0.968	46.5	97
22440	-4.058	20.166	6.44	1.1	51.1	107
23760	-3.81	21.3	6.25	1.27	50.7	110
25080	-3.562	22.433	7.13	1.27	46.6	95
26400	-3.314	23.567	6.76	1.27	48.1	113
27720	-3.065	24.7	6.04	1.27	45.5	128
29040	-2.817	25.834	7.86	1.27	46.5	96
30360	-2.569	26.968	7.01	1.16	42	102
31680	-2.321	28.101	5.65	1.1	43.4	107
33000	-2.073	29.235	6.06	1.27	47.6	120
34320	-1.825	30.368	6.29	1.16	55.4	130
35640	-1.577	31.502	5.56	1.21	56.7	135
36960	-1.329	32.635	5.88	1.04	44.1	115
38280	-1.081	33.769	6.18	1.04	59.1	89
39600	-0.833	34.902	6.762333	1.201267	48.94667	138
40920	-0.585	36.036				105
42240	-0.337	37.169				122
43560	-0.089	38.303				134

44880	0.159	39.436				135
46200	0.408	40.57				134
47520	0.656	41.703				150
48840	0.904	42.837				143
50160	1.152	43.97				122
51480	1.4	45.104				145
52800	1.648	46.238				111
54120	1.896	47.371				123
55440	2.144	48.505				148
56760	2.392	49.638				144
58080	2.64	50.772				140
59400	2.888	51.905				111
60720	3.136	53.039				139
62040	3.384	54.172				143
63360	3.632	55.306				143
64680	3.881	56.439				160
	4.129	57.573				116
	4.377	58.706				116
	4.625	59.84				132
	4.873	60.973				163
	5.121	62.107				131
	5.369	63.24				131
	5.617	64.374				117
	5.865	65.507				128
	6.113	66.641				135
	6.361	67.775				123
	6.609	68.908				153
	6.857	70.042				123
	7.106	71.175				131
	7.354	72.309				107
	7.602	73.442				114
	7.85	74.576				135
	4.0046	37.7360				120

Operating conditions:
P = 5 bar
Liquid Flow rate = 5 l/min

University of
Salford
MANCHESTER

Bubble Diameter (mm)	Bubble Velocity (m/s)	Equivalent Bubble Diameter (mm)	Average Bubble Diameter (mm)	Minimum Bubble size (mm)	Maximum Bubble size (mm)	Bubbles accounts
0	-7.272	0.896	5.18	1.21	40.8	134
1320	-7.041	1.943	4.46	1.03	32.8	175
2640	-6.809	2.991	5.43	1.21	50	107
3960	-6.578	4.038	4.31	1.27	28.6	187
5280	-6.346	5.086	4.6	1.27	42.7	169
6600	-6.115	6.133	4.16	1.27	50.7	165
7920	-5.883	7.181	5.11	1.21	56.5	128
9240	-5.652	8.228	5.1	1.27	43.3	144
10560	-5.42	9.276	5.42	1.21	41.3	151
11880	-5.189	10.324	5.22	1.27	36.6	143
13200	-4.957	11.371	5.15	1.21	45.4	145
14520	-4.726	12.419	5.28	1.27	64.4	132
15840	-4.494	13.466	4.69	1.1	38.5	168
17160	-4.263	14.514	5.87	1.27	38.3	125
18480	-4.031	15.561	4.89	1.1	36.8	160
19800	-3.8	16.609	5.03	1.27	45.3	142
21120	-3.568	17.656	5.26	1.27	39.7	143
22440	-3.336	18.704	4.61	1.1	35	182
23760	-3.105	19.752	4.46	1.16	38.6	182
25080	-2.873	20.799	5	1.27	41.1	144
26400	-2.642	21.847	4.89	0.967	50.6	131
27720	-2.41	22.894	4.52	1.1	46	166
29040	-2.179	23.942	5.63	1.16	49.4	113
30360	-1.947	24.989	5.26	0.967	43	149
31680	-1.716	26.037	5.49	1.21	36.2	144
33000	-1.484	27.084	4.92	1.27	32.4	164
34320	-1.253	28.132	4.82	1.27	40	163
35640	-1.021	29.18	6.32	0.967	45	114
36960	-0.79	30.227	5.37	1.27	58	118
38280	-0.558	31.275	5.47	1.27	52.9	140
39600	-0.327	32.322	5.064	1.1897	43.33	133
40920	-0.095	33.37				112
42240	0.136	34.417				141
43560	0.368	35.465				134

44880	0.599	36.512				120
46200	0.831	37.56				164
47520	1.062	38.608				184
48840	1.294	39.655				177
50160	1.525	40.703				155
51480	1.757	41.75				137
52800	1.988	42.798				127
54120	2.22	43.845				133
55440	2.451	44.893				153
56760	2.683	45.94				161
58080	2.914	46.988				123
59400	3.146	48.036				153
60720	3.377	49.083				156
62040	3.609	50.131				150
63360	3.84	51.178				177
64680	4.072	52.226				130
	4.304	53.273				145
	4.535	54.321				173
	4.767	55.368				159
	4.998	56.416				173
	5.23	57.464				144
	5.461	58.511				168
	5.693	59.559				144
	5.924	60.606				165
	6.156	61.654				157
	6.387	62.701				172
	6.619	63.749				170
	6.85	64.796				185
	7.082	65.844				182
	7.313	66.892				154
	7.545	67.939				176
	7.776	68.987				157
	3.9562	34.941				140

		SEGMENT :1　　　　Video- 8781 Operating conditions: P =0.5 bar Liquid Flow rate = 10 l/min		University of Salford MANCHESTER	

Bubble Diameter (mm)	Bubble Velocity (m/s)	Equivalent Bubble Diameter (mm)	Average Bubble Diameter (mm)	Minimum Bubble size (mm)	Maximum Bubble size (mm)	Bubbles accounts
0	-8.49	1.213	8.36	1.27	34.5	
2	-8.148	2.232	9.28	1.27	28.8	28
4	-7.805	3.251	8.69	1.42	29	24
6	-7.463	4.269	9.59	1.27	30.6	24
8	-7.12	5.288	10.3	1.27	33.5	23
10	-6.778	6.306	12.2	1.46	30.8	16
12	-6.436	7.325	9.86	1.27	29.7	16
14	-6.093	8.343	9.59	1.64	27.7	19
16	-5.751	9.362	10.1	1.27	33.5	17
18	-5.408	10.38	8.99	1.27	32	22
20	-5.066	11.399	11.4	1.68	31.3	16
22	-4.724	12.417	9.02	1.46	28.9	20
24	-4.381	13.436	7.63	1.27	30.2	25
26	-4.039	14.454	11.6	1.27	28.3	16
28	-3.697	15.473	7.85	1.27	36.7	22
30	-3.354	16.491	10.9	2	35.2	14
32	-3.012	17.51	7.59	1.37	28.8	20
34	-2.669	18.529	7.81	1.27	32.7	20
36	-2.327	19.547	11.8	1.27	37.1	16
38	-1.985	20.566	12.4	1.27	34.8	18
40	-1.642	21.584	8.92	1.51	27.2	14
42	-1.3	22.603	11.7	1.27	35.1	14
44	-0.958	23.621	10.8	1.51	30	22
46	-0.615	24.64	10.8	1.27	27.4	20
48	-0.273	25.658	9.82	1.51	29.4	23
50	0.07	26.677	9.62	1.27	28.6	20
52	0.412	27.695	9.97	1.27	24.6	22
54	0.754	28.714	8.25	1.27	25.6	31
56	1.097	29.732	8.26	1.27	25.9	29
58	1.439	30.751	10.2	1.51	27.96	22
60	1.782	31.769	9.776667	1.373333	30.52867	23
62	2.124	32.788				21
64	2.466	33.807				22
66	2.809	34.825				17

68	3.151	35.844				24
70	3.493	36.862				27
72	3.836	37.881				26
74	4.178	38.899				28
76	4.521	39.918				27
78	4.863	40.936				22
80	5.205	41.955				28
82	5.548	42.973				28
84	5.89	43.992				25
86	6.233	45.01				24
88	6.575	46.029				24
90	6.917	47.048				28
92	7.26	48.066				26
94	7.602	49.085				28
96	7.944	50.103				23
98	8.287	51.122				25

Bubble Diameter (mm)	Bubble Velocity (m/s)	Equivalent Bubble Diameter (mm)	Average Bubble Diameter (mm)	Minimum Bubble size (mm)	Maximum Bubble size (mm)	Bubbles accounts
0	-8.171	1.267	11.9	1.46	44.4	17
2	-7.836	2.226	12.5	2.1	33.1	13
4	-7.502	3.185	13.9	2.97	34.8	13
6	-7.168	4.144	8.47	1.27	30.3	17
8	-6.833	5.103	11	1.27	27.4	15
10	-6.499	6.062	11.2	1.72	31.2	11
12	-6.165	7.02	9.83	1.27	32.7	18
14	-5.83	7.979	8.45	1.51	37.6	20
16	-5.496	8.938	10.1	1.27	40.4	17
18	-5.161	9.897	11.1	1.27	41.8	19
20	-4.827	10.856	11.6	1.51	34.9	21
22	-4.493	11.815	11.2	1.27	31.2	14
24	-4.158	12.774	9.85	1.27	32.1	22
26	-3.824	13.732	11.2	1.46	30.4	21
28	-3.49	14.691	13.7	1.27	27.5	18
30	-3.155	15.65	11.9	1.27	29.5	18
32	-2.821	16.609	10.7	1.27	26.4	19
34	-2.486	17.568	12.9	1.64	38.4	18
36	-2.152	18.527	15.2	1.46	37.8	12
38	-1.818	19.486	16.9	6.33	36.1	13
40	-1.483	20.445	13	1.64	37.6	15
42	-1.149	21.403	11.6	1.46	33.7	19
44	-0.815	22.362	11.5	1.72	35.6	23
46	-0.48	23.321	11.8	1.27	41.1	19
48	-0.146	24.28	15.2	1.64	38	17
50	0.189	25.239	11.2	1.27	45.2	20
52	0.523	26.198	11.4	1.42	37.4	24
54	0.857	27.157	11.7	2.04	27.3	18
56	1.192	28.116	11.1	1.27	28.7	19
58	1.526	29.074	9.9	1.42	25.3	19
60	1.86	30.033	11.73333	1.667	34.26333	19
62	2.195	30.992				23
64	2.529	31.951				19
66	2.864	32.91				9

68	3.198	33.869				15
70	3.532	34.828				16
72	3.867	35.786				15
74	4.201	36.745				14
76	4.535	37.704				17
78	4.87	38.663				16
80	5.204	39.622				21
82	5.539	40.581				13
84	5.873	41.54				14
86	6.207	42.499				20
88	6.542	43.457				22
90	6.876	44.416				8
92	7.21	45.375				12
94	7.545	46.334				14
96	7.879	47.293				13
98	8.214	48.252				13

SEGMENT :1   Video- 8793

Operating conditions:
P =0.5 bar
Liquid Flow rate = 30 l/min

University of
Salford
MANCHESTER

P etroleum
T echnology
R esearch
G roup

Bubble Diameter (mm)	Bubble Velocity (m/s)	Equivalent Bubble Diameter (mm)	Average Bubble Diameter (mm)	Minimum Bubble size (mm)	Maximum Bubble size (mm)	Bubbles accounts
0	-8.133	1.214	16.8	1.87	31.2	14
2	-7.795	2.371	13.8	1.27	32	20
4	-7.458	3.528	12.3	1.27	33.8	15
6	-7.121	4.685	8.49	1.27	32.6	24
8	-6.783	5.842	15.3	1.87	32.9	13
10	-6.446	6.998	16.2	1.6	33.3	20
12	-6.109	8.155	11.2	1.51	32.7	17
14	-5.771	9.312	12.9	1.6	36.1	17
16	-5.434	10.469	14.9	1.87	37.5	14
18	-5.096	11.626	14.2	1.51	38.4	19
20	-4.759	12.782	13	1.27	43.1	16
22	-4.422	13.939	15	1.27	42.6	18
24	-4.084	15.096	10.2	1.27	42.9	15
26	-3.747	16.253	11.5	1.9	46.6	18
28	-3.41	17.41	12.6	1.46	41.7	16
30	-3.072	18.566	14.3	2.1	43	17
32	-2.735	19.723	18.4	1.27	48	21
34	-2.398	20.88	15.8	1.51	45.8	16
36	-2.06	22.037	13.6	1.27	38	18
38	-1.723	23.194	16.4	1.27	27.2	22
40	-1.386	24.35	12.7	1.46	34.7	17
42	-1.048	25.507	15.6	1.87	39.8	18
44	-0.711	26.664	16.2	1.27	30.6	15
46	-0.373	27.821	15.7	1.27	38.7	16
48	-0.036	28.978	18.1	1.46	39.8	14
50	0.301	30.134	10.4	1.27	49.6	18
52	0.639	31.291	10.6	3.04	34.1	18
54	0.976	32.448	15.1	2.34	30.6	16
56	1.313	33.605	16.3	1.51	30.2	18
58	1.651	34.761	13.3	2.29	37.1	21
60	1.988	35.918	14.02967	1.600333	37.48667	20
62	2.325	37.075				14
64	2.663	38.232				15
66	3	39.389				16

68	3.337	40.545				14
70	3.675	41.702				15
72	4.012	42.859				14
74	4.35	44.016				20
76	4.687	45.173				14
78	5.024	46.329				17
80	5.362	47.486				13
82	5.699	48.643				21
84	6.036	49.8				19
86	6.374	50.957				20
88	6.711	52.113				19
90	7.048	53.27				26
92	7.386	54.427				14
94	7.723	55.584				11
96	8.06	56.741				11
98	8.398	57.897				14
		29.5559				19

8.3 Appendix –B

Pressure-drop data along simulated column for SNIT

Pipe length (mm)	50000 Pa (0.5 bar)	100000 Pa (1 bar)	200000 Pa (2 bar)	300000 Pa (3 bar)	400000 Pa (4 bar)	500000 Pa (5 bar)
0.00	34772.47	32670.42	31793.19	28934.29	29222.25	28411.57
0.02	34574.97	32472.74	31594.95	28726.54	29033.84	28221.75
0.04	34377.42	32274.20	31403.68	28593.37	28885.47	28073.17
0.06	34180.07	32084.63	31211.28	28467.75	28783.79	27982.32
0.08	33982.64	31899.64	31020.96	28336.38	28693.99	27892.60
0.10	33785.09	31709.15	30840.66	28255.68	28609.92	27810.80
0.12	33596.70	31520.98	30669.97	28164.25	28500.30	27739.68
0.14	33409.88	31341.16	30504.08	28040.80	28383.14	27658.76
0.16	33224.03	31162.08	30341.47	27924.54	28256.93	27568.12
0.18	33040.48	30997.02	30180.89	27818.54	28131.86	27462.30
0.20	32858.87	30850.25	30021.92	27711.40	27998.45	27350.57
0.22	32677.88	30717.26	29871.18	27599.81	27857.88	27255.71
0.24	32497.72	30588.81	29724.71	27486.58	27728.34	27145.74
0.26	32315.14	30443.01	29572.85	27367.64	27602.02	27032.96
0.28	32130.12	30278.04	29418.19	27243.99	27471.16	26928.72
0.30	31947.04	30109.85	29268.16	27121.59	27341.51	26826.12
0.32	31765.57	29941.19	29119.52	27004.33	27212.12	26722.81
0.34	31585.22	29770.71	28937.23	26886.77	27081.24	26615.45
0.36	31403.27	29601.30	28759.09	26761.13	26954.73	26503.22

0.38	31221.45	29436.01	28611.46	26630.15	26837.51	26385.70
0.40	31043.44	29271.72	28481.47	26502.00	26723.52	26274.62
0.42	30865.11	29102.63	28346.48	26382.91	26604.15	26171.08
0.44	30684.05	28931.31	28216.04	26268.52	26478.15	26074.99
0.46	30500.66	28765.63	28096.83	26150.70	26354.81	25987.03
0.48	30315.74	28604.41	27974.52	26031.11	26234.50	25892.79
0.51	30130.06	28439.42	27850.30	25912.40	26112.82	25779.57
0.53	29948.89	28268.17	27724.26	25796.00	25991.85	25667.14
0.55	29772.15	28093.84	27589.80	25682.25	25872.33	25560.45
0.57	29590.34	27921.05	27445.59	25574.90	25753.10	25456.61
0.59	29411.71	27751.19	27295.44	25467.68	25633.35	25353.45
0.61	29242.49	27579.35	27146.44	25347.56	25511.83	25249.19
0.63	29075.14	27403.03	27006.53	25220.33	25391.05	25148.90
0.65	28903.11	27226.44	26871.96	25096.07	25276.23	25058.47
0.67	28729.35	27053.13	26736.65	24976.79	25176.27	24965.58
0.69	28558.57	26882.01	26598.49	24865.86	25076.78	24867.11
0.71	28391.95	26710.87	26462.14	24760.87	24960.08	24773.47
0.73	28224.39	26540.33	26332.77	24661.51	24826.19	24686.82
0.75	28054.55	26372.50	26208.70	24567.48	24681.83	24605.52
0.77	27884.45	26208.48	26085.94	24474.60	24534.87	24526.57
0.79	27715.16	26049.89	25961.88	24381.98	24389.17	24451.47

0.81	27546.27	25896.49	25834.50	24289.36	24245.53	24382.35
0.83	27376.46	25743.14	25699.13	24208.89	24105.29	24314.64
0.85	27206.55	25588.70	25481.07	24138.82	23969.09	24240.90
0.87	27036.39	25438.46	25327.94	24066.87	23837.04	24151.64
0.89	26864.60	25298.89	25217.64	24000.43	23712.22	24053.69
0.91	26690.80	25172.14	25098.38	23873.90	23593.51	23952.74
0.93	26515.32	25033.65	24962.86	23734.23	23482.00	23847.81
0.95	26339.63	24889.79	24822.93	23586.80	23373.39	23738.18
0.97	26165.63	24750.63	24685.76	23442.97	23271.15	23625.83
0.99	25994.61	24614.52	24546.79	23323.71	23178.89	23513.69
1.01	25825.08	24477.79	24404.31	23213.55	23095.83	23394.21
1.03	25649.23	24327.50	24260.94	23090.57	23006.14	23244.70
1.05	25471.95	24184.61	24117.54	22956.08	22843.19	23105.43
1.07	25300.32	24049.39	23979.32	22823.82	22659.67	22995.50
1.09	25132.21	23904.60	23846.99	22695.63	22520.20	22911.03
1.11	24962.27	23745.42	23718.33	22576.42	22385.22	22839.72
1.13	24789.54	23580.50	23591.48	22454.16	22236.35	22769.09
1.15	24614.42	23420.78	23463.45	22320.59	22070.55	22691.76
1.17	24438.19	23257.04	23330.20	22187.29	21894.32	22609.02
1.19	24260.03	23103.68	23185.05	22059.29	21718.18	22525.48
1.21	24082.20	22952.85	23023.41	21939.13	21547.09	22402.56

1.23	23905.44	22802.60	22867.65	21810.42	21386.76	22251.70
1.25	23731.84	22658.35	22723.68	21689.84	21238.91	22106.69
1.27	23561.17	22518.70	22596.47	21580.49	21097.86	21949.57
1.29	23391.75	22376.15	22470.40	21465.03	20955.52	21809.92
1.31	23227.94	22235.89	22324.92	21342.47	20808.13	21654.47
1.33	23062.17	22101.22	22172.14	21198.34	20632.78	21485.53
1.35	22891.29	21968.29	22019.84	21047.13	20448.46	21313.02
1.37	22715.63	21835.20	21864.97	20878.90	20285.48	21130.80
1.39	22535.57	21705.05	21707.51	20686.78	20151.28	20958.86
1.41	22357.54	21579.06	21546.81	20506.00	20030.65	20800.35
1.43	22183.96	21447.84	21388.93	20355.45	19912.98	20652.05
1.45	22011.14	21297.93	21233.91	20226.16	19792.70	20511.94
1.47	21837.86	21118.41	21077.97	20109.61	19672.78	20377.91
1.49	21661.78	20926.95	20920.77	19931.45	19551.70	20252.90
1.52	21484.95	20742.27	20769.67	19718.36	19435.27	20144.59
1.54	21309.56	20578.45	20624.09	19549.86	19324.92	20057.68
1.56	21135.24	20439.39	20479.61	19392.66	19222.59	19980.98
1.58	20962.26	20298.79	20332.06	19225.20	19114.79	19891.38
1.60	20791.13	20134.54	20178.88	19025.73	18973.96	19782.28
1.62	20620.83	19948.30	20021.70	18862.29	18888.32	19659.61
1.64	20451.23	19745.12	19868.06	18735.92	18829.99	19528.73

1.66	20281.83	19575.64	19720.58	18627.32	18779.84	19400.97
1.68	20113.70	19431.67	19576.43	18513.60	18733.51	19277.62
1.70	19944.87	19296.66	19430.72	18403.91	18688.11	19150.84
1.72	19780.18	19158.93	19286.21	18300.60	18646.38	19017.96
1.74	19615.48	19024.39	19145.43	18193.73	18439.08	18877.88
1.76	19442.08	18896.99	19004.68	18085.23	18369.38	18742.09
1.78	19248.99	18775.28	18862.34	17982.13	18363.49	18622.60
1.80	19053.08	18654.58	18719.13	17854.84	18349.88	18517.33
1.82	18860.04	18530.67	18576.66	17701.04	18332.93	18403.42
1.84	18671.12	18402.31	18436.70	17649.75	18311.78	18282.82
1.86	18486.69	18271.43	18295.58	17626.39	18286.47	18124.25
1.88	18305.17	18140.94	18141.51	17611.75	18238.20	17947.86
1.90	18125.31	18014.77	17978.12	17597.81	18120.00	17783.29
1.92	17947.69	17894.91	17817.01	17577.76	17914.28	17634.47
1.94	17765.49	17730.40	17664.91	17536.70	17736.53	17508.30
1.96	17574.41	17534.02	17522.25	17461.03	17562.11	17401.77
1.98	17398.31	17378.02	17382.77	17357.53	17395.01	17315.21
2.00	17231.35	17227.78	17236.90	17236.01	17232.20	17220.62

8.4 Appendix -B:

Pressure-drop data along simulated column for MNIT

Pipe length (mm)	50000 Pa (0.5 bar)	100000 Pa (1 bar)	200000 Pa (2 bar)	300000 Pa (3 bar)	400000 Pa (4 bar)	500000 Pa (5 bar)
0.00	31539.17	29293.50	26259.45	27306.89	26842.67	25739.58
0.02	31341.46	29150.76	26008.30	27156.90	26741.18	25548.27
0.04	31171.08	28919.36	25985.82	27093.58	26701.31	25517.71
0.06	31079.37	28833.32	25884.72	27030.97	26664.15	25398.22
0.08	30992.22	28804.23	25870.03	26978.80	26635.21	25375.77
0.10	30906.38	28752.84	25825.93	26908.70	26620.44	25320.25
0.12	30815.90	28708.40	25750.00	26910.51	26586.48	25244.07
0.14	30732.70	28627.96	25722.47	26855.46	26510.01	25170.25
0.16	30658.97	28543.02	25685.58	26785.70	26422.28	25102.15
0.18	30581.57	28461.04	25612.81	26721.70	26351.38	25032.11
0.20	30504.94	28396.96	25540.37	26662.30	26305.27	24972.48
0.22	30430.72	28349.32	25470.94	26597.46	26247.07	24926.65
0.24	30360.71	28277.49	25412.70	26531.63	26180.64	24875.76
0.26	30284.95	28194.23	25366.72	26476.18	26118.67	24815.02
0.28	30201.23	28113.01	25306.36	26428.41	26070.05	24742.07
0.30	30114.63	28031.63	25240.79	26370.23	26024.66	24654.67
0.32	30025.51	27948.46	25177.86	26287.17	25961.35	24572.11
0.34	29935.70	27862.38	25116.56	26201.81	25872.48	24496.71
0.36	29852.44	27775.00	25051.08	26124.79	25781.61	24421.54

0.38	29773.01	27688.49	24979.58	26050.99	25695.40	24342.84
0.40	29693.40	27603.23	24905.02	25977.38	25614.19	24267.07
0.42	29616.18	27518.79	24833.46	25902.30	25540.52	24198.67
0.44	29543.71	27436.86	24770.64	25828.22	25474.74	24139.75
0.46	29471.78	27360.07	24715.23	25758.40	25406.66	24092.06
0.48	29392.54	27289.16	24663.32	25692.84	25331.50	24052.2
0.51	29306.46	27220.93	24608.47	25627.21	25257.35	24007.57
0.53	29218.42	27151.03	24543.40	25561.13	25187.94	23954.7
0.55	29132.54	27078.43	24474.54	25496.95	25117.81	23902.63
0.57	29040.62	27004.81	24411.06	25435.12	25041.72	23860.93
0.59	28942.33	26930.74	24352.05	25382.37	24963.52	23832.04
0.61	28847.91	26856.07	24295.02	25335.48	24887.36	23810.6
0.63	28760.82	26781.49	24234.59	25280.63	24814.36	23786.7
0.65	28662.06	26707.72	24171.20	25212.44	24742.29	23750.82
0.67	28567.39	26635.04	24109.92	25134.95	24667.50	23694.69
0.69	28480.14	26563.40	24052.75	25057.73	24592.79	23624.04
0.71	28394.04	26491.81	23999.27	24985.10	24522.21	23550.96
0.73	28299.12	26419.82	23946.92	24916.88	24454.60	23479.32
0.75	28206.88	26348.40	23894.64	24852.95	24388.65	23409.66
0.77	28117.90	26277.89	23842.38	24792.44	24324.11	23342.46
0.79	28023.27	26207.27	23789.75	24734.00	24262.82	23277.85

0.81	27927.19	26135.87	23737.78	24676.72	24207.90	23215.46
0.83	27823.95	26064.54	23687.13	24620.10	24159.22	23154.08
0.85	27717.38	25993.15	23637.85	24564.51	24114.94	23096.09
0.87	27615.23	25919.47	23589.64	24511.35	24073.32	23044.55
0.89	27513.41	25843.58	23542.93	24461.10	24031.72	22997.83
0.91	27409.77	25769.92	23493.72	24413.21	23985.10	22953.28
0.93	27304.71	25702.38	23439.02	24367.69	23931.22	22912.12
0.95	27199.21	25635.72	23388.13	24324.37	23874.87	22875.29
0.97	27091.44	25564.76	23345.98	24283.31	23822.22	22842.27
0.99	26981.75	25494.16	23312.96	24243.02	23776.48	22810.97
1.01	26871.82	25426.42	23283.06	24203.87	23739.76	22780.2
1.03	26765.83	25360.09	23247.82	24169.91	23711.71	22750
1.05	26665.43	25293.55	23199.83	24142.11	23690.25	22720.71
1.07	26567.65	25225.71	23138.39	24117.62	23671.59	22693.11
1.09	26478.70	25154.54	23074.37	24092.58	23652.26	22667.76
1.11	26404.60	25073.27	23010.83	24059.66	23624.40	22644.32
1.13	26341.83	24976.74	22946.93	24008.78	23579.19	22622.32
1.15	26271.52	24867.60	22882.32	23933.09	23519.68	22602.11
1.17	26165.74	24754.51	22818.03	23847.69	23464.09	22584.1
1.19	26047.96	24641.57	22753.53	23759.85	23415.57	22566.61
1.21	25930.68	24532.69	22688.16	23668.85	23371.72	22545.84

1.23	25814.10	24429.18	22623.62	23579.13	23330.73	22519.64
1.25	25696.98	24329.58	22561.97	23495.37	23292.58	22488.65
1.27	25578.61	24231.38	22503.19	23417.42	23257.38	22455.55
1.29	25459.24	24129.98	22446.78	23342.15	23224.90	22423.98
1.31	25325.54	24021.40	22392.35	23267.23	23194.90	22395.18
1.33	25184.54	23904.02	22340.64	23190.95	23165.98	22368.74
1.35	25043.49	23779.15	22292.30	23106.60	23134.76	22344.04
1.37	24891.06	23648.22	22244.33	23006.73	23095.85	22320.98
1.39	24732.57	23510.83	22193.25	22894.51	23038.46	22299.98
1.41	24579.85	23359.81	22136.81	22777.78	22957.56	22280.55
1.43	24438.48	23229.88	22073.56	22663.09	22868.35	22262.76
1.45	24303.73	23158.65	22002.83	22554.80	22785.73	22248.64
1.47	24177.74	23113.99	21923.84	22453.09	22709.98	22239.27
1.49	24055.04	23019.09	21835.90	22353.59	22637.52	22231.67
1.52	23928.02	22822.10	21756.58	22265.57	22568.02	22220.39
1.54	23799.33	22650.27	21703.19	22192.24	22497.54	22197.38
1.56	23663.98	22531.68	21660.93	22134.67	22417.05	22151.17
1.58	23531.91	22415.14	21620.61	22083.71	22364.12	22072.91
1.60	23411.46	22309.94	21583.79	22041.27	22315.61	21994.12
1.62	23264.42	22240.41	21536.80	21997.94	22234.08	21928.64
1.64	23105.74	22196.27	21501.46	21944.88	22162.38	21867.43

1.66	22959.89	22160.71	21474.24	21874.14	22029.59	21796.88
1.68	22814.87	22129.56	21449.93	21788.33	21933.55	21725.17
1.70	22669.27	22102.28	21431.49	21693.43	21887.37	21677.42
1.72	22524.54	22080.98	21416.31	21589.25	21782.21	21628.68
1.74	22383.82	22054.85	21389.71	21484.98	21630.62	21562.66
1.76	22248.94	22011.60	21342.88	21380.76	21506.06	21497.49
1.78	22118.80	21938.23	21294.30	21274.46	21393.76	21437.81
1.80	21989.38	21822.26	21250.50	21178.55	21307.61	21374.48
1.82	21855.96	21684.46	21205.70	21094.06	21235.04	21326.67
1.84	21714.88	21549.60	21157.96	21022.19	21173.60	21298.46
1.86	21571.61	21420.32	21110.13	20968.52	21123.23	21259.56
1.88	21435.61	21287.13	21059.89	20920.71	21099.81	21194.04
1.90	21300.51	21151.85	20961.07	20874.52	21073.06	21118.26
1.92	21161.07	21033.77	20920.25	20832.52	20870.29	21031.3
1.94	21026.86	20927.99	20892.43	20799.13	20741.20	20935.35
1.96	20903.11	20834.48	20855.20	20771.48	20643.68	20845.68
1.98	20792.42	20760.58	20793.04	20745.09	20706.12	20769.61
2.00	20684.00	20676.44	20684.00	20684.00	20684.00	20684

8.5   Appendix C:

LIST OF PUBLICATIONS